arXiv:hep-ph/0003033 v1 4 Mar 2000

# TOP QUARK PHYSICS*

**Conveners**: *M. Beneke, I. Efthymiopoulos, M.L. Mangano, J. Womersley*
**Contributing authors**: *A. Ahmadov, G. Azuelos, U. Baur, A. Belyaev, E.L. Berger, W. Bernreuther, E.E. Boos, M. Bosman, A. Brandenburg, R. Brock, M. Buice, N. Cartiglia, F. Cerutti, A. Cheplakov, L. Chikovani, M. Cobal-Grassmann, G. Corcella, F. del Aguila, T. Djobava, J. Dodd, V. Drollinger, A. Dubak, S. Frixione, D. Froidevaux, B. González Piñeiro, Y.P. Gouz, D. Green, P. Grenier, S. Heinemeyer, W. Hollik, V. Ilyin, C. Kao, A. Kharchilava, R. Kinnunen, V.V. Kukhtin, S. Kunori, L. La Rotonda, A. Lagatta, M. Lefebvre, K. Maeshima, G. Mahlon, S. Mc Grath, G. Medin, R. Mehdiyev, B. Mele, Z. Metreveli, D. O'Neil, L.H. Orr, D. Pallin, S. Parke, J. Parsons, D. Popovic, L. Reina, E. Richter-Was, T.G. Rizzo, D. Salihagic, M. Sapinski, M.H. Seymour, V. Simak, L. Simic, G. Skoro, S.R. Slabospitsky, J. Smolik, L. Sonnenschein, T. Stelzer, N. Stepanov, Z. Sullivan, T. Tait, I. Vichou, R. Vidal, D. Wackeroth, G. Weiglein, S. Willenbrock, W. Wu*

## 1. INTRODUCTION

The top quark, when it was finally discovered at Fermilab in 1995 [1, 2, 3], completed the three-generation structure of the Standard Model (SM) and opened up the new field of top quark physics. Viewed as just another SM quark, the top quark appears to be a rather uninteresting species. Produced predominantly, in hadron-hadron collisions, through strong interactions, it decays rapidly without forming hadrons, and almost exclusively through the single mode $t \to Wb$. The relevant CKM coupling $V_{tb}$ is already determined by the (three-generation) unitarity of the CKM matrix. Rare decays and CP violation are unmeasurably small in the SM.

Yet the top quark is distinguished by its large mass, about 35 times larger than the mass of the next heavy quark, and intriguingly close to the scale of electroweak (EW) symmetry breaking. This unique property raises a number of interesting questions. Is the top quark mass generated by the Higgs mechanism as the SM predicts and is its mass related to the top-Higgs-Yukawa coupling? Or does it play an even more fundamental role in the EW symmetry breaking mechanism? If there are new particles lighter than the top quark, does the top quark decay into them? Could non-SM physics first manifest itself in non-standard couplings of the top quark which show up as anomalies in top quark production and decays? Top quark physics tries to answer these questions.

Several properties of the top quark have already been examined at the Tevatron. These include studies of the kinematical properties of top production [4], the measurements of the top mass [5, 6], of the top production cross-section [7, 8], the reconstruction of $t\bar{t}$ pairs in the fully hadronic final states [9, 10], the study of $\tau$ decays of the top quark [11], the reconstruction of hadronic decays of the $W$ boson from top decays [12], the search for flavour changing neutral current decays [13], the measurement of the $W$ helicity in top decays [14], and bounds on $t\bar{t}$ spin correlations [15]. Most of these measurements are limited by the small sample of top quarks collected at the Tevatron up to now. The LHC is, in comparison, a top factory, producing about 8 million $t\bar{t}$ pairs per experiment per year at low luminosity (10 fb$^{-1}$/year), and another few million (anti-)tops in EW single (anti-)top quark production. We therefore expect that top quark properties can be examined with significant precision at the LHC. Entirely new measurements can be contemplated on the basis of the large available statistics.

In this chapter we summarize the top physics potential of the LHC experiments. An important aspect of this chapter is to document SM model properties of the top quark against which anomalous behaviour has to be compared. In each section (with the exception of the one devoted to anomalous couplings) we begin by summarizing SM expectations and review the current theoretical status on a particular topic. This is followed by a detailed description of experimental analysis strategies in the

*To appear in the Report of the "1999 CERN Workshop on SM physics (and more) at the LHC".

context of the ATLAS and CMS experiments. Particular emphasis is given to new simulations carried out in the course of this workshop. In detail, the outline of this chapter is as follows:

In Section 2. we summarize *SM precision calculations* of the *top quark mass relations* and of the *total top quark width*. We then recall the importance of the top quark mass in EW precision measurements. We discuss, in particular, the role of EW precision measurements under the assumption that a SM Higgs boson has been discovered.

Section 3. deals with the $t\bar{t}$ *production process*: expectations for and measurements of the total cross section, the transverse momentum and $t\bar{t}$ invariant mass distribution are discussed. A separate subsection is devoted to EW radiative corrections to $t\bar{t}$ production, and to radiative corrections in the Minimal Supersymmetric SM (MSSM).

The prospects for an accurate *top quark mass measurement* are detailed in Section 4. Next to "standard" measurements in the lepton+jets and di-lepton channels, two mass measurements are discussed that make use of the large number of top quarks available at the LHC: the selection of top quarks with large transverse momentum in the lepton+jets channel and the measurement of $\ell J/\psi$ correlations in $t \to \ell J/\psi X$ decays. This decay mode appears to be particularly promising and the systematic uncertainties are analyzed in considerable detail.

*Single top quark production* through EW interactions provides the only known way to directly measure the CKM matrix element $V_{tb}$ at hadron colliders. It also probes the nature of the top quark charged current. In Section 5. the SM expectations for the three basic single top production mechanisms and their detection are documented, including the possibility to measure the high degree of polarisation in the SM.

The issue of top quark spin is pursued in Section 6. Here we summarize expectations on *spin correlations in* $t\bar{t}$ *production*, the construction of observables sensitive to such correlations and the results of a simulation study of di-lepton angular correlations sensitive to spin correlations. Possible non-SM CP violating couplings of the top quark can be revealed through anomalous spin-momentum correlations and are also discussed here.

As mentioned above, the search for *anomalous (i.e. non-SM) interactions* is one of the main motivations for top quark physics. In Section 7. the sensitivity of the LHC experiments to the following couplings is investigated: $gt\bar{t}$ couplings and anomalous $Wtb$ couplings in top production, flavour-changing neutral currents (FCNCs) in top production and decay.

Section 8. is devoted to *rare top decays*. The SM expectations for radiative top decays and FCNC decays are documented. Decay rates large enough to be of interest require physics beyond the SM. The two Higgs Doublet Models, the MSSM and generic anomalous couplings are considered explicitly followed by ATLAS and CMS studies on the expected sensitivity in particular decay channels.

Finally, the measurement of the *top quark Yukawa coupling in* $t\bar{t}H$ *production* is considered (Section 9.). The SM cross sections are tabulated in the various production channels at the LHC. For the case of a low mass Higgs boson, the results of a realistic study using a simulation of the ATLAS detector are discussed.

The following topics are collected in the appendices: $b$-quark tagging and the calibration of the jet energy scale in top events; the direct measurement of the top quark spin (as opposed to that of a top squark) and and of top quark electric charge; the total cross section for production of a fourth generation heavy quark; a compendium of Monte Carlo event generators available for top production and its backgrounds.

The internal ATLAS and CMS notes quoted in the bibliography can be obtained from the collaborations' web pages [16, 17]. Updated versions of this document, as well as a list of addenda and errata, will be available on the web page of the LHC Workshop top working group [18].

## 2. TOP QUARK PROPERTIES AND ELECTROWEAK PRECISION MEASUREMENTS[1]

The top quark is, according to the Standard Model (SM), a spin-1/2 and charge-$2/3$ fermion, transforming as a colour triplet under the group $SU(3)$ of the strong interactions and as the weak-isospin partner of the bottom quark. None of these quantum numbers has been directly measured so far, although a large amount of indirect evidence supports these assignments. The analysis of EW observables in $Z^0$ decays [19] requires the existence of a $T_3 = 1/2$, charge-2/3 fermion, with a mass in the range of 170 GeV, consistent with the direct Tevatron measurements. The measurement of the total cross section at the Tevatron, and its comparison with the theoretical estimates, are consistent with the production of a spin-1/2 and colour-triplet particle. The LHC should provide a direct measurement of the top quantum numbers. We present the results of some studies in this direction in Appendix B.

### 2.1 Top quark mass and width

In addition to its quantum numbers, the two most fundamental properties of the top quark are its mass $m_t$ and width $\Gamma_t$, defined through the position of the single particle pole $m_t^\star = m_t - i\Gamma_t/2$ in the perturbative top quark propagator. In the SM $m_t$ is related to the top Yukawa coupling:

$$y_t(\mu) = 2^{3/4} G_F^{1/2} m_t \left(1 + \delta_t(\mu)\right), \tag{1}$$

where $\delta_t(\mu)$ accounts for radiative corrections. Besides the top quark pole mass, the top quark $\overline{\rm MS}$ mass $\overline{m}_t(\mu)$ is often used. The definition of $\overline{m}_t(\mu)$ including EW corrections is subtle (see the discussion in [20]). As usually done in the literature, we define the $\overline{\rm MS}$ mass by including only pure QCD corrections:

$$\overline{m}_t(\mu) = m_t \left(1 + \delta_{\rm QCD}(\mu)\right)^{-1}. \tag{2}$$

The conversion factor $\delta_{\rm QCD}(\mu)$ is very well known [21]. Defining $\overline{m}_t = \overline{m}_t(\overline{m}_t)$ and $a_s = \alpha_s^{\overline{\rm MS}}(\overline{m}_t)/\pi$, we have

$$\begin{aligned} \delta_{\rm QCD}(\overline{m}_t) &= \frac{4}{3}\, a_s + 8.2366\, a_s^2 + 73.638\, a_s^3 + \ldots \\ &= (4.63 + 0.99 + 0.31 + 0.11^{+0.11}_{-0.11})\% = (6.05^{+0.11}_{-0.11})\%. \end{aligned} \tag{3}$$

This assumes five massless flavours besides the top quark and we use $a_s = 0.03475$ which corresponds to $\alpha_s^{\overline{\rm MS}}(m_Z) = 0.119$ and $\overline{m}_t = 165\,$GeV. The error estimate translates into an absolute uncertainty of $\pm 180\,$MeV in $m_t - \overline{m}_t$ and uses an estimate of the four-loop contribution. Note that the difference between the two mass definitions, $m_t - \overline{m}_t$, is about $10\,$GeV. This means that any observable that is supposed to measure a top quark mass with an accuracy of 1–2 GeV and which is known only at leading order (LO) must come with an explanation for why higher order corrections are small when the observable is expressed in terms of that top quark mass definition that it is supposed to determine accurately. We will return to this point in Section 4.

The on-shell decay width $\Gamma_t$ is less well known, but the theoretical accuracy ($< 1\%$) is more than sufficient compared to the accuracy of foreseeable measurements. The decay through $t \to bW$ is by far dominant and we restrict the discussion to this decay mode. It is useful to quantify the decay width in units of the lowest order decay width with $M_W$ and $m_b$ set to zero and $|V_{tb}|$ set to 1:

$$\Gamma_0 = \frac{G_F m_t^3}{8\pi\sqrt{2}} = 1.76\,{\rm GeV}. \tag{4}$$

Incorporating $M_W$ the leading order result reads

$$\Gamma_{\rm LO}(t \to bW)/|V_{tb}|^2 = \Gamma_0 \left(1 - 3\frac{M_W^4}{m_t^4} + 2\frac{M_W^6}{m_t^6}\right) = 0.885\,\Gamma_0 = 1.56\,{\rm GeV}. \tag{5}$$

[1] Section coordinators: M. Beneke, G. Weiglein.

Table 1: Corrections to the top quark width $\Gamma_0$ ($M_W = 0$, lowest order) in units of $\Gamma_0$. The best estimate of $\Gamma(t{\to}bW)/|V_{tb}|^2$ is obtained by adding all corrections together. Parameters: $a_s = 0.03475$, $M_W = 80.4\,\text{GeV}$ and $m_t = 175\,\text{GeV}$.

| | |
|---|---|
| $M_W \neq 0$ correction at lowest order, see (5) | $-11.5\%$ |
| $\alpha_s$ correction, $M_W = 0$ | $-9.5\%$ |
| $\alpha_s$ correction, $M_W \neq 0$ correction | $+1.8\%$ |
| $\alpha_s^2$ correction, $M_W = 0$ [22, 23] | $-2.0\%$ |
| $\alpha_s^2$ correction, $M_W \neq 0$ correction [23] | $+0.1\%$ |
| EW correction [24] | $+1.7\%$ |

The correction for non-vanishing bottom quark mass is about $-0.2\%$ in units of $\Gamma_0$. Likewise corrections to treating the $W$ boson as a stable particle are negligible. Radiative corrections are known to second order in QCD and to first order in the EW theory. Table 1 summarises the known corrections to the limiting case (4). Putting all effects together we obtain:

$$\Gamma(t{\to}bW)/|V_{tb}|^2 \approx 0.807\,\Gamma_0 = 1.42\,\text{GeV}. \tag{6}$$

The top quark lifetime is small compared to the time scale for hadronisation [25]. For this reason, top-hadron spectroscopy is not expected to be the subject of LHC measurements.

### 2.2 Role of $\mathbf{m_t}$ in EW precision physics

The EW precision observables serve as an important tool for testing the theory, as they provide an important consistency test for every model under consideration. By comparing the EW precision data with the predictions (incorporating quantum corrections) within the SM or its extensions, most notably the minimal supersymmetric extension of the Standard Model (MSSM) [26], it is in principle possible to derive indirect constraints on all parameters of the model. The information obtained in this way, for instance, on the mass of the Higgs boson in the SM or on the masses of supersymmetric particles is complementary to the information gained from the direct production of these particles.

In order to derive precise theoretical predictions, two kinds of theoretical uncertainties have to be kept under control: the uncertainties from unknown higher-order corrections, as the predictions are derived only up to a finite order in perturbation theory, and the parametric uncertainties caused by the experimental errors of the input parameters. The top quark mass enters the EW precision observables as an input parameter via quantum effects, i.e. loop corrections. As a distinctive feature, the large numerical value of $m_t$ gives rise to sizable corrections that behave as powers of $m_t$. This is in contrast to the corrections associated with all other particles of the SM. In particular, the dependence on the mass of the Higgs boson is only logarithmic in leading order and therefore much weaker than the dependence on $m_t$. In the MSSM large corrections from SUSY particles are only possible for large splittings in the SUSY spectrum, while the SUSY particles in general decouple for large masses.

The most important $m_t$-dependent contribution to the EW precision observables in the SM and the MSSM enters via the universal parameter $\Delta\rho$ which is proportional to $m_t^2$ [27],

$$\Delta\rho = \left(\frac{\Sigma^Z(0)}{M_Z^2} - \frac{\Sigma^W(0)}{M_W^2}\right)_{t,b} = N_C \frac{\alpha}{16\pi s_W^2 c_W^2} \frac{m_t^2}{M_Z^2}, \tag{7}$$

where the limit $m_b{\to}0$ has been taken, $s_W$ ($c_W$) is the sin (cos) of the weak mixing angle, and $\Sigma^Z(0)$ and $\Sigma^W(0)$ indicate the transverse parts of the gauge-boson self-energies at zero momentum transfer.

The theoretical prediction for $M_W$ is obtained from the relation between the vector-boson masses

and the Fermi constant,

$$M_W^2 \left(1 - \frac{M_W^2}{M_Z^2}\right) = \frac{\pi\alpha}{\sqrt{2}G_F}\,(1+\Delta r)\,, \tag{8}$$

where the quantity $\Delta r$ [28] is derived from muon decay and contains the radiative corrections. At one-loop order, $\Delta r$ can be written as $\Delta r = \Delta\alpha - \frac{c_W^2}{s_W^2}\Delta\rho + (\Delta r)_{\rm nl}$, where $\Delta\alpha$ contains the large logarithmic contributions from the light fermions, and the non-leading terms are collected in $(\Delta r)_{\rm nl}$.

The leptonic effective weak mixing angle is determined from the effective couplings of the neutral current at the Z-boson resonance to charged leptons, $J_\mu^{\rm NC} = \left(\sqrt{2}G_F M_Z^2\right)^{1/2}[g_V\gamma_\mu - g_A\gamma_\mu\gamma_5]$, according to

$$\sin^2\theta_{\rm eff}^{\rm lept} = \frac{1}{4}\left(1 - \frac{{\rm Re}\,(g_V)}{{\rm Re}\,(g_A)}\right). \tag{9}$$

In $\sin^2\theta_{\rm eff}^{\rm lept}$ the leading $m_t$-dependent contributions enter via $\delta\sin^2\theta_{\rm eff}^{\rm lept} = -(c_W^2 s_W^2)/(c_W^2 - s_W^2)\Delta\rho$.

The precision observables $M_W$ and $\sin^2\theta_{\rm eff}^{\rm lept}$ are currently known with experimental accuracies of $0.05\%$ and $0.07\%$, respectively [19]. The accuracy in $M_W$ will be further improved at the LHC by about a factor of three (see the EW chapter of this Yellow Report). Besides the universal correction $\Delta\rho$, there is also a non-universal correction proportional to $m_t^2$ in the $Zb\bar{b}$ coupling, which however is less accurately measured experimentally compared to $M_W$ and $\sin^2\theta_{\rm eff}^{\rm lept}$. The strong dependence of the SM radiative corrections to the precision observables on the input value of $m_t$ made it possible to predict the value of $m_t$ from the precision measurements prior to its actual experimental discovery, and the predicted value turned out to be in remarkable agreement with the experimental result [5, 6].

Within the MSSM, the mass of the lightest CP-even Higgs boson, $m_h$, is a further observable whose theoretical prediction strongly depends on $m_t$. While in the SM the Higgs-boson mass is a free parameter, $m_h$ is calculable from the other SUSY parameters in the MSSM and is bounded to be lighter than $M_Z$ at the tree level. The dominant one-loop corrections arise from the top and scalar-top sector via terms of the form $G_F m_t^4 \ln(m_{\tilde{t}_1} m_{\tilde{t}_2}/m_t^2)$ [29]. As a rule of thumb, a variation of $m_t$ by 1 GeV, keeping all other parameters fixed, roughly translates into a shift of the predicted value of $m_h$ by 1 GeV. If the lightest CP-even Higgs boson of the MSSM will be detected at the LHC, its mass will be measurable with an accuracy of about $\Delta m_h = 0.2$ GeV [30].

Due to the sensitive dependence of the EW precision observables on the numerical value of $m_t$, a high accuracy in the input value of $m_t$ is very important for stringent consistency tests of a model, for constraints on the model's parameters (e.g. the Higgs boson mass within the SM), and for a high sensitivity to possible effects of new physics. It should be noted that this calls not only for a high precision in the experimental measurement of the top quark mass, but also for a detailed investigation of how the quantity that is actually determined experimentally is related to the parameter $m_t$ used as input in higher-order calculations. While these quantities are the same in the simplest approximation, their relation is non-trivial in general due to higher-order contributions and hadronisation effects. A further discussion of this problem, which can be regarded as a systematic uncertainty in the experimental determination of $m_t$, is given in Section 4.

### 2.3 Physics gain from improving $\Delta m_t$ from $\Delta m_t = 2$ GeV to $\Delta m_t = 1$ GeV

During this workshop the question was investigated of how much information one could gain from the EW precision observables by improving the experimental precision in $m_t$ from $\Delta m_t = 2$ GeV, reachable within the first year of LHC running (see Section 4.2), to $\Delta m_t = 1$ GeV, possibly attainable on a longer time scale (see Section 4.6).

In order to analyse this question quantitatively, we have considered the case of the SM and the MSSM and assumed that the Higgs boson has been found at the LHC. For the uncertainty in $\Delta\alpha_{\rm had}$ (the

Table 2: Comparison of the current theoretical uncertainty from unknown higher-order corrections ($\Delta_{\rm theo}$) in $M_W$ and $\sin^2\theta_{\rm eff}^{\rm lept}$ with the parametric uncertainties from the error in $\Delta\alpha_{\rm had}$ and $m_t$.

| | $\Delta_{\rm theo}$ | $\delta(\Delta\alpha_{\rm had}) = 0.00016$ | $\Delta m_t = 2$ GeV | $\Delta m_t = 1$ GeV |
|---|---|---|---|---|
| $\Delta M_W/{\rm MeV}$ | 6 | 3.0 | 12 | 6.1 |
| $\Delta\sin^2\theta_{\rm eff}^{\rm lept}\times 10^5$ | 4 | 5.6 | 6.1 | 3.1 |

hadronic contribution to the electromagnetic coupling at the scale $M_Z$) we have adopted $\delta(\Delta\alpha_{\rm had}) = 0.00016$, which corresponds to the "theory driven" analyses of [31].

Concerning the current theoretical prediction for $M_W$ and $\sin^2\theta_{\rm eff}^{\rm lept}$ in the SM, the theoretical uncertainty from unknown higher-order corrections has been estimated to be about $\Delta M_W = 6$ MeV and $\Delta\sin^2\theta_{\rm eff}^{\rm lept} = 4\times 10^{-5}$ [32]. In Table 2 the theoretical uncertainties for $M_W$ and $\sin^2\theta_{\rm eff}^{\rm lept}$ from unknown higher-order corrections are compared with the parametric uncertainty from the input parameters $\Delta\alpha_{\rm had}$ and $m_t$ for $\Delta m_t = 2$ GeV as well as $\Delta m_t = 1$ GeV. The parametric uncertainties from the other parameters, supposing that the SM Higgs boson has been found at the LHC in the currently preferred range, are negligible compared to the uncertainties from $\Delta\alpha_{\rm had}$ and $m_t$. The resulting uncertainties in $M_W$ and $\sin^2\theta_{\rm eff}^{\rm lept}$ have been obtained using the parameterisation of the results for these quantities given in [33]. As can be seen in the table, for $\Delta m_t = 2$ GeV the parametric uncertainty in $m_t$ gives rise to the largest theoretical uncertainty in both precision observables. While for $\sin^2\theta_{\rm eff}^{\rm lept}$ the uncertainty induced from the error in $m_t$ is comparable to the one from the error in $\Delta\alpha_{\rm had}$, for $M_W$ the uncertainty from the error in $m_t$ is twice as big as the one from unknown higher-order corrections and four times as big as the one from the error in $\Delta\alpha_{\rm had}$. A reduction of the error from $\Delta m_t = 2$ GeV to $\Delta m_t = 1$ GeV will thus mainly improve the precision in the prediction for $M_W$. The uncertainty induced in $M_W$ by $\Delta m_t = 1$ GeV is about the same as the current uncertainty from unknown higher-order corrections. The latter uncertainty can of course be improved by going beyond the present level in the perturbative evaluation of $\Delta r$.

In Fig. 1 the theoretical predictions for $M_W$ and $\sin^2\theta_{\rm eff}^{\rm lept}$ (see [34] and references therein) are compared with the expected accuracies for these observables at LEP2/Tevatron and at the LHC (for the central values, the current experimental values are taken). The parametric uncertainties corresponding to $\delta(\Delta\alpha_{\rm had}) = 0.00016$ and $\Delta m_t = 2$ GeV, $\Delta m_t = 1$ GeV are shown for two values of the Higgs boson mass, $m_H = 120$ GeV and $m_H = 200$ GeV, and the present theoretical uncertainty is also indicated (here $m_H$ is varied within 100 GeV$\leq m_H \leq 400$ GeV and $\Delta m_t = 5.1$ GeV). The figure shows that, assuming that the Higgs boson will be discovered at the LHC, the improved accuracy in $m_t$ and $M_W$ at the LHC will allow a stringent consistency test of the theory. A reduction of the experimental error in $m_t$ from $\Delta m_t = 2$ GeV to $\Delta m_t = 1$ GeV leads to a sizable improvement in the accuracy of the theoretical prediction. In view of the precision tests of the theory a further reduction of the experimental error in $M_W$ and $\sin^2\theta_{\rm eff}^{\rm lept}$ would clearly be very desirable.

While within the MSSM the improved accuracy in $m_t$ and $M_W$ at the LHC will have a similar impact on the analysis of the precision observables as in the SM, the detection of the mass of the lightest CP-even Higgs boson will provide a further stringent test of the model. The prediction for $m_h$ within the MSSM is particularly sensitive to the parameters in the $t$–$\tilde{t}$ sector, while in the region of large $M_A$ and large $\tan\beta$ (giving rise to Higgs masses beyond the reach of LEP2) the dependence on the latter two parameters is relatively mild. A precise measurement of $m_h$ can thus be used to constrain the parameters in the $t$–$\tilde{t}$ sector of the MSSM.

In Fig. 2 it is assumed that the mass of the lightest scalar top quark, $m_{\tilde{t}_1}$, is known with high precision, while the mass of the heavier scalar top quark, $m_{\tilde{t}_2}$, and the mixing angle $\theta_{\tilde{t}}$ are treated as free parameters. The Higgs boson mass is assumed to be known with an experimental precision of $\pm 0.5$ GeV and the impact of $\Delta m_t = 2$ GeV and $\Delta m_t = 1$ GeV is shown (the theoretical uncertainty in the Higgs-

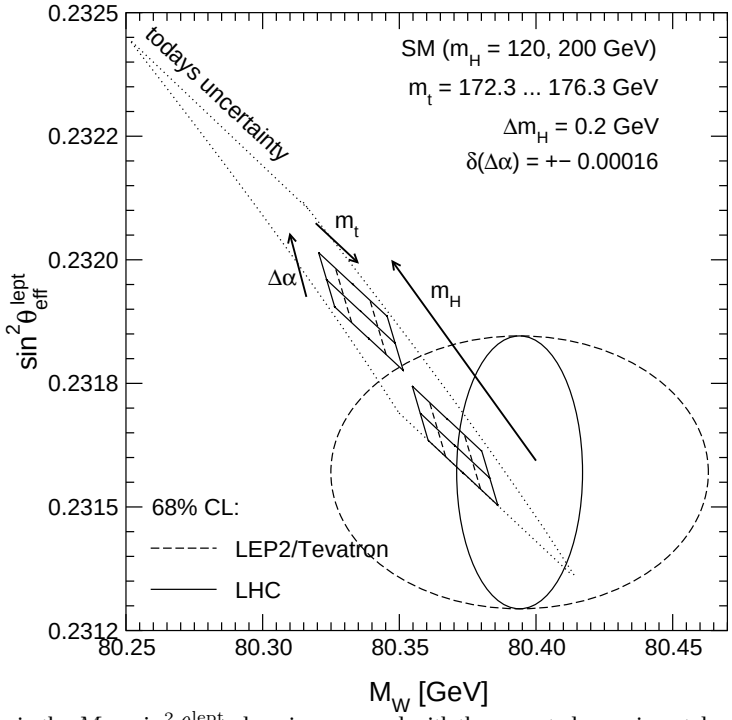


Fig. 1: The SM prediction in the $M_W$–$\sin^2\theta_{\rm eff}^{\rm lept}$ plane is compared with the expected experimental accuracy at LEP2/Tevatron ($\Delta M_W = 30$ MeV, $\sin^2\theta_{\rm eff}^{\rm lept} = 1.7\times10^{-4}$) and at the LHC ($\Delta M_W = 15$ MeV, $\sin^2\theta_{\rm eff}^{\rm lept} = 1.7\times10^{-4}$). The theoretical uncertainties induced by $\delta(\Delta\alpha_{\rm had}) = 0.00016$ and $\Delta m_t = 2$ GeV (full line) as well as $\Delta m_t = 1$ GeV (dashed line) are shown for two values of the Higgs boson mass $m_H$.

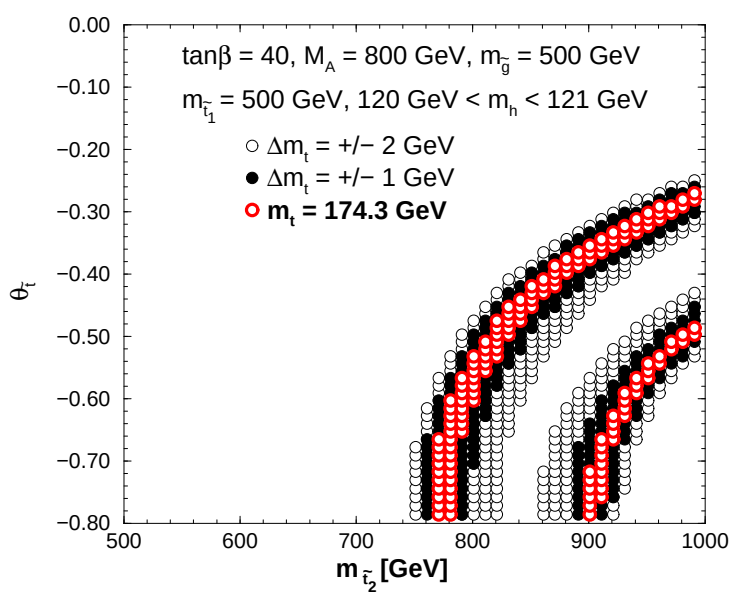


Fig. 2: Indirect constraints on the parameters of the scalar top sector of the MSSM from the measurement of $m_h$ at the LHC. The effect of the experimental error in $m_t$ is shown for $\Delta m_t = 2$ GeV and $\Delta m_t = 1$ GeV.

mass prediction from unknown higher-order contributions and the parametric uncertainties besides the ones induced by $m_{\tilde{t}_2}$, $\theta_{\tilde{t}}$ and $m_t$ have been neglected here). The two bands represent the values of $m_{\tilde{t}_2}$, $\theta_{\tilde{t}}$ which are compatible with a Higgs-mass prediction of $m_h = 120.5 \pm 0.5$ GeV, where the two-loop result of [35] has been used (the bands corresponding to smaller and larger values of $m_{\tilde{t}_2}$ are related to smaller and larger values of the off-diagonal entry in the scalar top mixing matrix, respectively). Combining the constraints on the parameters in the scalar top sector obtained in this way with the results of the direct search for the scalar top quarks will allow a sensitive test of the MSSM. As can be seen in the figure, a reduction of $\Delta m_t$ from $\Delta m_t = 2$ GeV to $\Delta m_t = 1$ GeV will lead to a considerable reduction of the allowed parameter space in the $m_{\tilde{t}_2}$–$\theta_{\tilde{t}}$ plane.

## 3. $t\bar{t}$ PRODUCTION AT THE LHC[2]

The determination of the top production characteristics will be one of the first measurements to be carried out with the large statistics available at the LHC. The large top quark mass ensures that top production is a short-distance process, and that the perturbative expansion, given by a series in powers of the small parameter $\alpha_S(m_t) \sim 0.1$, converges rapidly. Because of the large statistics (of the order of $10^7$ top quark pairs produced per year), the measurements and their interpretation will be dominated by experimental and theoretical systematic errors. Statistical uncertainties will be below the percent level for most observables. It will therefore be a severe challenge to reduce experimental and theoretical systematic uncertainties to a comparable level. In addition to providing interesting tests of QCD, accurate studies of the top production and decay mechanisms will be the basis for the evaluation of the intrinsic properties of the top quark and of its EW interactions. An accurate determination of the production cross section, for example, provides an independent indirect determination of $m_t$. Asymmetries in the rapidity distributions of top and antitop quarks [36] are sensitive to the light-quark parton distribution functions of the proton. Anomalies in the total $t\bar{t}$ rate would indicate the presence of non-QCD production channels, to be confirmed by precise studies of the top quark distributions (*e.g.* $p_T$ and $t\bar{t}$ invariant mass spectra). These would be distorted by the presence of anomalous couplings or $s$-channel resonances expected in several beyond-the-SM (BSM) scenarios. Parity-violating asymmetries (for example in the rapidity distributions of right and left handed top quarks) are sensitive to the top EW couplings, and can be affected by the presence of BSM processes, such as the exchange of supersymmetric particles. As already observed at the Tevatron [5, 6], the structure of the $t\bar{t}$ final state affects the direct determination of $m_t$. Initial and final-state gluon radiation do in fact contribute to the amount of energy carried by the jets produced in the decay of top quarks, and therefore need to be taken into proper account when jets are combined to extract $m_t$. The details of the structure of these jets (*e.g.* their fragmentation function and their shapes), will also influence the experimental determination of the jet energy scales (important for the extraction of $m_t$), as well as the determination of the efficiency with which $b$-jets will be tagged (important for the measurement of the production cross section).

It is therefore clear that an accurate understanding of the QCD dynamics is required to make full use of the rich statistics of $t\bar{t}$ final states in the study of the SM properties of top quarks, as well as to explore the presence of possible deviations from the SM. In this section we review the current state of the art in predicting the production properties for top quark pairs (for a more detailed review of the theory of heavy quark production, see [37]). The study of single top production will be presented in Section 5.

### 3.1 Tools for QCD calculations

Full next-to-leading-order (NLO, $\mathcal{O}(\alpha_S^3)$) calculations are available for the following quantities:

1. Total cross sections [38]
2. Single-inclusive $p_T$ and $y$ spectra [39]
3. Double-differential spectra ($m_{t\bar{t}}$, azimuthal correlations $\Delta\Phi$, etc.) [40]

[2]Section coordinators: M.L. Mangano, D. Wackeroth, M. Cobal (ATLAS), J. Parsons (ATLAS).

All of the above calculations are available in the form of Fortran programs [40, 41], so that kinematical distributions can be evaluated at NLO [42] even in the presence of analysis cuts.

Theoretical progress over the last few years has led to the resummation of Sudakov-type logarithms [43] which appear at all orders in the perturbative expansion for the total cross sections [44, 45]. More recently, the accuracy of these resummations has been extended to the next-to-leading logarithmic (NLL) level [46, 47]. For a review of the theoretical aspects of Sudakov resummation, see the QCD chapter of this report. As will be shown later, while the inclusion of these higher-order terms does not affect significantly the total production rate, it stabilises the theoretical predictions under changes in the renormalisation and factorisation scales, hence improving the predictive power.

Unfortunately, the results of these resummed calculations are not available in a form suitable to implement selection cuts, as they only provide results for total cross-sections, fully integrated over all of phase space. The formalism has been generalised to the case of one-particle inclusive distributions in [48], although no complete numerical analyses have been performed yet.

The corrections of $\mathcal{O}(\alpha_S^3)$ to the full production and decay should include the effect of gluon radiation off the quarks produced in the top decay. Interference effects are expected to take place between soft gluons emitted before and after the decay, at least for gluon energies not much larger than the top decay width. While these correlations are not expected to affect the measurement of generic distributions, even small soft-gluon corrections can have an impact on the determination of the top mass. Matrix elements for hard-gluon emission in $t\bar{t}$ production and decay ($p\bar{p}\to W^+bW^-\bar{b}g$, with $t$ and $\bar{t}$ intermediate states) are implemented in a parton-level generator [49]. The one-gluon emission off the light quarks from the $W$ decays was implemented, in the soft-gluon approximation, in the parton-level calculation of [50].

The above results refer to the production of top quarks treated as free, stable partons. Parton-shower Monte Carlo programs are available (HERWIG [51], PYTHIA [52], ISAJET [53]) for a complete description of the final state, including the full development of the perturbative gluon shower from both initial and final states, the decay of the top quarks, and the hadronisation of the final-state partons. These will be reviewed in Appendix D. Recently, $\mathcal{O}(\alpha_S)$ matrix element corrections to the decay of the top quark ($t\to Wbg$) have been included in the HERWIG Monte Carlo [54]. The impact of these corrections will be reviewed in Sections 3.3 and 4.62.

### 3.2 Total $t\bar{t}$ production rates

In this section we collect the current theoretical predictions for cross sections and distributions, providing our best estimates of the systematic uncertainties. The theoretical uncertainties we shall consider include renormalisation ($\mu_R$) and factorisation ($\mu_F$) scale variations, and the choice of parton distribution functions (PDF's);

We shall explore the first two by varying the scales over the range $\mu_0/2 < \mu < 2\mu_0$, where $\mu = \mu_R = \mu_F$ and

- $\mu_0 = m_t$ for the total cross sections
- $\mu_0 = \sqrt{m_t^2 + p_T^2}$ for single inclusive distributions
- $\mu_0 = \sqrt{m_t^2 + (p_{T,t}^2 + p_{T,\bar{t}}^2)/2}$ for double inclusive distributions

In the case of PDF's, we shall consider the latest fits of the CTEQ [55] and of the MRST [56, 57] groups:

- MRST ($\alpha_S(M_Z) = 0.1175$, $\langle k_T \rangle = 0.4$ GeV) (default)
- MRST($g\downarrow$) ($\alpha_S = 0.1175$, $\langle k_T \rangle = 0.64$ GeV)
- MRST($g\uparrow$) ($\alpha_S = 0.1175$, $\langle k_T \rangle = 0$)
- MRST($\alpha_S\downarrow\downarrow$) ($\alpha_S = 0.1125$, $\langle k_T \rangle = 0.4$ GeV)

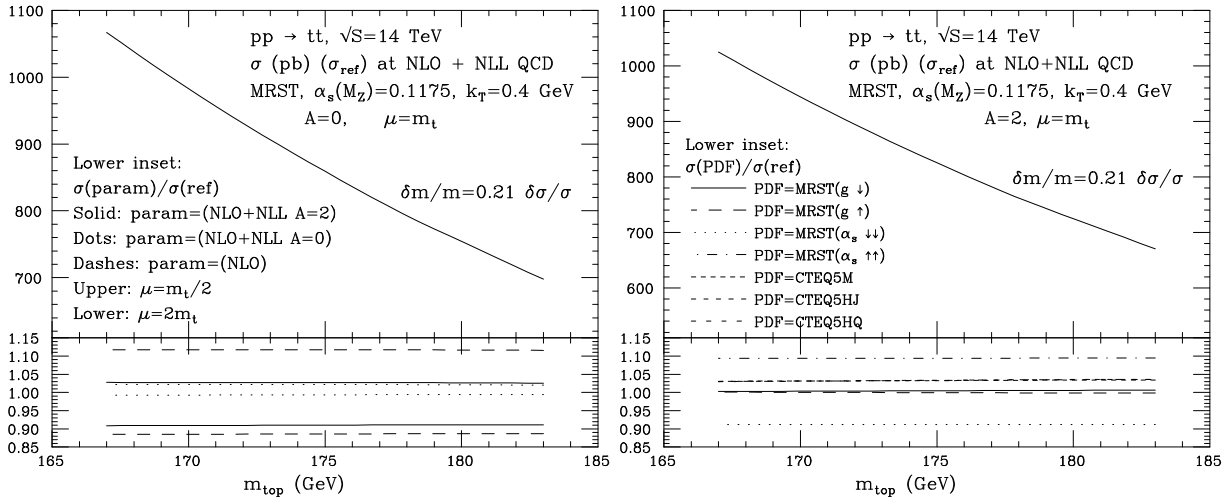


Fig. 3: $t\bar{t}$ production rates. Left: scale dependence at fixed order (NLO, dashed lines in the lower inset), and at NLO+NLL (solid lines). Right: PDF dependence. See the text for details.

- MRST($\alpha_S \uparrow\uparrow$) ($\alpha_S = 0.1225$, $\langle k_T \rangle = 0.4$ GeV)
- CTEQ5M ($\alpha_S = 0.118$)
- CTEQ5HJ ($\alpha_S = 0.118$, enhanced weight for Tevatron high-$E_T$ jets)
- CTEQ5HQ ($\alpha_S = 0.118$, using the ACOT heavy flavour scheme [58].)

All our numerical results relative to the MRST sets refer to the updated fits provided in [57]. These give total rates which are on average 5% larger than the fits in [56]. The total $t\bar{t}$ production cross section is given in Fig. 3, as a function of the top mass. As a reference set of parameters, we adopt $\mu_0 = m_t$ and MRST. Full NLO+NLL corrections are included. The upper inset shows the dependence of the cross section on the top mass. A fit to the distribution shows that $\Delta\sigma/\sigma \sim 5\Delta m_t/m_t$. As a result, a 5% measurement of the total cross section is equivalent to a 1% determination of $m_t$ (approximately 2 GeV). As will be shown later on, 2 GeV is a rather safe estimate of the expected experimental accuracy in the determination of $m_t$ (1 GeV being the optimistic ultimate limit). It follows that 5% should be a minimal goal in the overall precision for the measurement of $\sigma(t\bar{t})$. The scale uncertainty of the theoretical predictions is shown in the lower inset of Fig. 3. The dashed lines refer to the NLO scale dependence, which is of the order of $\pm 12\%$. The dotted lines refer to the inclusion of the NLL corrections, according to the results of [47]. The solid lines include the resummation of NLL effects, but assume a different structure of yet higher order (NNLL) corrections, relative to those contained in the reference NLL results (this is indicated by the value of the $A$ parameter equal to 2, see [47] for the details). The scale uncertainty, after inclusion of NLL corrections, is significantly reduced. In the most conservative case of $A = 2$, we have a $\pm 6\%$ variation. A detailed breakdown of the NLO $\mathcal{O}(\alpha_S^2 + \alpha_S^3)$ and higher-order $\mathcal{O}(\alpha_S^{\geq 4})$ contributions, as a function of the scale and of the value of the parameter $A$, is given in Table 3. A recent study [59] of resummation effects on the total cross section for photo- and hadro-production of quarkonium states indicates that allowing $\mu_R \neq \mu_F$ increases the scale dependence of the NLL resummed cross-sections to almost match the scale dependence of the NLO results [60]. Preliminary results of this study also suggest a similar increase of scale dependence in the case of $t\bar{t}$ production, if $\mu_R$ and $\mu_F$ are varied independently. This dependence can however be reduced by replacing $\mu_R$ with $\mu_F$ as the argument of $\alpha_S$ in the sub-leading coefficients of the resummed exponent [61].

The PDF dependence is shown on the right hand side of Fig. 3, and given in detail for $m_t = 175$ GeV in Table 4. The current uncertainty is at the level of $\pm 10\%$. Notice that the largest deviations from the default set occur for sets using different input values of $\alpha_S(M_Z)$. The difference between the reference sets of the two groups (MRST and CTEQ5M) is at the level of 3%. It is interesting to explore potential correlations between the PDF dependence of top production, and the PDF dependence of other

Table 3: Resummation contributions to the total $t\bar{t}$ cross-sections ($m_t = 175$ GeV) in pb. PDF set MRST.

| | | NLL resummed, A=2 | | NLL resummed, A=0 | |
|---|---|---|---|---|---|
| $\mu_R = \mu_F$ | NLO | $\mathcal{O}(\alpha_S^{\geq 4})$ | NLO+NLL | $\mathcal{O}(\alpha_S^{\geq 4})$ | NLO+NLL |
| $m_t/2$ | 890 | $-7$ | 883 | $-12$ | 878 |
| $m_t$ | 796 | 29 | 825 | 63 | 859 |
| $2m_t$ | 705 | 77 | 782 | 148 | 853 |

Table 4: Total $t\bar{t}$ cross-sections ($m_t = 175$ GeV) in pb. NLO+NLL ($A = 0$).

| PDF | $\mu = m_t/2$ | $\mu = m_t$ | $\mu = 2m_t$ |
|---|---|---|---|
| MRST | 877 | 859 | 853 |
| MRST $g \uparrow$ | 881 | 862 | 857 |
| MRST $g \downarrow$ | 876 | 858 | 852 |
| MRST $\alpha_S \downarrow$ | 796 | 781 | 777 |
| MRST $\alpha_S \uparrow$ | 964 | 942 | 934 |
| CTEQ5M | 904 | 886 | 881 |
| CTEQ5HJ | 905 | 886 | 881 |

processes induced by initial states with similar parton composition and range in $x$. One such example is given by inclusive jet production. Fig. 4 shows the initial-state fraction of inclusive jet final states (with $|\eta| < 2.5$) as a function of the jet-$E_T$ threshold. For values of $E_T \sim 200$ GeV, 90% of the jets come from processes with at least one gluon in the initial state. This fraction is similar to that present in $t\bar{t}$ production, where 90% of the rate is due to $gg$ collisions. On the right side of Fig. 4 we show the double ratios:

$$\frac{\left[\sigma(t\bar{t})/\sigma(\text{jet}, E_T > E_T^{\min})\right]_{\text{PDF}}}{\left[\sigma(t\bar{t})/\sigma(\text{jet}, E_T > E_T^{\min})\right]_{\text{MRST}}} \tag{10}$$

As the plot shows, there is a strong correlation between the PDF dependences of the two processes. The correlation is maximal for $E_T^{\min} \sim 200$ GeV, as expected, since for this value the flavour composition of the initial states and the range of partonic momentum fractions probed in the two production processes are similar. In the range $180 \lesssim E_T^{\min} \lesssim 260$ GeV the PDF dependence of the ratio $\sigma(t\bar{t})/\sigma(\text{jet}, E_T > E_T^{\min})$ is reduced to a level of $\pm 1\%$, even for those sets for which the absolute top cross-section varies by $\pm 10\%$. The jet cross-sections were calculated [62] using a scale $\mu^{jet} = E_T \equiv \mu_0^{jet}$. If we vary the scales for $t\bar{t}$ and jet production in a correlated way (*i.e.* selecting $\mu^{jet}/\mu_0^{jet} = \mu^{t\bar{t}}/\mu_0^{t\bar{t}}$), no significant scale dependence is observed. There is however no a-priori guarantee that the scales should be correlated. Unless this correlation can be proved to exist, use of the inclusive-jet cross section to normalise the $t\bar{t}$ cross section will therefore leave a residual systematic uncertainty which is no smaller than the scale dependence of the jet cross section. We do not expect this to become any smaller than the PDF dependence in the near future.

Combining in quadrature the scale and PDF dependence of the total $t\bar{t}$ cross section, we are left with an overall 12% theoretical systematic uncertainty, corresponding to a 4 GeV uncertainty on the determination of the top mass from the total cross section.

### 3.3 Kinematical properties of $t\bar{t}$ production

We start from the most inclusive quantity, the top $p_T$ spectrum. The NLO predictions are shown in Fig. 5. Here we also explore the dependence on scale variations and on the choice of PDF. The uncertainties are

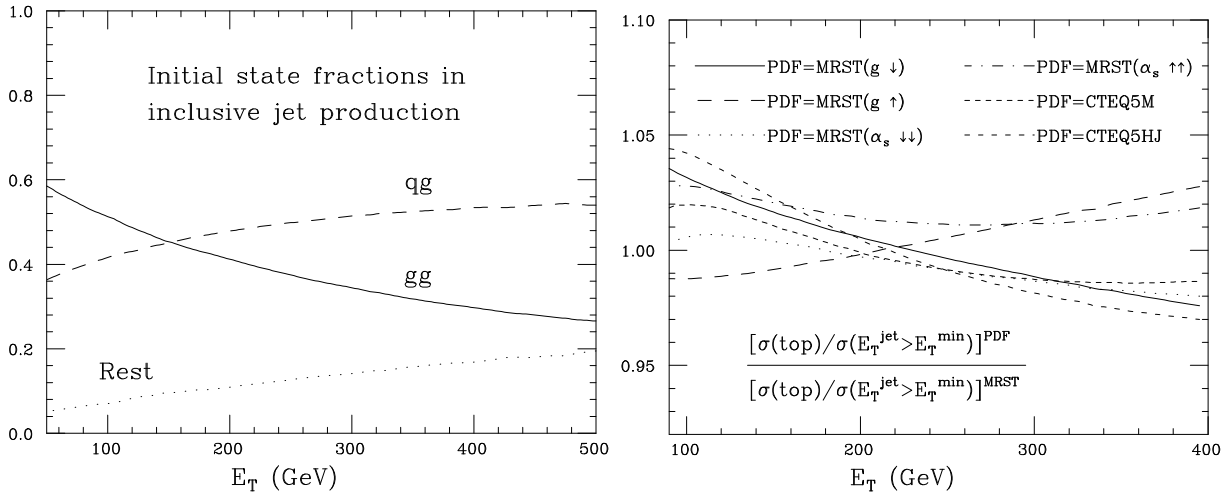


Fig. 4: Left: initial state composition in inclusive jet events, as a function of the jet $E_T$ ($|\eta| < 2.5$). Right: PDF dependence of the top-to-jet cross-section ratio, as a function of the minimum jet $E_T$.

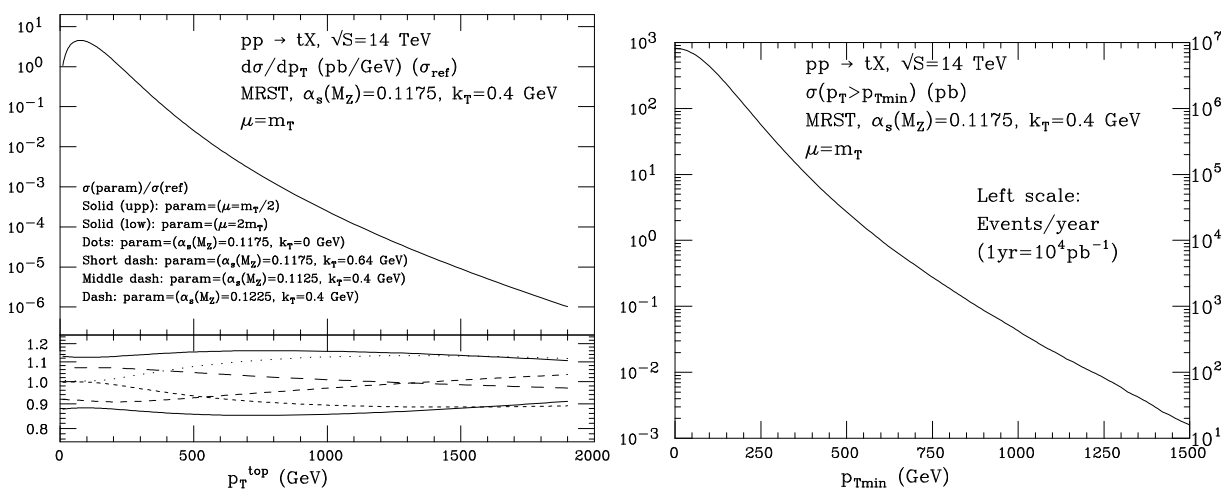


Fig. 5: Inclusive top $p_T$ spectrum. Left: scale and PDF dependence at NLO. Right: event rates above a given $p_T$ threshold.

$\pm 15\%$ and $\pm 10\%$, respectively. The reconstruction of top quarks and their momenta, as well as the determination of the reconstruction efficiencies and of the possible biases induced by the experimental selection cuts, depend on the detailed structure of the final state. It is important to verify that inclusive distributions as predicted by the most accurate NLO calculations are faithfully reproduced by the shower Monte Carlo calculations, used for all experimental studies. This is done in Fig. 6, where the NLO calculation is compared to the result of the HERWIG Monte Carlo, after a proper rescaling by an overall constant $K$-factor. The bin-by-bin agreement between the two calculations is at the level of 10%, which should be adequate for a determination of acceptances and efficiencies at the percent level.

Similar results are obtained for the invariant mass distribution of top quark pairs, shown in the plot of Fig. 6. The scale and PDF dependence of the NLO calculation are similar to those found for the inclusive $p_T$ spectrum, and are not reported in the figure.

Contrary to the case of inclusive $p_T$ and $M_{t\bar{t}}$ spectra, other kinematical distributions show large differences when comparing NLO and Monte Carlo results [42]. This is the case of distributions which are trivial at LO, and which are sensitive to Sudakov-like effects, such as the azimuthal correlations or the spectrum of the $t\bar{t}$ pair transverse momentum $p_T^{t\bar{t}}$. These two distributions are shown in the two plots of Fig. 7. Notice that the scale uncertainty at NLO is larger for these distributions than for previous inclusive

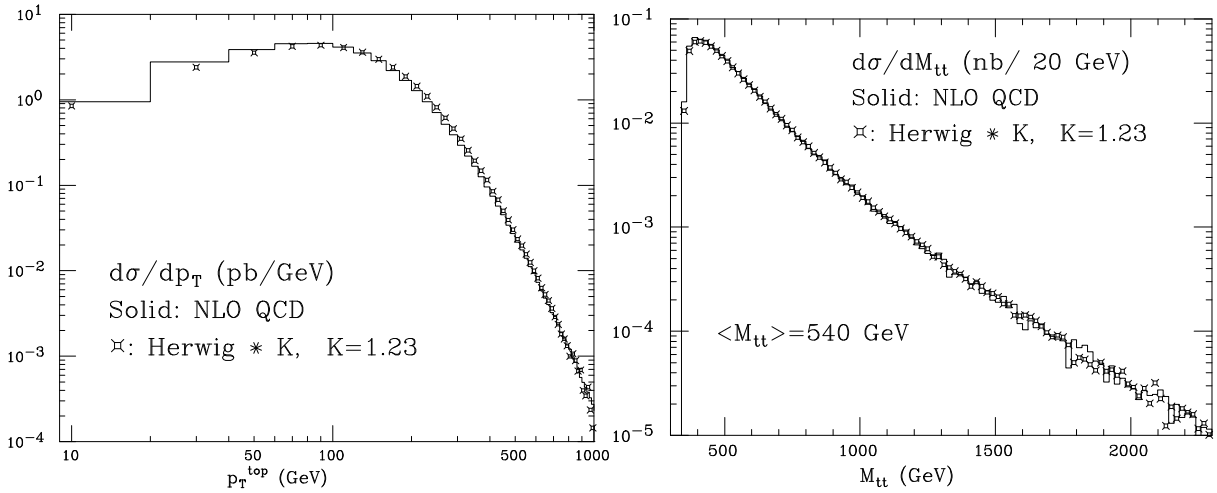


Fig. 6: Comparison of NLO and (rescaled) HERWIG spectra. Left: inclusive top $p_T$ spectrum. Right: inclusive $M_{t\bar{t}}$ spectrum.

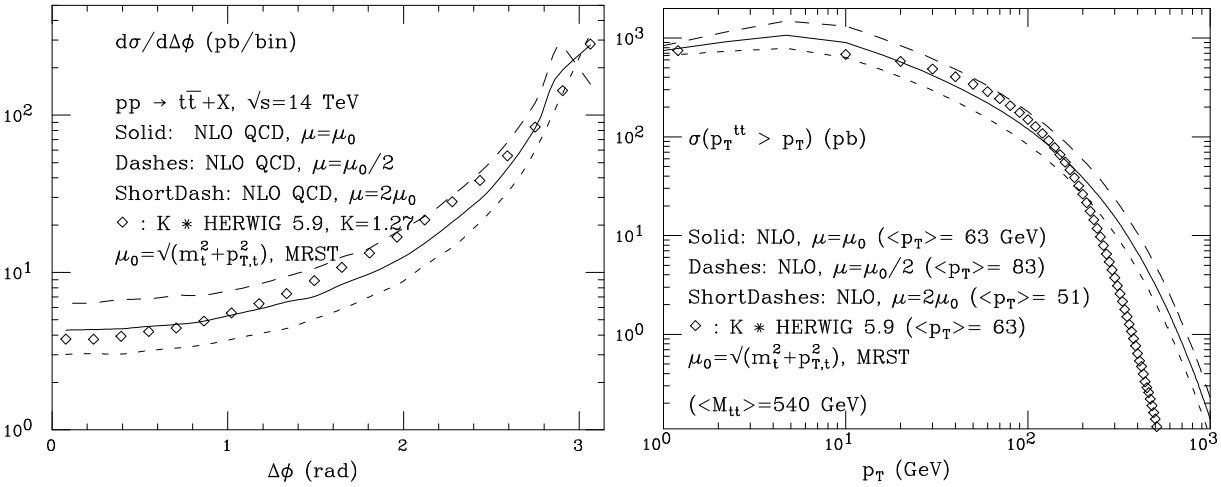


Fig. 7: Left: azimuthal correlation between the $t$ and $\bar{t}$. Right: integrated transverse momentum spectrum of the top quark pair. Continuous lines correspond to the parton-level NLO calculation, for different scale choices; the plots correspond to the result of the HERWIG Monte Carlo.

quantities. These kinematical quantities are in fact trivial at $\mathcal{O}(\alpha_S^2)$ (proportional to $\delta$-functions), and their evaluation at $\mathcal{O}(\alpha_S^3)$ is therefore not a true NLO prediction. The regions $p_T^{t\bar{t}}\to 0$ and $\Delta\phi\to\pi$ are sensitive to multiple soft-gluon emission, and the differences between the NLO calculation (which only accounts for the emission of one gluon) and the Monte Carlo prediction (which includes the multi-gluon emission) is large. The region $p_T^{t\bar{t}} \gg m_t$ is vice-versa sensitive to the emission of individual hard gluons, a process which is more accurately accounted for by the full $\mathcal{O}(\alpha_S^3)$ matrix elements included in the NLO calculation than by the Monte Carlo approach. Notice that the average value of $p_T^{t\bar{t}}$ is quite large, above 50 GeV. This is reasonable, as it is of the order of $\alpha_S$ times the average value of the hardness of the process ($\langle M_{t\bar{t}}\rangle \sim 540$ GeV). It is found that this large transverse momentum is compensated by the emission of a jet recoiling against the top pair, with a smaller fraction of events where the $p_T^{t\bar{t}}$ comes from emission of hard gluons from the final state top quarks. The large-$p_T^{t\bar{t}}$ discrepancy observed in Fig. 7 should be eliminated once the matrix element corrections to top production will be incorporated in HERWIG, along the lines of the work done for Drell-Yan production in [63].

Emission of extra jets is also expected from the evolution of the decay products of the top quarks ($b$'s, as well as the jets from the hadronic $W$ decays). Gluon radiation off the decay products is included

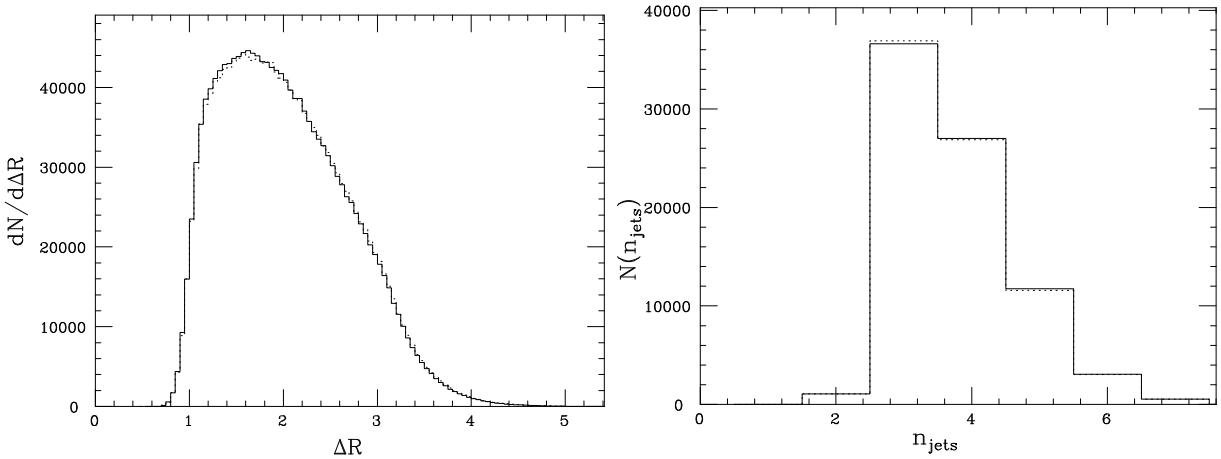


Fig. 8: Left: Distributions of the minimum invariant opening angle $\Delta R$ among the three hardest jets, with (HERWIG 6.1, solid line) and without (6.0, dotted) matrix element corrections in the $t \to bW$ decay. Right: jet multiplicity distributions.

in the shower Monte Carlo calculations. In the case of the latest version of HERWIG (v6.1) [51], the emission of the hardest gluon from the $b$ quarks is evaluated using the exact matrix elements [54]. This improvement, in addition to a few bug fixes, resolve the discrepancies uncovered in [49] between an exact parton level calculation and previous versions of HERWIG. The matrix-element corrections do not alter significantly most of the inclusive jet observables. As examples, we show in Fig. 8 the $\Delta R$ and the jet multiplicity distributions for events where both $W$'s decay leptonically. More details can be found in [64]. Jets are defined using the $k_T$ algorithm [65], with radius parameter $R = 1$. As can be seen, the impact of the exact matrix element corrections is limited, mostly because the extra-jet emission is dominated by initial-state radiation.

The impact on quantities which more directly affect the determination of the top mass remains to be fully evaluated. Given the large rate of high-$E_T$ jet emissions, their proper description will be a fundamental ingredient in the accurate reconstruction of the top quarks from the final state jets, and in the determination of the top quark mass. A complete analysis will only be possible once the matrix element corrections to the $t\bar{t}$ production will be incorporated in the Monte Carlos. Work in this direction is in progress (G. Corcella and M.H. Seymour).

### 3.4 Non-QCD radiative corrections to $t\bar{t}$ production

The production and decay of top quarks at hadron colliders is a promising environment for the detection and study of loop induced SUSY effects: at the parton level there is a large center of mass energy $\hat{s}$ available and owing to its large mass, the top quark strongly couples to the (virtual) Higgs bosons, a coupling which is additionally enhanced in SUSY models. Moreover, it might turn out that SUSY loop effects in connection with top and Higgs boson interactions less rapidly decouple than the ones to gauge boson observables.

To fully explore the potential of precision top physics at the LHC and at the Tevatron [66] to detect, discriminate and constrain new physics, the theoretical predictions for top quark observables need to be calculated beyond leading order (LO) in perturbation theory. Here we will concentrate on the effects of non-QCD radiative corrections to the production processes $gg \to t\bar{t}$ and $q\bar{q} \to t\bar{t}$, including supersymmetric corrections. When searching for quantum signatures of new physics also the SM loop effects have to be under control. The present SM prediction for $t\bar{t}$ observables includes the QCD corrections as discussed above and the EW one-loop contributions to the QCD $t\bar{t}$ production processes [67, 68, 69]. The latter modify the $gt\bar{t}(q\bar{q}g)$ vertex by the virtual presence of the EW gauge bosons and the SM Higgs boson. At the parton level, the EW radiative corrections can enhance the LO cross sections by up to $\approx 30\%$ close to the threshold $\sqrt{\hat{s}} \gtrsim 2m_t$ when the SM Higgs boson is light and reduce the LO cross sections with increasing $\hat{s}$ by up to the same order of magnitude. After convoluting with the parton distribution

functions (PDF's), however, they only reduce the LO production cross section $\sigma(pp\to t\bar{t}X)$ at the LHC by a few percent [67]: up to $2.5(1.8)\%$ for the following cuts on the transverse momentum $p_T$ and the pseudo rapidity $\eta$ of the top quark: $p_T > 100(20)$ GeV and $|\eta| < 2.5$.

So far, the studies of loop induced effects of BSM physics in $t\bar{t}$ production at hadron colliders include the following calculations:

**The $\mathcal{O}(\alpha)$ corrections** within a general two Higgs doublet model (G2HDM) (=SM with two Higgs doublets but without imposing SUSY constraints) to $q\bar{q}\to t\bar{t}$ [70, 71] and $gg\to t\bar{t}$ [71]. In addition to the contribution of the $W$ and $Z$, the $gt\bar{t}(q\bar{q}g)$ vertex is modified by the virtual presence of five physical Higgs bosons which appear in any G2HDM after spontaneous symmetry breaking: $H^0, h^0, A^0, H^\pm$. Thus, the G2HDM predictions for $t\bar{t}$ observables depend on their masses and on two mixing angles, $\beta$ and $\alpha$. The G2HDM radiative corrections are especially large for light Higgs bosons and for very small ($< 1$) and very large values of $\tan\beta$ due to the enhanced Yukawa-like couplings of the top quark to the (virtual) Higgs bosons. Moreover, there is a possible source for large corrections due to a threshold effect in the renormalised top quark self-energy, i.e. when $m_t \approx M_{H^\pm} + m_b$. In [71] the $s$-channel Higgs exchange diagrams in the gluon fusion subprocess, $gg\to h^0, H^0\to t\bar{t}$, had been included. For this workshop we also considered the $gg\to A^0\to t\bar{t}$ contribution [72]. A study of the $s$-channel Higgs exchange diagrams alone, can be found in [73] ($H^0$) and [74, 75] ($H^0$ and $A^0$). They are of particular interest, since they can cause a peak-dip structure in the invariant $t\bar{t}$ mass distribution for heavy Higgs bosons, $M_{H^0,A^0} > 2m_t$, when interfered with the LO QCD $t\bar{t}$ production processes.

**The SUSY EW $\mathcal{O}(\alpha)$ corrections** within the MSSM to $q\bar{q}\to t\bar{t}$ [71, 76, 77, 78] and $gg\to t\bar{t}$ [71, 79]. In [71] also the squark loop contribution to the $gg\to h^0, H^0$ production process in the $s$ channel Higgs exchange diagrams has been taken into account. The SUSY EW corrections comprise the contributions of the supersymmetric Higgs sector, and the genuine SUSY contributions due to the virtual presence of two charginos $\tilde{\chi}^\pm$, four neutralinos $\tilde{\chi}^0$, two top squarks $\tilde{t}_{L,R}$ and two bottom squarks $\tilde{b}_{L,R}$. The MSSM input parameters can be fixed in such a way that the $t\bar{t}$ observables including MSSM loop corrections depend on a relatively small set of parameters [71]: $\tan\beta, M_{A^0}, m_{\tilde{t}_1}, m_{\tilde{b}_L}, \Phi_{\tilde{t}}, \mu, M_2$, where LR mixing is considered only in the top squark sector, parametrized by the mixing angle $\Phi_{\tilde{t}}$. $m_{\tilde{t}_1}$ and $m_{\tilde{b}_L} = m_{\tilde{b}_R}$ denote the mass of the lighter top squark and the bottom squark, respectively. The effects of the supersymmetric Higgs sector tend to be less pronounced than the ones of the G2HDM: since supersymmetry tightly correlates the parameters of the Higgs potential, the freedom to choose that set of parameters which yield the maximum effect is rather limited. On the other hand, they can be enhanced by the genuine SUSY contribution depending on the choice of the MSSM input parameters. The SUSY EW corrections can become large close to the threshold for the top quark decay $t\to\tilde{t} + \tilde{\chi}^0$. They are enhanced for very small ($< 1$) and very large values of $\tan\beta$ and when there exists a light top squark ($m_{\tilde{t}_1} \approx 100$ GeV).

**The SUSY QCD $\mathcal{O}(\alpha_s)$ corrections** to $q\bar{q}\to t\bar{t}$ [78, 80, 81, 82, 83] and $gg\to t\bar{t}$ [84]. So far, there are only results available separately for the $q\bar{q}\to t\bar{t}$ (Tevatron) and the $gg\to t\bar{t}$ (LHC) production processes. The combination of both is work in progress and will be presented in [85]. The SUSY QCD contribution describes the modification of the $gt\bar{t}(q\bar{q}g)$ vertex and the gluon vacuum polarisation due to the virtual presence of gluinos and squarks. Thus, additionally to the dependence on squarks masses (and on mixing angles if LR mixing is considered) the SUSY QCD corrections introduce a sensitivity of $t\bar{t}$ observables on the gluino mass $m_{\tilde{g}}$. As expected, the effects are the largest the lighter the gluino and/or the squarks. Again, there are possible enhancements due to threshold effects, for instance close to the anomalous threshold $m_t^2 = m_{\tilde{g}}^2 + m_{\tilde{t}_1}^2$.

The $t\bar{t}$ observables under investigation so far comprise the total $t\bar{t}$ production cross section $\sigma_{t\bar{t}}$, the invariant $t\bar{t}$ mass distribution $d\sigma/dM_{t\bar{t}}$ and parity violating asymmetries $\mathcal{A}_{LR}$ in the production of left and right handed top quark pairs. At present, the numerical discussion is concentrated on the impact of BSM quantum effects on $t\bar{t}$ observables in $p\overset{(-)}{p}\to t\bar{t}X$. A parton level Monte Carlo program for $p\overset{(-)}{p}\to t\bar{t}\to W^+W^-b\bar{b}\to(f_i\bar{f}_i')(f_j'\bar{f}_j)b\bar{b}$ is presently under construction [72]. This will allow a more

Table 5: The relative corrections to $pp \to t\bar{t}X$ at the LHC when only including SUSY QCD one-loop corrections [84] (with $p_T >$20 GeV, $|\eta| < 2.5$) or only the EW one-loop corrections within the G2HDM and the MSSM [71] ($p_T > 100$ GeV). For comparison the SM prediction is also listed.

| | SM ($M_H = 100$ GeV) | G2HDM | SUSY EW | SUSY QCD |
|---|---|---|---|---|
| $\lvert\sigma_{t\bar{t}}^{NLO} - \sigma_{t\bar{t}}^{LO}\rvert/\sigma_{t\bar{t}}^{LO}$ | $2.5\%$ | $\leq 4\%$ | $\leq 10\%$ | $\leq 4\%$ |

realistic study of the sensitivity of a variety of kinematical distributions to SUSY quantum signatures in the $t\bar{t}$ production processes, for instance by taking into account detector effects.

In the following we give an overview of the present status of BSM quantum effects in $t\bar{t}$ observables at the LHC:

$\underline{\sigma_{\mathbf{t\bar{t}}}}$ : In Table 5 we provide the relative corrections for $\sigma_{t\bar{t}}$ at the LHC for different BSM physics scenarios. They reflect the typical maximum size of the radiative corrections within the models under consideration. As already mentioned there are possible enhancements due to threshold effects, which can yield much larger relative corrections. However, they only arise for very specific choices of the MSSM input parameters. The SUSY EW one-loop corrections always reduce the LO production cross sections and range from SM values, to up to $\approx -5\%$ for heavy squarks and up to $\approx -20\%$ close to $m_t = m_{\tilde{t}_1} + m_{\tilde{\chi}^0}$. The SUSY QCD one-loop corrections, however, can either reduce or enhance $\sigma_{t\bar{t}}$. The relative corrections are negative for small $m_{\tilde{g}}$ and increase with decreasing gluino and/or squark masses. They change sign when approaching the threshold for real sparticle production and reach a maximum at $m_{\tilde{g}} \approx 200$ GeV of about $+2\%$ [84]. Again, very large corrections arise in the vicinity of a threshold for real sparticle production, $m_t = m_{\tilde{g}} + m_{\tilde{t}_1}$. The SUSY EW and QCD one-loop corrections, so far, have only been combined for the $q\bar{q} \to t\bar{t}$ production process and numerical results are provided for the Tevatron $p\bar{p}$ collider in [78, 83]. To summarise, apart from exceptional regions in the MSSM parameter space, it will be difficult to detect SUSY through loop contributions to the $t\bar{t}$ production rate. If light sparticles exist, they are most likely directly observed first. Then, the comparison of the precisely measured top production rate with the MSSM predictions will test the consistency of the model under consideration at quantum level and might yield additional information on the parameter space, for instance constraints on $\tan\beta$ and $\Phi_{\tilde{t}}$.

$\underline{\mathbf{d}\sigma/\mathbf{dM_{t\bar{t}}}}$ : More promising are the distributions of kinematic variables. Here we will concentrate on the impact of SUSY quantum signatures on the invariant $t\bar{t}$ mass distribution. Results for the effects of EW one-loop corrections within the G2HDM and the MSSM on $d\sigma/dM_{t\bar{t}}$ at the LHC are provided in [71]. So far, the impact of the SUSY QCD one-loop contribution on $d\sigma/M_{t\bar{t}}$ has only been discussed for the Tevatron $p\bar{p}$ collider [81], where it turned out that they can significantly change the normalisation and distort the shape of $d\sigma/dM_{t\bar{t}}$. As already mentioned, there is the possibility for an interesting peak-dip structure due to a heavy neutral Higgs resonance in $gg \to t\bar{t}$ within two Higgs doublet models. The potential of the LHC for the observation of such resonances has been studied in [74, 86]. In Section 3.5 the results of an ATLAS analysis of the observability of the $H/A \to t\bar{t}$ channel for different luminosities are presented. In Fig. 9 we show preliminary results for the invariant $t\bar{t}$ mass distribution to $pp \to t\bar{t} \to W^+W^-b\bar{b} \to (\nu_e e^+)(d\bar{u})b\bar{b}$ at the LHC when including MSSM EW one-loop corrections [72]. When $M_{A^0} > 2m_t$ the $gg \to H^0, A^0 \to t\bar{t}$ contributions can cause an excess of $t\bar{t}$ events at $M_{t\bar{t}}$ slightly below $M_{A^0}$, when the Higgs bosons are not too heavy, and a dip in the distribution slightly above $M_{t\bar{t}} = M_{A^0}$. For the choice of MSSM parameters used in Fig. 9 the peak vanishes for $M_{A^0} > 400$ GeV and only a deficiency of events survives which decreases rapidly for increasing $M_{A^0}$. These effects can be enhanced when the SUSY QCD contributions are taken into account.

$\underline{\mathcal{A}_{\mathbf{LR}}}$ : Parity violating asymmetries in the distribution of left and right-handed top quark pairs at hadron colliders directly probe the parity non-conserving parts of the non-QCD one-loop corrections to the $t\bar{t}$ production processes within the model under consideration and have been studied at the Tevatron [77, 82, 87, 68, 81, 83] and at the LHC [88]. In Fig. 10 we show the left-right asymmetries $\mathcal{A}_{LR}$ in

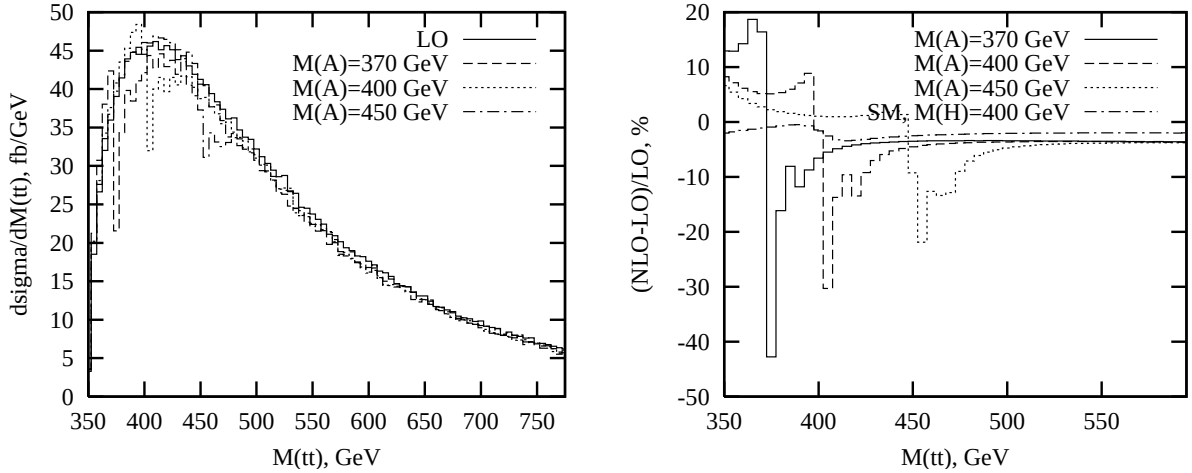


Fig. 9: The LO and NLO invariant mass distributions $d\sigma/dM_{t\bar{t}}$ (left) and the relative corrections (right) to the reaction $pp{\to}t\bar{t}{\to}(\nu_e e^+)(d\bar{u})b\bar{b}$ at the LHC with $p_T(e,q) > 20$ GeV, $E_T(\nu) > 20$ GeV and $|\eta(e,q)| < 3.2$ for different values of $M_{A^0}$ ($\tan\beta = 1.6$, $\Phi_{\tilde{t}} = \pi/8$, $m_{\tilde{t}_1} = 160$ GeV, $m_{\tilde{b}_L} = 500$ GeV, $\mu = 120$ GeV and $M_2 = 3|\mu|$.). For comparison the relative correction when only taking into account the EW SM one-loop contribution is also shown. The CTEQ3LO set of PDF's is used and $m_t = 174$ GeV.

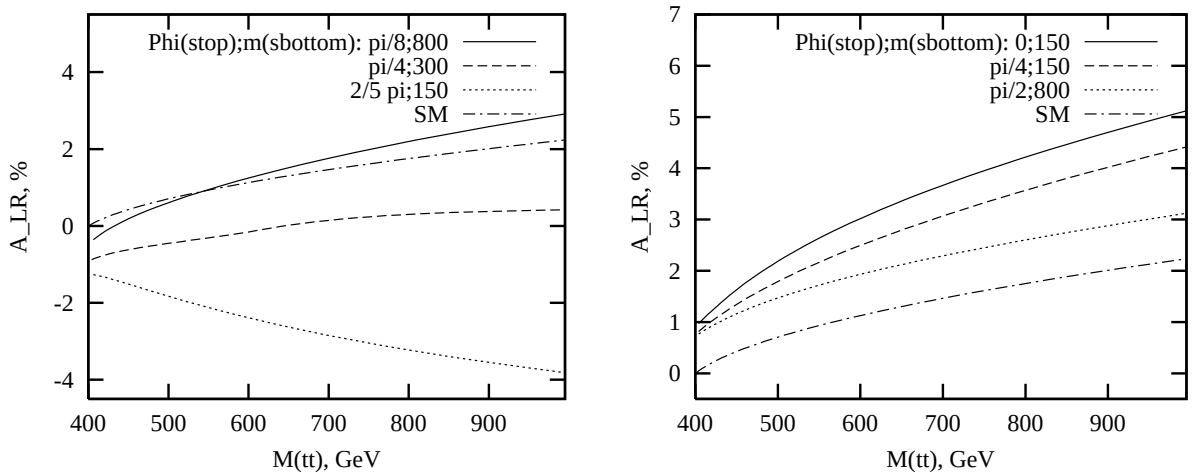


Fig. 10: The left-right asymmetry $\mathcal{A}_{LR}$ in the invariant $t\bar{t}$ mass distribution to $pp{\to}t\bar{t}X$ at the LHC with $p_T > 100$ GeV for different values of $\Phi_{\tilde{t}}$ and $m_{\tilde{b}_L}$ and for two extreme choices of $\tan\beta$: $\tan\beta = 0.7$ (left) and $\tan\beta = 50$ (right) (with $m_{\tilde{t}_1} = 90$ GeV, $M_{H^\pm}$=110 GeV, $\mu = 120$ GeV and $M_2 = 3|\mu|$).

the invariant mass distribution of (longitudinally) polarised top quark pairs in $pp{\to}t_{L,R}\bar{t}_{L,R}X$, induced by SM and MSSM EW one-loop corrections [88]. The parity violating asymmetry within the MSSM results from the interplay of the supersymmetric Higgs sector ($M_{H^\pm}$) and the genuine SUSY contributions ($\tilde{\chi}^\pm, \tilde{\chi}^0$). The contribution from the charged Higgs boson can either be enhanced or diminished depending on the values of $m_{\tilde{t}_1}$ and $\Phi_{\tilde{t}}$. Within the G2HDM the loop-induced asymmetries are most pronounced for a light charged Higgs boson and very small and very large values of $\tan\beta$. At the LHC, the G2HDM and MSSM EW one-loop corrections induce asymmetries in the total production rate of left and right-handed top quark pairs of up to about $2.5\%$ and $3.2\%$, respectively, and thus can be considerably larger than the SM expectation (SM: $1.2\%$). When the squarks are non-degenerate in mass also the SUSY QCD one-loop corrections induce parity violating asymmetries in strong $t\bar{t}$ production. So far, there exist only studies for the Tevatron [82, 81, 83].

### 3.5 Measurement of $\mathrm{t\bar{t}}$ production properties

According to the SM, the top quark decays almost exclusively via $t \to Wb$. The final state topology of $t\bar{t}$ events then depends on the decay modes of the $W$ bosons. In approximately 65.5% of $t\bar{t}$ events,

both $W$ bosons decay hadronically via $W \to jj$, or at least one $W$ decays via $W \to \tau\nu$. These events are difficult to extract cleanly above the large QCD multi-jet background, and are for the most part not considered further. Instead, the analyses presented here concentrate on leptonic $t\bar{t}$ events, where at least one of the $W$ bosons decays via $W \to \ell\nu$ ($\ell = e, \mu$). The lepton plus large $E_T^{miss}$, due to the escaping neutrino(s), provide a large suppression against multi-jet backgrounds. The leptonic events, which account for approximately 34.5% of all $t\bar{t}$ events, can be subdivided into a "single lepton plus jets" sample and a "di-lepton" sample, depending on whether one or both W bosons decay leptonically. As discussed below, the selection cuts and background issues are quite different for the various final state topologies.

An important experimental tool for selecting clean top quark samples is the ability to identify $b$-jets. Techniques for $b$-tagging, using secondary vertices, semi-leptonic $b$-decays, and other characteristics of $b$-jets, have been extensively studied. Both ATLAS and CMS expect to achieve, for a $b$-tagging efficiency of 60%, a rejection of at least 100 against prompt jets (i.e. jets containing no long-lived particles) at low luminosity. At high luminosity, a rejection factor of around 100 can be obtained with a somewhat reduced $b$-tagging efficiency of typically 50%.

All the results presented in this section are obtained using for the signal the PYTHIA Monte Carlo program. Most background processes have also been generated with PYTHIA, with the exception of $Wb\bar{b}$, which has been produced using the HERWIG implementation [89] of the exact massive matrix-element calculation.

### *3.51 Single lepton plus jets sample*

The single lepton plus jets topology, $t\bar{t} \to WWb\bar{b} \to (\ell\nu)(jj)b\bar{b}$ arises in $2 \times 2/9 \times 6/9 \approx 29.6\%$ of all $t\bar{t}$ events. One expects, therefore, production of almost 2.5 million single lepton plus jet events for an integrated luminosity of 10 fb$^{-1}$, corresponding to one year of LHC running at $10^{33}$ cm$^{-2}$ s$^{-1}$. The presence of a high $p_T$ isolated lepton provides an efficient trigger. The lepton and the high value of $E_T^{miss}$ give a large suppression of backgrounds from QCD multi-jets and $b\bar{b}$ production.

For the single lepton plus jets sample, it is possible to fully reconstruct the final state. The four-momentum of the missing neutrino can be reconstructed by setting $M^\nu$ = 0, assigning $E_T^\nu$ = $E_T^{miss}$, and calculating $p_z^\nu$, with a quadratic ambiguity, by applying the constraint that $M^{\ell\nu}$ = $M_W$.

An analysis by ATLAS [30] examined a typical set of selection cuts. First, the presence of an isolated electron or muon with $p_T > 20$ GeV and $|\eta| < 2.5$ was required, along with a value of $E_T^{miss} >$ 20 GeV. At least four jets with $p_T > 20$ GeV were required, where the jets were reconstructed using a fixed cone algorithm with cone size of $\Delta R$ = 0.7. After cuts, the major sources of backgrounds were $W$+jet production with $W \to \ell\nu$ decay, and $Z$+jet events with $Z \to \ell^+\ell^-$. Potential backgrounds from $WW$, $WZ$, and $ZZ$ gauge boson pair production have also been considered, but are reduced to a negligible level after cuts.

A clean sample of $t\bar{t}$ events was obtained using $b$-tagging. Requiring that at least one of the jets be tagged as a $b$-jet yielded a selection efficiency (not counting branching ratios) of 33.3%. For an integrated luminosity of 10 fb$^{-1}$, this would correspond to a signal of 820,000 $t\bar{t}$ events. The total background, dominated by $W$+jet production, leads to a signal-to-background ratio (S/B) of 18.6. Tighter cuts can be used to select a particularly clean sample. Examples of this will be given in Section 4.

### *3.52 Di-lepton sample*

Di-lepton events, where each W decays leptonically, provide a particularly clean sample of $t\bar{t}$ events, although the product of branching ratios is small, $2/9 \times 2/9 \approx$ 4.9%. With this branching ratio, one expects the production of over 400,000 di-lepton events for an integrated luminosity of 10 fb$^{-1}$.

The presence of two high $p_T$ isolated leptons allows these events to be triggered efficiently. Backgrounds arise from Drell-Yan processes associated with jets, $Z \to \tau^+\tau^-$ associated with jets, $WW$+jets,

and $b\bar{b}$ production. Typical selection criteria [30, 90] require two opposite-sign leptons within $|\eta| < 2.5$, with $p_T > 35$ and 25 GeV respectively, and with $E_T^{miss} > 40$ GeV. For the case of like-flavour leptons ($e^+e^-$ and $\mu^+\mu^-$), an additional cut $|M^{\ell\ell} - M^Z| > 10$ GeV was made on the di-lepton mass to remove $Z$ candidates. Requiring, in addition, at least two jets with $p_T > 25$ GeV produced a signal of 80,000 events for 10 fb$^{-1}$, with S/B around 10. Introducing the requirement that at least one jet be tagged as a $b$-jet reduced the signal to about 58,000 events while improving the purity to S/B $\approx$ 50.

### *3.53 Multi-jet sample*

The largest sample of $t\bar{t}$ events consists of the topology $t\bar{t} \to WWb\bar{b} \to (jj)(jj)b\bar{b}$. The product of branching ratios of $6/9 \times 6/9 \approx$ 44.4% implies production of 3.7 million multi-jet events for an integrated luminosity of 10 fb$^{-1}$. However, these events suffer from a very large background from QCD multi-jet events. In addition, the all-jet final state poses difficulties for triggering. For example, the trigger menus examined so far by ATLAS [30] consider multi-jet trigger thresholds only up to four jets, for which a jet $E_T$ threshold of 55 GeV is applied at low luminosity. Further study is required to determine appropriate thresholds for a six-jet topology.

At the Fermilab Tevatron Collider, both the CDF and D0 collaborations have shown that it is possible to isolate a $t\bar{t}$ signal in this channel. The CDF collaboration has obtained a signal significance over background of better than three standard deviations [9] by applying simple selection cuts and relying on the high $b$-tagging efficiency ($\simeq$ 46%). To compensate for the less efficient $b$-tagging, the D0 collaboration has developed a more sophisticated event selection technique [10]. Ten kinematic variables to separate signal and background were used in a neural network, and the output was combined in a second network together with three additional variables designed to best characterise the $t\bar{t}$ events.

ATLAS has made a very preliminary investigation [30, 91] of a simple selection and reconstruction algorithm for attempting to extract the multi-jet $t\bar{t}$ signal from the background. Events were selected by requiring six or more jets with $p_T > 15$ GeV, and with at least two of them tagged as $b$-jets. Jets were required to satisfy $|\eta| < 3$ ($|\eta| < 2.5$ for $b$-jet candidates). In addition, the scalar sum of the transverse momenta of the jets was required to be greater than 200 GeV. The $t\bar{t}$ signal efficiency for these cuts was 19.3%, while only 0.29% of the QCD multi-jet events survived. With this selection, and assuming a QCD multi-jet cross-section of 1.4 $\times 10^{-3}$ mb for $p_T$(hard process) $> 100$ GeV, one obtains a signal-to-background ratio S/B $\approx$ 1/57.

Reconstruction of the $t\bar{t}$ final state proceeded by first selecting di-jet pairs, from among those jets not tagged as $b$-jets, to form $W \to jj$ candidates. A $\chi^2_W$ was calculated from the deviations of the two $M_{jj}$ values from the known value of $M_W$. The combination which minimised the value of $\chi^2_W$ was selected, and events with $\chi^2_W > 3.5$ were rejected. For accepted events, the two $W$ candidates were then combined with $b$-tagged jets to form top and anti-top quark candidates, and a $\chi^2_t$ was calculated as the deviation from the condition that the top and anti-top masses are equal. Again, the combination with the lowest $\chi^2_t$ was selected, and events with $\chi^2_t > 7$ were rejected. After this reconstruction procedure and cuts, the value of S/B improved to 1/8 within the mass window 130-200 GeV. Increasing the $p_T$ threshold for jets led to some further improvement; for example, requiring $p_T^j > 25$ GeV yielded S/B = 1/6.

The isolation of a top signal can be further improved in a number of ways, such as using a multivariate discriminant based on kinematic variables like aplanarity, sphericity or $\Delta R$(jet-jet), or restricting the analysis to a sample of high $p_T^{top}$ events. These techniques are undergoing further investigation, but it will be very difficult to reliably extract the signal from the background in this channel. In particular, the multi-jet rates and topologies suffer from very large uncertainties.

### *3.54 Measurement of the $t\bar{t}$ invariant mass spectrum*

As discussed previously, properties of $t\bar{t}$ events provide important probes of both SM and BSM physics. For example, a heavy resonance decaying to $t\bar{t}$ might enhance the cross-section, and might produce a

peak in the $M_{t\bar{t}}$ invariant mass spectrum. Deviations from the SM top quark branching ratios, due for example to a large rate of $t \to H^+b$, could lead to an apparent deficit in the $t\bar{t}$ cross-section measured with the assumption that BR($t \to Wb$) $\approx$ 1.

Due to the very large samples of top quarks which will be produced at the LHC, measurements of the total cross-section $\sigma(t\bar{t})$ will be limited by the uncertainty of the integrated luminosity determination, which is currently estimated to be 5%-10%. The cross-section relative to some other hard process, such as $Z$ production, should be measured more precisely.

Concerning differential cross-sections, particular attention has thus far been paid by ATLAS [30] to measurement of the $M_{t\bar{t}}$ invariant mass spectrum. A number of theoretical models predict the existence of heavy resonances which decay to $t\bar{t}$. An example within the SM is the Higgs boson, which will decay to $t\bar{t}$ provided the decay is kinematically allowed. However, the strong coupling of the SM Higgs boson to the $W$ and $Z$ implies that the branching ratio to $t\bar{t}$ is never very large. For example, for $M_H$ = 500 GeV, the SM Higgs natural width would be 63 GeV, and BR($H \to t\bar{t}$) $\approx$ 17%. The resulting value of $\sigma\times$BR for $H \to t\bar{t}$ in the SM is not sufficiently large to see a Higgs peak above the large background from continuum $t\bar{t}$ production. In the case of MSSM, however, if $M_{H,A} > 2m_t$, then BR($H/A \to t\bar{t}$) $\approx$ 100% for $\tan\beta \approx 1$. For the case of scalar or pseudo-scalar Higgs resonances, it has been pointed out [73, 74] that interference can occur between the amplitude for the production of the resonance via $gg \to H/A \to t\bar{t}$ and the usual gluon fusion process $gg \to t\bar{t}$. The interference effects become stronger as the Higgs' mass and width increase, severely complicating attempts to extract a resonance signal.

The possible existence of heavy resonances decaying to $t\bar{t}$ arises in technicolor models [92] as well as other models of strong EW symmetry breaking [93]. Recent variants of technicolor theories, such as Topcolor [94], posit new interactions which are specifically associated with the top quark, and could give rise to heavy particles decaying to $t\bar{t}$. Since $t\bar{t}$ production at the LHC is dominated by $gg$ fusion, colour octet resonances ("colourons") could also be produced [95].

Because of the large variety of models and their parameters, ATLAS performed a study [30, 96] of the sensitivity to a "generic" narrow resonance decaying to $t\bar{t}$. Events of the single lepton plus jets topology $t\bar{t} \to WWb\bar{b} \to (\ell\nu)(jj)b\bar{b}$ were selected by requiring $E_T^{miss} > 20$ GeV, and the presence of an isolated electron or muon with $p_T > 20$ GeV and $|\eta| < 2.5$. In addition, it was required that there were between four and ten jets, each with $p_T > 20$ GeV and $|\eta| < 3.2$. At least one of the jets was required to be tagged as a $b$-jet. After these cuts, the background to the $t\bar{t}$ resonance search was dominated by continuum $t\bar{t}$ production.

The momentum of the neutrino was reconstructed, as described previously, by setting $M_\nu$ = 0, assigning $E_T^\nu$ = $E_T^{miss}$, and calculating $p_z^\nu$ (with a quadratic ambiguity) by applying the constraint that $M_{\ell\nu}$ = $M_W$. The hadronic $W \to jj$ decay was reconstructed by selecting pairs of jets from among those not tagged as $b$-jets. In cases where there were at least two $b$-tagged jets, candidates for $t \to Wb$ were formed by combining the $W$ candidates with each $b$-jet. In events with only a single $b$-tagged jet, this was assigned as one of the $b$-quarks and each of the still unassigned jets was then considered as a candidate for the other $b$-quark.

Among the many different possible jet-parton assignments, the combination was chosen that minimised the following $\chi^2$:

$$\chi^2 = (M_{jjb} - m_t)^2/\sigma^2(M_{jjb}) + (M_{\ell\nu b} - m_t)^2/\sigma^2(M_{\ell\nu b}) + (M_{jj} - M_W)^2/\sigma^2(M_{jj})$$

Events were rejected if either $M_{\ell\nu b}$ or $M_{jjb}$ disagreed with the known value of $m_t$ by more than 30 GeV.

For events passing the reconstruction procedure, the measured energies were rescaled, according to their resolution, to give the correct values of $M_W$ and $m_t$ for the appropriate combinations. This procedure improved the resolution of the mass reconstruction of the $t\bar{t}$ pair to $\sigma(M_{t\bar{t}})/M_{t\bar{t}} \approx 6.6\%$. As an example, Fig. 11 shows the reconstructed $M_{t\bar{t}}$ distribution for a narrow resonance of mass 1600 GeV. The width of the Gaussian core is well described by the resolution function described above. The size

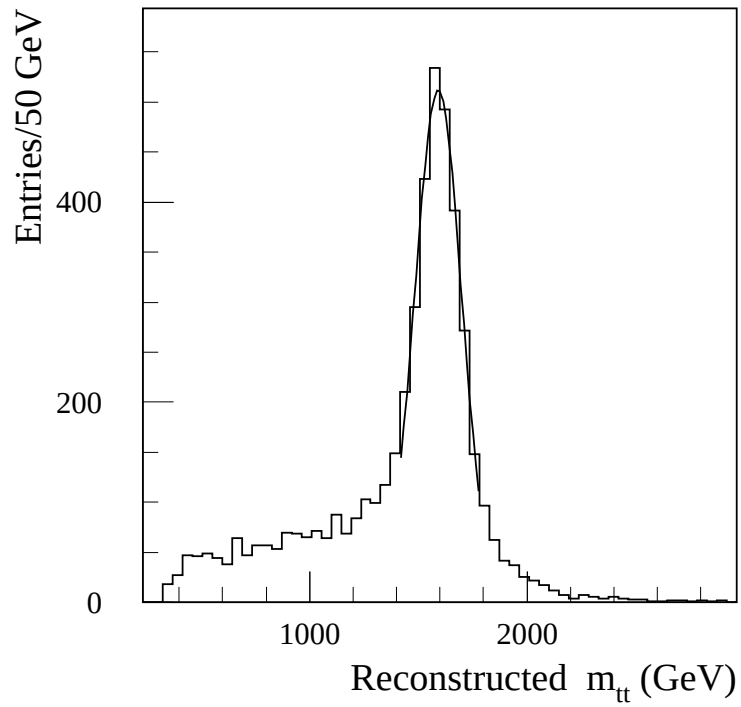


Fig. 11: Measured $t\bar{t}$ invariant mass distribution for reconstruction of a narrow resonance of mass 1600 GeV decaying to $t\bar{t}$.

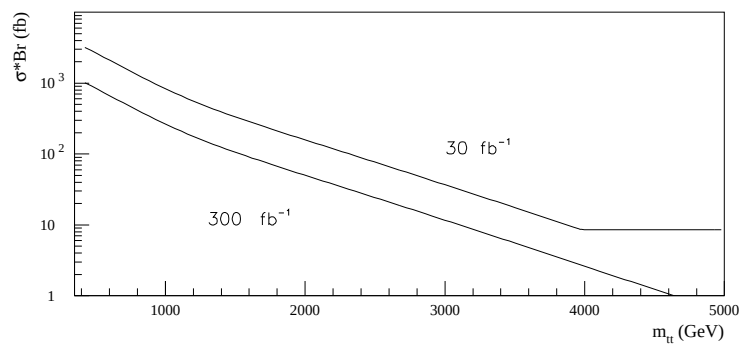


Fig. 12: Value of $\sigma\times$ BR required for a $5\sigma$ discovery potential for a narrow resonance decaying to $t\bar{t}$, as a function of $M_{t\bar{t}}$, and for an integrated luminosity of either 30 or 300 fb$^{-1}$.

of the tails, which are dominated by incorrect jet-parton assignments, is such that approximately 65% of the events are contained within $\pm 2\sigma$ of the peak.

The reconstruction efficiency, not including branching ratios, for $t\bar{t} \to WWb\bar{b} \to (\ell\nu)(jj)b\bar{b}$ was about 20% for a resonance of mass 400 GeV, decreasing gradually to about 15% for $M_{t\bar{t}}$ = 2 TeV.

For a narrow resonance $X$ decaying to $t\bar{t}$, Fig. 12 shows the required $\sigma\times$ BR($X \to t\bar{t}$) for discovery of the resonance. The criterion used to define the discovery potential was observation within a $\pm 2\sigma$ mass window of a signal above the $t\bar{t}$ continuum background, where the required signal must have a statistical significance of at least $5\sigma$ and must contain at least ten events. Results are shown versus $M_X$ for integrated luminosities of 30 fb$^{-1}$ and 300 fb$^{-1}$. For example, with 30 fb$^{-1}$, a 500 GeV resonance could be discovered provided its $\sigma\times$ BR is at least 2560 fb. This value decreases to 830 fb for $M_X$ = 1 TeV, and to 160 fb for $M_X$ = 2 TeV. The corresponding values for an integrated luminosity of 300 fb$^{-1}$ are 835 fb, 265 fb, and 50 fb for resonances masses $M_X$ = 500 GeV, 1 TeV, and 2 TeV, respectively.

Once predictions from models exist for the mass, natural width, and $\sigma\times$ BR for a specific resonance, the results in Fig. 12 can be used to determine the sensitivity and discovery potential for those models. As discussed above, for the case of scalar or pseudo-scalar Higgs resonances, extra care must be taken due to possible interference effects. While such effects are small for the case of a narrow resonance,

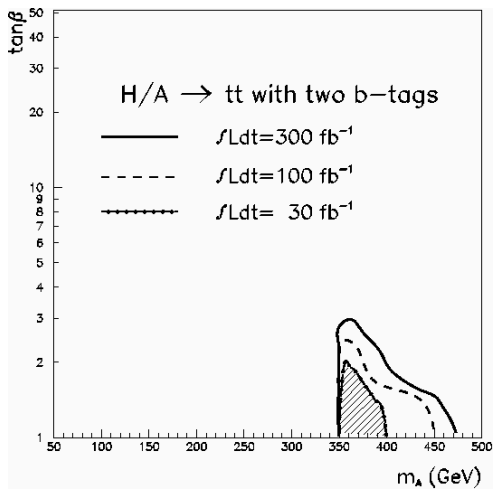


Fig. 13: For various integrated luminosities, $5\sigma$ discovery contours in the MSSM ($M^A$, $\tan\beta$) plane for the channel $H, A \to t\bar{t}$.

they can be significant once the finite widths of heavy resonances are taken into account. For example, ATLAS has performed an analysis [30, 97] of the decays $H/A \to t\bar{t}$ in MSSM with $\tan\beta = 1.5$ and $M_{H,A} > 2m_t$. Assuming the $t\bar{t}$ continuum background is well known, a combined $H + A$ signal would be visible for Higgs masses in the range of about 370 - 450 GeV. However, the interference effects produce an effective suppression of the combined $H + A$ production rates of about 30% for $M_{H,A} = 370$ GeV, increasing to 70% for masses of 450 GeV, essentially eliminating the possibility to extract a signal for higher Higgs masses, and thereby severely limiting the MSSM parameter space for which this channel has discovery potential (see Fig. 13).

## 4. TOP QUARK MASS[3]

As discussed in Section 2.2 one of the main motivations for top physics at the LHC is an accurate measurement of the top mass. Currently the best Tevatron single-experiment results on $m_t$ are obtained with the lepton plus jets final states. These yield: $m_t$= 175.9 $\pm$ 4.8 (stat.) $\pm$ 5.3 (syst.) (CDF) [6] and 173.3 $\pm$ 5.6 (stat.) $\pm$ 5.5 (syst.) (DØ) [5]. The systematic errors in both measurements are largely dominated by the uncertainty on the jet energy scale which amounts to 4.4 GeV and 4 GeV for CDF and DØ, respectively. On the other hand, the systematic errors in the di-lepton channels are somewhat less, but the statistical errors are significantly larger, by a factor of $\gtrsim$ 2, as compared to the lepton plus jets final states. Future runs of the Tevatron with an about 20-fold increase in statistics promise a measurement of the top mass with an accuracy of up to $\sim$ 3 GeV [98]; in the lepton plus jets channel the error is dominated by the systematics while in the di-lepton channels the limiting factor is still the statistics.

Several studies of the accuracy which can be expected with the LHC experiments have been performed in the past [99]. It is interesting to see whether one can use the large statistics available after a few years of high-luminosity running to push the precision further. In particular, it is interesting to study the ultimate accuracy achievable at a hadronic collider, and the factors that limit this accuracy.

In the following subsections, we begin with general remarks on the top quark mass and a very brief review of the present status of the theoretical understanding of top quark mass measurement in the threshold scan at a future $e^+e^-$ collider. We then present the results of a recent studies of top mass reconstruction at the LHC. The techniques used include the study of the lepton plus jets final states (inclusive, as well as limited to high-$p_T$ top quarks), di-lepton final states (using the di-leptons from the leptonic decay of both $W$'s, as well as samples where the isolated $W$ lepton is paired with a non-isolated

[3]Section coordinators: M. Beneke, M.L. Mangano, I. Efthymiopoulos (ATLAS), P. Grenier (ATLAS), A. Kharchilava (CMS).

lepton from the decay of the companion $b$ hadron). A very promising analysis using the $J/\psi$ from the $b$ hadron decay paired with the lepton from the leptonic decay of the $W$ is discussed at the end. The conclusions of these studies indicate that an accuracy of 2 GeV should be achievable with the statistics available after only 1 year of running at low luminosity. An accuracy of 1 GeV accuracy could be achieved after the high luminosity phase.

### 4.1 General remarks and the top mass measurement in $\mathbf{e^+e^-}$ annihilation

Although one speaks of "the" top quark mass, one should keep in mind that the concept of quark mass is convention-dependent. The top quark pole mass definition is often implicit, but in a confining theory it can be useful to choose another convention. This is true even for top quarks when one discusses mass measurements with an accuracy of order of or below the strong interaction scale. Since different mass conventions can differ by 10 GeV (see Section 2.1), the question arises which mass is actually determined to an accuracy of 1-2 GeV by a particular measurement.

The simple answer is that a particular measurement determines those mass parameters accurately in terms of which uncalculated higher order corrections to the matrix elements of the process are small. This in turn may depend on the accuracy one aims at and the order to which the process has already been calculated. To clarify these statements we briefly discuss the top quark mass measurement at a high energy $e^+e^-$ collider.

"The" top quark mass can be measured in $e^+e^-$ collisions by recontructing top quark decay products in much the same way as at the LHC. In addition, there exists the unique possibility of determining the mass in pair production near threshold. This is considered to be the most accurate method [100] and it appears that an uncertainty of $\delta\overline{m}_t \approx 0.15\,\mathrm{GeV}$ can be achieved *for the top quark $\overline{MS}$ mass* with the presently available theoretical input [101]. This is a factor two improvement compared to the accuracy that could be achieved with the same theoretical input if the cross section were parametrised in terms of the top quark pole mass. The fundamental reason for this difference is the fact that the concept of a quark pole mass is intriniscally ambiguous by an amount of order $\Lambda_{\mathrm{QCD}}$ [102] and this conclusion remains valid even if the quark decays on average before hadronisation [103]. In the context of perturbation theory this ambiguity translates into sizeable higher order corrections to the matrix elements of a given process renormalized in the pole mass scheme. This makes it preferable to choose another mass convention if large corrections disappear in this way as is the case for the total cross section in $e^+e^-$ annihilation, because the total cross section is less affected by non-perturbative effects than the pole mass itself. Note, however, that despite this preference the position of the threshold is closer to twice the pole mass than twice the $\overline{\mathrm{MS}}$ mass, hence a leading order calculation determines the pole mass more naturally. It is possible to introduce intermediate mass renormalizations that are better defined than the pole mass and yet adequate to physical processes in which top quarks are close to mass shell [101, 104]. The conclusion that the top quark pole mass is disfavoured is based on the existence of such mass redefinitions and the existence of accurate theoretical calculations.

The situation with mass determinations at the LHC appears much more complicated, since the mass reconstruction is to a large extent an experimental procedure based on leading order theoretical calculations, which are not sensitive to mass renormalization at all. Furthermore the concept of invariant mass of a top quark decay system is prone to "large" non-perturbative corrections of relative order $\Lambda_{\mathrm{QCD}}/m_t$, because the loss or gain of a soft particle changes the invariant mass squared by an amount of order $m_t\Lambda_{\mathrm{QCD}}$. The parametric magnitude of non-perturbative corrections is of the same order of magnitude as for the top quark pole mass itself and cannot be decreased by choosing another mass renormalization prescription. For this reason, top mass measurements based on reconstructing $m_t$ from the invariant mass of the decay products of a single top quark should be considered as measurements of the top quark pole mass. From the remarks above it follows that there is a limitation of principle on the accuracy of such measurements. However, under LHC conditions the experimental systematic uncertainty discussed later in this section is the limiting factor in practice. A potential exception is the measure-

Table 6: Efficiencies (in percent) for the inclusive $t\bar{t}$ single lepton plus jets signal and for background processes, as a function of the selection cuts applied. No branching ratios are included in the numbers. The last column gives the equivalent number of events for an integrated luminosity of 10 fb$^{-1}$, and the signal-to-background ratio.

| Process | $p_T^\ell > 20$ GeV $E_T^{miss} > 20$ GeV | as before, plus $N_{jet} \geq 4$ | as before, plus $N_{b-jet} \geq 2$ | events, per 10 fb$^{-1}$ |
|---|---|---|---|---|
| $t\bar{t}$ signal | 64.7 | 21.2 | 5.0 | 126000 |
| $W + jets$ | 47.9 | 0.1 | 0.002 | 1658 |
| $Z + jets$ | 15.0 | 0.05 | 0.002 | 232 |
| $WW$ | 53.6 | 0.5 | 0.006 | 10 |
| $WZ$ | 53.8 | 0.5 | 0.02 | 8 |
| $ZZ$ | 2.8 | 0.04 | 0.008 | 14 |
| Total background | | | | 1922 |
| $S/B$ | | | | 65 |

ment of $m_t$ in the decay mode $\ell J/\psi X$ discussed at the end of this section, since the systematic error is estimated to be below 1 GeV and since the systematic error is to a large extent theoretical. It would be interesting to investigate non-perturbative power corrections and principle obstructions to an accurate mass measurement for this process. This analysis has however not yet been carried out in any detail, comparable to the threshold scan in $e^+e^-$ annihilation.

### 4.2 $\mathbf{m_t}$ in the lepton plus jets channel. Inclusive sample

The inclusive lepton plus jets channel provides a large and clean sample of top quarks for mass reconstruction. Considering only electrons and muons, the branching ratio of this channel is 29.6%. Therefore, one can expect more than 2 millions events for one year of running at low luminosity. ATLAS performed an analysis in that channel using events generated using PYTHIA [52] and the ATLAS detector fast simulation package ATLFAST [105]. The top mass is determined using the hadronic part of the decay, as the invariant mass of the three jets coming from the same top: $m_t$= $m_{jjb}$. The leptonic top decay is used to tag the event with the presence of a high $p_T$ lepton and large $E_T^{miss}$ . For the background processes, the HERWIG [51, 89] generator was used for the background process $Wb\bar{b}$.

The following background processes have been considered: $b\bar{b}$, $W + jets$ with $W \to \ell\nu$, $Z + jets$ with $Z \to \ell^+\ell^-$, $WW$ with one $W \to \ell\nu$ and the other $W \to q\bar{q}$, $WZ$ with $W \to \ell\nu$ and $Z \to q\bar{q}$, $ZZ$ with one $Z \to \ell^+\ell^-$ and $Z \to q\bar{q}$, and $Wb\bar{b}$ with $W \to \ell\nu$. Events are selected by requiring an isolated lepton with $p_T >$ 20 GeV and $|\eta| < 2.5$, $E_T^{miss} > 20$ GeV, and four jets with $p_T >$ 40 GeV and $|\eta| < 2.5$, of which two of them were required to be tagged as $b$-jets. Jets were reconstructed using a fixed cone algorithm with $\Delta R$= 0.4. Although at production level the signal over background is very unfavourable, after the selection cuts and for an integrated luminosity of 10 fb$^{-1}$, 126000 signal events and 1922 background events were kept, yielding a value of $S/B = 65$ (see Table 6).

The reconstruction of the decay $W \to jj$ is first performed. The invariant mass $m_{jj}$ of all the combinations of jets (with $p_T >$ 40 GeV and $|\eta| < 2.5$) that were not tagged as $b$-jets is computed and the jet pair with an invariant mass closest to $m_W$ is selected as the $W$ candidate. Fig. 14 represents the invariant mass distribution of the selected jet pairs. The reconstructed $W$ mass is consistent with the generated value, the mass resolution being 7.8 GeV. Within a window of $\pm$20 GeV around the $W$ mass, the purity (P) and the overall efficiency (E) of the $W$ reconstruction are respectively P=67% and E=1.7%. Additional pair association criteria, such as requiring the leading jet to be part of the combination, did not improve significantly the purity and have not been considered further in the analysis. $W$ candidates, retained if $|m_{jj} - M_W| < 20$ GeV, have then to be associated with one $b$-tagged jet to reconstruct the decay $t \to Wb$. To reconstruct the right combination, some association criteria have been tried, such as choosing the $b$-jet furthest from the isolated lepton, the $b$-jet closest to the reconstructed $W$, and choosing

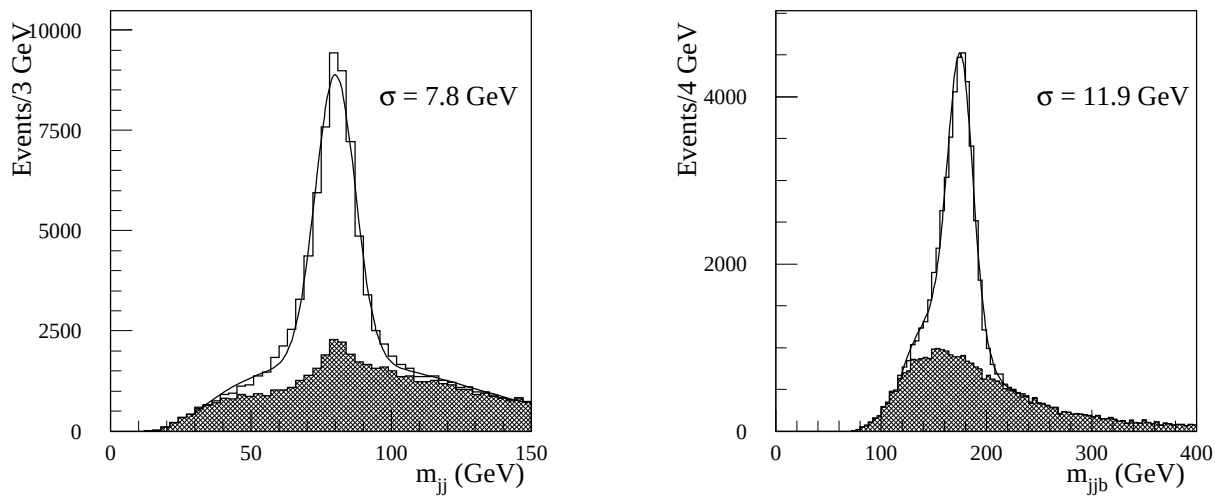


Fig. 14: Left: invariant mass distribution of the selected $jj$ pairs. Right: invariant mass distribution of the selected $jjb$ combination. Both distributions are normalised to an integrated luminosity of 10fb$^{-1}$. The shaded area shows the combinatorial background.

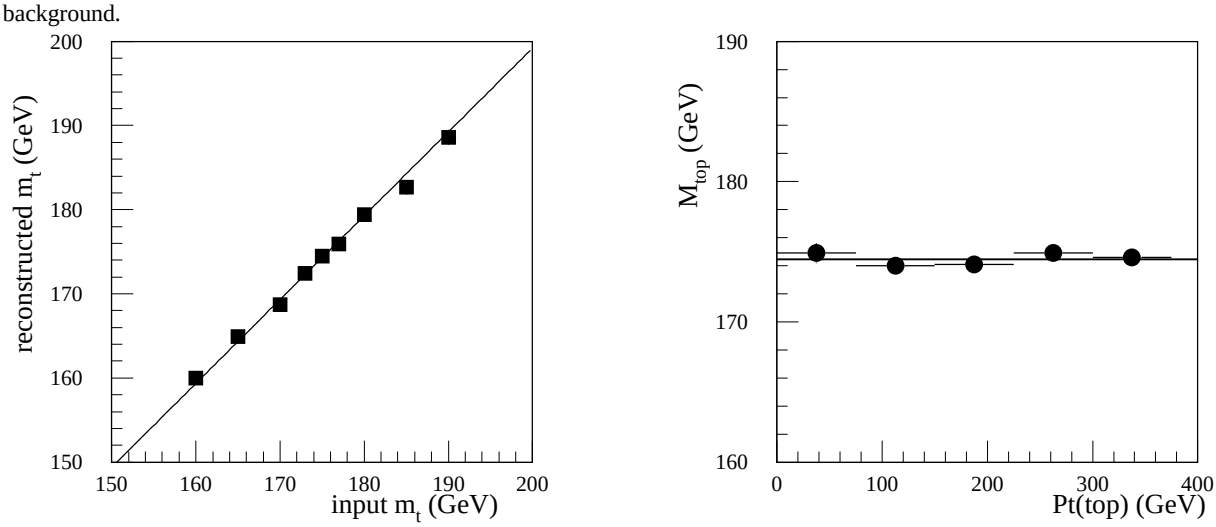


Fig. 15: Left: dependence of the reconstructed top mass on the generated value. Right: dependence of the reconstructed top mass on the transverse momentum($p_T$) of the reconstructed top.

the $jjb$ combination having the highest $p_T$ for the reconstructed top. These various methods gave similar results. Fig. 14 presents the invariant mass distribution of the reconstructed top when the $jjb$ combination having the highest $p_T$ has been used as association criteria. No $M_W$ constraint is applied for the light quark jets. For an integrated luminosity of 10fb$^{-1}$, the total number of reconstructed top is 32000 events, of which 30000 are within a window of $\pm 35$ GeV around the generated top mass $m_t$= 175 GeV. The total number of combinatorial events is 34000, of which 14000 are within the mass window. The number of background events coming from other processes is negligible. The $m_{jjb}$ distribution fitted by a Gaussian plus a third order polynomial yields a top mass consistent with the generated value of 175 GeV and a top mass resolution of 11.9 GeV. The resulting statistical uncertainty for an integrated luminosity of 10fb$^{-1}$ is $\delta m_t$= 0.070 GeV.

The dependence of the top reconstruction algorithm on the top mass has been checked using several samples of $t\bar{t}$ events generated with different values of $m_t$ ranging from 160 to 190 GeV. The results, shown in Fig. 15, demonstrate a linear dependence of the reconstructed top mass on the generated value: the data points are fitted to a linear function with $\chi^2/\mathrm{ndf} = 6.7/8$. The stability of the mass value as a function of the transverse momentum of the reconstructed top ($p_T$(top)) was also checked. As shown in Fig. 15, no significant $p_T$(top) dependence is observed: the data points are fitted to a constant with $\chi^2/\mathrm{ndf} = 6.25/5$. For more details of this analysis, see [106].

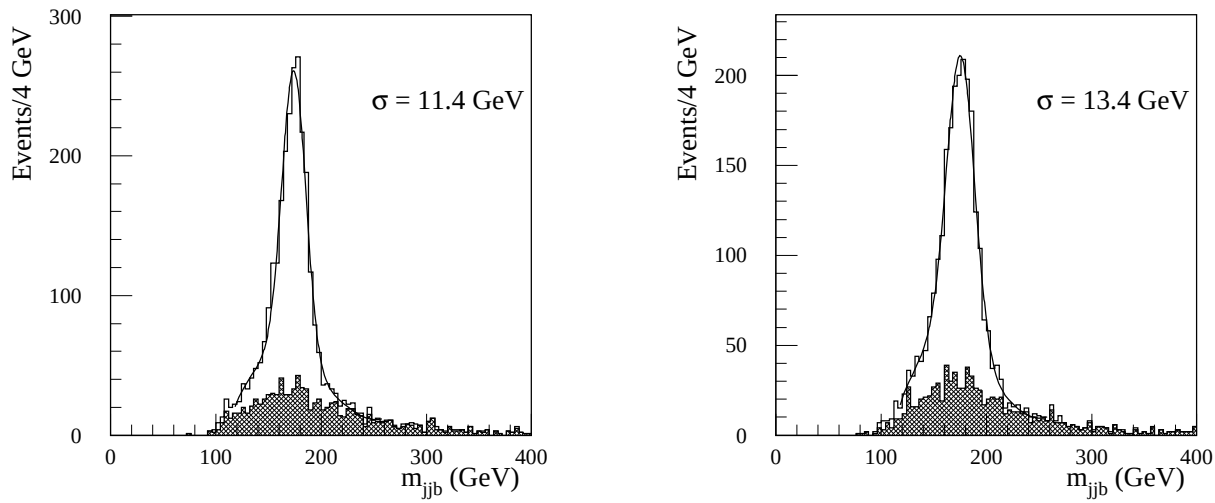


Fig. 16: Invariant $jjb$ mass distributions. Left: from fast simulation. Right: from full simulation.

The results presented above, obtained with a fast simulation package, have been cross-checked with 30000 events passed through the ATLAS GEANT-based full simulation package [107]. In full simulation, in order to save computing time, events have been generated under restrictive conditions at the generator level. The comparison is done by using the same generated events which have been passed through both the fast and full simulation packages. The results, in terms of purity, efficiency and mass resolutions show a reasonable agreement between fast and full simulation. In addition, as it is shown in Fig. 16, the shape and amount of the combinatorial background for the $m_{jjb}$ distributions are in good agreement between the two types of simulations.

It has to be noted that for this analysis as well as for the other top mass reconstruction studies performed within ATLAS, the jets were calibrated using the ratio $p_T$(parton)/$p_T$(jet) obtained from Monte Carlo samples of di-jet events or $H \rightarrow b\bar{b}$ with $m_H = 100$ GeV. In that aspect this calibration does not include all possible detector effects and corrections. More details can be found in Chapter 20 of [30] and in Appendix A.

### 4.3 $\mathbf{m_t}$ in the lepton plus jets channel. High $\mathbf{p_T}$ sample

An interesting possibility at the LHC, thanks to the large $t\bar{t}$ production rate, is the use of special sub-samples, such as events where the top and anti-top quarks have high $p_T$. In this case, they are produced back-to-back in the lab-frame, and the daughters from the two top decays will appear in distinct "hemispheres" of the detector. This topology would greatly reduce the combinatorial background as well as the backgrounds from other processes. Furthermore, the higher average energy of the jets to be reconstructed should reduce the sensitivity to systematic effects due to the jet energy calibration and to effects of gluon radiation. However, in this case a competing effect appears which can limit the resulting precision: as the top $p_T$ increases, the jet overlapping probability increases as well, which again affects the jet calibration. ATLAS performed a preliminary study of this possibility using two different reconstruction methods:

- in the first one an analysis similar to the inclusive case is done, with $m_t$ being reconstructed from the three jets in the one hemisphere ($m_t$=$m_{jjb}$);
- in the second one, $m_t$ is reconstructed summing up the energies in the calorimeter towers in a large cone around the top direction.

In the following paragraphs, highlights of these analyses are discussed.

#### *4.31 Jet Analysis*

High $p_T$ $t\bar{t}$ events were generated using PYTHIA 5.7 [52] with a $p_T$ cut on the hard scattering process above 200 GeV. The expected cross-section in this case is about 120 pb, or about 14.5% of the total

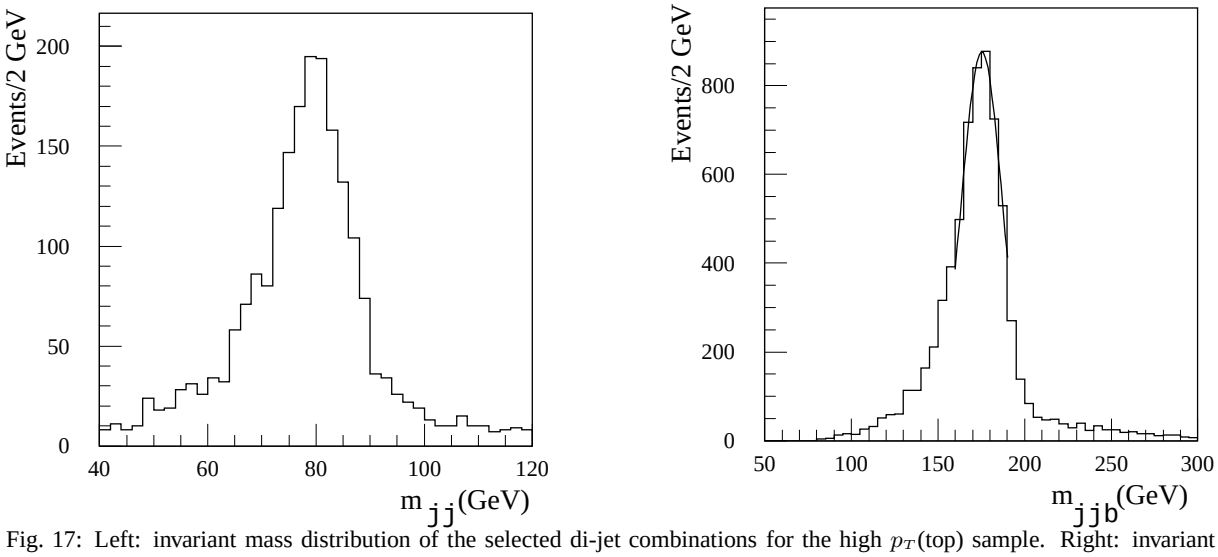


Fig. 17: Left: invariant mass distribution of the selected di-jet combinations for the high $p_T$(top) sample. Right: invariant mass distribution of the accepted combinations for the high $p_T$(top) sample. Both distributions are normalised to an integrated luminosity of 10fb$^{-1}$.

$t\bar{t}$ production cross-section. The selection cuts required the presence of an isolated lepton with $p_T>$ 30 GeV and $|\eta|< 2.5$, and $E_T^{miss} > 30$ GeV. The total transverse energy of the event was required to be greater than 450 GeV. Jets were reconstructed using a cone algorithm with radius $\Delta R$=0.4. The plane perpendicular to the direction of the isolated lepton was used to divide the detector into two hemispheres. Considering only jets with $p_T> 40$ GeV and $|\eta|< 2.5$, the cuts required one $b$-tagged jet in the same hemisphere as the lepton, and three jets, one of which was $b$-tagged, in the opposite hemisphere. Di-jet candidates for the $W \to jj$ decay were selected among the non-$b$-tagged jets in the hemisphere opposite to the lepton. The resultant $m_{jj}$ invariant mass distribution is shown in Fig. 17 (left). Fitting the six bins around the peak of the mass distribution with a Gaussian, yielded a $W$ mass consistent with the generated value, and a $m_{jj}$ resolution of 7 GeV, in good agreement with that obtained for the inclusive sample. Di-jets with 40 GeV$<m_{jj}<$120 GeV were then combined with the $b$-tagged jet from the hemisphere opposite to the lepton to form $t \to jjb$ candidates. Finally, the high $p_T$(top) requirement was imposed by requiring $p_T(jjb)> 250$ GeV. With these cuts, the overall signal efficiency was 1.7%, and the background from sources other than $t\bar{t}$ was reduced to a negligible level. The invariant mass distribution of the accepted $jjb$ combinations is shown in Fig. 17 (right). Fitting the six bins around the peak of the mass distribution with a Gaussian, yielded a top mass consistent with the generated value of 175 GeV, and a $m_{jjb}$ mass resolution of 11.8 GeV. For an integrated luminosity of 10 fb$^{-1}$, a sample of 6300 events would be collected in ATLAS, leading to a statistical error of $\delta m_t$(stat.) = $\pm$0.25 GeV, which remains well below the systematic uncertainty. As in the case of the inclusive sample, no strong $p_T$ dependence was observed and the reconstructed mass depends linearly on the Monte Carlo input value.

### *4.32 Using a large calorimeter cluster*

For sufficiently high $p_T$(top) values, the jets from the top decay are close to each other with a large possibility of overlap. In such a case it might be possible to reconstruct the top mass by collecting all the energy deposited in the calorimeter in a large cone around the top quark direction. Such a technique has the potential to reduce the systematic errors, since it is less sensitive to the calibration of jets and to the intrinsic complexities of effects due to leakage outside the smaller cones, energy sharing between jets, etc. Some results from a preliminary investigation of the potential of this technique are discussed here. More details of the analysis can be found in [30, 108].

Similar event selection criteria as in the previous case were used: an isolated lepton with $p_T>$ 20 GeV and $|\eta|< 2.5$, $E_T^{miss} > 20$ GeV, one $b$-tagged jet (with $\Delta R$=0.4 and $p_T> 20$ GeV) in the lepton hemisphere, and at least 3 jets in the hemisphere opposite to the lepton ($\Delta R$=0.2, $p_T> 20$ GeV) with

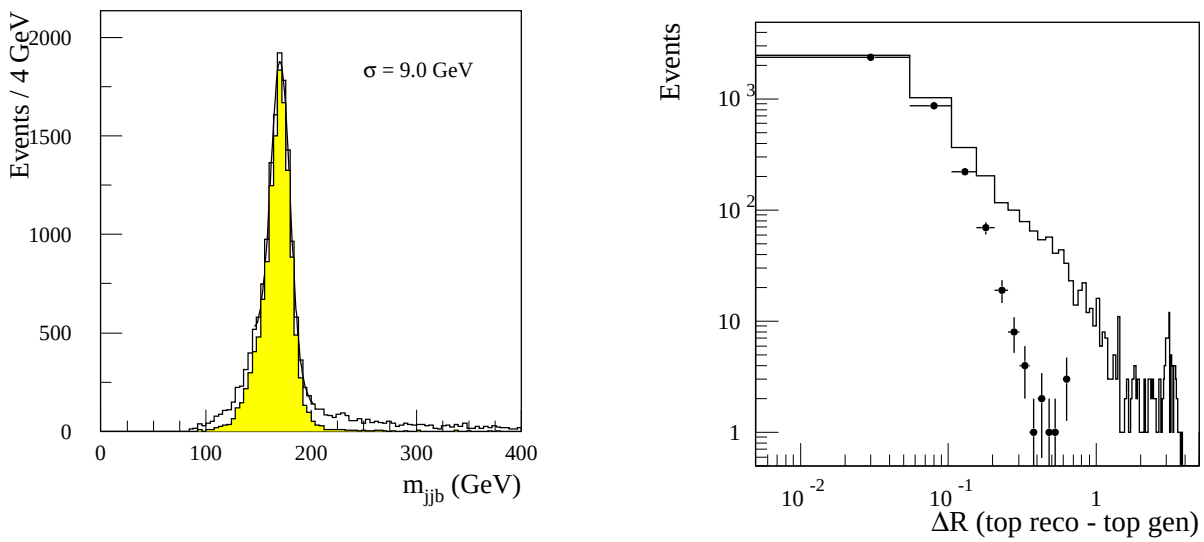


Fig. 18: Left: invariant mass distribution of the selected $jjb$ combination, using $\Delta R$= 0.2 cones for the high $p_T$(top) sample, normalised to an integrated luminosity of 10fb$^{-1}$. The shaded area corresponds to the combinations with the correct jet-parton assignments. Right: distance $\Delta R$ between the reconstructed and the parton level direction of the top quark. The dots correspond to the correct $jjb$ combinations.

one of them $b$-tagged. For the accepted events, the two highest $p_T$ non-$b$-tagged jets were combined with the highest $p_T$ $b$-jet candidate in the hemisphere opposite to the lepton to form candidates for the $jjb$ hadronic top decay. The selected $jjb$ combination was required to have $p_T > 150$ GeV and $|\eta| < 2.5$. With these selection criteria, about 13000 events would be expected in the mass window from 145 to 200 GeV, with a purity of 90%, for an integrated luminosity of 10fb$^{-1}$. The reconstructed invariant mass of the $jjb$ combination is shown in Fig. 18 (left). The direction of the top quark was then determined from the jet momenta. Figure 18 (right) shows the distance $\Delta R$ in $(\eta, \phi)$ space between the reconstructed and the true top direction at the parton level, demonstrating good agreement.

A large cone of radius $\Delta R$ was then drawn around the top quark direction, and the top mass was determined by adding the energies of all calorimeter "towers" within the cone. A calorimeter tower has a size of $\delta\eta \times \delta\phi$= 0.1×0.1, combining the information of both the EM and hadronic calorimeters. The invariant mass spectrum is shown in Fig. 19 (left) for a cone size $\Delta R$= 1.3, and exhibits a clean peak at the top quark mass. The fitted value of the reconstructed top mass is shown in Fig. 19 (right), where it displays a strong dependence on the cone size. If initial (ISR) and final (FSR) state radiation in PYTHIA are turned off, the fitted mass remains constant (to within 2%), independently of cone size.

The large dependence of the reconstructed top mass on the cone size can be attributed to the underlying event (UE) contribution. A method was developed to evaluate and subtract the underlying event contribution using the calorimeter towers not associated with the products of the top quark decay. The UE contribution was calculated as the average $E_T$ deposited per calorimeter tower, averaged over those towers which were far away from the reconstructed jets of the event. As expected, the average $E_T$ per calorimeter tower increases as more activity is added, especially in the case of ISR. However, only a rather small dependence is observed on the radius $\Delta R$ used to isolate the towers associated with the hard scattering process. The resulting value of the reconstructed mass ($m_{cone}$), with and without UE subtraction, is also shown in Fig. 19 (right) as a function of the cone radius. As can be seen, after the UE subtraction, the reconstructed top mass is independent of the cone size used. As a cross-check, the mean $E_T$ per cell subtracted was varied by $\pm$10% and the top mass recalculated in each case. As shown superimposed on Fig. 19 (right), these "miscalibrations" lead to a re-emergence of a dependence of $m_t$ on the cone size. While the prescription for the UE subtraction does lead to a top mass which is independent of the cone size, it should be noted that the reconstructed mass is about 15 GeV (or 8.6%) below the nominal value, $m_t$= 175 GeV, implying that a rather large correction is needed.

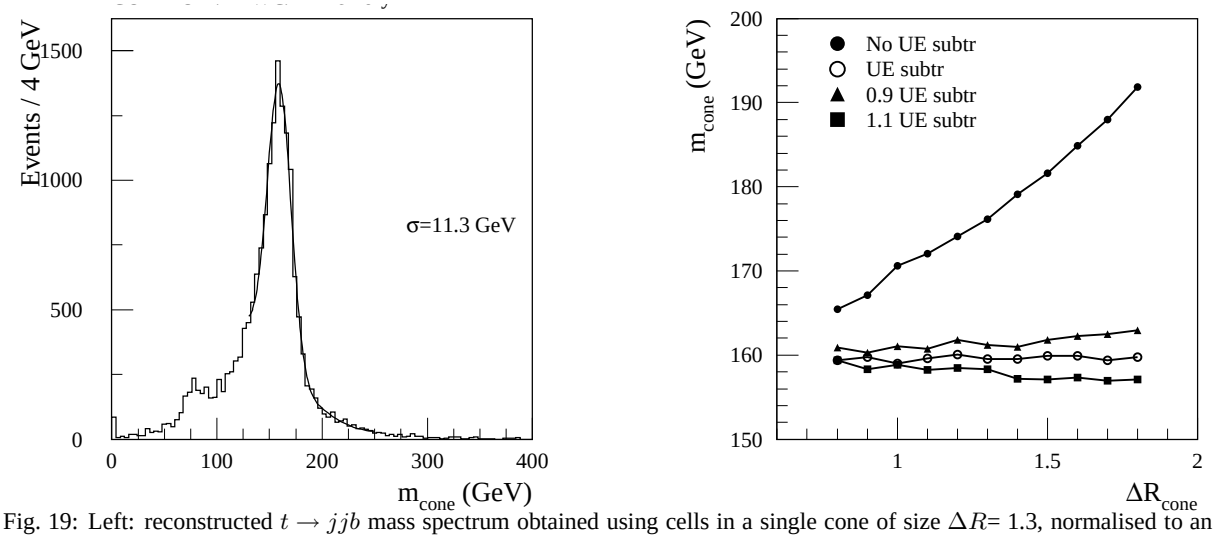


Fig. 19: Left: reconstructed $t \to jjb$ mass spectrum obtained using cells in a single cone of size $\Delta R$= 1.3, normalised to an integrated luminosity of 10 fb$^{-1}$. Right: the fitted top mass using cells in a single cone, before and after the underlying event (UE) subtraction and as a function of the cone size.

To investigate if this correction can be extracted from the data without relying on Monte Carlo simulations, the same procedure was applied to a sample of $W+$ jet events generated with a range of $p_T$ comparable to that of the top sample. The $W$ was forced to decay hadronically into jets. The UE contribution was estimated with the same algorithm as described above. The results agreed within 1% with the values determined for the high $p_T$(top) sample. As in the case of the top events, the reconstructed $W$ mass after UE subtraction is independent of the cone size. The average value of $m_{jj}$ after the UE subtraction is about 8.5 GeV (or 10.6%) below the nominal value of $m_W$. The fractional error on $m_{jj}$, as measured with the $W$+jet sample, was used as a correction factor to $m_{cone}$ in the high $p_T$(top) sample. For a cone of radius $\Delta R$= 1.3, the top mass after UE subtraction increases from 159.9 GeV to 176.0 GeV after rescaling. The rescaled values of $m_{cone}$ are about 1% higher than the generated top mass. This over-correction of $m_t$ using the value of $m_W$ measured with the same method, is mainly due to ISR contributions. If ISR is switched off, the rescaling procedure works to better than 1%.

### 4.4 Systematic uncertainties on the measurement of $\mathrm{m_t}$ in the single lepton plus jets channel

For the analyses presented above within ATLAS, a number of sources of systematic error have been studied using samples of events generated with PYTHIA and simulated mainly with the fast detector package ATLFAST, but also using a relatively large number of fully simulated events in order to cross-check some of the results. The results of these studies are summarised in Fig. 20 and discussed below.

*Jet energy scale:* The measurement of $m_t$ via reconstruction of $t \to jjb$ relies on a precise knowledge of the energy calibration for both light quark jets and $b$-jets. The jet energy scale depends on a variety of detector and physics effects, including non-linearities in the calorimeter response, energy lost outside the jet cone (due, for example, to energy swept away by the magnetic field or to gluon radiation at large angles with respect to the original parton), energy losses due to detector effects (cracks, leakage, etc.), and "noise" due to the underlying event. Preliminary studies done in ATLAS indicate that a jet energy scale calibration at the level of 1% for both light quark and $b$-jets would be feasible at the LHC (see discussion in the Appendix A). In the case of the $m_t$ reconstructed from the invariant mass of the three jets ($m_{jjb}$) the $b$-jet energy scale enters directly in the measurement and therefore it must be calibrated from other sources, while the energy of the two light quark jets can be calibrated event-by-event using the $W$ mass constraint. This would work quite well at least for the inclusive sample, where the jets are well separated. In the high $p_T$ case, energy sharing algorithms and corrections for the two jets are needed, and therefore in order to be conservative we assume in the following that no such an event-by-event correction can be made. To estimate the effect of an absolute jet energy scale uncertainty,

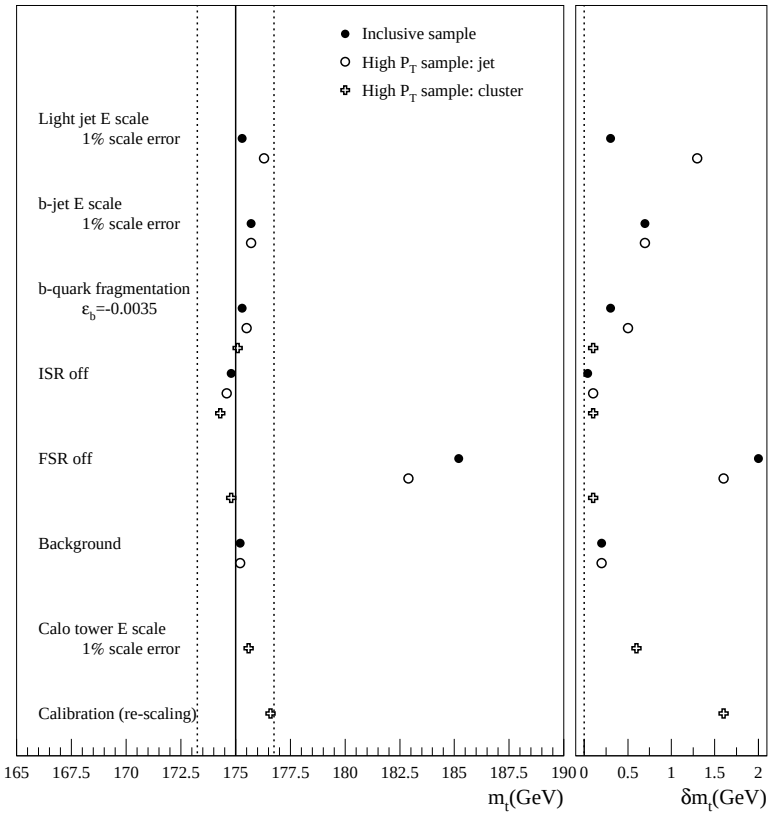


Fig. 20: Summary of systematic errors in the $m_t$ measurement. Left: the observed mass shifts for different effects studied. The dashed lines indicates a 1% mass window. Right: the quoted error in the $m_t$ measurement.

different "miscalibration" coefficients were applied to the measured jet energies. A linear dependence was observed.

*$b$-quark fragmentation:* The fraction of the original $b$-quark momentum which will appear as visible energy in the reconstruction cone of the corresponding $b$-jet depends on the fragmentation function of the $b$-quark. This function is usually parametrised in PYTHIA in terms of one variable, $\epsilon_b$, using the Peterson fragmentation function [109]. To estimate the systematic error in $m_t$, the "default" value for $\epsilon_b$ (=-0.006) was varied within its experimental uncertainty (0.0025) [110, 19] and the difference in the reconstructed $m_t$ was taken as the systematic error $\delta m_t$.

*Initial and final state radiation:* The presence of ISR or FSR can impact the measurement of $m_t$. To estimate the systematic error due to these, data samples were generated where ISR or FSR in the PYTHIA generator were switched off. In the case of FSR, a large mass shift was observed for a jet cone of $\Delta R$=0.4. This is reduced as expected when a larger cone is used. Clearly this case is rather pessimistic since the knowledge in both ISR and FSR is typically at the level of 10%. Therefore as a conservative estimate of the resultant systematic errors in $m_t$, 20% of the mass shifts were used.

An alternative approach uses the measured jet multiplicity to search, event-by-event, for the presence of hard gluon radiation. Following the convention for this approach adopted at the Tevatron [5, 6], the mass shift would be defined not by comparing events with radiation switched on and events with radiation switched off, but by the difference, $\Delta m_t$, between the value of $m_t$ determined from events with exactly four jets and that determined from events with more than four jets. The systematic error due to effects of initial and final radiation would then be considered as $\delta m_t$= $\Delta m_t/\sqrt{12}$. Such a calculation would yield systematic errors of approximately 0.4-1.1 GeV, smaller than the more conservative approach adopted here.

*Background:* Uncertainties in the size and shape of the background, which is dominated by "wrong combinations" in $t\bar{t}$ events, can affect the top mass reconstruction. The resultant systematic uncertainty

on $m_t$ was estimated by varying the assumptions on the background shape in the fitting procedure. Fits of the $m_{jjb}$ distribution were performed assuming a Gaussian shape for the signal and either a polynomial or a threshold function for the background. Varying the background function resulted in a systematic error on $m_t$ of 0.2 GeV. The structure of the UE can affect the top mass reconstruction. However, as discussed above, it is possible to estimate and correct for this effect using data. Given the large statistics available at the LHC, it is assumed that the residual uncertainty from the underlying event will be small compared to the other errors (note that the UE denotes here a minimum bias event, since the impact of ISR has already been accounted for).

For the particular case of the $m_t$ reconstructed using a large calorimeter cluster, similar procedures were adopted to estimate the the systematic errors. It is important to notice that, as expected, the use of a large cone substantially reduces the effects of FSR and $b$-quark fragmentation, each of which gives rise to a systematic error of 0.1 GeV. The uncertainty arising from ISR, which can affect the determination of the UE subtraction, is about 0.1 GeV as well. However, the main uncertainty in this technique comes from the calibration procedure. The calibration with the $W+$ jet sample produces a value of $m_t$ which is about 1% above the generated value. Furthermore, the $W \to jj$ events would suffer from background from QCD multi-jet events. On-going studies suggest that one could calibrate using $W \to jj$ decays from the high $p_T$(top) events themselves, selecting those events in which the $b$-tagged jet is far away from the other two jets of the $W$ decay and then reconstructing the $W \to jj$ decay using a single cone of size $\Delta R$= 0.8. Further study is required to reliably estimate the potential of this calibration procedure, and therefore a conservative systematic uncertainty of 1% is assigned to it.

### 4.5 $\mathbf{m_t}$ in the di-lepton channel

Di-Lepton events can provide a measurement of the top quark mass complementary to that obtained from the single lepton plus jets mode. The signature of a di-lepton event consists of two isolated high $p_T$ leptons, high $E_T^{miss}$ due to the neutrinos, and two jets from the $b$-quarks. The measurement of $m_t$ using di-lepton events is not a direct measurement as in the previous case but it relies on the relation between the kinematical distributions of the top decay products and $m_t$, and on how they can be reproduced by the Monte Carlo simulation. About 400000 di-lepton $t\bar{t}$ events are expected to be produced in a data sample corresponding to an integrated luminosity of 10 fb$^{-1}$. Backgrounds arise from Drell-Yan processes associated with jets, $Z \to \tau\tau$ associated with jets, $WW+$ jets and $b\bar{b}$ production.

Of the many possible kinematic variables which could be studied, ATLAS performed a preliminary study using: the mass $m_{\ell b}$ of the lepton+$b$-jet system, the energy of the two highest $E_T$ jets, and the mass $m_{\ell\ell}$ of the di-lepton system formed with both leptons originating from the same top decay (i.e. $t \to \ell\nu b$ followed by $b \to \ell\nu c$). The event selection criteria required two opposite-sign leptons within $|\eta|< 2.5$, with $p_T>$ 35 and 25 GeV respectively, and with $E_T^{miss} > 40$ GeV. Two jets with $p_T > 25$ GeV were required in addition. After the selection cuts, 80000 signal events survived, with $S/B$ around 10.

#### *4.51 Top mass measurement using $m_{\ell b}$*

In this analysis, the value of $m_t$ was estimated using the expression:

$$m_t{}^2 = M_W^2 + 2\langle m_{\ell b}^2\rangle/[1 - \langle\cos\theta_{\ell b}\rangle] \tag{11}$$

Here, $\langle m_{\ell b}^2\rangle$ is the squared mean invariant mass of the lepton and $b$-jet from the same top decay. The mean value of $\langle\cos\theta_{\ell b}\rangle$, the angle between the lepton and the $b$-jet in the $W$ rest frame, can be regarded as an input parameter to be taken from Monte Carlo. To obtain a very clean sample, the two highest $p_T$ jets were required to be tagged as $b$-jets, leaving a total of about 15200 signal events per 10 fb$^{-1}$. One cannot determine, in general, which lepton should be paired with which $b$-jet. The pairing which gave the smaller value of $\langle m_{\ell b}^2\rangle$ was chosen, and checking the parton-level information showed that this criterion selected the correct pairing in 85% of the cases, for a generated top mass of 175 GeV. The mean

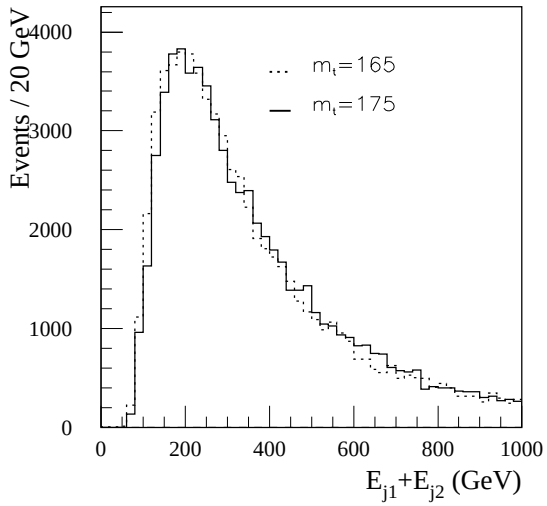


Fig. 21: Template distributions of the total energy of the two leading jets in $t\bar{t}$ events for top quark masses of 165 and 175 GeV. The two distributions are normalised to the same area.

value $\langle m^2_{\ell b}\rangle$ was measured for samples generated with different input top masses $m$, and then $m_t$ was calculated from the expression above. For an integrated luminosity of 10 fb$^{-1}$, the expected statistical uncertainty on $m_t$ using this method is $\pm 0.9$ GeV. Major sources of systematics include uncertainty on the $b$-quark fragmentation function, which produces a systematic error on $m_t$ of 0.7 GeV if defined as described in Section 4.4. Systematic errors due to the effects of FSR and ISR together are about 1 GeV, while those due to varying the jet energy scale by 1% are 0.6 GeV. Further studies are required to estimate the uncertainties due to the reliance upon the Monte Carlo modelling of the $t\bar{t}$ kinematics.

### *4.52 Top mass measurement using the energy of the two leading jets*

Increased sensitivity could be obtained with a technique which utilises not only the mean, but also the shape of the kinematic distribution. As an example, a study has been made of the sensitivity to $m_t$ obtained by comparing to "template" distributions the energy of the two highest-$E_T$ jets. The template distributions were made by generating PYTHIA samples of $t\bar{t}$ events with different values of $m_t$ in the range 160-190 GeV, in steps of 5 GeV. Figure 21 shows, as an example, the templates obtained for $m_t = 165$ GeV and 175 GeV. For each possible top mass value $m$, a $\chi^2(m)$ was obtained by comparing the kinematical distribution of the simulated data with the templates of mass $m$. The best value for the mass was the value which, for the "data" set, generated with $m_t$= 175 GeV, gave the minimum $\chi^2$. For an integrated luminosity of 10 fb$^{-1}$, the expected statistical sensitivity on $m_t$ corresponds to about $\pm$0.4 GeV. Varying the calorimeter jet energy scale by 1% produced a systematic error on $m_t$ of 1.5 GeV. Other sources of systematic error result from the dependence of the method on the Monte Carlo modelling of the $t\bar{t}$ kinematics, and require further study. As an example, changing the choice of the structure functions used in the Monte Carlo simulation (for example, from CTEQ2L to CTEQ2M or EHQL1) led to differences in the top mass of $\pm$0.7 GeV.

### *4.53 Top mass measurement using $m_{ll}$ in tri-lepton events*

The invariant mass distribution of the two leptons from the same top quark decay (*i.e.* $t \to \ell\nu b$ followed by $b \to \ell\nu c$) is quite sensitive to $m_t$. It has been shown that the mass distribution of lepton pairs from the same top quark decay is much less sensitive to the top quark transverse momentum distribution than that of lepton pairs from different top quarks [99]. Signal events are expected to contain two leptons from the decay of the $W$ bosons produced directly in the top and anti-top quark decays, and one lepton from the $b$-quark decay. In addition to the cuts described above, one non-isolated muon with $p_T >$ 15 GeV was required. For an integrated luminosity of 10 fb$^{-1}$, the expected signal would be about 7250 events,

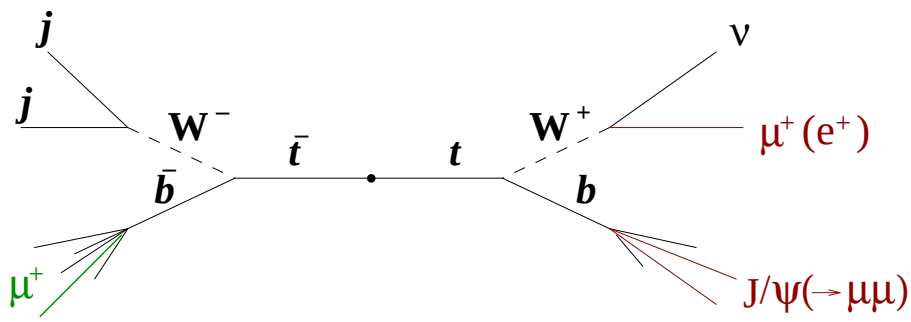


Fig. 22: Schematics of the top decay to leptonic final states with $J/\psi$.

yielding a statistical uncertainty on the measurement of $m_t$ of approximately $\pm 1$ GeV. This technique is insensitive to the jet energy scale. The dominant uncertainties arise from effects of ISR and FSR and from the $b$-quark fragmentation, which sum up to about 1.5 GeV.

### 4.6 $\mathbf{m_t}$ from $\mathbf{t \to l + J/\psi + X}$ decays

An interesting proposal [111] by CMS, explored in detail during the workshop [112], is to take advantage of the large top production rates and exploit the correlation between the top mass and the invariant mass distribution of the system composed of a $J/\psi$ (from the decay of a $b$ hadron) and of the lepton ($\ell = e, \mu$) from the associated $W$ decay (see Fig. 22).

The advantage of using a $J/\psi$ compared to the other studies involving leptons as presented above is twofold: first, the large mass of the $J/\psi$ induces a stronger correlation with the top mass (as will be shown later). Second, the identification of the $J/\psi$ provides a much cleaner signal. In order to uniquely determine the top decay topology one can tag the charge of the $b$ decaying to $J/\psi$ by requiring the other $b$-jet to contain a muon as well. The overall branching ratio is $5.3 \times 10^{-5}$, taking into account the charge conjugate reaction and $W \to e\nu$ decays. In spite of this strong suppression, we stress that these final states are experimentally very clean and can be exploited even at the highest LHC luminosities. Furthermore, one can also explore other ways to associate the $J/\psi$ with the corresponding isolated lepton – for example by measuring the jet charge of identified $b$'s. One should say that all these methods of top mass determination essentially rely on the Monte-Carlo description of its production and decay. Nonetheless the model, to a large extent, can be verified and tuned to the data.

#### *4.61 Analysis*

In the following we assume a $t\bar{t}$ production cross-section of 800 pb for $m_t$ = 175 GeV. Events are simulated with the PYTHIA5.7 [52] or HERWIG 5.9 [51] event generators. Particle momenta are smeared according to parameterisations obtained from detailed simulation of the CMS detector performance. Four-lepton events are selected by requiring an isolated lepton with $p_T$>15 GeV and $|\eta|$<2.4, and three non-isolated, centrally produced muons of $p_T$>4 GeV and $|\eta|$<2.4, with the invariant mass of the two of them being consistent with the $J/\psi$ mass. These cuts significantly reduce the external (non-$t\bar{t}$) background, mainly $Wb\bar{b}$ production,[4] which can be further reduced by employing, in addition, two central jets from another $W$. The resulting kinematical acceptance of the selection criteria is 30%; this rather small value is largely due to soft muons from $J/\psi$ and $b$. In one year high luminosity running of LHC, corresponding to an integrated luminosity of 100 fb$^{-1}$, and assuming trigger plus reconstruction efficiency of 0.8, we expect about $10^5 \times 800 \times 5.3 \cdot 10^{-5} \times 0.3 \times 0.8 = 1000$ events.

An example of the $\ell J/\psi$ mass distribution with the expected background is shown in Fig. 23. The background is internal (from the $t\bar{t}$ production) and is due to the wrong assignment of the $J/\psi$ to the corresponding isolated lepton. These tagging muons of wrong sign are predominantly originating from

[4]PYTHIA results indicate that with the above cuts this source of the background can be kept at a per cent level.

$B^0/\overline{B}^0$ oscillations, $b{\to}c{\to}\mu$ transitions, $W(\to c,\ \tau){\to}\mu$ decays, $\pi$/K decays in flight and amount to $\sim$ 30% of the signal combinations. The shape of the signal $\ell J/\psi$ events (those with the correct sign of the tagging muon) is consistent with a Gaussian distribution over the entire mass interval up to its kinematical limit of $\sim$ 175 GeV. The background shape is approximated by a cubic polynomial. The parameters of this polynomial are determined with "data" made of the wrong combinations of $\ell J/\psi$ with an admixture of signal. In such a way the shape of the background is determined more precisely and in situ. Thus, when the signal distribution is fitted, only the background normalisation factor is left as a free parameter along with the three parameters of a Gaussian. The result of the fit is shown in Fig. 23. We point out that this procedure allows to absorb also the remaining external background (if any) into the background fit function.

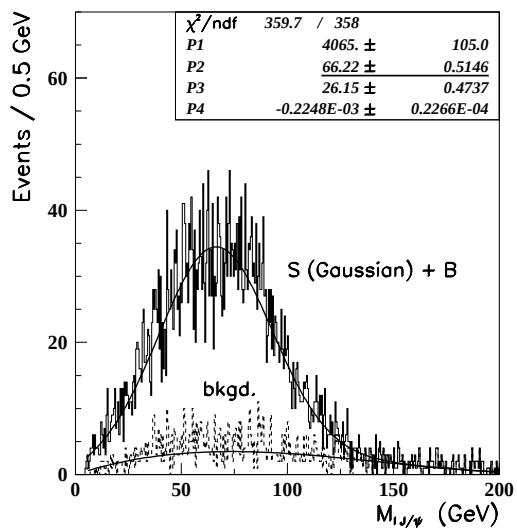


Fig. 23: Example of the $\ell J/\psi$ invariant mass spectrum in four-lepton final states. The number of events corresponds to four years running at LHC high luminosity.

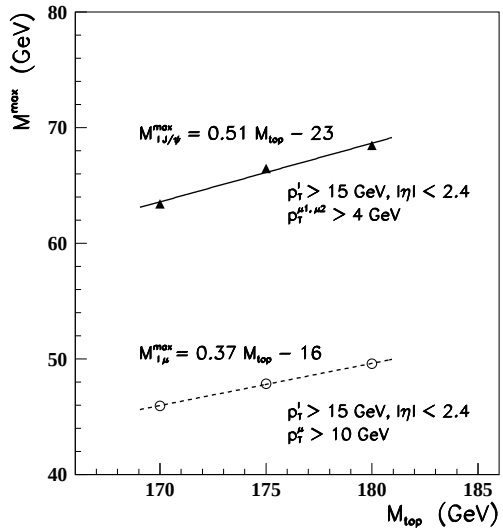


Fig. 24: Correlation between $M^{max}$ and the top quark mass in isolated lepton plus $J/\psi$ (solid line) and isolated lepton plus $\mu$-in-jet (dashed line) final states.

As a measure of the top quark mass we use the mean value (position of the maximum of the distribution) of the Gaussian, $M^{max}_{\ell J/\psi}$. In four years running at LHC with high luminosity the typical errors on this variable, including the uncertainty on the background, are about 0.5 GeV. It is composed of $\lesssim$ 0.5 GeV statistical error and $\lesssim$ 0.15 GeV systematics contribution due to the uncertainty on the measurement of the background shape.[5]

The measurement of the $M^{max}_{\ell J/\psi}$ can then be related to the generated top quark mass. An example of the correlation between the $M^{max}$ and $m_t$ is shown in Fig. 24 along with the parameters of a linear fit. For comparison, we also show the corresponding dependence in a more traditional isolated lepton plus $\mu$-in-jet channel. Not surprisingly, the stronger correlation, and thus a better sensitivity to the top mass, is expected in the $\ell J/\psi$ final states as compared to the isolated lepton plus $\mu$-in-jet channel. This is because, in the former case, we pickup a heavy object (the $J/\psi$) which carries a larger fraction of the $b$-jet momentum. The $M^{max}_{\ell J/\psi}$ measurement error, statistical and systematic, scales as the inverse slope value of the fit, which is a factor of 2 in our case. Hence the statistical error on the top mass in this particular example is $\sim$ 1 GeV.

It is appropriate to comment on the ways to obtain a larger event sample. Encouraging results have been obtained in [113] to reconstruct the $b{\to}J/\psi{\to}e^+e^-$ decays for low luminosity runs. The extension of these studies for a high luminosity environment is very desirable. Another possibility would be to relax the kinematical requirements. The choice of $p_T$ cut on soft muons is not dictated by the

[5]The statistical power of the sample can be further improved by exploiting full spectrum, rather than its Gaussian part.

background considerations but by the trigger rates, and is set here to 4 GeV rather arbitrarily. For example, the di-muon trigger with $\eta$-dependent thresholds which is available in CMS for low luminosity runs [114] allows to significantly increase the kinematical acceptance, practically to the limit determined by muon penetration up to the muon chambers. Therefore, the assessment of the trigger rates at high luminosity with lower $p_T$ thresholds and in multi-lepton events clearly deserves a dedicated study.

An even larger event sample can be obtained in three lepton final states, using instead the jet-charge technique to determine the $t\bar{t}$ decay topology instead of the tagging muon. The jet charge is defined as a $p_T$-weighted charge of particles collected in a cone around the $J/\psi$ direction. Obviously, this kind of analysis requires detailed simulations with full pattern recognition which are under way. However, particle level simulations performed with PYTHIA and with realistic assumptions on track reconstruction efficiency give event samples comparable to the muon-tag performance, with about 10 times less integrated luminosity. In any case, through the LHC lifetime, one can collect enough events so that the overall top mass measurement accuracy would not be hampered by the lack of statistics; it would rather be limited by the systematic uncertainties which are tightly linked with the Monte-Carlo tools in use, as will be argued in the following section.

### *4.62 Systematics*

An essential aspect of the current analysis is to understand limitations which would arise from the Monte-Carlo description of the top production and decay. It is important to realize that the observable used in this study enjoys two properties: it is Lorentz invariant an it does not depend on the detailed structure of the jets, but only on the momentum spectrum of the $b$-hadron and of the $J/\psi$ from its decay.

As a result, were it not for distortions of the $\ell J/\psi$ mass distribution induced by acceptance effects and by the presence of an underlying background, the measurement would be entirely insensitive with respect to changes in the top production dynamics, and in the structure of the underlying event. As a result, typical systematics such as those induced by higher-order corrections to the production process, or by the ISR and by the structure of the minimum bias event, are strongly reduced relative to other measurements of $m_t$. This expectation will be shown to be true in the following of this section.

The main limitations to an accurate extraction of the top mass using this technique are expected to come from: i) the knowledge of the fragmentation function of the $b$ hadrons contained in the $b$-jet and, ii) the size of the non-perturbative corrections to the relation between the top quark mass and the $\ell J/\psi$ mass distribution. The $J/\psi$ spectrum in the decay of the $b$-hadrons will be measured with high accuracy in the next generation of $B$-factory experiments. It should be pointed out, however, that the composition of $b$-hadrons measured at the $\Upsilon(4S)$ and in the top decays will not be the same. In this second case, one expects a non-negligible contribution from baryons and from $B_s$ states. The size of the relevant corrections to the inclusive $J/\psi$ spectrum in top decays is not known, and, although expected to be small, it needs to be studied. Additional effects, such as QED corrections to the $W$ leptonic decay, $W$ polarisation and spin correlation effects can all be controlled and included in the theoretical simulations.

The rest of this section presents the results of a detailed study [112] of the systematics, mostly based on PYTHIA.

*Detector resolution:* Here we have considered only Gaussian smearing of particle momenta and the effect on the $M_{\ell J/\psi}^{max}$ measurement uncertainty is negligible. A possible nonlinearity of the detector response can be well controlled with the huge sample of $J/\psi$, $\Upsilon$ and $Z$ leptonic decays that will be available.

*Background:* The uncertainty would be mainly due to an inaccurate measurement of the background shape and the systematics contribution of $\lesssim 0.15$ GeV quoted in previous section would scale down with increasing statistics. For example, already with $\sim 10^4$ events the induced uncertainty is $\lesssim 0.1$ GeV.

*PDF:* Depending on the relative fraction of gluon/quarks versus $x$ in various PDF's the top production kinematics might be different. No straightforward procedure is available for the moment to evaluate uncertainties due to a particular choice of PDF. We compared results obtained with the default set

CTEQ2L [115] and a more recent CTEQ4L [116] parameterisations of PDF's. The observed change in the $M_{\ell J/\psi}^{max}$ value is well within 0.1 GeV.

*Top $p_T$ spectrum:* As shown in Section 3.3, one does not expect significant uncertainties in the prediction of the top $p_T$ spectrum. However, to see an effect we have artificially altered the top $p_T$ spectrum by applying a cut at the generator level. We found that even requiring all top quarks to have $p_T > 100$ GeV gives rise to only a $1\sigma$ change ($\pm 0.7$ GeV) in the fitted value of $m_t$.

*Initial state radiation:* The $M_{\ell J/\psi}^{max}$ value is unchanged even switching off completely the ISR.

*Top and $W$ widths:* Kinematical cuts that are usually applied affect the observed Breit-Wigner shape (tails) of decaying particles. Conversely, poor knowledge of the widths may alter the generated $lJ/\psi$ mass spectrum depending on the cuts. In our case, only a small change in the $M_{\ell J/\psi}^{max}$ value is seen relative to the zero-width approximation.

*$W$ polarisation:* A significant shift is found for the isotropic decays of W when compared to the SM expectation of its $\sim$ 70% longitudinal polarisation. In future runs of the Tevatron the $W$ polarisation will be measured with a $\sim$ 2% accuracy [98], and at the LHC this would be further improved, so that it should not introduce additional uncertainties in simulations.

*$t\bar{t}$ spin correlations:* A "cross-talk" between $t$ and $\bar{t}$ decay products is possible due to experimental cuts. To examine this effect in detail the $2\to 6$ matrix elements have been implemented in PYTHIA preserving the spin correlations [117]. No sizeable difference in the $M_{\ell J/\psi}^{max}$ value is seen compared to the default $2\to 2$ matrix elements.

*QED bremsstrahlung:* Only a small effect is observed when it is switched off. Furthermore, QED radiation is well understood and can be properly simulated.

*Final State Radiation:* A large shift of $\sim$ 7 GeV is observed when the FSR is switched off. This is due to the absence of evolution for the $b$ quark, whose fragmentation function will be unphysically hard. To evaluate the uncertainty we varied the parton virtuality scale $m_{min}$, the invariant mass cut-off below which the showering is terminated. A $\pm 50$% variation of it around the default (tuned to data) value of 1 GeV induces an uncertainty of $^{+0.1}_{-0.15}$ GeV.

*$b$ fragmentation, except FSR:* As a default, in PYTHIA we have used the Peterson form for the $b$-quark fragmentation function with $\varepsilon_b = 0.005$. Variation of this value by $\pm$10% [118] leads to an uncertainty of $^{-0.3}_{+0.25}$ GeV. (The $\pm$10% uncertainty on $\varepsilon_b$ is inferred from LEP/SLD precision of $\sim$ 1% on the average scaled energy of $B$-hadrons.) It should be pointed out that recent accurate measurements of the $b$-quark fragmentation function [119] are not well fitted by the Peterson form.

The last two items of this list deserve some additional comments. While the separation between the FSR and the non-perturbative fragmentation phases seems unnecessary, and liable to lead to an over-estimate of the uncertainty, it is important to remark that our knowledge of the non-perturbative hadronisation comes entirely from the production of $b$-hadrons in $Z^0$ decays at LEP and SLC. It is important to ensure that the accuracy of both perturbative and non-perturbative effects is known, since the perturbative evolution of $b$ quarks from $Z^0$ and top decays are not the same owing to the different scales involved. An agreement between data and Monte Carlo calculations for the $b$-hadron fragmentation function at the $Z^0$ does not guarantee a correct estimate of the $b$-hadron fragmentation function in top decays.

To be specific, we shall consider here the effects induced by the higher-order matrix element corrections to the radiative top decays $t\to bWg$ [54]. These effects cannot be simulated by a change in the virtuality scale $m_{min}$ as explored above in the study based on PYTHIA, as they have a different physical origin. The extended phase-space available for gluon emission after inclusion of the matrix-element corrections leads to a softening of the $b$-quark, and, as a result, of the $\ell J/\psi$ spectrum. For simplicity, we study here the invariant mass of the system $B\ell$. The resulting invariant mass distributions, for $m_t$= 175 GeV, with (HERWIG 6.1) and without (HERWIG 6.0) matrix element corrections are shown in Fig. 25. The averages of the two distributions, as a function of the top mass, are given on the right of the figure, and the difference of the averages are given in Table 7. Given the slopes of the correlation

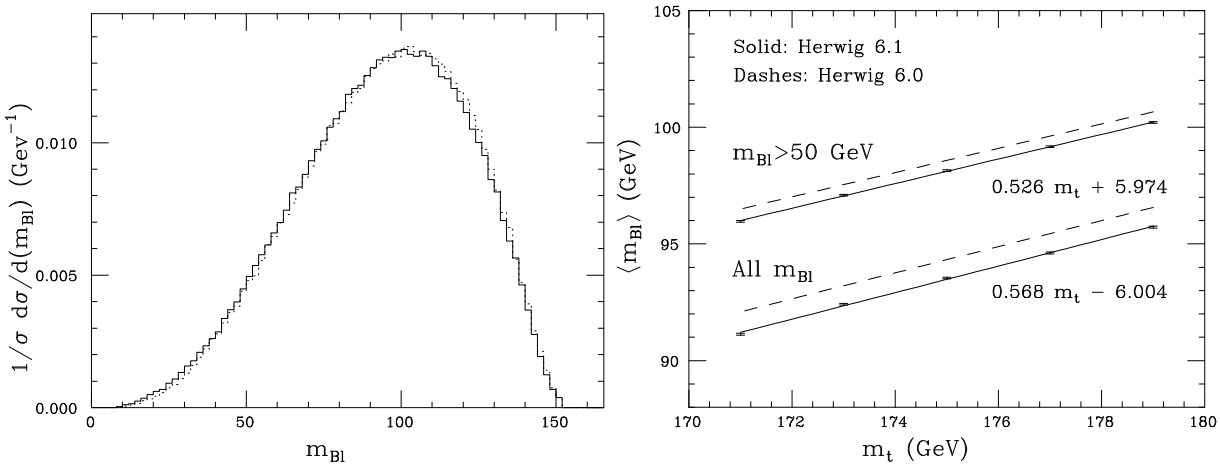


Fig. 25: Left: invariant mass of the $B$-lepton system for $m_t = 175$ GeV, according to HERWIG 6.0 (dotted) and 6.1 (with matrix element corrections, solid). Right: linear fits to the average invariant mass $\langle m_{B\ell}\rangle$ as a function of $m_t$.

Table 7: Negative shift in the average invariant mass $\langle m_{B\ell}\rangle$ after inclusion of matrix element corrections for the top decay in HERWIG. Left: average over all values of $m_{B\ell}$. Right: average over the sample with $m_{B\ell} > 50$ GeV.

| $m_t$ | $\langle m^{6.0}_{B\ell}\rangle - \langle m^{6.1}_{B\ell}\rangle$ (all $m_{B\ell}$) | $\langle m^{6.0}_{B\ell}\rangle - \langle m^{6.1}_{B\ell}\rangle$ ($m_{B\ell} > 50$ GeV) |
|---|---|---|
| 171 GeV | $(0.891 \pm 0.038)$ GeV | $(0.479 \pm 0.036)$ GeV |
| 173 GeV | $(0.844 \pm 0.038)$ GeV | $(0.479 \pm 0.034)$ GeV |
| 175 GeV | $(0.843 \pm 0.039)$ GeV | $(0.510 \pm 0.035)$ GeV |
| 177 GeV | $(0.855 \pm 0.039)$ GeV | $(0.466 \pm 0.035)$ GeV |
| 179 GeV | $(0.792 \pm 0.040)$ GeV | $(0.427 \pm 0.036)$ GeV |

between $\langle m_{B\ell}\rangle$ and $m_t$, we see that the corrections due to inclusion of the exact matrix elements are between 1 GeV (for $m_{B\ell} > 50$ GeV) and 1.5 GeV (for the full sample).

More details of the analysis will be found in [64]. It is also found there that the dependence of $\langle m_{B\ell}\rangle$ on the hadronic center of mass energy, or on the partonic initial state producing the $t\bar{t}$ pair, is no larger than 100 MeV. We take this as an indication that the effects of non-factorisable non-perturbative corrections (such as those induced by the neutralisation of the colour of the top quark decay products) are much smaller than the 1 GeV accuracy goal on the mass.

A summary of these studies is given in Fig. 26. One sees an impressive stability of the results for reasonable choices of parameters. The expected systematic error in the $M^{max}_{\ell J/\psi}$determination is $\lesssim {}^{+0.3}_{-0.4}$ GeV which translates into a systematic error on the top mass of $\delta m_t \lesssim {}^{+0.6}_{-0.8}$ GeV.

In addition to the above studies, we also compared directly the results of HERWIG (v5.9) and PYTHIA. With HERWIG we have tried various tunings from LEP experiments as well as its default settings [51]. They all yield comparable results to each other and to PYTHIA results, and are within $\lesssim 0.5$ GeV. This corresponds to a systematic uncertainty $\delta m_t \lesssim 1$ GeV.

### 4.7 Conclusions for the top mass measurement at the LHC

The very large samples of top quark events which will be accumulated at the LHC lead to a precision measurement of the top quark mass. Different statistically independent channels have been investigated and from the studies so far a precision of better than 2 GeV in each case can be obtained. In particular for the lepton plus jets channel where the $m_t$ is measured directly reconstructing the invariant mass of the $m_{jjb}$ candidates, such a precision can be achieved within a year or running at low luminosity. For the channels involving two or more leptons, data from several years have to be combined to limit the statistical error in the measurement beyond the expected systematic errors.

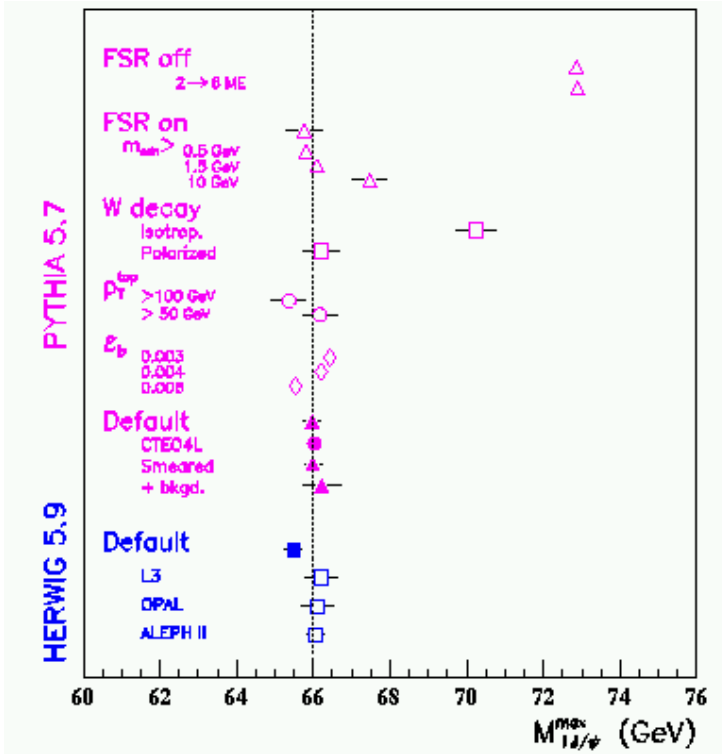


Fig. 26: Observed $m_t$ shifts for the various systematic effects studied for the $\ell + J/\psi$ channel.

With the statistical error not being a problem, the emphasis of the work was devoted to estimate the systematic error involved in each method. For each sample, the contributing systematic errors are different, a fact which will allow important cross-checks to be made. The results indicate that a total error below 2 GeV should be feasible. In the case of the lepton plus jet channel the major contribution to the uncertainty is identified in the jet energy scale (in particular for the $b$-jets) and in the knowledge of FSR. When a special sub-sample of high $p_T$ top events is used and the $m_t$ is reconstructed using a large calorimeter cluster the FSR sensitivity is reduced, but further work is required to validate it. For the channels using two or more leptons for the top decay, the major contribution in the systematic error comes from the Monte Carlo and from how well the kinematic observable used for the mass measurement is related to the mass of the top quark.

In $\ell J/\psi$ final states the top mass can be determined with a systematic uncertainty of $\lesssim$ 1 GeV. These final states are experimentally very clean and can be exploited even at highest LHC luminosities. The precision would be limited by the theoretical uncertainties which is basically reduced to the one associated with the $t \to B$ meson transition. This method of top mass determination looks very promising, and a final definition of its ultimate reach will rely on a better understanding of theoretical issues, and on the possibility to minimise the model dependence using the LHC data themselves.

## 5. SINGLE TOP PRODUCTION[6]

At the LHC, top quarks are mostly produced in pairs, via the strong process $gg \to t\bar{t}$ (and, to a lesser extent, $q\bar{q} \to t\bar{t}$). However, there are a significant number of top quarks that are produced singly, via the weak interaction. There are three separate single-top quark production processes of interest at the LHC, which may be characterised by the virtuality of the $W$ boson (of four-momentum $q$) in the process:

- $t$-channel: The dominant process involves a space-like $W$ boson ($q^2 \leq 0$), as shown in Fig. 27(a) [120]. The virtual $W$ boson strikes a $b$ quark in the proton sea, promoting it to a top quark. This

[6]Section coordinators: S. Willenbrock, D. O'Neil (ATLAS), J. Womersley (CMS).

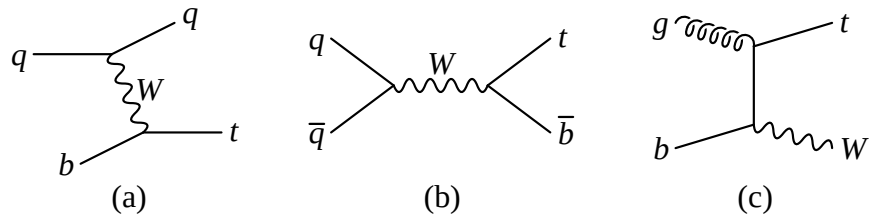


Fig. 27: Feynman diagrams for single-top quark production in hadron collisions: (a) $t$-channel process; (b) $s$-channel process; (c) associated production (only one of the two diagrams for this process is shown).

Table 8: Total cross sections (pb) for single-top quark production and top quark pair production at the LHC, for $m_t$=175 $\pm$2 GeV. The NLO $t$-channel cross section is from [125]. The NLO $s$-channel cross section is from [126]. The cross section for the $Wt$ process is from [124]; it is leading order, with a subset of the NLO corrections included. The uncertainties are due to variation of the factorisation and renormalisation scales; uncertainty in the parton distribution functions; and uncertainty in the top quark mass (2 GeV).

| process: | $t$-channel | $s$-channel | $Wt$ | $t\bar{t}$ |
|---|---|---|---|---|
| $\sigma$(pb): | $245 \pm 27$ | $10.2 \pm 0.7$ | $51 \pm 9$ | $\sim 800$ |

process is also referred to as $W$-gluon fusion, because the $b$ quark ultimately arises from a gluon splitting to $b\bar{b}$.

- $s$-channel: If one rotates the $t$-channel diagram such that the virtual $W$ boson becomes time-like, as shown in Fig. 27(b), one has another process that produces a single top quark [121, 122]. The virtuality of the $W$ boson is $q^2 \geq (m_t + m_b)^2$.
- Associated production: A single top quark may also be produced via the weak interaction in association with a real $W$ boson ($q^2 = M_W^2$), as shown in Fig. 27(c) [123, 124]. One of the initial partons is a $b$ quark in the proton sea, as in the $t$-channel process.

The total cross sections for these three single-top quark production processes are listed in Table 8, along with the cross section for the strong production of top quark pairs. The $t$-channel process has the largest cross section; it is nearly one third as large as the cross section for top quark pairs. The $s$-channel process has the smallest cross section, more than an order of magnitude less than the $t$-channel process. The $Wt$ process has a cross section intermediate between these two. We will argue that all three processes are observable at the LHC. The $t$-channel and $s$-channel processes will first be observed at the Fermilab Tevatron [127]; the $Wt$ process will first be seen at the LHC.

There are several reasons for studying the production of single top quarks at the LHC:

- The cross sections for single-top quark processes are proportional to $|V_{tb}|^2$. These processes provide the only known way to directly measure $V_{tb}$ at hadron colliders.
- Single-top quark events are backgrounds to other signals. For example, single-top quark events are backgrounds to some signals for the Higgs boson [128].
- Single top quarks are produced with nearly $100\%$ polarisation, due to the weak interaction [123, 129, 130, 131]. This polarisation serves as a test of the $V - A$ structure of the top quark charged-current weak interaction.
- New physics may be discernible in single-top quark events. New physics can influence single-top quark production by inducing non-SM weak interactions [129, 132, 133, 134, 135], via loop effects [136, 137, 138, 139, 140], or by providing new sources of single-top quark events [133, 137, 141, 142].

In the next three subsections we separately consider the three single-top quark production processes. The subsection after these discusses the polarisation of single top quarks. In the concluding section, we discuss the accuracy with which $V_{tb}$ can be measured in single-top quark events at the LHC.

## 5.1 t-channel single-top production

### *5.11 Theory*

The largest source of single top quarks at the LHC is via the $t$-channel process, shown in Fig. 27(a) [120, 123, 125, 129, 143, 144, 145]. A space-like ($q^2 \leq 0$) $W$ boson strikes a $b$ quark in the proton sea, promoting it to a top quark. As shown in Table 8, the cross section for this process is about one third that of the strong production of top quark pairs. Thus there will be an enormous number of single top quarks produced via the $t$-channel process at the LHC.

It is perhaps surprising that the cross section for the weak production of a single top quark, of order $\alpha_W^2$, is comparable to that of the strong production of top quark pairs, of order $\alpha_s^2$. There are several enhancements to the $t$-channel production of a single top quark that are responsible for this:

- The differential cross section for the $t$-channel process is proportional to $d\sigma/dq^2 \sim 1/(q^2 - M_W^2)^2$, due to the $W$-boson propagator. The total cross section is therefore dominated by the region $|q^2| \leq M_W^2$, and is proportional to $1/M_W^2$. In contrast, the total cross section for the strong production of top quark pairs is proportional to $1/s$, where $s \geq 4m_t^2$ is the parton center-of-mass energy.
- Since only a single top quark is produced, the typical value of the parton momentum fraction $x$ is half that of top quark pair production. Since parton distribution functions scale roughly like $1/x$ at small values of $x$, and there are two parton distribution functions, this leads to an enhancement factor of roughly four.

The fact that the total cross section is dominated by the region $|q^2| \leq M_W^2$ also has the implication that the final-state light quark tends to be emitted at small angles, *i.e.*, high rapidities. This characteristic feature of the signal proves to be useful when isolating it from backgrounds.

The $b$ distribution function in the proton sea arises from the splitting of virtual gluons into nearly-collinear $b\bar{b}$ pairs. Thus it is implicit that there is a $\bar{b}$ in the final state, which accompanies the top quark and the light quark. The final-state $\bar{b}$ tends to reside at small $p_T$, so it is usually unobservable.

The total cross section for the $t$-channel production of single top quarks has been calculated at NLO [125, 143]; the result is given in Table 8. A subset of the NLO corrections is shown in Fig. 28(a). This correction arises from an initial gluon which splits into a $b\bar{b}$ pair. If the $b\bar{b}$ pair is nearly collinear, then this process contributes to the generation of the $b$ distribution function, which is already present at leading order; hence, one does not include this kinematic region as a contribution to the NLO correction. This is indicated schematically in Fig. 28(b). Only the contribution where the $b\bar{b}$ pair is non-collinear is a proper NLO correction to the total cross section.[7] The other corrections to this process, due to final-state and virtual gluons, as well as corrections associated with the light quark, are also included in the cross section given in Table 8.

The central value for the cross section is obtained by setting the factorisation scale[8] of the $b$ distribution function equal to $\mu^2 = -q^2 + m_t^2$. The uncertainty in the NLO cross section due to the variation of the factorisation scale between one half and twice its central value is $4\%$. Due to the similarity with deep-inelastic scattering, the factorisation scale of the light quark is $\mu^2 = -q^2$, and is not varied [125].

Since the $\bar{b}$ tends to reside at low $p_T$, the dominant final state is $Wbj$, where the $Wb$ are the decay products of the top quark, and the jet is at high rapidity. However, the $\bar{b}$ is at $p_T > 20$ GeV in roughly $40\%$ of the events, in which case the final state is $Wb\bar{b}j$. From a theoretical perspective, the optimal strategy is to isolate both final states and thereby measure the total cross section, which has an uncertainty of only $4\%$ from varying the factorisation scale, as mentioned above. However, the $Wb\bar{b}j$ final state has a large background from $t\bar{t}$, and it has not yet been established by ATLAS or CMS that this signal can be isolated, although the analysis of [145] gives cause for optimism. Thus we focus on the $Wbj$ final state,

[7] The formalism for separating the nearly-collinear and non-collinear regions, and for generating the $b$ distribution function, was developed in Refs. [146, 58].

[8] The factorisation and renormalisation scales are set equal.

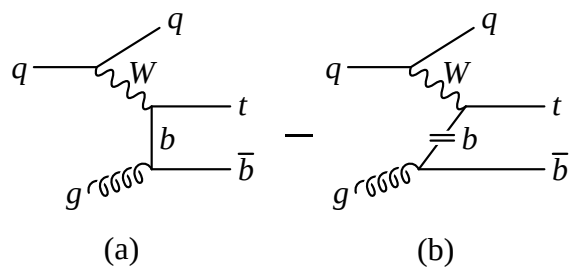


Fig. 28: (a) Initial-gluon correction to single-top quark production via the $t$-channel process (the diagram with the $W$ and gluon lines crossed is not shown); (b) the kinematic region in which the gluon splits to a nearly-collinear $b\bar{b}$ pair (the double line through the $b$ propagator indicates that it is nearly on shell) is subtracted from the correction, as it is already included at leading order.

demanding that the $\bar{b}$ have $p_T < p_{Tcut}$. For $p_{Tcut} = 20$ GeV,[9] the cross section for this semi-inclusive process is 164 pb, with an uncertainty of $10\%$ from varying the factorisation scale [144], about twice the uncertainty of the total cross section. Work is in progress to calculate the differential cross section $d\sigma/dp_{T\bar{b}}$ at NLO with the goal of reducing this uncertainty [147]. It would also be desirable to calculate the total cross section at next-to-next-to-leading order (NNLO).

Additional theoretical uncertainties stem from the top quark mass and the parton distribution functions. An uncertainty in the top quark mass of 2 GeV yields an uncertainty of only $2\%$ in the cross section, which is negligible. This is due to the fact that the cross section scales like $1/M_W^2$ rather than $1/s$. The uncertainty in the cross section due to the parton distribution functions is estimated in [148] to be $10\%$. That analysis suggests that the uncertainty can be reduced below this value. Combining all uncertainties in quadrature, we conclude that the total theoretical uncertainty is presently $15\%$ in the $Wbj$ cross section ($11\%$ in the total cross section). The discussion above suggests that this can be significantly reduced with further effort.

### *5.12 Phenomenology*

Studies of the $t$-channel process have been carried out by both ATLAS and CMS. We will first describe the CMS study, and then that of ATLAS.

In order to reject the large $t\bar{t}$ background in this channel, it is necessary to impose a cut on jet multiplicity. Accurate modelling of jet response and resolution is therefore desirable, and so CMS [149] used a full GEANT calorimeter simulation of the detector. The GEANT simulation also allows a more realistic modelling of the missing-$p_T$ response of the detector, which is important in understanding the mass resolution which can be obtained on the reconstructed $t$ quark. The detailed calorimeter simulation was combined with a parameterised $b$-tagging efficiency.

Signal events were generated using PYTHIA 5.72 [52], with $m_t = 175$ GeV and the CTEQ2L parton distribution functions. Events were preselected at the generator level to have one and only one charged lepton (with $p_T > 25$ GeV and $|\eta| < 2.5$) and one or two jets (generator-level jets were found using the LUCELL clustering algorithm, which is part of PYTHIA). Generated events were then passed through the parameterised $b$-tagging and the GEANT detector simulation. The CMS $b$-tagging performance is taken from a study which used a detailed detector simulation combined with existing CDF data on impact-parameter resolutions. The tagging efficiency for $p_T > 50$ GeV is typically 50% for $b$-jets, 10% for $c$-jets, and 1–2% for light quarks and gluons. These efficiencies fall quite rapidly for lower transverse momenta, and it was assumed no tagging could be performed for $p_T < 20$ GeV or $|\eta| > 2.4$. The generated luminosity corresponded to about 100 pb$^{-1}$ – only 30 hours of running at $10^{33}\mathrm{cm}^{-2}\mathrm{s}^{-1}$.

The $t\bar{t}$ and $WZ$ backgrounds were also generated using PYTHIA 5.72. The same pre-selections were applied at the generator level. The $W+$ jets backgrounds were generated using the VECBOS

[9] The CMS analysis presented below uses $p_{Tcut} = 20$ GeV; the ATLAS analysis uses $p_{Tcut} = 15$ GeV.

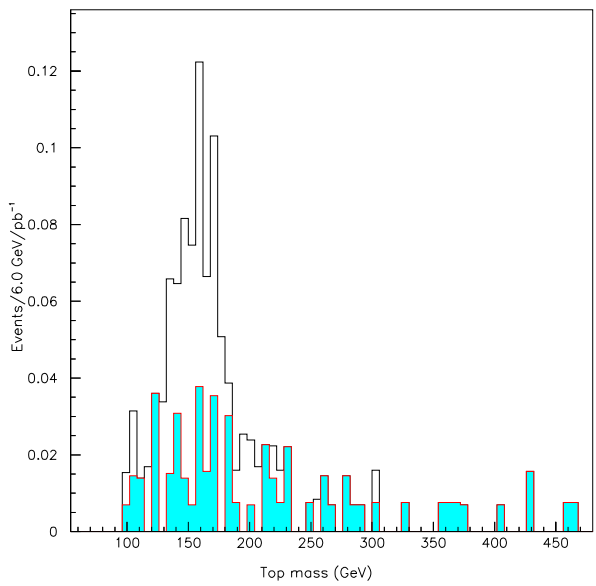


Fig. 29: Reconstructed top mass for signal plus backgrounds (open histogram) and backgrounds only (shaded). The backgrounds considered are $t\bar{t}$, $W+2$ jets and $W+3$ jets. The vertical scale is events per 6 GeV mass bin per pb$^{-1}$ of luminosity.

generator [150], combined with HERWIG 5.6 [51] to fragment the outgoing partons.[10] $W+2$ jets and $W+3$ jets processes were generated separately. Again, events were preselected to have a charged lepton with $p_T > 25$ GeV and $|\eta| < 2.5$, and to have a (parton-level) $p_T > 15$ GeV for the final-state jets.

Events were then selected which passed the following requirements:

- One and only one isolated lepton ($\ell = e$ or $\mu$) with $p_T > 20$ GeV and $|\eta| < 2.5$. This allows the events to pass a reasonable lepton trigger.
- Missing $p_T > 20$ GeV, and transverse mass (of the lepton and missing $p_T$) $50 < m_T < 100$ GeV. These two requirements select $W \to \ell\nu$ candidates.
- Exactly two jets with $p_T > 20$ GeV and $|\eta| < 4$. Requiring at least two jets reduces the $W+$ jets background, while requiring no more than two jets rejects the $t\bar{t}$ background which naively would produce four jets in the final state.
- One jet with $p_T > 20$ GeV and $|\eta| < 2.5$, the other jet with $p_T > 50$ GeV and $2.5 < |\eta| < 4.0$. The requirement that the second jet be at forward rapidities tends to select the desired $t$-channel process.
- Leading jet $p_T < 100$ GeV. This helps to reduce the $t\bar{t}$ background.
- Exactly one $b$-tagged jet (given the $b$-tagging acceptance, this is always the central jet). This requirement again reduces $t\bar{t}$, and of course rejects $W+$ jets processes with light-quark or gluon jets.
- Invariant mass of the two jets in the $80-100$ GeV range. This rejects $WZ$ events with $Z \to b\bar{b}$.

The single-top signal is then searched for in the invariant mass of the $W$ and the $b$-tagged jet (which should peak at the top quark mass). The mass was reconstructed assuming the solution for the $W$ kinematics which yields the lower $|p_z^\nu|$. (It is possible to use other choices, for example the solution which gives the $Wb$ mass closest to $m_t$. This would result in an apparently better top mass resolution but would also severely bias the background shape; the statistical significance of the signal would not be improved.)

Figure 29 shows the reconstructed mass distribution for signal and background combined. The signal is apparent as an excess over the background (the shaded histogram) around 160 GeV. (Since jet

[10] The version of VECBOS used here, and its interface to HERWIG, were developed for use in CDF [151], and were adapted for CMS by R. Vidal.

energy scale corrections have not been applied to the simulated events, the top mass reconstructs to less than its true value.) The signal-to-background ratio in a window of $160 \pm 20$ GeV is 3.5 with a clear peak visible in the $Wb$ invariant-mass distribution. The number of signal events is 66 in 100 pb$^{-1}$, giving a signal efficiency of 1.2% (after the $W \to \ell\bar{\nu}$ branching ratio). We then find that 10 fb$^{-1}$ would yield 6600 signal events ($S$) and 1900 background ($B$), sufficient for a statistical accuracy on the number of signal events of $\sqrt{S+B}/S = 1.4\%$.

The largest background comes from $Wcj$ with the charm jet mistagged as a $b$-jet. It would be worthwhile to develop a $b$-tagging algorithm having greater rejection against such mistags, even at the cost of some signal efficiency. The $Wb\bar{b}$ background was found to be a small contribution to the $W+2$ jets background at the parton level for the selection cuts employed here, and was therefore not explicitly included in the analysis.

The use of the forward jet tag substantially improves the signal-to-background ratio, and allows a clear reconstructed top-mass peak to be seen. However, it does not significantly improve $\sqrt{S+B}/S$ [144]. One could therefore imagine omitting the forward jet requirement if the systematic uncertainty could thereby be reduced.

Compared with earlier studies (for example [144]), this analysis uses more realistic jet and missing-$p_T$ resolutions, and includes initial- and final-state gluon radiation. As a result, the top-mass resolution is worsened; but the resolution found here compares well with the result of a full simulation of single-top production in CDF.

A study of the cross-section measurement for the $t$-channel process was also carried out by ATLAS [152]. Signal events were generated using the ONETOP parton-level Monte Carlo [153] with fragmentation, radiation, and underlying event simulated by PYTHIA 5.72. Backgrounds containing top quarks ($t\bar{t}$ and other single-top production) were also generated using ONETOP, while $W+$ jets and $Wb\bar{b}$ backgrounds were generated by HERWIG 5.6.[11] These events were processed by the ATLAS parameterised detector simulation assuming a 60% $b$-tagging efficiency for $b$-jets, 10% for $c$-jets, and 1% for light quarks and gluons. The events were then analysed with a view towards separating $t$-channel single top from background and measuring its cross section.

Event selection criteria were divided into two types: pre-selection and selection cuts. The pre-selection criteria were as follows:

- at least one isolated lepton with $p_T > 20$ GeV;
- at least one $b$-tagged jet with $p_T > 50$ GeV;
- at least one other jet with $p_T > 30$ GeV.

These were followed by the selection cuts:

- two and only two jets in the event (a jet has $p_T > 15$ GeV);
- one jet is a central $b$-tagged jet;
- the other jet is a forward ($|\eta| > 2.5$) untagged jet with $p_T > 50$ GeV.

The application of these cuts, and also the requirement of a reconstructed top mass between 150 and 200 GeV, yields the number of events shown in Table 9. The final signal efficiency is 3% and the signal-to-background ratio is 2.4. This implies a statistical precision on the cross-section measurement of $\sqrt{S+B}/S = 0.9\%$ with 10 fb$^{-1}$ of data. Introducing other event selection variables (see [30, 154, 155]) it is possible to improve the signal-to-background ratio to nearly 5, but this does not improve the cross-section measurement due to the small remaining signal efficiency.

Both the CMS and ATLAS studies indicate that it will be possible to observe $t$-channel single-top production with a good signal-to-background ratio and a statistical uncertainty in the cross section of less than 2% with 10 fb$^{-1}$. Thus the uncertainty in the extracted value of $V_{tb}$ will almost certainly be dominated by systematic uncertainties, as discussed in the conclusions.

[11] The $Wb\bar{b}$ background was generated using the matrix element from [89] interfaced to HERWIG 5.6.

Table 9: Cumulative effect of cuts on $t$-channel signal and backgrounds. The first four rows of this table refer to cumulative efficiencies of various cuts. The last two rows refer to the number of events for 10 fb$^{-1}$. Only events in which $W \to e\nu$ or $\mu\nu$ are considered in this table. Uncertainties quoted in this table are due entirely to Monte Carlo statistics.

| cut | $t$-channel eff(%) | $t\bar{t}$ eff(%) | $Wb\bar{b}$ eff(%) | $W+$ jets eff(%) |
|---|---|---|---|---|
| pre-selection | 18.5 | 44.4 | 2.53 | 0.66 |
| njets=2 | 12.1 | 0.996 | 1.55 | 0.291 |
| fwd jet $\lvert\eta\rvert > 2.5$ $p_T$ >50 GeV | 4.15 | 0.035 | 0.064 | 0.043 |
| $M_{\ell\nu b}$ 150-200 GeV | 3.00 | 0.017 | 0.023 | 0.016 |
| events/10 fb$^{-1}$ (before cuts) | $5.43 \times 10^5$ | $2.40 \times 10^6$ | $6.67 \times 10^5$ | $4.00 \times 10^7$ |
| events/10 fb$^{-1}$ (after cuts) | 16515±49 | 455±74 | 155±17 | 6339±265 |

## 5.2 s-channel single-top production

### *5.21 Theory*

The $s$-channel production of single top quarks is shown in Fig. 27(b) [121, 122, 123, 126, 144, 145]. The cross section is much less than that of the $t$-channel process because it scales like $1/s$ rather than $1/M_W^2$. However, the $s$-channel process has the advantage that the quark and antiquark distribution functions are relatively well known, so the uncertainty from the parton distribution functions is small. Furthermore, the parton luminosity can be constrained by measuring the Drell-Yan process $q\bar{q}\to W^*\to\ell\bar{\nu}$, which has the identical initial state [122, 156].[12]

The total cross section for the $s$-channel process has been calculated at NLO [126]; the result is given in Table 8. The factorisation and renormalisation scales are set equal to $\mu^2 = q^2$; varying each, independently, between one-half and twice its central value yields uncertainties in the cross section of $2\%$ from each source. The uncertainty in the cross section from the parton distribution functions is estimated to be $4\%$. The largest single source of uncertainty is the top quark mass; an uncertainty of 2 GeV yields an uncertainty in the cross section of $5\%$. The relatively large sensitivity of the cross section to the top quark mass is a manifestation of the $1/s$ scaling. Combining all theoretical uncertainties in quadrature yields a total uncertainty in the cross section of $7\%$. This is much less than the present theoretical uncertainty in the $t$-channel cross section.

The Yukawa correction to this process, of order $\alpha_W m_t^2/M_W^2$, is less than one percent [126]. However, this correction could be significant in a two-Higgs-doublet model for low values of $\tan\beta$, in which the Yukawa coupling is enhanced [138].

### *5.22 Phenomenology*

In order to evaluate the potential to separate the $s$-channel signal from its backgrounds, Monte Carlo events have been processed by a fast (parameterised) simulation of an LHC detector. At parton level the signal and the $t\bar{t}$ background were generated by the ONETOP Monte Carlo [153]. Radiation, showering, and the underlying event were added by PYTHIA 5.72 [52]. The $W+$ jets and $Wb\bar{b}$ backgrounds were generated using HERWIG 5.6 [51].[13] Table 8 presents the cross sections assumed for the processes

[12] The parton luminosity can only be constrained, not directly measured, with this process. Since the neutrino longitudinal momentum is unknown, the $q^2$ of the virtual $W$ cannot be reconstructed.

[13] The $Wb\bar{b}$ background was generated using the matrix element from [89] interfaced to HERWIG 5.6.

Table 10: Cumulative effect of cuts on $s$-channel signal and backgrounds. The first five rows of this table refer to cumulative efficiencies of various cuts. The last two rows refer to the number of events for 30 fb$^{-1}$. Only events in which W$\rightarrow$ e$\nu$ or $\mu\nu$ are considered in this table. Uncertainties quoted in this table are due entirely to Monte Carlo statistics.

| cut | $s$-channel eff(%) | $t$-channel eff(%) | $Wt$ eff(%) | $t\bar{t}$ eff(%) | $Wb\bar{b}$ eff(%) | $W+$ jets eff (%) |
|---|---|---|---|---|---|---|
| pre-selection | 27.0 | 18.5 | 25.5 | 44.4 | 2.53 | 0.667 |
| njets=2 | 18.4 | 12.1 | 4.03 | 0.996 | 1.55 | 0.291 |
| nbjet=2 $p_T > 75$ GeV | 2.10 | 0.035 | 0.018 | 0.023 | 0.034 | 0.0005 |
| $\sum^{\text{jets}} p_T$ >175 GeV | 1.92 | 0.031 | 0.016 | 0.021 | 0.028 | 0.0005 |
| M$_{\ell\nu b}$ 150-200 GeV | 1.36 | 0.023 | 0.006 | 0.012 | 0.0097 | 0.00014 |
| events/30 fb$^{-1}$ (before cuts) | $6.66 \times 10^4$ | $1.63 \times 10^6$ | $4.5 \times 10^5$ | $6.9 \times 10^6$ | $2.0 \times 10^6$ | $1.2 \times 10^8$ |
| events/30 fb$^{-1}$ (after cuts) | $908 \pm 35$ | $375 \pm 13$ | $27 \pm 15$ | $853 \pm 175$ | $194 \pm 34$ | $169 \pm 76$ |

containing top quarks. The cross section for the $W+$ jets background is normalised to that predicted by the VECBOS Monte Carlo [150] and is taken to be 18000 pb.[14] The $Wb\bar{b}$ cross section is taken from [144] to be 300 pb.

From a phenomenological standpoint the most important distinction between the $s$-channel and $t$-channel sources of single top is the presence of a second high-$p_T$ $b$-jet in the $s$-channel process. As mentioned previously, in $t$-channel events the second $b$-jet tends to be at low $p_T$ and is often not seen. Therefore, requiring two $b$-jets above 75 GeV $p_T$ will eliminate most of the $t$-channel background. Requiring two high-$p_T$ $b$-jets in the event also suppresses the $W+$ jets background relative to the signal.

In addition to suppressing the $t$-channel background it is also necessary, as in other single-top signals, to design cuts to reduce the $W+$ jets and $t\bar{t}$ backgrounds. In order to reduce contamination by $W+$ jets events, the reconstructed top mass in each event must fall within a window about the known top mass (150-200 GeV), and the events must have a total transverse jet momentum[15] above 175 GeV. Only events containing exactly two jets (both tagged as $b$'s) are kept in order to reduce the $t\bar{t}$ background.

Table 10 presents the cumulative effect of all cuts on the $s$-channel signal and on the backgrounds. Events from $t$-channel single-top production are included in this table as a background to the $s$-channel process. From this table the predicted signal-to-background ratio for the $s$-channel signal is calculated to be 0.56. The results also imply a signal statistical significance ($S/\sqrt{B}$) of 23 with an integrated luminosity of 30 fb$^{-1}$. The statistical precision on the cross section, calculated from $\sqrt{S+B}/S$, is 5.5% with 30 fb$^{-1}$.

This study indicates that, despite the large anticipated background rate, it should be possible to perform a good statistical measurement of the $s$-channel single-top cross section. The accuracy with which $V_{tb}$ can be measured is discussed in the conclusions.

### 5.3 Associated production

#### *5.31 Theory*

Single top quarks may also be produced in association with a $W$ boson, as shown in Fig. 27(c) [123, 124, 145]. Like the $t$-channel process, one of the initial partons is a $b$ quark. However, unlike the $t$-channel

[14] This cross section is defined for events containing at least two jets, each with $p_T > 15$ GeV and $|\eta| < 5$.

[15] Scalar sum of the transverse momentum of all jets in the event.

process, this process scales like $1/s$. This, combined with the higher values of $x$ needed to produce both a top quark and a $W$ boson, leads to a cross section for associated production which is about a factor of five less than that of the the $t$-channel process, despite the fact that it is of order $\alpha_s\alpha_W$ rather than $\alpha_W^2$.

The total cross section for associated production has been calculated at leading order, with a subset of the NLO corrections included [124, 145]; the result is given in Table 8. This subset is analogous to the initial-gluon correction to the $t$-channel process, discussed previously. The other corrections have not yet been evaluated.[16] The initial-gluon correction contains an interesting feature which has no analogue in the $t$-channel process. One of the contributing diagrams to the initial-gluon correction ($gg\to Wt\bar{b}$) corresponds to $gg\to t\bar{t}$, followed by $\bar{t}\to W\bar{b}$. This should not be considered as a correction to associated production, but rather as a background (it is in fact the dominant background, as discussed below). Thus, when evaluating the initial-gluon correction, it is necessary to subtract the contribution in which the $\bar{t}$ is on shell. This is done properly in [124].

The cross section is evaluated with the common factorisation and renormalisation scales set equal to $\mu^2 = s$. The uncertainty in the cross section due to varying these scales between one half and twice their central value is $15\%$. This uncertainty would presumably be reduced with a full NLO calculation. The uncertainty in the cross section from the parton distribution functions is estimated to be $10\%$ [148],[17] although this could be improved with further study. The uncertainty in the cross section due to an uncertainty in the top quark mass of 2 GeV is $4\%$, relatively large due to the $1/s$ scaling of the cross section. Combining all theoretical uncertainties in quadrature yields a total uncertainty at present of $18\%$, the largest of the three single-top processes.

### *5.32 Phenomenology*

The strategy for measuring the cross section for associated production ($Wt$ mode) is similar to that for the $t$-channel process, as they share the same backgrounds. However, the nature of associated production makes it relatively easy to separate from $W+$ jets and difficult to separate from $t\bar{t}$ events. This difficulty in removing the $t\bar{t}$ background does not preclude obtaining a precise cross-section measurement in this channel, assuming the rate for $t\bar{t}$ can be well measured at the LHC.

Two studies designed to separate signal from background have been performed using two different final states. The first is a study by ATLAS [30] which attempts to isolate $Wt$ signal events in which one $W$ decays to jets and the other decays to leptons. The second study, which is presented in [124], attempts to isolate signal events in which both $W$'s decay leptonically.

The first study presented here was done by ATLAS using the same event sample described in Section 5.1. Since the presence of a single isolated high-$p_T$ lepton is one of the preconditions of this study, the second $W$ must decay to two jets to be accepted by the event pre-selection. Therefore requiring a two-jet invariant mass within a window around the $W$ mass will serve to eliminate most events that do not contain a second $W$. The two-jet invariant-mass distribution is shown in Fig. 30 and clearly demonstrates the presence of a sharp peak in the associated-production signal and the $t\bar{t}$ background. This effectively leaves $t\bar{t}$ as the only background to $Wt$ events.

In addition to these special distinguishing features of the $Wt$ signal, there are several simple kinematic requirements which can be employed to reduce the $t\bar{t}$ background. By choosing events with exactly three jets and with exactly one of them tagged as a $b$-jet, some rejection of the $t\bar{t}$ background is possible. Some further rejection is obtained by limiting the selection to events with invariant mass less than 300 GeV, where the invariant mass of an event is defined as the invariant mass obtained by adding the four-vectors of all reconstructed jets and charged leptons ($e$ and $\mu$). However, even with these cuts the $t\bar{t}$ background is significantly larger than the $Wt$ signal.

Table 11 presents the cumulative effect of all cuts on the $Wt$ signal and on the $t\bar{t}$ and $W+$ jets

[16] The analogous calculation for $Wc$ production has been performed in [157].

[17] This is the uncertainty in the gluon-gluon luminosity at $\sqrt{\tau} = (m_t + M_W)/\sqrt{S} \approx 0.02$, where $\sqrt{S} = 14$ TeV.

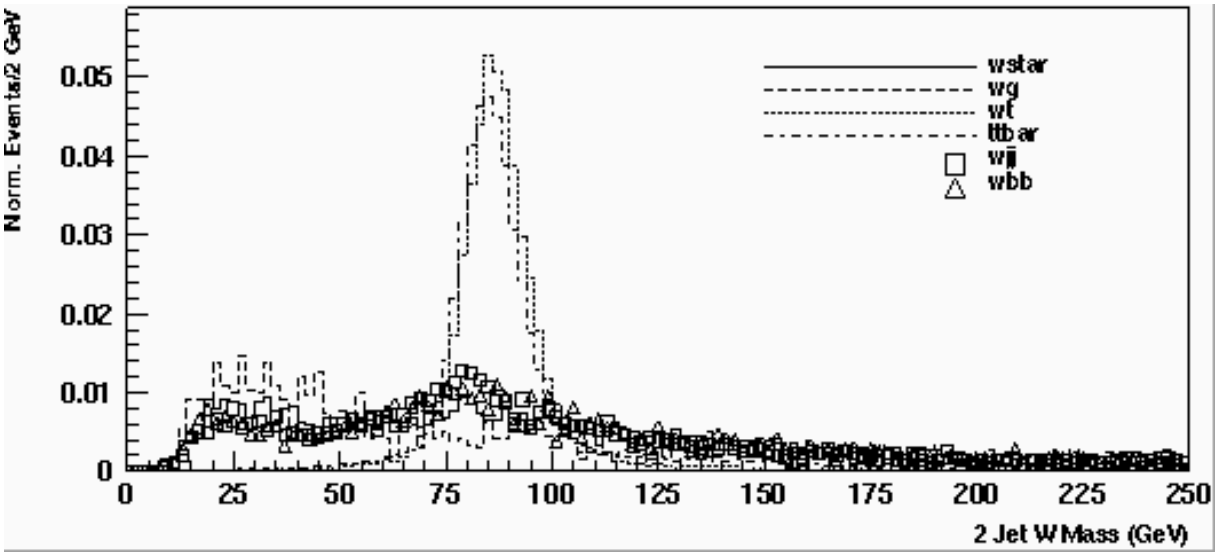


Fig. 30: The normalised two-jet invariant-mass distribution. For each event the two-jet combination with mass closest to the $W$ mass is plotted. This clearly shows a peak in the distribution for $Wt$ and $t\bar{t}$ which is not present for the other backgrounds.

backgrounds. The $Wb\bar{b}$ and $t$-channel single-top backgrounds are virtually eliminated by the cuts and so are not included in the table. From this table the predicted signal-to-background ratio for the $Wt$ signal is calculated to be 0.24. After three years of running at low luminosity (30 fb$^{-1}$), this implies a signal statistical significance ($S/\sqrt{B}$) of 25 and a statistical error on the $Wt$ cross section ($\sqrt{S+B}/S$) of 4.4%.

The second study [124] was done at parton level and involved the separation of signal from background in the mode in which both $W$'s decay to leptons. This signal contains two high $p_T$ leptons and only one jet (the $b$-jet produced from the top decay). In this decay channel it was found that, after applying detector acceptance cuts, requiring precisely one $b$-tagged jet with $p_T > 15$ GeV is enough to yield a signal-to-background ratio of nearly unity. Also, the signal efficiency is significantly higher than in the ATLAS analysis, allowing more total signal events to pass the cuts despite the lower branching ratio for this decay mode. The statistical precision on the cross section measured in this analysis is 1.3% with an integrated luminosity of 30 fb$^{-1}$. The accuracy with which $V_{tb}$ can be extracted is discussed in the conclusions.

### 5.4 Polarisation in single-top production

#### *5.41 Theory*

Because single top quarks are produced through the weak interaction, they are highly polarised [123, 129, 130, 131, 144]. In the ultra-relativistic limit, the top quarks are produced in helicity eigenstates with helicity $-1/2$ (the top antiquarks have helicity $+1/2$), because the $V-A$ structure of the weak interaction selects quarks of a definite chirality. However, if the top quarks are not ultra-relativistic, chirality is not the same as helicity. Nevertheless, it was shown in [130] that there is a basis in which the top quark is $100\%$ polarised, regardless of its energy. The top quark spin points along the direction of the $d$-type or $\bar{d}$-type quark in the event, in the top quark rest frame (the $\bar{t}$ spin points opposite this direction). In $t$-channel production, this is the direction of the final-state light quark ($ub \to dt$) or the beam direction ($\bar{d}b \to \bar{u}t$). In $s$-channel production, this is the beam direction ($u\bar{d} \to t\bar{b}$). In associated production ($gb \to Wt$), this is the direction of the $d$ quark (or charged lepton) from the $W$ decay.

We focus our attention on the $t$-channel single-top process for the remainder of this section. The top quark polarisation in the $t$-channel process has been calculated at NLO [131]; the results below are taken from this study. In the case of $t$ production, $80\%$ of the events have the $d$-type quark in the final state. This suggests using the direction of the light-quark jet, as observed in the top quark rest frame, to

Table 11: Cumulative effect of cuts on $Wt$ signal and backgrounds. Pre-selection cuts are defined in the same way as for the ATLAS $t$-channel analysis described earlier in this report. The first five rows of this table refer to cumulative efficiencies of various cuts. The last two rows refer to the number of events for 30 fb$^{-1}$. Only events in which W$\rightarrow$ e$\nu$ or $\mu\nu$ are considered in this table. Uncertainties quoted in this table are due entirely to Monte Carlo statistics.

| cut | $Wt$ eff(%) | $t\bar{t}$ eff(%) | $W+$ jets eff(%) |
|---|---|---|---|
| pre-selection | 25.5 | 44.4 | 0.66 |
| njets=3 $p_T > 50$ GeV | 3.41 | 4.4 | 0.030 |
| nbjet=1 $p_T > 50$ GeV | 3.32 | 3.24 | 0.028 |
| Invariant Mass $< 300$ GeV | 0.55 | 0.36 | 0.00051 |
| $65 < M_{jj} < 95$ | 0.49 | 0.14 | 0.000085 |
| events/30 fb$^{-1}$ (before cuts) | 5.3$\times 10^5$ | 7.2$\times 10^6$ | 1.2$\times 10^8$ |
| events/30 fb$^{-1}$ (after cuts) | $2608 \pm 166$ | $10616 \pm 625$ | $102 \pm 59$ |

measure the spin. This has been dubbed the "spectator basis" [130]. The polarisation of the top quark in this basis (defined as $P = (N_\uparrow - N_\downarrow)/(N_\uparrow + N_\downarrow)$) is $0.89$. However, the polarisation is increased to nearly $100\%$ when the cuts used in the $t$-channel analysis are imposed. This is because the polarisation is diluted by events in which the $\bar{b}$ is produced at high $p_T$; but such events are eliminated by the requirement of only two jets.

In the case of $\bar{t}$ production, $69\%$ of the events have the $d$-type quark in the initial state. This suggests using the beam direction to measure the $\bar{t}$ spin. However, it turns out that the spectator basis again yields the largest polarisation, $P = -0.87$. This polarisation is increased to $P = -0.96$ when cuts are applied.[18]

Since the top quark decays via the weak interaction, its spin is analysed by the angular distribution of its decay products. The most sensitive spin analyser in top decay is the charged lepton, which has a (leading order) angular distribution with respect to the top quark spin of

$$\frac{1}{\Gamma}\frac{d\Gamma}{d\cos\theta_\ell} = \frac{1}{2}(1 + \cos\theta_\ell) \tag{12}$$

in the top quark rest frame [158]. Hence the charged lepton tends to point along the direction of the spectator jet.

### *5.42 Phenomenology*

The goal of this analysis is to estimate the sensitivity of ATLAS and CMS to the measurement of the polarisation of the top quarks produced by the $t$-channel single-top process. The $t$-channel process was chosen due to the large statistics available in this channel and the relative ease with which it is separated from its backgrounds. The $t$-channel events produced by the ONETOP generator and passed through PYTHIA and a parameterised detector simulation are analysed to attempt to recover the predicted SM top polarisation in the presence of background and detector effects. Details of the study are presented in [152, 154].

[18] With cuts applied, the polarisation in the so-called "$\eta$-beamline basis" is slightly higher, $P = -0.97$.

The experimental measurement of the polarisation of the top quark is essentially a measurement of the angular distribution of its decay products in the top quark rest frame. As explained above, the most sensitive angle is between the charged lepton from top decay and the direction of the spectator jet, in the top quark rest frame. In the absence of background or detector effects the angular distribution of the charged lepton is given by

$$f(\cos\theta_\ell) = \frac{1}{2}(1 + P\cos\theta_\ell) \tag{13}$$

where $P$ is the polarisation of the sample and can range from $-1$ to $1$.

Experimentally, in order to measure the angular distribution of the charged lepton in the top quark rest frame, it is necessary to first reconstruct the four-momentum of the top quark. However, the reconstruction of the top four-momentum suffers from an ambiguity due to the unknown longitudinal momentum of the neutrino produced in the top decay. Using the $W$ and top masses as constraints,[19] one can reconstruct the top four-momentum, but the quality of the reconstruction is degraded by this ambiguity. Once the top four-momentum has been reconstructed, one can determine the direction of the spectator jet and the charged lepton in the top quark rest frame. The angle between these two directions is $\theta_\ell$.

In order to extract the value of the top polarisation from the angular distribution, reference event samples were created with 100% alignment with the polarisation axis (spin up, $P = +1$) and with 100% anti-alignment with the polarisation axis (spin down, $P = -1$). These reference distributions were compared to a statistically-independent data set with the predicted SM top quark polarisation. This comparison was done by minimising

$$\chi^2 = \sum_{(\cos\theta)_i} \frac{(f_{\rm th}(\cos\theta_\ell)_i - f_{\rm d}(\cos\theta_\ell)_i)^2}{\sigma^2_{{\rm th}_i} + \sigma^2_{{\rm d}_i}} \tag{14}$$

where the subscript d represents quantities calculated for the data distribution and the subscript th refers to the generated reference distribution. The theoretical value $f_{\rm th}(\cos\theta_\ell)$ is calculated via

$$f_{\rm th}(\cos\theta_\ell) = \frac{1}{2}((1-P)f_D(\cos\theta_\ell) + (1+P)f_U(\cos\theta_\ell)) \tag{15}$$

where $f_D$ and $f_U$ refer to the value of the generated theoretical distribution for the 100% spin-down and the 100% spin-up tops, respectively, and $P$ is the polarisation of the top sample. The procedure returns an estimate of the top polarisation and an error on that estimate. In this way the sensitivity to changes in top polarisation can be quantified.

Moving from the parton-level simulation to a simulation which includes both hadronisation and detector effects is certain to complicate the measurement of the polarisation of the top quark. In addition, the signal could be biased by an event selection designed to eliminate background and will be contaminated by residual background events.

The first histogram in Fig. 31 shows the angular distribution for signal only, at parton-level. The second histogram in Fig. 31 shows the angular distribution of the charged lepton after detector effects have been simulated. In addition to effects associated with detector energy smearing, jet and cluster definitions, *etc.*, this distribution includes the effects of ambiguities in reconstructing the top quark due to the absence of information about the neutrino longitudinal momentum. It does not, however, contain the effects of any event selection in order to separate signal from background. This histogram demonstrates that the effect of hadronisation and detector resolution changes the shape of the angular distribution but still produces a highly asymmetric distribution.

In addition to the effects introduced by the detector resolution, the effect of applying the event-selection criteria can be evaluated by applying them one at a time and observing the change in shape of this distribution. For the purposes of the polarisation analysis the event-selection criteria are:

[19] The $W$ mass can be used to calculate the neutrino longitudinal momentum to within a two-fold ambiguity. Of these two solutions the one which produces the best top mass is chosen.

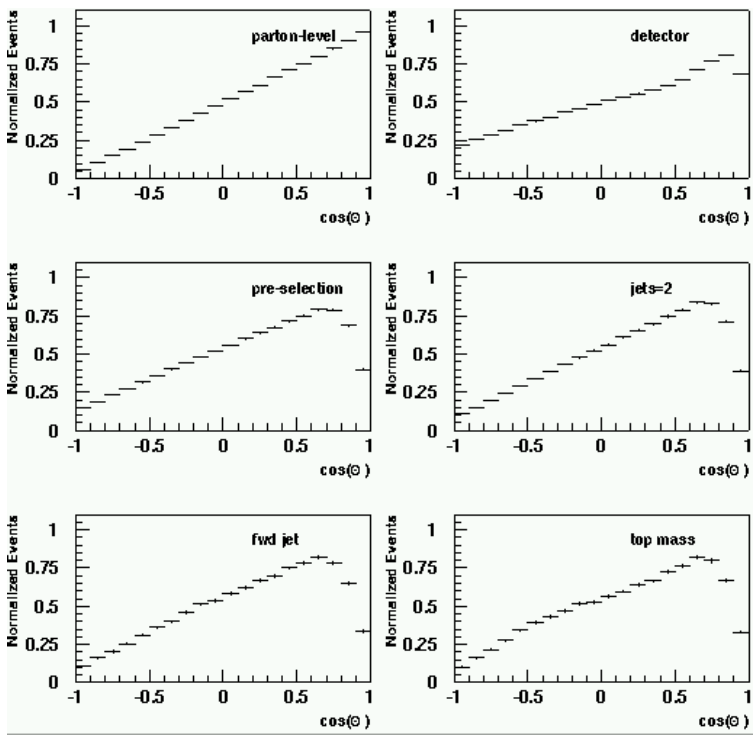


Fig. 31: Angular distribution of charged lepton in top rest frame for various data samples. The histograms progress from left-to-right, top-to-bottom. The first histogram shows the parton-level distribution. The second histogram is after the simulation of detector and reconstruction effects. The final four histograms illustrate the influence of event selection criteria on the angular distribution. The effects of the cuts are cumulative and are the result of adding pre-selection cuts, a jet-multiplicity requirement, a forward jet tag, and a top mass window, respectively.

- Pre-selection (trigger) cuts as in ATLAS $t$-channel analysis described previously;
- number of jets = 2;
- forward jet ($|\eta| > 2.5$) with $p_T > 50$ GeV;
- reconstructed top mass in the range 150–200 GeV.

This set of criteria leads to a signal efficiency of 3.0%, corresponding to more than 16000 events in 10 fb$^{-1}$ of integrated luminosity. Fig. 31 demonstrates the effect of applying these cuts in a cumulative manner. Again the asymmetry of the $t$-channel angular distribution is preserved, though more degradation is clearly evident, in particular near $\cos\theta_\ell = 1$. The degradation is worse at these values of $\cos\theta_\ell$ because the leptons from these events are emitted in the direction opposite to the top boost. This reduces the momentum of the leptons causing more of them to fail $p_T$-based selection criteria.

Since $W+$ jet events dominate the background remaining after cuts, they are taken as the only background in this analysis. Fig. 32 shows the cumulative effect of cuts on the angular distribution of the charged lepton from $W+$ jets events. A peculiar feature of these events is evident in all of these distributions. This is the tendency for events to be grouped near $\cos\theta_\ell = 1$. The events which populate this region tend to be the highest $p_T$ events. This shows that even basic jet and isolated-lepton definitions and pre-selection cuts bias the angular distribution of $W+$ jets events.

When the event-selection criteria described in the previous sections are applied, the signal-to-background ratio (treating $W+$ jets as the only background) is found to be 2.6. Using the methods described earlier it is possible to estimate the polarisation of a mixed sample of $t$-channel signal and $W+$ jets background. The reference distributions for 100% spin-down and 100% spin-up top quarks mixed with background in a ratio of 2.6 are shown in Fig. 33. Also shown is the angular distribution corresponding to a statistically-independent data sample with SM polarisation mixed with background

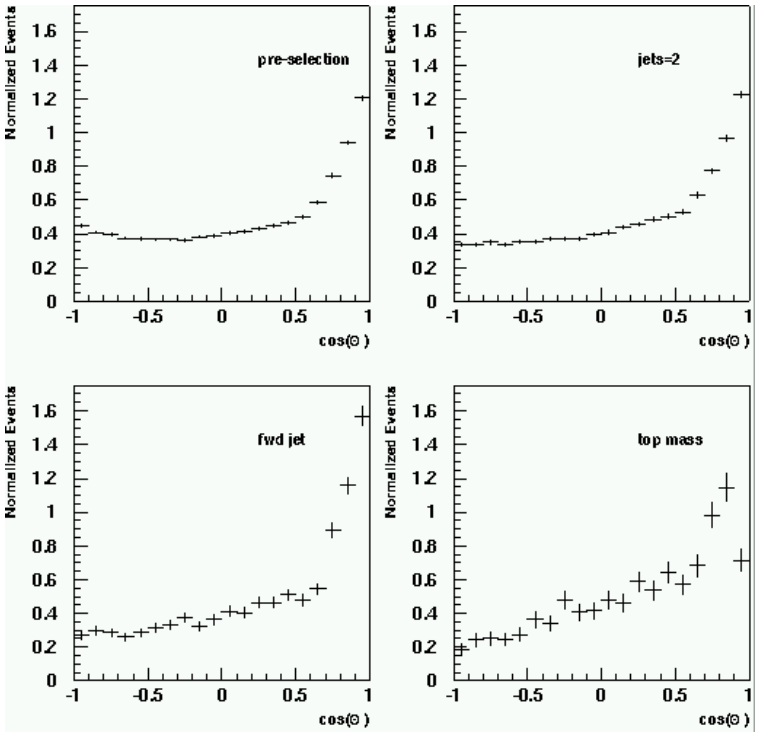


Fig. 32: The effect of event selection cuts on the angular distribution of the charged lepton in $Wjj$ events. The effects of the cuts are cumulative. The first distribution is the result of applying the pre-selection (trigger) cuts only. Further cuts are applied cumulatively from left-to-right, top-to-bottom.

in the ratio 2.6. The $\chi^2$ function presented in (14) is minimised to obtain an estimate of the polarisation of the top. To estimate the precision for one year of data-taking, the fit was done with 3456 signal events and 1345 background events, corresponding to 2 fb$^{-1}$ of integrated luminosity ($\sim$ 1/5 of a year). For this integrated luminosity the error on the polarisation measurement is 4.0%. Then, assuming the statistics on the reference distributions, $f_D(\cos\theta_\ell)$ and $f_U(\cos\theta_\ell)$, will lead to a negligible source of error, this precision improves to 3.5%. Projecting these results to one year of data-taking at low luminosity (10 fb$^{-1}$), assuming that the errors scale as the square root of the number of events, yields a predicted statistical precision of 1.6% on the measurement of the top polarisation.

### 5.5 Conclusions on single top production

As mentioned in the introduction, single-top quark production is the only known way to directly measure $V_{tb}$ at a hadron collider. In this section we estimate the accuracy with which $V_{tb}$ can be extracted at the LHC, and discuss what will be required to achieve that accuracy.

There are four sources of uncertainty in the extraction of $|V_{tb}|^2$ from the single-top cross section: theoretical, experimental, statistical, and machine luminosity. As we have seen, the statistical uncertainty with 30 fb$^{-1}$ of integrated luminosity is less than $2\%$ for both the $t$-channel process[20] and associated production, and is $5.5\%$ for the $s$-channel process ($3\%$ with 100 fb$^{-1}$). It will be a challenge to reduce the other sources of uncertainty to $5\%$, so we regard the statistical accuracy as being sufficient in all three processes.

The traditional uncertainty in the machine luminosity is about $5\%$ [159]. It may be possible to reduce the uncertainty below this value using Drell-Yan data, but this relies on accurate knowledge of the quark distribution functions. However, the process $q\bar{q}\to W^*\to\ell\bar{\nu}$ involves the identical combination

[20]Only 10 fb$^{-1}$ are required to achieve this accuracy in the $t$-channel process.

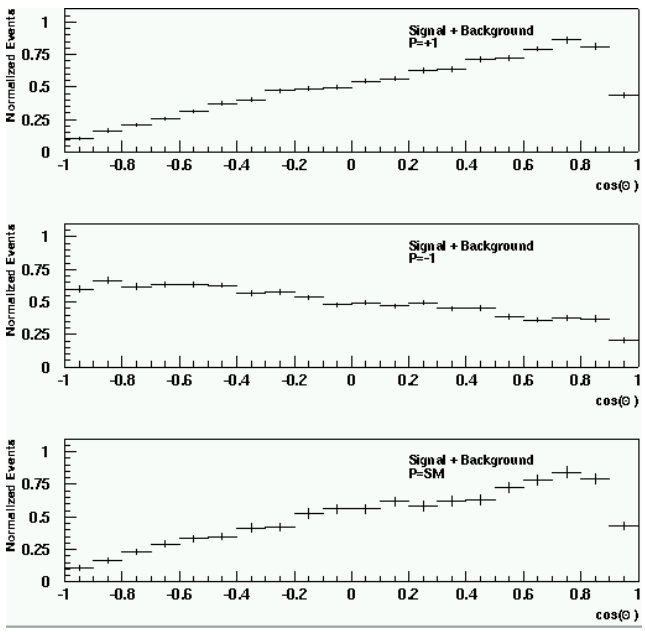


Fig. 33: The first histogram shows the reference distribution for 100% spin-up top quarks after detector effects and event-selection criteria have been applied and the appropriate level of background has been mixed in. The second histogram shows the reference distribution for 100% spin-down top quarks. The third histogram represents the expected SM distribution for a statistically-independent sample of signal and background.

of parton distribution functions as the $s$-channel process, so it can be used to almost directly measure the relevant parton luminosity, thereby avoiding the need to measure the machine luminosity [156].

The theoretical uncertainty is under the best control in the $s$-channel process. The theoretical uncertainty is dominated by the uncertainty in the top quark mass; an uncertainty of 2 GeV yields an uncertainty of $5\%$. This is cut in half if the uncertainty in the top mass is reduced to 1 GeV. The small uncertainty due to variation of the factorisation and renormalisation scales can be reduced to a negligible amount by calculating the cross section at NNLO order, which should be possible in the near future. The small uncertainty from the parton distribution functions can be further reduced as described in the previous paragraph; this also obviates the need for a measurement of the machine luminosity.

The theoretical uncertainty in the $t$-channel process is presently dominated by the factorisation-scale dependence and the parton luminosity. Although the scale dependence of the total cross section is small ($4\%$), the uncertainty in the semi-inclusive cross section ($\sigma(p_{T\bar{b}}) < 20$ GeV) is about $10\%$. This can be reduced by calculating the $p_T$ spectrum of the $\bar{b}$ at NLO. It may also prove possible to measure the total cross section, although this has yet to be demonstrated. It is therefore plausible that the factorisation-scale dependence will be about $5\%$ once the LHC is operating. It is also likely that the uncertainty from the parton distribution functions will be reduced below its present value of $10\%$. The parton luminosity could be directly measured using $Wj$ production, which is dominated by $gq \rightarrow Wq$, and therefore involves the identical combination of parton distribution functions as the $t$-channel process. Again, this has the desirable feature of eliminating the need to measure the machine luminosity.

The theoretical uncertainty in the associated-production cross section can be reduced far below its present value of $18\%$. A full NLO calculation should reduce the factorisation-scale dependence to roughly $5\%$. It is likely that the uncertainty from the parton distribution functions will also be reduced. Unless it is possible to measure the $gg$ luminosity directly, the uncertainty from the parton distribution functions will be augmented by the uncertainty in the machine luminosity.

As far as experimental systematic uncertainties are concerned, the extraction of a signal cross section requires knowledge of the backgrounds and of the efficiency and acceptance for the signal. These

analyses require hard cuts on both signal and background, and so the processes need to be modelled and understood very well.

For all of these processes, the major backgrounds are $t\bar{t}$ and $W+$ jets. The largest background for the $s$-channel process (where a double $b$-tag is employed) and associated production is $t\bar{t}$. The $t\bar{t}$ process can be isolated in other decay modes and in principle well measured. In the $t$-channel process the biggest background comes from $Wcj$ with the charm jet mistagged as a $b$-jet. Obviously it would be worthwhile to develop a $b$-tagging algorithm having greater rejection against such mistags, even at the cost of some signal efficiency, given that the signal rate is large. It may be possible to understand the $W+$jets backgrounds by comparing with a sample of $Z+$ jets events after applying similar selections to those used to select the single-top sample in $W+$ jets. The $Z+$ charm rate will be suppressed compared to the $W+$ charm rate since the latter is mostly produced from the strange sea, which is bigger than the charm sea; nonetheless, the cross section, kinematics, jet multiplicities and so on can all be compared to our simulations using the $Z+$ jets sample.

The forward jet tag is very effective in enhancing the signal-to-background ratio in the $t$-channel process. This means that jets need to be found with good efficiency up to large rapidities, at least $|\eta| \sim 4$ in the calorimeter. Unfortunately these observations also imply that the background estimate is very sensitive to the Monte Carlo predicting the correct mix of jet flavours and jet rapidities in the $W+$ jets events. (We note that VECBOS generates very few jets in the tagging region, and so far there is no collider data on forward jets in vector-boson events which could verify whether this is correct.) Of course, effort applied to understanding $W+$ heavy-flavour jets backgrounds will pay off in many other searches besides this one, and will be a very worthwhile investment. We also look forward to the results of ongoing efforts to improve the Monte Carlo simulation of vector-boson plus jet production [160]. Requiring exactly two jets (as was done here to reject the $t\bar{t}$ background) also means that we will be very sensitive to our knowledge of jet efficiencies, QCD radiation, *etc*. The cross-section measurement also requires knowledge of the $b$-tagging efficiency. This should be measurable at the few-percent level using control samples of $t\bar{t}$ events selected with kinematic cuts alone.

As mentioned above, the purely statistical uncertainty in the cross-section measurement will be less than 5%, as will most of the theoretical uncertainties. It will be a considerable challenge to reduce the experimental systematic uncertainty to this level. At the present time, the experimental systematic uncertainty in the $t\bar{t}$ cross section at the Tevatron (which is a similar challenge in many respects, involving jets, $b$-tagging, and background subtraction) is about $19\%$ [10]. This total is made up of many components which are each at the 5% level, so while it will be a lot of work to reduce them, there is no obvious "brick wall" that would prevent this.

Many of these systematic issues can also be addressed by comparing the $t$-channel and $s$-channel single-top processes. It will be a powerful tool to be able to measure $V_{tb}$ in two channels which have different dominant backgrounds, different selection cuts, and a different balance between theoretical and experimental systematic uncertainties.

We are only just now entering the era of precision top physics with Run II at the Tevatron. Single-top production has not yet even been observed. We will learn a great deal over the next few years about how to model top events and their backgrounds, and how to understand the systematic uncertainties. The LHC will undoubtedly benefit from all this experience.

If all sources of uncertainty are kept to the $5\%$ level or less, it should be possible to measure $|V_{tb}|^2$ to $10\%$ or less. We therefore regard the measurement of $V_{tb}$ with an accuracy of $5\%$ or less as an ambitious but attainable goal at the LHC. We have also seen that a measurement of the polarisation of single top quarks produced via the $t$-channel process will be possible with a statistical accuracy of $1.6\%$ with 10 fb$^{-1}$. We have not attempted to estimate the systematic uncertainty in this measurement.

## 6. $t\bar{t}$ SPIN CORRELATIONS AND CP VIOLATION[21]

For $t\bar{t}$ production at the LHC quantities associated with the spins of the top and antitop quark will be "good" observables as well. The reason for this is well known. Because of its extremely short lifetime $\tau_t$ (see Section 2.1) the top quark decays before it can form hadronic bound states. Thus the information on the spin of the top quark does not get diluted. As the spin-flip time is much larger than $\tau_t$ it is, moreover, very unlikely that the top quark changes its spin-state by emitting gluon(s) via a chromomagnetic dipole transition before it decays. In any case this amplitude is calculable with QCD perturbation theory. Hence by measuring the angular distributions and correlations of the decay products of $t$ and $\bar{t}$ the spin-polarisations and the spin-spin correlations that were imprinted upon the $t\bar{t}$ sample by the production mechanism can be determined and compared with predictions made within the SM or its extensions. Therefore these spin phenomena are an additional important means to study the fundamental interactions involving the top quark.

In this section we are concerned with the production and decay of top-antitop pairs. At the LHC the main $t\bar{t}$ production process is gluon-gluon fusion, $q\bar{q}$ annihilation being sub-dominant. As the main SM decay mode is $t \to W^+ b$ we shall consider here the parton reactions

$$gg, q\bar{q} \to t\bar{t} + X \to b\bar{b} + 4f + X, \tag{16}$$

where $f$ denotes either a quark, a charged lepton or a neutrino. If the final state in (16) contains two, one, or no high $p_T$ charged lepton(s) then we call these reactions, as usual, the di-lepton, single lepton, and non-leptonic $t\bar{t}$ decay channels, respectively. To lowest order QCD the matrix elements for (16), including the complete $t\bar{t}$ spin correlations and the effects of the finite top and $W$ widths, were given in [161, 162]. Spin correlation effects in $t\bar{t}$ production in hadron collisions were studied within the SM in [162, 163, 164, 165, 166, 167, 168].

In order to discuss the top spin-polarisation and correlation phenomena that are to be expected at the LHC it is useful to employ the narrow-width approximation for the $t$ and $\bar{t}$ quarks. Because $\Gamma_t/m_t \ll 1$ one can write, to good approximation, the squares of the exact Born matrix elements $\mathcal{M}^{(\lambda)}$, $\lambda = gg, q\bar{q}$, in the form

$$|\mathcal{M}^{(\lambda)}|^2 \propto \mathrm{Tr}\,[\rho R^{(\lambda)} \bar{\rho}] \equiv \rho_{\alpha'\alpha} R^{(\lambda)}_{\alpha\alpha',\beta\beta'} \bar{\rho}_{\beta'\beta}. \tag{17}$$

The complete spin information is contained in the (unnormalised) spin density matrices $R^{(\lambda)}$ for the production of on-shell $t\bar{t}$ pairs and in the density matrices $\rho, \bar{\rho}$ for the decay of polarised $t$ and $\bar{t}$ quarks into the above final states. The trace in (17) is to be taken in the $t$ and $\bar{t}$ spin spaces. The decay density matrices will be discussed below. The matrix structure of $R^{(\lambda)}$ is

$$R^{(\lambda)}_{\alpha\alpha',\beta\beta'} = A^{(\lambda)} \delta_{\alpha\alpha'} \delta_{\beta\beta'} + B^{(\lambda)}_i (\sigma^i)_{\alpha\alpha'} \delta_{\beta\beta'} + \bar{B}^{(\lambda)}_i \delta_{\alpha\alpha'} (\sigma^i)_{\beta\beta'} + C^{(\lambda)}_{ij} (\sigma^i)_{\alpha\alpha'} (\sigma^j)_{\beta\beta'}\,, \tag{18}$$

where $\sigma^i$ are the Pauli matrices. Using rotational invariance the "structure functions" $B^{(\lambda)}_i, \bar{B}^{(\lambda)}_i$ and $C^{(\lambda)}_{ij}$ can be further decomposed. A general discussion of the symmetry properties of these functions is given in [169]. The function $A^{(\lambda)}$, which determines the $t\bar{t}$ cross section, is known in QCD at NLO [38]. Because of parity (P) invariance the vectors $\mathbf{B}^{(\lambda)}, \bar{\mathbf{B}}^{(\lambda)}$ can have, within QCD, only a component normal to the scattering plane. This component, which amounts to a normal polarisation of the $t$ quark, $\mathcal{P}^t_\perp$, is induced by the absorptive part of the respective scattering amplitude and was computed for the above LHC processes to order $\alpha_s^3$ [170]. ($\mathcal{P}^t_\perp = \mathcal{P}^{\bar{t}}_\perp$ if CP invariance holds.) The size of the normal polarisation depends on the top quark scattering angle and on the c.m. energy. In the gluon-gluon fusion process $\mathcal{P}^t_\perp$ reaches peak values of about 1.5%. In $t\bar{t}$ production at the LHC the polarisation of the top quark within the partonic scattering plane, which is P-violating, is small as well within the SM. Therefore the $t$ and $\bar{t}$ polarisations in the scattering plane are good observables to search for P-violating non-SM interactions in the reactions (16) – see Section 3.4.

[21] Section coordinators: W. Bernreuther, A. Brandenburg, V. Simak (ATLAS), L. Sonnenschein (CMS).

The $t\bar{t}$ production by the strong interactions leads, on the other hand, to a significant correlation between the $t$ and $\bar{t}$ spins. This correlation is encoded in the functions $C_{ij}^{(\lambda)}$. Using P- and charge-conjugation (C) invariance they have, in the case of a $t\bar{t}$ final state, the structure

$$C_{ij}^{(\lambda)} = c_1^{(\lambda)}\delta_{ij} + c_2^{(\lambda)}\hat{p}_i\hat{p}_j + c_3^{(\lambda)}\hat{k}_{ti}\hat{k}_{tj} + c_4^{(\lambda)}(\hat{k}_{ti}\hat{p}_j + \hat{p}_i\hat{k}_{tj}), \tag{19}$$

where $\hat{\mathbf{p}}$ and $\hat{\mathbf{k}}_t$ are the directions of flight of the initial quark or gluon and of the $t$ quark, respectively, in the parton c.m. frame. So far the functions $c_r^{(\lambda)}$ are known to lowest-order QCD only (see, e.g., [164]). For a $t\bar{t}X$ final state a decomposition similar to (19) can be made.

From (19) one may read off the following set of spin-correlation observables [164]:

$$(\hat{\mathbf{k}}_t \cdot \mathbf{s}_t)(\hat{\mathbf{k}}_{\bar{t}} \cdot \mathbf{s}_{\bar{t}}), \tag{20}$$

$$(\hat{\mathbf{p}} \cdot \mathbf{s}_t)(\hat{\mathbf{p}} \cdot \mathbf{s}_{\bar{t}}), \tag{21}$$

$$\mathbf{s}_t \cdot \mathbf{s}_{\bar{t}}, \tag{22}$$

$$(\hat{\mathbf{p}} \cdot \mathbf{s}_t)(\hat{\mathbf{k}}_{\bar{t}} \cdot \mathbf{s}_{\bar{t}}) + (\hat{\mathbf{p}} \cdot \mathbf{s}_{\bar{t}})(\hat{\mathbf{k}}_t \cdot \mathbf{s}_t), \tag{23}$$

where $\mathbf{s}_t, \mathbf{s}_{\bar{t}}$ are the $t$ and $\bar{t}$ spin operators, respectively. The observables (20), (21), and (23) determine the correlations of different $t, \bar{t}$ spin projections. Eq. (20) corresponds to a correlation of the $t$ and $\bar{t}$ spins in the helicity basis, while (21) correlates the spins projected along the beam line. We note that the "beam-line basis" defined in [166] refers to spin axes being parallel to the left- and right-moving beams in the $t$ and $\bar{t}$ rest frames, respectively. The $t\bar{t}$ spin correlation in this basis is a linear combination of (20), (21), and (23).

A natural question is: what is – assuming only SM interactions – the best spin basis or, equivalently, the best observable for investigating the $t\bar{t}$ spin correlations? For quark-antiquark annihilation, which is the dominant production process at the Tevatron, it turns out that the spin correlation (21) [164, 168] and the correlation in the beam-line basis [166] is stronger than the correlation in the helicity basis. In fact, for $\bar{q}q$ annihilation a spin-quantisation axis was constructed in [167] with respect to which the $t$ and $\bar{t}$ spins are 100% correlated. At the LHC the situation is different. For $gg\to t\bar{t}$ at threshold conservation of total angular momentum dictates that the $t\bar{t}$ is in a ${}^1S_0$ state. Choosing spin axes parallel to the right- and left-moving beams this means that we have $t_L\bar{t}_L$ and $t_R\bar{t}_R$ states at threshold. On the other hand at very high energies helicity conservation leads to the dominant production of unlike helicity pairs $t_R\bar{t}_L$ and $t_L\bar{t}_R$. One can show that no spin quantisation axis exists for $gg\to t\bar{t}$ with respect to which the $t$ and $\bar{t}$ spins are 100% correlated. The helicity basis is a good choice, but one can do better. This is reflected in the above observables. Computing their expectation values and statistical fluctuations one finds [164] that (22) has a higher statistical significance than the helicity correlation (20) which in turn is more sensitive than (21) or the correlation in the beam-line basis.

The spins of the $t$ and $\bar{t}$ quarks are to be inferred from their P-violating weak decays, i.e., from $t\to bW^+\to b\ell^+\nu_\ell$ or $bq\bar{q}'$ and likewise for $\bar{t}$ if only SM interactions are relevant. As already mentioned and used in previous sections, in this case the charged lepton from $W$ decay is the best analyser of the top spin. This is seen by considering the decay distribution of an ensemble of polarised $t$ quarks decaying into a particle $f$ (plus anything) with respect to the angle between the polarisation vector $\xi_t$ of the top quark and the direction of flight $\hat{\mathbf{q}}_f$ of the particle $f$ in the $t$ rest frame. This distribution has the generic form

$$\frac{1}{\Gamma}\frac{d\Gamma}{d\cos\theta_f} = \frac{1}{2}(1 + \kappa_f \xi_t \cdot \hat{\mathbf{q}}_f), \tag{24}$$

where the magnitude of the coefficient $\kappa_f$ signifies the spin-analyser quality of $f$. The SM values for some $f$, collected from [171, 172, 173, 174], are given in Table 12. The corresponding $t$ decay density matrix in the $t$ rest frame is read off from (24) to be $\rho_{\alpha'\alpha} = (\mathbb{1} + \kappa_f\, \boldsymbol{\sigma} \cdot \hat{\mathbf{q}}_f)_{\alpha'\alpha}$. The distributions for

Table 12: Correlation coefficient $\kappa_f$ for $V-A$ charged current. In the last column l.e.j. stands for least energetic jet in the $t$ rest frame.

| $f$ | $\ell^+, \bar{d}, \bar{s}$ | $\nu_\ell, u, c$ | $b$ | $W^+$ | l.e.j. from $q\bar{q}'$ |
|---|---|---|---|---|---|
| $\kappa_f$ | 1 | $-0.31$ | $-0.41$ | 0.41 | 0.51 |

the decay of polarised antitop quarks are obtained by replacing $\kappa_f \to -\kappa_f$ in (24). The order $\alpha_s$ QCD corrections to the decays $t \to b\ell\nu$ and $t \to Wb$ of polarised $t$ quarks were computed in [171] and [175], respectively. For $t, \bar{t}$ polarisation observables these corrections are small.

From the above table it is clear that the best way to analyse the $t\bar{t}$ spin correlations is through angular correlations among the two charged leptons $\ell^+\ell'^-$ in the di-lepton final state. Using the production and decay density matrices in (17), neglecting the 1-loop induced QCD normal polarisation, and integrating over the azimuthal angles of the charged leptons one obtains the following normalised double distribution, e.g. in the helicity basis

$$\frac{1}{\sigma}\frac{d^2\sigma}{d\cos\theta_+ d\cos\theta_-} = \frac{1 + C\kappa_{\ell^+}\kappa_{\ell^-}\cos\theta_+\cos\theta_-}{4} \ , \tag{25}$$

where $\kappa_{\ell^+}\kappa_{\ell^-} = -1$ and $\theta_+(\theta_-)$ is the angle between the $t(\bar{t})$ direction in the $t\bar{t}$ c.m. frame and the $\ell^+(\ell^-)$ direction of flight in the $t(\bar{t})$ rest frame. The coefficient $C$, which is the degree of the spin correlation in the helicity basis, results from the $c_i^{(\lambda)}$ in (19) and it is related to [165]:

$$C = \frac{N(t_L\bar{t}_L + t_R\bar{t}_R) - N(t_L\bar{t}_R + t_R\bar{t}_L)}{N(t_L\bar{t}_L + t_R\bar{t}_R) + N(t_L\bar{t}_R + t_R\bar{t}_L)} \ . \tag{26}$$

For partonic final states and to lowest order in $\alpha_s$ one gets $C = 0.332$ for the LHC. (The number depends somewhat on the parton distributions used. Here and below the set CTEQ4L [116] was used.) The optimum would be to find a spin axis with respect to which $|C| = 1$. But, as stated above, this is not possible for $gg$ fusion. In addition to (25), analogous correlations among $\ell^+$ from $t$ and jets from $\bar{t}$ decay (and vice-versa) in the single lepton channels, and jet-jet correlations in the non-leptonic decay channels should, of course, also be studied. While the spin-analysing power is lower in these cases, one gains in statistics.

From the above example is quite obvious that, for a given $t\bar{t}$ decay channel, the $t\bar{t}$ spin correlation will be most visible when the angular correlations among the $t$ and $\bar{t}$ decay products are exhibited in terms of variables defined in the $t$ and $\bar{t}$ rest frames. An important question is therefore how well the 4-momenta of the $t$ and $\bar{t}$ quarks can be reconstructed experimentally? We briefly discuss the results of a simulation of the single lepton and di-lepton channels [176] which includes hadronisation and detector effects using PYTHIA [52] and the ATLFAST [105] software packages. The transverse momentum of every reconstructed object like a jet, a charged lepton, or the missing transverse energy of an event has to exceed a certain minimum value $p_T^{min}$. The detector acceptances impose further restrictions on the phase space of the detected objects in pseudo-rapidity.

In the case of the single lepton $t\bar{t}$ decay channels one isolated lepton ($e^\pm$ or $\mu^\pm$) is required. From the missing transverse energy of the event and the $W$ mass constraint the longitudinal momentum $p_z$ of the neutrino can be determined up to a twofold ambiguity. It turns out that in most cases the lower solution of $p_z$ is the correct one. To complete the event topology, four jets are demanded. Two of them have to be identified as $b$-jets coming from top decay.

The two non-tagged jets are often misidentified due to additional activity in the detector from initial and final state radiation. To suppress the QCD background the invariant mass of the two jets has to lie in a narrow mass window around the known mass of the $W$ boson. After this cut the two-jet system is rescaled to the $W$ mass. Finally there is a twofold ambiguity when the $b$-jets are combined with the reconstructed $W$ bosons. The combination which yields the lower reconstructed top mass turns out to be the correct one most of the time.

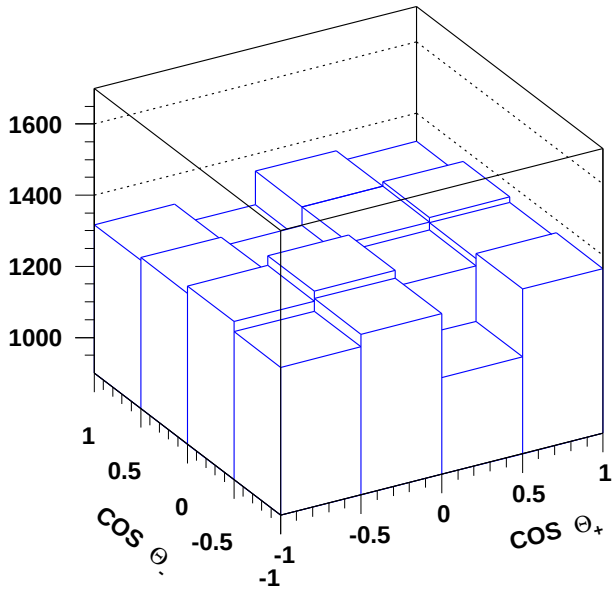


Fig. 34: Joint distribution $d^2N/d\cos\theta_+ d\cos\theta_-$ generated with default PYTHIA. The detector response was simulated with CMSJET.

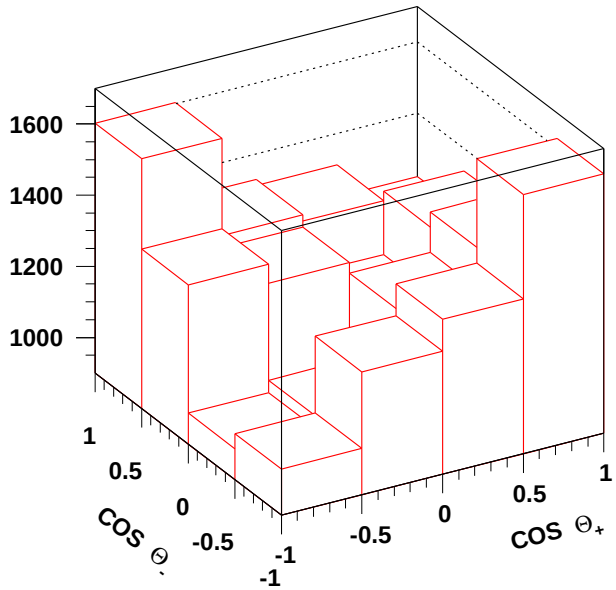


Fig. 35: Same distribution as in the figure to the left, but including the SM $t\bar{t}$ spin correlations. The detector response was simulated with CMSJET.

In the case of the di-lepton decay channels two isolated oppositely charged leptons are requested. Moreover two jets have to be detected and tagged as $b$-jets. With the known top and $W$ masses and with the missing transverse energy of the event the unknown 3-momenta of the neutrino and anti-neutrino can be computed using the kinematic constraints of the event. These result in a system of two linear and four quadratic equations. The equations can be solved numerically and usually several solutions arise. Since the experimentally determined momenta do not coincide with the corresponding variables at the parton level the kinematic constraints have to be relaxed somewhat in order to improve the reconstruction efficiency. The algorithm set up in [176] was used to solve these equations. The best solution can be obtained by computing weights from known distributions. Following [176] the highest efficiency was obtained using the weight given by the product of the energy distributions of $\nu_\ell$ and $\bar{\nu}_\ell$ and the $\cos\theta_t^*$ distribution in the $t\bar{t}$ c.m. frame.

For the LHC running at low luminosity ($\mathcal{L} = 10^{33}\,\mathrm{cm}^{-2}\mathrm{s}^{-1}$), about $4 \times 10^5$ $t\bar{t}$ events per year are expected in the di-lepton decay channels ($\ell = e, \mu$). A further simulation of these channels was performed in order to study the joint distribution (25). PYTHIA 5.7 [52] was used for the event generation, CMSJET [177] for the detector response and the algorithm of [176] for the reconstruction of the $t, \bar{t}$ momenta. The transverse momenta of the two isolated, oppositely charged leptons and of the two jets were required to exceed $20\,\mathrm{GeV}$. The minimal missing transverse energy of the event was chosen to be $40\,\mathrm{GeV}$. A further selection criterion was that each jet provides at least two tracks with a significance of the transverse impact parameter above $3.0$ to be tagged as $b$-jet. The processes were simulated in two different ways. First the SM matrix elements of [75] for the reactions (16), which contain the $t\bar{t}$ spin correlations, were implemented into PYTHIA. For comparison these channels were also simulated with the PYTHIA default matrix elements for $gg, q\bar{q}\to t\bar{t}$ which do not contain spin correlations. In both simulations initial and final state radiation, multiple interactions, and the detector response was included. In Figs. 34, 35 we have plotted the resulting double distributions $d^2N/d\cos\theta_+ d\cos\theta_-$. They have been corrected for the distortions of the phase space due to the cuts. A fit to the distribution Fig. 35 according to (25) yields the correlation coefficient $C = 0.331 \pm 0.023$, in agreement with the value $C = 0.332$ obtained at the parton level without cuts. A fit to Fig. 34 leads to $C = -0.021 \pm 0.022$ consistent with $C = 0$. Systematic errors, for instance due to background processes, e.g., $Z^*\to\ell^+\ell^-$ accompanied by two $b$-jets, remain to be investigated.

From these double distributions one may form one- or zero-dimensional projections, for instance asymmetries as considered in [166, 165, 168]. Another approach is to study distributions and expectation values of angular correlation observables which would be zero in the absence of the $t\bar{t}$ spin correlations. A suitable set of observables is obtained by transcribing, for instance, the spin observables given above into correlations involving the directions of flight of those final state particles that are used to analyse the $t$ and $\bar{t}$ spins. As an example we discuss the case of the single lepton channels $t \to bq\bar{q}', \bar{t} \to \bar{b}\ell^-\bar{\nu}_\ell$. One may choose to analyse the $t$ spin by the direction of flight $\hat{\mathbf{q}}_b^*$ of the $b$-jet in the rest frame of the $t$ quark and the $\bar{t}$ spin by the momentum direction $\hat{\mathbf{q}}_-$ of the $\ell^-$ in the laboratory frame. The latter is rather conservative in that no reconstruction of the $\bar{t}$ momentum is necessary. Then (20)-(22) are translated into the observables

$$\mathcal{O}_1 = (\hat{\mathbf{q}}_b^* \cdot \hat{\mathbf{p}}_p)(\hat{\mathbf{q}}_- \cdot \hat{\mathbf{p}}_p), \tag{27}$$

$$\mathcal{O}_2 = (\hat{\mathbf{q}}_b^* \cdot \hat{\mathbf{k}}_t)(\hat{\mathbf{q}}_- \cdot \hat{\mathbf{k}}_t), \tag{28}$$

$$\mathcal{O}_3 = \hat{\mathbf{q}}_b^* \cdot \hat{\mathbf{q}}_-, \tag{29}$$

where $\hat{\mathbf{p}}_p$ refers to the beam direction. The pattern of statistical sensitivities of the spin observables (20)-(22) stated above is present also in these angular correlations. Computing the expectation values $\langle \mathcal{O}_i \rangle$ and the statistical fluctuations $\Delta\mathcal{O}_i$ and those of the observables for the corresponding charge conjugated channels, one gets for the statistical significances of these observables at the parton level [164]: $\mathcal{S}_1 \approx 0.007\sqrt{N_{b\ell^-}}$, $\mathcal{S}_2 \approx 0.025\sqrt{N_{b\ell^-}}$, and $\mathcal{S}_3 \approx 0.055\sqrt{N_{b\ell^-}}$, where $N_{b\ell^-}$ is the number of reconstructed events in the specific single lepton channel. The linear combination

$$\mathcal{O}_4 = \mathcal{O}_3 - \mathcal{O}_1 \tag{30}$$

has a still higher sensitivity than $\mathcal{O}_1$, namely $\mathcal{S}_3 \approx 0.073\sqrt{N_{b\ell^-}}$. Even with $10^4$ reconstructed $b\ell^-$ and $\bar{b}\ell^+$ events each one would get a 7.3$\sigma$ spin-correlation signal with this observable. The significance of these observables after the inclusion of hadronisation and detector effects remains to be studied.

The results of the above simulations are very encouraging for the prospect of $t, \bar{t}$ spin physics. On the theoretical side the NLO QCD corrections to the helicity amplitudes, and to the spin density matrices should be computed in order to improve the precision of the predictions and simulation tools.

If $t\bar{t}$ production and/or decay is affected by non-SM interactions then the correlations above will be changed. One interesting possibility would be the existence of a heavy spin-zero resonance $X_0$ (for instance a heavy (pseudo)scalar Higgs boson as predicted, e.g., by SUSY models or some composite object) that couples strongly to top quarks. For a certain range of masses and couplings to $t\bar{t}$ such an object would be visible in the $t\bar{t}$ invariant mass spectrum [74, 75]. Suppose one will be fortunate and discover such a resonance at the LHC. Then the parity of this state may be inferred from an investigation of $t\bar{t}$ spin correlations. This is illustrated by the following example. As already mentioned above, close to threshold gluon-gluon fusion produces a $t\bar{t}$ pair in a $^1S_0$ state. On the other hand if the pair is produced by the $X_0$ resonance, $gg \to X_0 \to t\bar{t}$, then for a scalar (pseudo-scalar) $X_0$ the $t\bar{t}$ pair is in a $^3P_0$ ($^1S_0$) state and has therefore characteristic spin correlations. Let us evaluate, for instance, the observable (22). Its expectation value at threshold is $\langle \mathbf{s}_t \cdot \mathbf{s}_{\bar{t}} \rangle = 1/4$ $(-3/4)$ if $t\bar{t}$ is produced by a (pseudo)scalar spin-zero boson, ignoring the $gg \to t\bar{t}$ background. An analysis which includes the interference with the QCD $t\bar{t}$ amplitude shows characteristic differences also away from threshold. By investigating several correlation observables (i.e., employing different spin bases) one can pin down the scalar/pseudo-scalar nature of such a resonance for a range of $X_0$ masses and couplings to top quarks [75].

Another effect of new physics might be the generation of an anomalously large chromomagnetic form factor $\kappa$ (see Section 7.1) in the $t\bar{t}$ production amplitude which would change the spin correlations with respect to the SM predictions [178, 179] (see also [180, 181]). For the LHC with 100 fb$^{-1}$ integrated luminosity one obtains from a study of asymmetries (that were also used in [179]) at the parton level a statistical sensitivity of $\delta\kappa \simeq 0.02$.

The top quark decay modes $t \to b\ell^+\nu_\ell, bq\bar{q}'$ might also be affected by non-SM interactions, for instance by right-handed currents or by charged Higgs-boson exchange, and this would alter the angular correlations discussed above as well. A Michel-parameter type analysis of the sensitivity to such effects at the LHC remains to be done.

The large $t\bar{t}$ samples to be collected at the LHC offer, in particular, an excellent opportunity to search for CP-violating interactions beyond the SM in high energy reactions. (The Kobayashi-Maskawa phase induces only tiny effects in $t\bar{t}$ production and decay.) We mention in passing that such interactions are of great interest for attempts to understand the baryon asymmetry of the universe. Many proposals and phenomenological studies of CP symmetry tests in $t\bar{t}$ production and decay at hadron colliders have been made. The following general statements apply [169]: A P- and CP-violating interaction affecting $t\bar{t}$ production induces additional terms in the production density matrices $R^{(\lambda)}$ which generate two types of CP-odd spin-momentum correlations, namely

$$\hat{\mathbf{k}}_t \cdot (\mathbf{s}_t - \mathbf{s}_{\bar{t}}) \ , \tag{31}$$

and

$$\hat{\mathbf{k}}_t \cdot (\mathbf{s}_t \times \mathbf{s}_{\bar{t}}) \ , \tag{32}$$

and two analogous correlations where $\hat{\mathbf{k}}_t$ is replaced by $\hat{\mathbf{p}}$. The longitudinal polarisation asymmetry (31) requires a non-zero CP-violating absorptive part in the respective scattering amplitude. In analogy to the SM spin correlations above, (31) and (32) can also be transcribed into angular correlations among the $t$ and $\bar{t}$ decay products, which may serve as basic CP observables (see below).

As to the modelling of non-SM CP violation two different approaches have been pursued. One is to parameterise the unknown dynamics with form factors or, neglecting possible dependences on kinematic variables, with couplings representing the strength of effective interactions [180, 182, 173, 183, 178, 179, 184, 185], and compute the effects on suitable observables. This yields estimates of the sensitivities to the respective couplings. For instance if $t\bar{t}$ production is affected by a new CP-violating interaction with a characteristic energy scale $\Lambda_{CP} > \sqrt{\hat{s}}$ then this interaction may effectively generate a chromoelectric dipole moment (CEDM) $d_t$ of the top quark (see Section 7.1). Assuming $10^7$ non-leptonic, $6\times10^6$ single lepton, and $10^6$ $t\bar{t}$ di-lepton events, the analysis of [185], using optimal CP observables, comes to the conclusion that a $1\sigma$ sensitivity of $\delta(Re\, d_t) \simeq 5\times10^{-20} g_s$ cm may be reached at the LHC. A detector-level study of CP violation in $t\bar{t}$ decays with di-lepton final states was performed in [186].

Alternatively one may consider specific extensions of the SM where new CP-violating interactions involving the top quark appear and compute the induced effects in $t\bar{t}$ production and decay, in particular for the reactions (16). We mention two examples. In supersymmetric extensions of the SM, in particular in the minimal one (MSSM), the fermion-sfermion-neutralino interactions contain in general CP-violating phases which originate from SUSY-breaking terms. These phases are unrelated to the Kobayashi-Maskawa phase. The interaction Lagrangian for the top quark coupling to a scalar top $\tilde{t}_{1,2}$ and a gluino $\tilde{G}$ reads in the mass basis

$$\mathcal{L}_{\tilde{G}t\tilde{t}} = i\sqrt{2} g_s \sum_{l=1,2} (e^{-i\phi_t} \bar{t}_L \Gamma_l \tilde{G}^a T^a \tilde{t}_l + e^{+i\phi_t} \bar{t}_R \Gamma'_l \tilde{G}^a T^a \tilde{t}_l) + \text{h.c.}, \tag{33}$$

where $g_s$ is the QCD coupling. A priori the phase $\phi_t$ is unrelated to the analogous phases in the light quark sector which are constrained by the experimental upper bound on the electric dipole moment of the neutron. The CP-violating one-loop contributions of (33) to $gg, \bar{q}q \to t\bar{t}$ were computed in [187, 185]. A non-zero CP effect requires, apart from a non-zero phase $\phi_t$, also non-degeneracy of the masses of $\tilde{t}_{1,2}$. For fixed phase and $\tilde{t}_1 - \tilde{t}_2$ mass difference the effect decreases with increasing gluino and scalar top masses. Assuming the same data samples as in the CEDM analysis above, [185] concludes from a computation of optimal CP observables that a sensitivity $|\phi_t| \gtrsim 0.1$ can be reached at the LHC if the gluino and squark masses do not exceed 400 GeV.

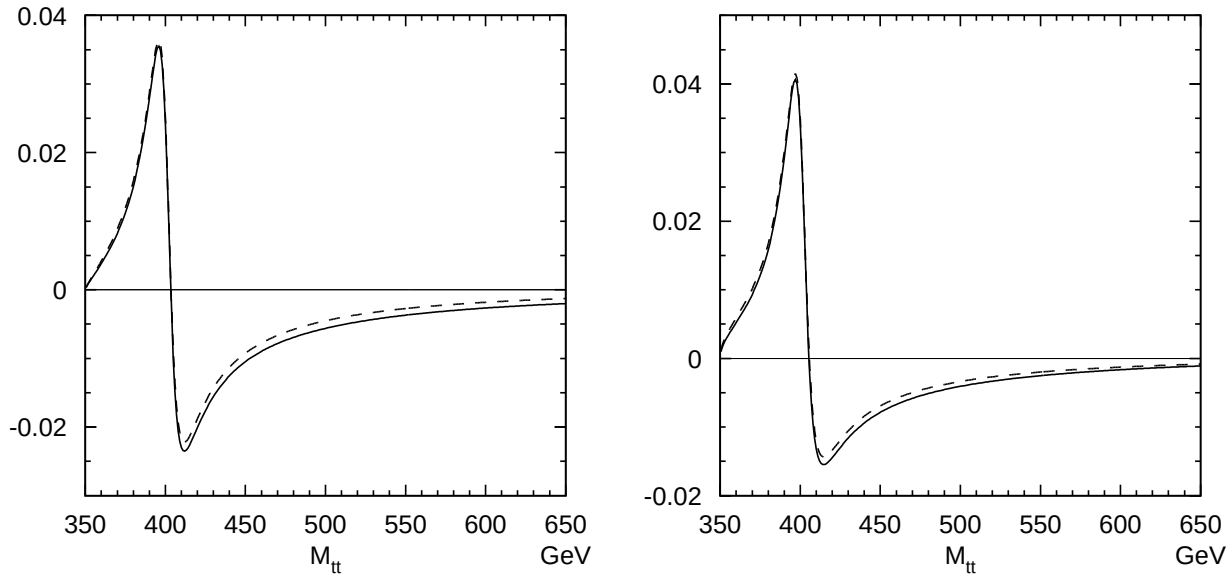


Fig. 36: Right: differential expectation value of $Q_1$ as a function of the $t\bar{t}$ invariant mass at $\sqrt{s} = 14$ TeV for reduced Yukawa couplings $a_t = 1$, $\tilde{a}_t = -1$, and a Higgs boson mass $m_\varphi = 400$ GeV. The dashed line represents the resonant and the solid line the sum of the resonant and non-resonant $\varphi$ contributions. Left: same as figure to the left, but for the observable $Q_2$ [86].

Another striking possibility would be CP violation by an extended scalar sector manifesting itself through the existence of non-degenerate neutral Higgs bosons with undefined CP parity. Higgs sector CP violation can occur already in extensions of the SM by an extra Higgs doublet (see, for instance [188]). It may also be sizable in the MSSM within a certain parameter range [189]. The coupling of such a neutral Higgs boson $\varphi$ with undefined CP parity to top quarks reads

$$\mathcal{L}_Y = -(\sqrt{2}G_F)^{1/2} m_t (a_t \bar{t}t + \tilde{a}_t \bar{t} i \gamma_5 t)\, \varphi \ , \tag{34}$$

where $a_t$ and $\tilde{a}_t$ denote the reduced scalar and pseudo-scalar Yukawa couplings, respectively (in the SM $a_t = 1$ and $\tilde{a}_t = 0$). The CP-violating effects of (34) on $gg, \bar{q}q \to t\bar{t}$ were investigated for light $\varphi$ in [190] and for $\varphi$ bosons of arbitrary mass in [191, 169] (see also [185, 86]). The exchange of $\varphi$ bosons induces, at the level of the $t\bar{t}$ states, both types of correlations (32), (31) (the CP asymmetry $\Delta N_{LR} = [N(t_L \bar{t}_L) - N(t_R \bar{t}_R)]/(\mathrm{all}\, t\bar{t})$ considered in [190] corresponds to the longitudinal polarisation asymmetry $\langle \hat{\mathbf{k}}_t \cdot (\mathbf{s}_{\bar{t}} - \mathbf{s}_t) \rangle$). If the mass of $\varphi$ lies in the vicinity or above $2m_t$ the $s$-channel $\varphi$-exchange diagram $gg \to \varphi \to t\bar{t}$ becomes resonant and is by far the most important $\varphi$ contribution.

Simple and highly sensitive observables and asymmetries were investigated for the different $t\bar{t}$ decay channels in [86]. For the di-lepton channels the following transcriptions of (31) and (32) may be used:

$$Q_1 = \hat{\mathbf{k}}_t \cdot \hat{\mathbf{q}}_+ - \hat{\mathbf{k}}_{\bar{t}} \cdot \hat{\mathbf{q}}_- \ , \tag{35}$$

$$Q_2 = (\hat{\mathbf{k}}_t - \hat{\mathbf{k}}_{\bar{t}}) \cdot (\hat{\mathbf{q}}_- \times \hat{\mathbf{q}}_+)/2 \ , \tag{36}$$

where $\hat{\mathbf{k}}_t$, $\hat{\mathbf{k}}_{\bar{t}}$ are here the $t$, $\bar{t}$ momentum directions in the $t\bar{t}$ c.m. frame and $\hat{\mathbf{q}}_+$,$\hat{\mathbf{q}}_-$ are the $\ell^+$, $\ell^-$ momentum directions in the $t$ and $\bar{t}$ quark rest frames, respectively. Note that $Q_1 = \cos\theta_+ - \cos\theta_-$ where $\theta_\pm$ are defined after (25). When taking expectation values of these observables the channels $\ell^+$, $\ell'^-$ with $\ell, \ell' = e, \mu$ are summed over. The sensitivity to the CP-violating product of couplings $\gamma_{CP} \equiv -a_t \tilde{a}_t$ of heavy Higgs bosons is significantly increased when expectation values of (35), (36) are taken with respect to bins of the $t\bar{t}$ invariant mass $M_{t\bar{t}}$. Two examples of these "differential expectation values" are shown in Fig. 36. In order to estimate the measurement errors we have used a sample of di-lepton events, obtained from a simulation at the detector level using the same selection criteria as in the simulation described above, and determined the resulting error on the expectation value of $Q_1$, choosing $M_{t\bar{t}}$ bins with a width of 10 GeV. With $2 \times 10^5$ reconstructed di-lepton events in the whole $M_{t\bar{t}}$ range

we find that the error on $\langle Q_1 \rangle_{M_{t\bar{t}}}$ is slightly below $1\%$ for a bin at, say, $M_{t\bar{t}} = 400$ GeV. In addition one may employ the following asymmetries which are experimentally more robust than $\langle Q_i \rangle$:

$$A(Q_i) = \frac{N_{\ell\ell}(Q_i > 0) - N_{\ell\ell}(Q_i < 0)}{N_{\ell\ell}}\,, \tag{37}$$

where $i = 1, 2$ and $N_{\ell\ell}$ is the number of di-lepton events. From an analysis of these observables and asymmetries and analogous ones for the single lepton channels at the level of partonic final states the conclusion can be drawn [86] that one will be sensitive to $|\gamma_{CP}| \gtrsim 0.1$ at the LHC. This will constitute rather unique CP tests.

## 7. TOP QUARK ANOMALOUS INTERACTIONS[22]

In the SM the gauge couplings of the top quark are uniquely fixed by the gauge principle, the structure of generations and the requirement of a lowest dimension interaction Lagrangian. Due to the large top mass, top quark physics looks simple in this renormalisable and unitary quantum field theory. Indeed,

- the top quark production cross section is known with a rather good accuracy ($\sim (10-15)$ %),
- there are no top hadrons (mesons or baryons),
- the top quark decay is described by pure $(V-A)$ weak interactions,
- only one significant decay channel is present: $t \to bW^+$ (other decay channels are very suppressed by small mixing angles).

This simplicity makes the top quark a unique place to search for new physics beyond the SM. If anomalous top quark couplings exist, they will affect top production and decay at high energies, as well as precisely measured quantities with virtual top quark contributions.

We do not know which type of new physics will be responsible for a future deviation from the SM predictions. However, top quark couplings can be parametrized in a model independent way by an effective Lagrangian. The top quark interactions of dimension 4 can be written (in standard notation [192]):

$$\begin{aligned}\mathcal{L}_4 \;=\; & -g_s \bar{t}\gamma^\mu T^a t G^a_\mu - \frac{g}{\sqrt{2}} \sum_{q=d,s,b} \bar{t}\gamma^\mu (v^W_{tq} - a^W_{tq}\gamma_5) q W^+_\mu \\ & -\frac{2}{3} e \bar{t}\gamma^\mu t A_\mu - \frac{g}{2\cos\theta_W} \sum_{q=u,c,t} \bar{t}\gamma^\mu (v^Z_{tq} - a^Z_{tq}\gamma_5) q Z_\mu \end{aligned} \tag{38}$$

plus the hermitian conjugate operators for the flavour changing terms. $T^a$ are the Gell-Mann matrices satisfying $\mathrm{Tr}\,(T^a T^b) = \delta^{ab}/2$. Gauge invariance fixes the strong and electromagnetic interactions in (38) and hemiticity implies real diagonal couplings $v^Z_{tt}, a^Z_{tt}$, whereas the non-diagonal ones $v^{W,Z}_{tq}, a^{W,Z}_{tq}$ can be complex in general. Within the SM $v^W_{tq} = a^W_{tq} = \frac{V_{tq}}{2}$, with $V_{tq}$ the Cabbibo-Kobayashi-Maskawa (CKM) matrix elements, $v^Z_{tt} = \frac{1}{2} - \frac{4}{3}\sin^2\theta_W,\ a^Z_{tt} = \frac{1}{2}$, and the non-diagonal $Z$ couplings are equal to zero. Typically modifications of the SM couplings can be traced back to dimension 6 operators in the effective Lagrangian description valid above the EW symmetry breaking scale [193, 194, 195] (see also [196, 132, 197]). Hence, they are in principle of the same order as the other dimension 5 and 6 couplings below the EW scale. However, in specific models the new couplings in Eq. (38) can be large [198]. Moreover, the present experimental limits are relatively weak and these couplings can show up in simple processes and can be measured with much better precision at the LHC.

The dimension 5 couplings to one on-shell gauge boson, after gauge symmetry breaking, have the generic form: [199] :

$$\mathcal{L}_5 \;=\; -g_s \sum_{q=u,c,t} \frac{\kappa^g_{tq}}{\Lambda} \bar{t}\sigma^{\mu\nu} T^a (f^g_{tq} + i h^g_{tq}\gamma_5) q G^a_{\mu\nu} - \frac{g}{\sqrt{2}} \sum_{q=d,s,b} \frac{\kappa^W_{tq}}{\Lambda} \bar{t}\sigma^{\mu\nu} (f^W_{tq} + i h^W_{tq}\gamma_5) q W^+_{\mu\nu}$$

[22] Section coordinators: F. del Aguila, S. Slabospitsky, M. Cobal (ATLAS), E. Boos (CMS).

$$-e\sum_{q=u,c,t}\frac{\kappa^{\gamma}_{tq}}{\Lambda}\bar{t}\sigma^{\mu\nu}(f^{\gamma}_{tq}+ih^{\gamma}_{tq}\gamma_5)qA_{\mu\nu}-\frac{g}{2\cos\theta_W}\sum_{q=u,c,t}\frac{\kappa^{Z}_{tq}}{\Lambda}\bar{t}\sigma^{\mu\nu}(f^{Z}_{tq}+ih^{Z}_{tq}\gamma_5)qZ_{\mu\nu} \quad (39)$$

plus the hermitian conjugate operators for the flavour changing terms. $G^a_{\mu\nu}$ is $\partial_\mu G^a_\nu - \partial_\nu G^a_\mu$ (see, however, below) and similarly for the other gauge bosons. We normalise the couplings by taking $\Lambda = 1$ TeV. $\kappa$ is real and positive and $f, h$ are complex numbers satisfying for each term $|f|^2 + |h|^2 = 1$. As in the dimension 4 case these dimension 5 terms typically result from dimension 6 operators after the EW breaking. They could be large, although they are absent at tree level and receive small corrections in renormalizable theories. At any rate the LHC will improve appreciably their present limits.

There are also dimension 5 terms with two gauge bosons. However, the only ones required by the unbroken gauge symmetry $SU(3)_C \times U(1)_Q$, and taken into account here, are the strong couplings with two gluons and the EW couplings with a photon and a $W$ boson. They are obtained including also the bilinear term $g_s f^{abc} G^b_\mu G^c_\nu$, with $f^{abc}$ the $SU(3)_C$ structure constants, in the field strength $G^a_{\mu\nu}$ in (39) and the bilinear term $-ie(A_\mu W^+_\nu - A_\nu W^+_\mu)$ in $W^+_{\mu\nu}$, respectively. We do not consider any other dimension 5 term with two gauge bosons for their size is not constrained by $SU(3)_C \times U(1)_Q$ and/or they only affect to top quark processes with more complicated final states than those discussed here. We will not elaborate on operators of dimension 6, although the first $q^2$ corrections to dimension 4 terms could be eventually observed at large hadron colliders [134]. In this section we are not concerned with the effective top couplings to Higgs bosons either.

In what follows we study the LHC potential for measuring or putting bounds on the top quark anomalous interactions in (38), (39) through production processes. Results from top quark decays are presented is Section 8. The $t\bar{t}$ couplings to gluons are considered first, since they are responsible for $t\bar{t}$ production. Secondly we discuss the top quark couplings $\bar{t}bW$. In the SM this coupling is not only responsible for almost $100\%$ of the top decays but it also leads to an EW single top production mode, as reviewed in Section 5.. Finally we deal with the $t$ flavour changing neutral currents (FCNC). The $\gamma t\bar{t}$ and $Zt\bar{t}$ vertices have not been considered here because $e^+e^-$ and $\mu^+\mu^-$ colliders can give a cleaner environment for their study.

With the exception of the summary Table 23, we will quote limits from the literature without attempting to compare them. In Table 13 we illustrate statistics frequently used and which we will refer to in the text when presenting the bounds. As can be observed, the number of signal events, and the limit estimates, vary appreciably with the choice of statistics. We do correct for the different normalizations of the couplings used in the literature.

Table 13: Limits on the number of signal events $S$ obtained with different statistics. $B$ is the number of background events. In the other columns we gather $S$ for (1): $99\%$ CL (3 $\sigma$) measurement, $\frac{S}{\sqrt{S+B}} \geq 3$; (3): $99\%$ CL (3 $\sigma$) limit, $\frac{S}{\sqrt{B}} \geq 3$; and (5): $99\%$ CL for the Feldman-Cousins (FC) statistics [200]; and similarly for (2), (4), and (6), for the $95\%$ CL (1.96 $\sigma$), respectively.

| $B$ | (1) | (2) | (3) | (4) | (5) | (6) |
|---|---|---|---|---|---|---|
| 0 | 9 | 3.84 | 0 | 0 | 4.74 | 3.09 |
| 5 | 12.57 | 6.71 | 6.71 | 4.38 | 8.75 | 6.26 |
| 10 | 15 | 8.41 | 9.49 | 6.20 | 10.83 | 7.82 |
| 15 | 16.96 | 9.75 | 11.62 | 7.59 | 12.81 | 9.31 |

### 7.1 Probes of anomalous $\mathbf{g}\mathbf{t}\bar{\mathbf{t}}$ couplings

The combination $\frac{4m_t}{\Lambda}\kappa^g_{tt} f^g_{tt}$ (see (39)) can be identified with the anomalous chromomagnetic dipole moment of the top quark, which, as is the case of QED, receives one-loop contributions in QCD. Therefore, its natural size is of the order of $\alpha_s/\pi$. As we observed above, when this coupling is non-zero a direct $gg\bar{t}t$ four-point vertex is induced as a result of gauge invariance.

Table 14: Attainable $1\sigma$ limits on $Re(d_t)$ and $Im(d_t)$, through $T_{33}$, $A_E$ and $Q_{33}$ for one year of the LHC running at low luminosity (10 fb$^{-1}$) [204].

| Observable | Attainable $1\sigma$ limits |
|---|---|
| $T_{33}$ | $\lvert Re(d_t)\rvert = 0.899 \times 10^{-17} g_s \mathrm{cm}$ |
| $A_E$ | $\lvert Im(d_t)\rvert = 0.858 \times 10^{-18} g_s \mathrm{cm}$ |
| $Q_{33}$ | $\lvert Im(d_t)\rvert = 0.205 \times 10^{-17} g_s \mathrm{cm}$ |

On the other hand the combination $\frac{4m_t}{\Lambda}\kappa^g_{tt}h^g_{tt}$ can be identified as the anomalous chromoelectric dipole moment of the top quark. Within the SM this can arise only beyond two loops [201]. On the other hand it can be much larger in many models of CP violation such as multi-Higgs-doublet models and SUSY [202]. Therefore, such a non-vanishing coupling would be a strong indication of BSM physics.

Considering the gluonic terms in (38), (39) for the process of light quark annihilation into $\bar{t}t$ one obtains [181, 203]

$$\frac{d\sigma_{q\bar{q}}}{dt} = \frac{2\pi\alpha_s}{9\,\hat{s}^2}\left[2-\beta^2(1-z^2) - \frac{8m_t}{\Lambda}\kappa^g_{tt}(f^g_{tt}+f^{g*}_{tt}) + \frac{32m_t^2}{\Lambda^2}(\kappa^g_{tt})^2|f^g_{tt}|^2 + \frac{4\hat{s}}{\Lambda^2}(\kappa^g_{tt})^2\beta^2(1-z^2)\right], \tag{40}$$

$\hat{s}$ being the incoming parton total energy squared, $z$ being the cosine of the scattering angle $\theta^*$ in the cms of the incoming partons, and $\beta = \sqrt{1-4m_t^2/\hat{s}}$.

The squared matrix element for $gg$ annihilation is a more complicated expression; we refer to [181, 204] for exact formulas. If the (anomalous) couplings are assumed to be functions (form-factors) of $q^2$ and then corrected by operators of dimension higher than 5, the $gg$ annihilation amplitude would be evaluated at different scales (for the $\hat{t}(\hat{u})$ and $\hat{s}$ channels), and an additional violation of the $SU(3)_C$ gauge invariance could be made apparent. For a detailed discussion of this problem see, for example, [181] and references therein.

The effects associated with $\kappa^g_{tt}f^g_{tt}$ were examined in [181, 205, 206]. As shown in [134] they will be easily distinguishable from the effects of $q^2$ corrections to the strong coupling due to operators of dimension 6, which are relatively straightforward to analyse [195] in $t\bar{t}$ production since the effective coupling would be a simple rescaling of the strength of the ordinary QCD coupling by an additional $q^2$-dependent amount. It was shown in [206] that the high-end tail of the top quark $p_T$ and $M_{t\bar{t}}$ distributions are the observables most sensitive to non-zero values of $\kappa^g_{tt}f^g_{tt}$, with a reach for $\kappa = \frac{4m_t}{\Lambda}\kappa^g_{tt}f^g_{tt}$ as small as $\simeq 0.03$. For these values of $\kappa$, only a minor change in the total $t\bar{t}$ rate is expected (see Fig. 37). The effect of a non-zero $\kappa^g_{tt}h^g_{tt}$ was analysed, in particular, in [204, 207, 172]. It was shown in [204] that information on $\kappa^g_{tt}h^g_{tt}$ could be obtained by studying the following correlation observables between $\ell^+\ell^-$ lepton pairs produced in $t\bar{t}$ in di-lepton decays:

$$\begin{aligned} T_{33} &= 2(\boldsymbol{p}_{\bar{\ell}} - \boldsymbol{p}_\ell)_3(\boldsymbol{p}_{\bar{\ell}} \times \boldsymbol{p}_\ell)_3, \\ A_E &= E_{\bar{\ell}} - E_\ell, \qquad Q^\ell_{33} = 2(\boldsymbol{p}_{\bar{\ell}} + \boldsymbol{p}_\ell)_3(\boldsymbol{p}_{\bar{\ell}} - \boldsymbol{p}_\ell)_3 - \frac{2}{3}(\boldsymbol{p}^2_{\bar{\ell}} - \boldsymbol{p}^2_\ell). \end{aligned}$$

Table 14 shows the 1 $\sigma$ sensitivities of these correlations to $Re(d_t)$ and $Im(d_t)$ (where, $d_t \equiv g_s\frac{2}{\Lambda}\kappa^g_{tt}h^g_{tt}$). Quantitatively, $T_{33}$ and $Q_{33}$ enable us to probe $Re(d_t)$ and $Im(d_t)$ of the order of $10^{-17}g_s\mathrm{cm}$, respectively, and $A_E$ allows us to probe $Im(d_t)$ down to the order of $10^{-18}g_s\mathrm{cm}$ (see [204] for details).

### 7.2 Search for anomalous Wtb couplings

The $Wtb$ vertex structure can be probed and measured using either top pair or single top production processes. The total $t\bar{t}$ rate depends very weakly on the $Wtb$ vertex structure, as top quarks are dominantly produced on-shell [208]. However, more sensitive observables, like $C$ and $P$ asymmetries, top polarisation and spin correlations provide interesting information, as discussed in Section 6. The single

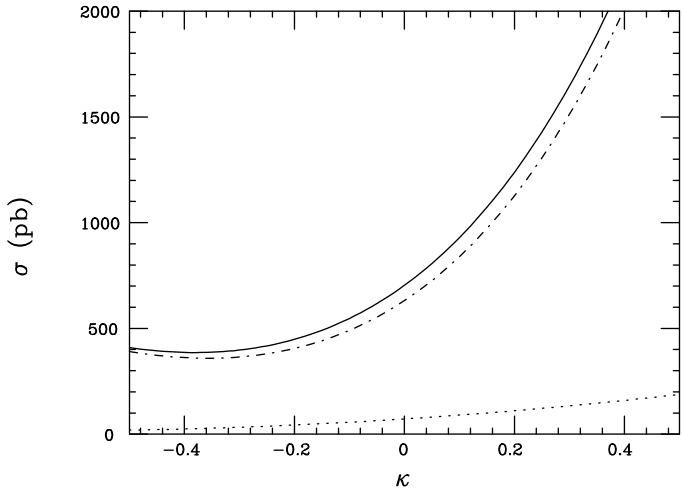


Fig. 37: Cross section for $t\bar{t}$ production (solid) at the LHC as a function of $\kappa$. The part of the cross section arising from the $gg(q\bar{q})$ annihilation is shown by the dash-dotted (dotted) curve (see [206] for details).

top production rate is directly proportional to the square of the $Wtb$ coupling, and therefore it is potentially very sensitive to the $Wtb$ structure. In single top events the study of the top polarisation properties potentially provides a way to probe a $Wtb$ coupling structure [209]. The potential to measure anomalous $Wtb$ couplings at LHC via single top from the production rate and from kinematical distributions has been studied in several papers [195, 210, 135, 30].

In the model independent effective Lagrangian approach [193, 194, 195] there are four independent form factors describing the $Wtb$ vertex (see [195] for details). The effective Lagrangian in the unitary gauge [211, 208, 135] is given in (38), (39). As already mentioned the $(V-A)$ coupling in the SM carries the CKM matrix element $V_{tb}$ which is very close to unity. The value of a $(V+A)$ coupling is already bounded by the CLEO $b \to s\gamma$ data [212, 213] at a level [195, 213] such that it will be out of reach even at the high energy $\gamma e$ colliders. Since we are looking for small deviations from the SM, in the following $v_{tb}^W$ and $a_{tb}^W$ will be set to $v_{tb}^W = a_{tb}^W = \frac{1}{2}$ and an analysis is presented only for the two 'magnetic' anomalous couplings $F_{L2} = \frac{2M_W}{\Lambda}\kappa_{tb}^W(-f_{tb}^{W*} - ih_{tb}^{W*})$, $F_{R2} = \frac{2M_W}{\Lambda}\kappa_{tb}^W(-f_{tb}^{W*} + ih_{tb}^{W*})$. Natural values for the couplings $|F_{L(R)2}|$ are in the region of $\frac{\sqrt{m_b m_t}}{v} \sim 0.1$ [196] and do not exceed the unitarity violation bounds for $|F_{L(R)2}| \sim 0.6$ [194].

Calculations of the complete set of diagrams for the two main processes $pp \to b\bar{b}W$ and $pp \to b\bar{b}W + \mathrm{jet}$ have been performed [135] for the effective Lagrangian in (38), (39), using the package CompHEP [214]. The calculation includes the single-top signal and the irreducible backgrounds. Appropriate observables and optimal cuts to enhance the single-top signal have been identified through an analysis of singularities of Feynman diagrams and explicit calculations. The known NLO corrections to the single top rate [126, 125] have been included, as well as a simple jet energy smearing. The upper part of Fig. 38 presents the resulting 2 $\sigma$ exclusion contour for an integrated luminosity of $100$ fb$^{-1}$, assuming $e, \mu$ and $\tau \to \ell$ decays of the $W$-boson. The combined selection efficiency in the kinematical region of interest, including the double $b$-tagging, is assumed to be $50\%$. Figure 38 demonstrates that it will be essential to measure both processes $pp \to b\bar{b}W$ and $pp \to b\bar{b}W + \mathrm{jet}$ at the LHC. The allowed region for each single process is a rather large annuli, but the overlapping region is much smaller and allows an improvement of the sensitivity on anomalous couplings of an order of magnitude with respect to the Tevatron. Since the production rate is large, even after strong cuts, expected statistical errors are rather small, and the systematic uncertainties (from luminosity measurements, parton distribution functions, QCD scales, $m_t$, $\ldots$) will play an important role. As it is not possible to predict them accurately before the LHC startup, we show here how the results depend on the assumed combined systematic uncertainty. Figure 38 (lower part) shows how the exclusion contours deteriorate when systematic errors of $1\%$ and $5\%$ are included.

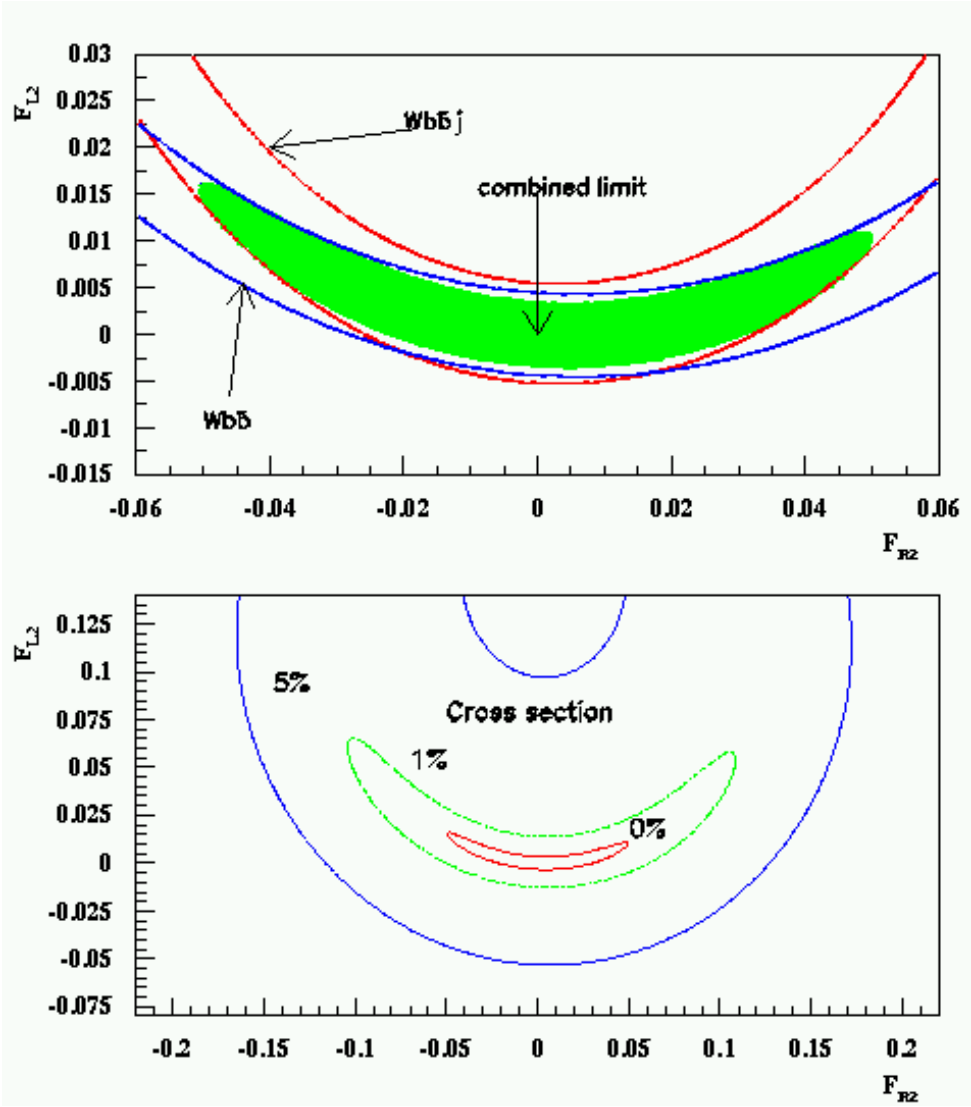


Fig. 38: Limits on anomalous couplings after optimised cuts from two processes $pp \to b\bar{b}W$ and $pp \to b\bar{b}W + \text{jet}$ (upper plot). Dependence of the combined limits on the values of systematic uncertainties (lower plot).

Note that a systematic error of 10% at the LHC will diminish the sensitivity significantly and the allowed regions will be comparable to those expected at the upgraded Tevatron.

The rate of single top production at LHC is different from the rate of single anti-top production. This asymmetry provides an additional observable at LHC that is not available at the Tevatron and which allows to reduce systematic uncertainties.

The potential of the hadron colliders can be compared to the potential of a next generation $e^+e^-$ linear collider (LC) where the best sensitivity could be obtained in high energy $\gamma e$-collisions [208, 215]. The results of this comparison are shown in Table 15. From the table we see that the upgraded Tevatron will be able to perform the first direct measurements of the structure of the $Wtb$ coupling. The LHC with $5\%$ systematic uncertainties will improve the Tevatron limits considerably, rivalling with the reach of a high-luminosity (500 fb$^{-1}$) 500 GeV LC option. The very high energy LC with 500 fb$^{-1}$ luminosity will eventually improve the LHC limits by a factor of three to eight, depending on the coupling under consideration.

Table 15: Uncorrelated limits on anomalous couplings from measurements at different machines.

| | $F_{L2}$ | | | $F_{R2}$ | | |
|---|---|---|---|---|---|---|
| Tevatron ($\Delta_{\rm sys.} \approx 10\%$) | $-0.18$ | $\ldots$ | $+0.55$ | $-0.24$ | $\ldots$ | $+0.25$ |
| LHC ($\Delta_{\rm sys.} \approx 5\%$) | $-0.052$ | $\ldots$ | $+0.097$ | $-0.12$ | $\ldots$ | $+0.13$ |
| $\gamma e$ ($\sqrt{s_{e^+e^-}} = 0.5\,\mathrm{TeV}$) | $-0.1$ | $\ldots$ | $+0.1$ | $-0.1$ | $\ldots$ | $+0.1$ |
| $\gamma e$ ($\sqrt{s_{e^+e^-}} = 2.0\,\mathrm{TeV}$) | $-0.008$ | $\ldots$ | $+0.035$ | $-0.016$ | $\ldots$ | $+0.016$ |

### 7.3 FCNC in top quark physics

In the previous subsections, we analysed top quark anomalous couplings as small deviations from the ordinary SM interactions ($gt\bar{t}$ and $tWb$ vertices). Here we consider new processes which are absent at tree-level and highly suppressed in the SM, namely the FCNC couplings $tVc$ and $tVu$ ($V = g, \gamma, Z$). The SM predicts very small rates for such processes [216] (see Table 16). The top quark plays therefore a unique rôle compared to the other quarks, for which the expected FCNC transitions are much larger: the observation of a top quark FCNC interaction would signal the existence of new physics. As an illustration, Table 16 shows predictions for the top quark decay branching ratios evaluated in the two-Higgs doublet model [217], the SUSY models [218], and the SM extension with exotic (vector-like) quarks [198].

Table 16: Branching ratios for FCNC top quark decays as predicted within the SM and in three SM extensions.

| | SM | two-Higgs [217] | SUSY [218] | Exotic quarks [198] |
|---|---|---|---|---|
| B($t\to qg$) | $5\times 10^{-11}$ | $\sim 10^{-5}$ | $\sim 10^{-3}$ | $\sim 5\times 10^{-4}$ |
| B($t\to q\gamma$) | $5\times 10^{-13}$ | $\sim 10^{-7}$ | $\sim 10^{-5}$ | $\sim 10^{-5}$ |
| B($t\to qZ$) | $\sim 10^{-13}$ | $\sim 10^{-6}$ | $\sim 10^{-4}$ | $\sim 10^{-2}$ |

In the effective Lagrangian description of (38), (39) it is straightforward to calculate the top quark decay rates as a function of the top quark FCNC couplings:

$$\Gamma(t\to qg) = \left(\frac{\kappa^g_{tq}}{\Lambda}\right)^2 \frac{8}{3}\alpha_s m_t^3 \quad , \quad \Gamma(t\to q\gamma) = \left(\frac{\kappa^\gamma_{tq}}{\Lambda}\right)^2 2\alpha m_t^3, \tag{41}$$

$$\Gamma(t\to qZ)_\gamma = \left(|v^Z_{tq}|^2 + |a^Z_{tq}|^2\right)\alpha\, m_t^3 \frac{1}{4M_Z^2\sin^2 2\theta_W}\left(1-\frac{M_Z^2}{m_t^2}\right)^2\left(1+2\frac{M_Z^2}{m_t^2}\right), \tag{42}$$

$$\Gamma(t\to qZ)_\sigma = \left(\frac{\kappa^Z_{tq}}{\Lambda}\right)^2 \alpha\, m_t^3 \frac{1}{\sin^2 2\theta_W}\left(1-\frac{M_Z^2}{m_t^2}\right)^2\left(2+\frac{M_Z^2}{m_t^2}\right). \tag{43}$$

For comparison, Table 17 collects the rare top decay rates normalised to $\kappa^g_{tq} = \kappa^\gamma_{tq} = |v^Z_{tq}|^2 + |a^Z_{tq}|^2 = \kappa^Z_{tq} = 1$, and for the SM. We assume $m_t = 175$ GeV, $\Lambda = 1$ TeV, $\alpha = \frac{1}{128}$, $\alpha_s = 0.1$ and sum the decays into $q = u, c$. In this 'extreme' case with the anomalous couplings equal to one the top can decay into a gluon or a $Z$ boson plus a light quark $q = u, c$ and into the SM mode $bW$ at similar rates.

#### *7.31 Current Constraints on FCNC in top quark physics*

Present constraints on top anomalous couplings are derived from low-energy data, direct searches of top rare decays, deviations from the SM prediction for $t\bar{t}$ production and searches for single top production at LEP2.

*Indirect constraints:* The top anomalous couplings are constrained by the experimental upper bounds on the induced FCNC couplings between light fermions. For example, the $\gamma^\mu$ term in the $Ztq$

Table 17: Top quark decay widths and corresponding branching ratios for the anomalous couplings equal to one and for the SM. In the fourth line we gather the values of the corresponding anomalous couplings giving the same decay rates as in the SM.

| | Top decay mode | | | | |
|---|---|---|---|---|---|
| | $W^+b$ | $(c+u)g$ | $(c+u)\gamma$ | $(c+u)Z_\gamma$ | $(c+u)Z_\sigma$ |
| FCNC coupling | | 1 | 1 | 1 | 1 |
| $\Gamma(\mathrm{GeV})$ | 1.56 | 2.86 | 0.17 | 2.91 | 0.14 |
| B | 0.20 | 0.37 | 0.022 | 0.38 | 0.018 |
| FCNC coupling | | $8\times10^{-6}$ | $3\times10^{-6}$ | $4\times10^{-7}$ | |
| $\Gamma_{\mathrm{SM}}(\mathrm{GeV})$ | 1.56 | $8\times10^{-11}$ | $8\times10^{-12}$ | $2.2\times10^{-13}$ | |
| $\mathrm{B}_{\mathrm{SM}}$ | 1 | $5\times10^{-11}$ | $5\times10^{-13}$ | $1.5\times10^{-13}$ | |

vertex generates an effective interaction of the form [219]

$$\mathcal{L}_{eff} = \frac{g}{\cos\theta_W} a_{ij} \bar{f}_i \gamma^\mu \frac{1-\gamma_5}{2} f_j Z_\mu \; + \; \mathrm{h.c.}, \tag{44}$$

where $f_{i,j}$ are two different light down-type quarks. The one-loop estimate of the vertex gives:

$$a_{ij} = \frac{1}{16\pi^2}\frac{m_t^2}{v^2}\left[V_{ti}^*(v_{tq}^Z + a_{tq}^Z)V_{qj} + V_{qi}^*(v_{tq}^{Z*} + a_{tq}^{Z*})V_{tj}\right]\ln\frac{\Lambda^2}{m_t^2}, \tag{45}$$

where $V_{ij}$ are the CKM matrix elements. Then, using the results of [219] and the experimental constraints from [192] on $K_L{\to}\mu^+\mu^-$, the $K_L$-$K_S$ mass difference, $B^0-\overline{B}^0$ mixing, $B{\to}\ell^+\ell^-X$ and $b{\to}s\gamma$, one obtains:

$$a_{sd} < 2\times10^{-5}, \;\; a_{bd} < 4\times10^{-4}, \;\; a_{bs} < 1.4\times10^{-3}, \tag{46}$$

and, taking $v = 250$ GeV, $m_t = 175$ GeV and $\Lambda = 1$ TeV:

$$|v_{tu}^Z + a_{tu}^Z| < 0.04, \;\; |v_{tc}^Z + a_{tc}^Z| < 0.11. \tag{47}$$

$v_{tq}^Z - a_{tq}^Z$ do not contribute to $a_{ij}$ for massless external fermions. However, both chiralities of the $Ztq$ vertex contribute, for instance, to the vacuum polarization tensor $\Pi^{\mu\nu}(q^2)$. Thus, using the recent value for the $\rho$ parameter, $\rho = 0.9998 \pm 0.0008\ (+0.0014)$ [192], the following $2\sigma$ limit is obtained:

$$\sqrt{|v_{tq}^Z|^2 + |a_{tq}^Z|^2} < 0.15. \tag{48}$$

*CDF results:* The CDF collaboration has searched for the decays $t{\to}\gamma c(u)$ and $t{\to}Zc(u)$ in the reaction $\bar{p}p \to \bar{t}tX$ at $\sqrt{s} = 1.8$ TeV, obtaining the following 95% CL limits [13]:

$$\mathrm{BR}(t{\to}c\gamma) + \mathrm{BR}(t{\to}u\gamma) < 3.2\%, \quad \mathrm{BR}(t{\to}cZ) + \mathrm{BR}(t{\to}uZ) < 33\% \; . \tag{49}$$

These translate into the bounds on the top anomalous couplings

$$\kappa_{tq}^\gamma < 0.78, \quad \sqrt{|v_{tq}^Z|^2 + |a_{tq}^Z|^2} < 0.73. \tag{50}$$

*$t\bar{t}$ production via FCNC:* Constraints on the vertex $gtq$ can be derived form the study of the $t\bar{t}$-pair production cross-section. Imposing that the $t\bar{t}$-pair production cross-section, including the possible effect of anomalous couplings, should not differ from the observed one (assumed in this study to be $\sigma_{t\bar{t}}^{\mathrm{exp}} = 6.7 \pm 1.3$ pb [6]) by more than 2 pb, leads to the constraint [220]:

$$\frac{\kappa_{tq}^g}{\Lambda} \leq 0.47\ \mathrm{TeV}^{-1}. \tag{51}$$

Table 18: Short summary of the LEP 2 results for $e^+e^- \to t\bar{q}$. The theoretical value $\sigma_{\rm th}$ is evaluated assuming the limit on the corresponding anomalous coupling in (50).

| Collab. | $\sqrt{s}$ (GeV) | $\mathcal{L}$(pb$^{-1}$) | $\sigma_{\rm exp}(95\% CL)$ | $\sigma_{\rm th}$ |
|---|---|---|---|---|
| DELPHI | 183 GeV [222] | 47.7 | $< 0.55$ pb | $< 0.15$ pb |
| ALEPH | 189 GeV [221] | 174 | $< 0.60$ pb | $< 0.30$ pb |
| DELPHI | 189 GeV [223] | 158 | $< 0.22$ pb | $< 0.30$ pb |

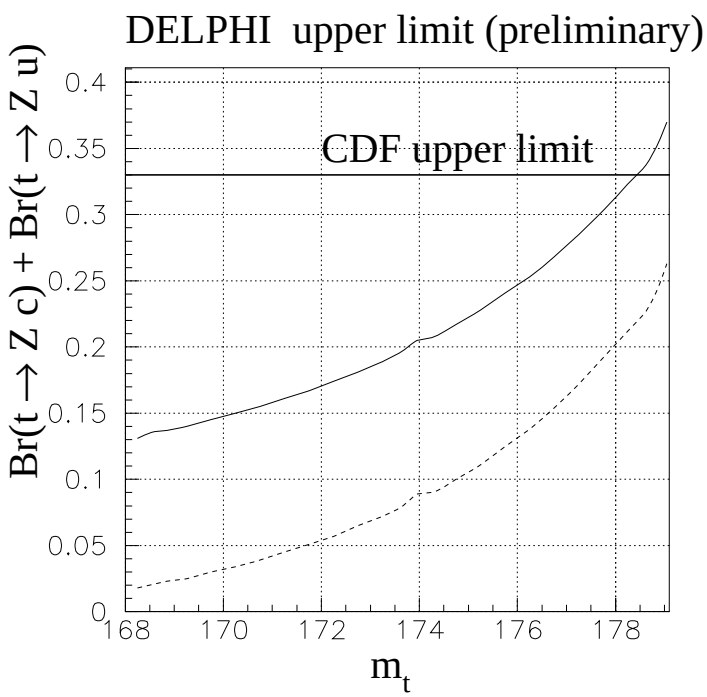


Fig. 39: Upper limit on branching fraction of $t \to Zq$ resulted from LEP 2 data. Dashed curve corresponds to $\kappa^{\gamma}_{tq} = 0$, while solid one corresponds to $\kappa^{\gamma}_{tq} < 0.78$.

*FCNC at LEP 2:* Since 1997, LEP2 has run at cms energies in excess of 180 GeV, making the production of single top quark kinematically possible through the reaction:

$$e^+ \, e^- \to \gamma^*(Z^*) \to \bar{q}. \tag{52}$$

Two LEP experiments [221, 222, 223] have presented the results of their search for this process. A short summary of these data is given in Table 18. The production cross section is very sensitive to the top quark mass, $\sigma_{tq} \sim (1 - \frac{m_t^2}{s})^2$ (see [224] for details). Therefore, the upper limit on the corresponding branching ratio depends from the exact value of $m_t$ as well, as shown in Fig.39. The current constraints on the top quark FCNC processes are summarised in Table 19. Note that the LEP2 limit is slightly better then that given by CDF (49). These constraints should further improve once the data from the highest-energy runs are analysed.

### 7.4 Search for FCNC in top quark production processes

FCNC interactions of top quarks will be probed through anomalous top decays (as discussed in Section 8.), and through anomalous production rates or channels, as discussed in the remainder of this

Table 19: Current constraints on top quark FCNC interactions.

| | | | |
|---|---|---|---|
| $t \to g\,q$ | BR$< 17\%$ | $\kappa^g_{tq} < 0.47$ | (other FCNC couplings zero) |
| $t \to \gamma\,q$ | BR$< 3.2\%$ | $\kappa^\gamma_{tq} < 0.78$ | (other FCNC couplings zero) |
| $t \to Z\,q$ | BR$< 22\%$ | $\sqrt{\lvert v^Z_{tq}\rvert^2 + \lvert a^Z_{tq}\rvert^2} < 0.55$ | (other FCNC couplings zero) |

Table 20: Upper bounds on the anomalous couplings $\kappa^g_{tu}$ and $\kappa^g_{tc}$ from single top production processes. The symbols $2 \to 1$ and $2 \to 2$ correspond to the reactions quark-gluon fusion, and single top production, respectively [225, 142].

| | Tevatron | | | LHC |
|---|---|---|---|---|
| | Run 1 | Run 2 | Run 3 | |
| $\sqrt{s}$ (TeV) | 1.8 | 2.0 | 2.0 | 14.0 |
| $\mathcal{L}(\mathrm{fb}^{-1})$ | 0.1 | 2 | 30 | 10 |
| $\kappa^g_{tu}(2 \to 1)$ | 0.058 | 0.019 | 0.0092 | 0.0033 |
| $\kappa^g_{tu}(2 \to 2)$ | 0.082 | 0.026 | 0.013 | 0.0061 |
| $\kappa^g_{tc}(2 \to 1)$ | 0.22 | 0.062 | 0.030 | 0.0084 |
| $\kappa^g_{tc}(2 \to 2)$ | 0.31 | 0.092 | 0.046 | 0.013 |

section.

### *7.41 Deviations from SM expectations for $t\bar{t}$ production*

As shown in the previous subsection, the FCNC $tgq$-vertex contributes to $gg \to t\bar{t}$ transitions, and to a possible enhancement of the top quark production at large $E_t$ and $M_{t\bar{t}}$. A recent study [220] shows that at the LHC the sensitivity to these couplings is equivalent to that found with the data of Run 1 at the Tevatron:

$$\left(\frac{\kappa^g_{tq}}{\Lambda}\right)_{\mathrm{LHC}} \simeq \left(\frac{\kappa^g_{tq}}{\Lambda}\right)_{\mathrm{FNAL}} \simeq 0.5\ \mathrm{TeV}^{-1}. \tag{53}$$

### *7.42 'Direct' top quark production ($2 \to 1$)*

The 'quark–gluon' fusion process [225] $g + u(c) \to t$ is characterised by the largest cross-section for top quark production through FCNC-interactions assuming equal anomalous couplings. At the LHC, using the CTEQ2L structure functions [115], these cross sections for $\frac{\kappa^g_{tq}}{\Lambda} = 1$ TeV$^{-1}$ are equal to:

$$\sigma(ug \to t) \simeq 4 \times 10^4\ \mathrm{pb} \quad , \quad \sigma(\bar{u}g \to t) \simeq 1 \times 10^4\ \mathrm{pb} \quad , \quad \sigma(cg \to t) \simeq 6 \times 10^3\ \mathrm{pb}. \tag{54}$$

Note that $\sigma(ug \to t)$ is about 50 times larger than the SM $t\bar{t}$ cross section. The major source of background to this is the $W+$ jet production. The additional background due to single top production, when the associated jets are not observed, should not exceed 20% of the total background and was therefore ignored. To reproduce the experimental conditions, a Gaussian smearing of the energy of the final leptons and quarks was applied (see [225] for details). Cuts on the transverse momentum ($p_T > 25$ GeV), pseudo-rapidity ($|\eta_j| < 2.0$, $|\eta_\ell| < 3.0$), and lepton-jet separation ($\Delta R \geq 0.4$) were applied. A $b$-tagging efficiency of 60% and a mistagging probability of 1% were assumed.

The criterion $S/\sqrt{S+B} \geq 3$ was used to determine the minimum values of anomalous couplings. The couplings $tgu$ and $tgc$ have been considered separately. The resulting constraints on $\kappa^g_{tu}$ and $\kappa^g_{tc}$ are given in Table 20, which also contains the results of an analysis done for the Tevatron.

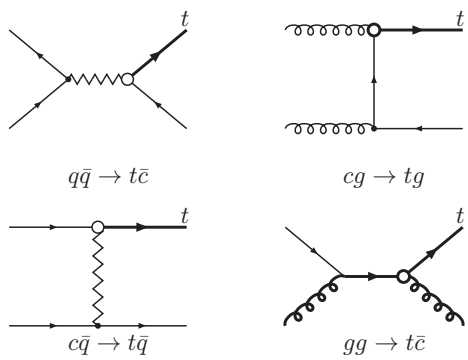


Fig. 40: 2→2 single top quark production.

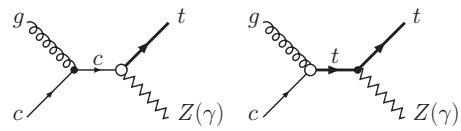


Fig. 41: $s$-channel diagrams for $tV$ ($V = Z, \gamma$) production

### *7.43 Single top quark production (2→2)*

Single top quark production in 2→2 processes has been studied as well [142]. There are four different subprocesses, which lead to one top quark in the final state together with one associated jet (see Fig. 40 and [142] for detailed considerations):

$$q\bar{q}\to t\bar{q}, \quad gg\to t\bar{q}, \quad qq\to tq, \quad qg\to tg \tag{55}$$

The major background comes from $W + 2$ jets and $W + b\bar{b}$ production, as well as from single top production. In addition to the cuts and tagging rates used in the above analysis of 'direct' top production, additional cuts on the reconstructed top mass (145 GeV $< M_{bW} <$ 205 GeV), on $p_{T\,b} > 35$ GeV, and on jet-jet and lepton-jet separation ($\Delta R_{jj} > 1.5$, $\Delta R_{lj} > 1.0$) were applied here to improve the signal/background separation. The corresponding limits on anomalous couplings in the top-gluon interaction with $c$ or $u$ quarks are given in Table 20.

### *7.44 $tZ$ and $t\gamma$ production*

All the anomalous couplings may contribute to the processes $q\,g \to t\,Z(\gamma)$, and were considered in [226, 227]. The left diagram in Fig. 41 corresponds to the $Z(\gamma)tq$ coupling, while the right one shows the top-gluon anomalous coupling (the corresponding $t$-channel diagrams are not shown). For all the calculations presented here, the MRSA PDF set [228] with $Q^2 = \hat{s}$ was used. The resulting total cross sections for $\kappa^{\gamma}_{tq} = \sqrt{|v^Z_{tq}|^2 + |a^Z_{tq}|^2} = 1$ are [227]:

$$\begin{aligned} \sigma(u\,g\to\gamma\,t) &= 73\,\mathrm{pb}, & \sigma(c\,g\to\gamma\,t) &= 10\,\mathrm{pb}, \\ \sigma(u\,g\to Z\,t) &= 746\,\mathrm{pb}, & \sigma(c\,g\to Z\,t) &= 114\,\mathrm{pb}. \end{aligned}$$

Different background sources ($W+$ jets, $Z+$ jets, $ZW+$ jets, $Wb\bar{b}+$ jets, $t\bar{t}$, and $Wt$ production) were considered. The experimental conditions were simulated by a Gaussian smearing of the lepton, photon and jet energies (see [227] for details). Cuts on the transverse momenta, $p_T(\ell,\, j,\, \gamma) > (15,\, 20,\, 40)$ GeV, on pseudo-rapidities, $|\eta_{j,\ell,\gamma}| < 2.5$, and on lepton-jet-photon separation ($\Delta R \geq 0.4$) were applied. A $b$-tagging efficiency of 60% and a mistagging probability of 1% were assumed. It was found that $b$-tagging plays an essential role in tracing the top quark and reducing backgrounds.

It has been shown that the best limits on the top quark FCNC couplings can be obtained from the decay channels $Zt\to\ell^+\ell^-\,\ell\nu b$ and $\gamma t\to\gamma\,\ell\nu b$ (see [226] and [227] for details). Upper bounds at 95% CL are derived using the FC statistics [200]. Table 21 collects the corresponding limits on eight top anomalous couplings. Like in previous cases the bounds on $u$ and $c$ couplings were obtained under the assumption that only one anomalous coupling at a time is non-zero. The analysis was done for both Tevatron and LHC but with different optimized cuts.

Table 21: Upper bounds on top anomalous couplings (see (38,39)) from $Zt$ and $\gamma t$ production. We have corrected for the different normalizations used in [226, 227].

| | Tevatron | | LHC | |
|---|---|---|---|---|
| | Run 1 | Run 2 | | |
| $\sqrt{s}$ (TeV) | 1.8 | 2.0 | 14.0 | 14.0 |
| $\mathcal{L}$ (fb$^{-1}$) | 0.1 | 2 | 10 | 100 |
| $\kappa^g_{tu}$ | 0.31 | 0.057 | 0.0097 | 0.0052 |
| $\kappa^g_{tc}$ | – | – | 0.020 | 0.011 |
| $\kappa^\gamma_{tu}$ | 0.86 | 0.18 | 0.013 | 0.0060 |
| $\kappa^\gamma_{tc}$ | – | – | 0.037 | 0.018 |
| $\sqrt{\lvert v^Z_{tu}\rvert^2 + \lvert a^Z_{tu}\rvert^2}$ | 0.49 | 0.13 | 0.016 | 0.0078 |
| $\sqrt{\lvert v^Z_{tc}\rvert^2 + \lvert a^Z_{tc}\rvert^2}$ | – | – | 0.032 | 0.016 |
| $\kappa^Z_{tu}$ | 1.71 | 0.43 | 0.040 | 0.018 |
| $\kappa^Z_{tc}$ | – | – | 0.097 | 0.046 |

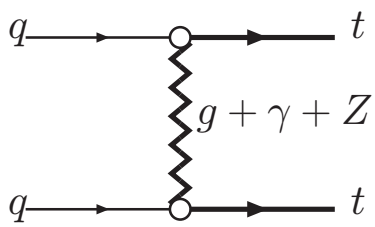


Fig. 42: Diagram describing like-sign top quark pair production

### *7.45 Like-sign $tt$ ($\bar{t}\,\bar{t}$) pair production*

Additional evidence for a FCNC $gtq$ coupling can be sought through the production of like-sign top pairs (see Fig. 42).

$$p\,p \to t\,t\,X, \quad p\,p \to \bar{t}\,\bar{t}\,X \tag{56}$$

The ATLAS collaboration performed a detailed investigation of this reaction for the case of high luminosity, $\mathcal{L}_{\rm int} = 100$ fb$^{-1}$ (see [30] and [220] for details). All the three anomalous couplings contribute to this process and the kinematics of the $tt$-pair is almost the same as for the conventional $t\bar{t}$-pair production.

An experimentally clean signature of $tt$ ($\overline{tt}$) production is the production of like-sign high $p_T$ leptons plus two hard $b$-jets. The main sources of background are $q\bar{q}' \to t\bar{t}W$ and $qq \to W^\pm q' W^\pm q'$. The expected cross sections for the signal (with $\kappa^g_{tq} = \kappa^\gamma_{tq} = |v^Z_{tc}|^2 + |a^Z_{tc}|^2 = 1$) and background processes are equal to:

$$\begin{aligned}
\sigma(tt) &= 1920 \text{ pb}, & \sigma(\overline{tt}) &= 64 \text{ pb},\\
\sigma(W^+t\bar{t}) &= 0.5 \text{ pb}, & \sigma(W^-t\bar{t}) &= 0.24 \text{ pb},\\
\sigma(W^+W^+qq) &= 0.5 \text{ pb}, & \sigma(W^-W^-qq) &= 0.23 \text{ pb}.
\end{aligned}$$

CTEQ2L structure functions [115] were used with the evolution parameter $Q^2 = m_t^2$ for the signal and $Q^2 = m_W^2$ for the background calculations. PYTHIA 5.7 [52] was used for the fragmentation and all events were passed through the ATLFAST detector simulation. An additional reducible like-sign di-lepton background is due to $t\bar{t}$ events with a $b$ semi-leptonic decay. The initial selection required therefore two like-sign *isolated* leptons with $p_T > 15$ GeV and $|\eta| < 2.5$ as well as at least two jets with $p_T > 20$ GeV and $|\eta| < 2.5$. In order to get a better signal/background separation jets with $p_T > 40$ GeV (with at least one tagged as a $b$-jet) were required (see [30, 220] for other cuts). The potential reach of this study, using the $S/\sqrt{S+B} \geq 3$ criterion, is given in Table 22.

Table 22: The limits on anomalous couplings from an improved ATLAS analysis [30, 220] of like-sign top-pair production at the LHC for the case of high luminosity, $\mathcal{L}_{\rm int} = 100$ fb$^{-1}$. The contribution from the $\sigma^{\mu\nu}$ term in the $Ztq$ vertex is ignored.

| $\kappa^g_{tu}$ | $\kappa^g_{tc}$ | $\kappa^\gamma_{tu}$ | $\kappa^\gamma_{tc}$ | $\sqrt{\vert v^Z_{tu}\vert^2 + \vert a^Z_{tu}\vert^2}$ | $\sqrt{\vert v^Z_{tc}\vert^2 + \vert a^Z_{tc}\vert^2}$ |
|---|---|---|---|---|---|
| 0.078 | 0.25 | 0.14 | 0.32 | 0.27 | 0.85 |

Table 23: Summary of the LHC sensitivity to the top quark anomalous couplings $\kappa^g_{tq}$, $\kappa^\gamma_{tq}$ and $\sqrt{|v^Z_{tu}|^2 + |a^Z_{tu}|^2}$. The resulting constraints are presented in terms of 'branching ratio', $\Gamma(t{\to}qV)/\Gamma_{SM}(= 1.56\ \mathrm{GeV})$. The results for the Tevatron option are also given (see text for explanation). $2{\to}1$, $2{\to}2$, $tV$, and $t\,t$ stand for quark-gluon fusion, single top production, $t+\gamma(Z)$ production, and like-sign top-pair final states, respectively. The 'decay', 'ATLAS', and 'CMS' labels denote the results obtained from the study of top decay channels, documented in Section 8.

| | Tevatron | | | LHC | | | |
|---|---|---|---|---|---|---|---|
| $\sqrt{s}$(TeV) | 1.8 | 2 | 2 | 14 | 14 | | |
| $\mathcal{L}$(fb$^{-1}$) | 0.1 | 2 | 30 | 10 | 100 | | |
| $tug$ | $3.1\times10^{-3}$ | $3.3\times10^{-4}$ | $7.8\times10^{-5}$ | $1.0\times10^{-5}$ | $3.2\times10^{-6}$ | $2{\to}1$ | [225] |
| | $6.2\times10^{-3}$ | $6.2\times10^{-4}$ | $1.5\times10^{-4}$ | $3.4\times10^{-5}$ | $1.1\times10^{-5}$ | $2{\to}2$ | [142] |
| | $1.8\times10^{-1}$ | $6.0\times10^{-3}$ | – | $1.7\times10^{-4}$ | $5.0\times10^{-5}$ | $tV$ | [226, 227] |
| | – | $1.9\times10^{-2}$ | $2.7\times10^{-3}$ | – | – | decay | [229] |
| | – | – | – | $1.5\times10^{-2}$ | $5.6\times10^{-3}$ | $t\,t$ | [220, 30] |
| $tcg$ | $4.4\times10^{-2}$ | $3.5\times10^{-3}$ | $8.3\times10^{-4}$ | $6.5\times10^{-5}$ | $2.1\times10^{-5}$ | $2{\to}1$ | [225] |
| | $8.8\times10^{-2}$ | $7.8\times10^{-3}$ | $2.0\times10^{-3}$ | $1.6\times10^{-4}$ | $4.9\times10^{-5}$ | $2{\to}2$ | [142] |
| | – | – | – | $7.3\times10^{-4}$ | $2.2\times10^{-4}$ | $tV$ | [226, 227] |
| | – | $1.9\times10^{-2}$ | $2.7\times10^{-3}$ | – | – | decay | [229] |
| | – | – | – | $1.6\times10^{-1}$ | $5.7\times10^{-2}$ | $t\,t$ | [220, 30] |
| $tu\gamma$ | $7.9\times10^{-2}$ | $3.5\times10^{-3}$ | – | $1.8\times10^{-5}$ | $3.9\times10^{-6}$ | $tV$ | [226, 227] |
| | – | – | – | $3.0\times10^{-3}$ | $1.1\times10^{-3}$ | $t\,t$ | [220, 30] |
| | – | – | – | $1.9\times10^{-4}$ | $4.8\times10^{-5}$ | ATLAS | [30] |
| | – | – | – | $8.6\times10^{-5}$ | $4.0\times10^{-5}$ | CMS | [230] |
| $tc\gamma$ | – | – | – | $1.5\times10^{-4}$ | $3.5\times10^{-5}$ | $tV$ | [226, 227] |
| | – | – | – | $1.7\times10^{-2}$ | $5.5\times10^{-3}$ | $t\,t$ | [220, 30] |
| | – | – | – | $1.9\times10^{-4}$ | $4.8\times10^{-5}$ | ATLAS | [30] |
| | – | – | – | $8.6\times10^{-5}$ | $4.0\times10^{-5}$ | CMS | [230] |
| $tuZ$ | $4.5\times10^{-1}$ | $3.2\times10^{-2}$ | – | $4.8\times10^{-4}$ | $1.1\times10^{-4}$ | $tV$ | [226, 227] |
| | – | $1.1\times10^{-2}$ | $5.2\times10^{-3}$ | $5.8\times10^{-4}$ | $1.9\times10^{-4}$ | decay | [219] |
| | – | – | – | $1.9\times10^{-1}$ | $6.8\times10^{-2}$ | $t\,t$ | [220, 30] |
| | – | – | – | $6.5\times10^{-4}$ | $1.0\times10^{-4}$ | ATLAS | [30] |
| | – | – | – | $1.4\times10^{-3}$ | $1.4\times10^{-4}$ | CMS | [230] |
| $tcZ$ | – | – | – | $1.9\times10^{-3}$ | $4.8\times10^{-4}$ | $tV$ | [226, 227] |
| | – | $1.1\times10^{-2}$ | $5.2\times10^{-3}$ | $5.8\times10^{-4}$ | $1.9\times10^{-4}$ | decay | [219] |
| | – | – | – | 1.9 | $6.7\times10^{-1}$ | $t\,t$ | [220, 30] |
| | – | – | – | $6.5\times10^{-4}$ | $1.0\times10^{-4}$ | ATLAS | [30] |
| | – | – | – | $1.4\times10^{-3}$ | $1.4\times10^{-4}$ | CMS | [230] |

### 7.5 Conclusion on $\mathrm{tqV}$ anomalous couplings

Table 23 presents a short summary of LHC sensitivities to anomalous FCNC couplings of the top quark. For comparison, we present also the estimates of the corresponding sensitivities at Tevatron. For completeness we anticipate and include here the results from rare decays discussed in the next section (see also [219, 229]). To unify the description of the LHC potential to detect top anomalous couplings from production and decay processes, all results in Table 23 are expressed in terms of limits on top decay branching ratios: $\Gamma(t{\to}qV)/\Gamma_{\rm SM}\,(=\,1.56\ {\rm GeV})$. The results were obtained using $m_t = 175$ GeV, $\alpha_s = 0.1$, and $\alpha = 1/128$. When needed the limits quoted in the table have been rescaled to the different luminosities and to the $S/\sqrt{S+B} \geq 3$ criterion by using a simple linear extrapolation of the available bounds (see [30, 230] and Section 8.). The limits on the top anomalous couplings from $tV$ production in Table 21 were obtained using the FC prescription [200] and have been multiplied by a factor of $\sqrt{2}$, which roughly relates this prescription with the statistical criterion adopted in Table 23 [226, 227].

At present, only few cases (like-sign top-pair production, $t{\to}qZ$ and $t{\to}q\gamma$ decays, see [30, 230]) were investigated with a more or less realistic detector simulation (ATLFAST and CMSJET). Other investigations were done at the parton level (the final quarks were considered as jets and a simple smearing of lepton, jet and photon energies was applied). Of course, more detailed investigations with a more realistic simulation of the detector response may change these results.

The most promising way to measure the anomalous FCNC top-gluon coupling seems to be the investigation of single top production processes, as the search for $t{\to}gq$ decays would be overwhelmed by background from QCD multi-jet events. At the same time, both top quark production and decay would provide comparable limits on top quark anomalous FCNC interactions with a photon or a $Z$-boson. In general, the studies shown above indicate that the LHC will improve by a factor of at least 10 the Tevatron sensitivity to top quark FCNC couplings. Of course, the results presented here are not complete, since other new kinds of interactions may lead to the appearance of unusual properties of the top quark. For example, recently proposed theories with large extra-dimensions predict a significant modification of $t\bar{t}$ pair production (see, for example, [231] and references therein). It was found that the exchange of spin-2 Kaluza-Klein gravitons leads to a modification of the total $t\bar{t}$ production rate as well as to a noticeable deviation in the $p_T$ and $M_{t\bar{t}}$ distributions with respect to the SM predictions. Naturally, we may expect also the modifications of spin-spin correlations due to graviton exchange.

It has to be stressed that different types of new interactions may affect the same observable quantity. Only a careful investigation of different aspects of top quark physics may provide a partial separation of these interactions.

## 8. RARE DECAYS OF THE TOP QUARK[23]

The production of $10^7 - 10^8$ top quark pairs per year at LHC will allow to probe the top couplings to both known and new particles involved in possible top decay channels different from the main $t{\to}bW$. Thanks to the large top mass, there are several decays that can be considered, even involving the presence of on-shell heavy vector bosons or heavy new particles in the final states. On a purely statistical basis, one should be able to detect a particular decay channel whenever its branching ratio (BR) is larger than about $10^{-6} - 10^{-7}$. In practice, we will see that background problems and systematics will lower this potential by a few orders of magnitude, the precise reduction being dependent of course on the particular signature considered. We will see, that the final detection threshold for each channel will not allow the study of many possible final states predicted in the SM, unless new stronger couplings come into play.

### 8.1 Standard Model top decays

In this section, we give an overview of the decay channels of the top quark in the framework of the SM. In the SM the decay $t{\to}bW$ is by far the dominant one. The corresponding width has been discussed in

[23]Section coordinators: B. Mele, J. Dodd (ATLAS), N. Stepanov (CMS).

Section 2.1. The rates for other decay channels are predicted to be smaller by several orders of magnitude in the SM. The second most likely decays are the Cabibbo-Kobajashi-Maskawa (CKM) non-diagonal decays $t \to sW$ and $t \to dW$. Assuming $|V_{ts}| \simeq 0.04$ and $|V_{td}| \simeq 0.01$, respectively [192], one gets

$$\mathrm{BR}(t \to sW) \sim 1.6 \times 10^{-3} \;\text{ and }\; \mathrm{BR}(t \to dW) \sim 1 \times 10^{-4} \tag{57}$$

in the SM with three families. From now on, for a generic decay channel $X$, we define

$$\mathrm{BR}(t \to X) = \frac{\Gamma(t \to X)}{\Gamma(t \to bW)_{\mathrm{SM}}}. \tag{58}$$

The two-body tree-level decay channels are the only ones that the LHC could detect in the framework of the SM. With the exception of higher-order QED and QCD radiative decays, the next less rare processes have rates no larger than $10^{-6}$.

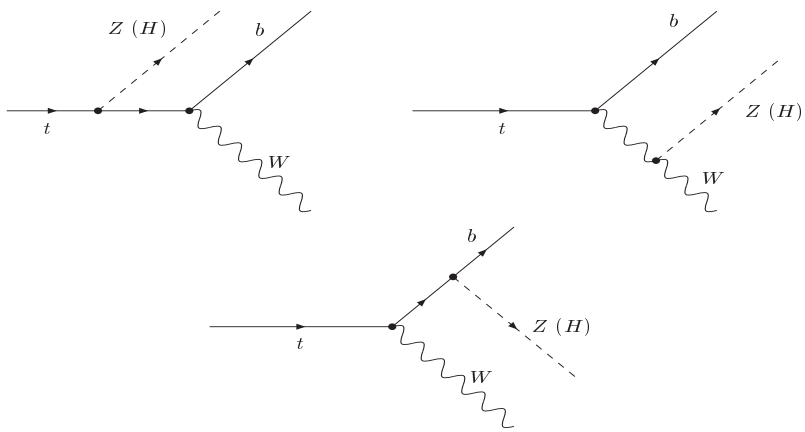


Fig. 43: Feynman graphs for the decay $t \to bWZ$ ($t \to bWH$).

At tree level, the decay $t \to bWZ$ (Fig. 43) has some peculiar features, since the process occurs near the kinematical threshold ($m_t \sim M_W + M_Z + m_b$) [232, 233, 234, 235]. This fact makes the $W$ and $Z$ finite-width effects crucial in the theoretical prediction of the corresponding width [233]. Because the $W$ and $Z$ are unstable and not observed directly, more than one definition of the $t \to bWZ$ branching ratio is possible. If defined according to

$$\tilde{\Gamma}(t \to bWZ) \equiv \frac{\Gamma(t \to b\mu\nu_\mu\nu_e\bar{\nu}_e)}{\mathrm{BR}(W \to \mu\nu_\mu)\mathrm{BR}(Z \to \nu_e\bar{\nu}_e)}, \tag{59}$$

including a consistent treatment of $W$ and $Z$ width effects, the branching ratio is to a very good approximation given by the double resonant set of diagrams (shown in Fig. 43), since the background to the neutrino decay of the $Z$ is negligible. One obtains [235], for $m_t = 175$ GeV,

$$\mathrm{BR}(t \to bWZ) = BR_{res}(t \to bWZ) = 2.1 \times 10^{-6}. \tag{60}$$

However, the signature $b\mu\nu_\mu\nu_e\bar{\nu}_e$ is not practical from an experimental point of view. In [233], a first estimate of $\mathrm{BR}(t \to bWZ)$ was given on the basis of the definition

$$\Gamma(t \to bWZ) \equiv \frac{\Gamma(t \to b\mu\nu_\mu e^+e^-)}{\mathrm{BR}(W \to \mu\nu_\mu)\mathrm{BR}(Z \to e^+e^-)}, \tag{61}$$

which involves experimentally well-observable decays, but includes contributions to the numerator from $t \to bW\gamma$ decays (with $\gamma \to e^+e^-$) and other "background" diagrams. The estimate for the corresponding branching ratio is

$$BR_{cut}(t \to bWZ) \simeq 6 \times 10^{-7}, \tag{62}$$

for $m_t = 175$ GeV, assuming a minimum cut of $0.8 M_Z$ on the $e^+e^-$-pair invariant mass. This cut tries to cope with the contribution of background graphs where the $e^+e^-$ pair comes not from a $Z$ boson but from a photon.

If the Higgs boson is light enough, one could also have the decay $t \to bWH$ (Fig. 43), although the present limits on $m_H$ strongly suppress its rate. For $m_H \gtrsim 100$ GeV, one gets [233]:

$$\mathrm{BR}(t \to bWH) \lesssim 7 \times 10^{-8}. \tag{63}$$

Finally, the decay $t \to cWW$ is very much suppressed by a GIM factor $\frac{m_b^2}{M_W^2}$ in the amplitude. One then gets [234]:

$$\mathrm{BR}(t \to cWW) \sim 10^{-13}. \tag{64}$$

One can also consider the radiative three-body decays $t \to bWg$ and $t \to bW\gamma$. These channels suffer from infrared divergences and the evaluation of their rate requires a full detector simulation, including for instance the effects of the detector resolution and the jet isolation algorithm. In an idealised situation where the rate is computed in the $t$ rest frame with a minimum cut of 10 GeV on the gluon or photon energies, one finds [236]:

$$\mathrm{BR}(t \to bWg) \simeq 0.3 \quad , \quad \mathrm{BR}(t \to bW\gamma) \simeq 3.5 \times 10^{-3}. \tag{65}$$

The FCNC decays $t \to cg$, $t \to c\gamma$ and $t \to cZ$ occur at one loop, and are also GIM suppressed by a factor $\frac{m_b^2}{M_W^2}$ in the amplitude. Hence, the corresponding rates are very small [249]:

$$\mathrm{BR}(t \to cg) \simeq 5 \times 10^{-11} \quad , \quad \mathrm{BR}(t \to c\gamma) \simeq 5 \times 10^{-13} \quad , \quad \mathrm{BR}(t \to cZ) \simeq 1.3 \times 10^{-13} \tag{66}$$

For a light Higgs boson, one can consider also the FCNC decay $t \to cH$ . A previous evaluation of its rates [249] has now been corrected. For $m_H \simeq 100\ (160)$ GeV, one gets [237]:

$$\mathrm{BR}(t \to cH) \simeq 0.9 \times 10^{-13}\ \ (4 \times 10^{-15}). \tag{67}$$

To conclude the discussion of rare SM decays of the top quark, we point out here the existence of some studies on *semi-exclusive* $t$-quark decays where the interaction of quarks among the $t$ decay products may lead to final states with one hadron (meson) recoiling against a jet. In [238] decays with an $\Upsilon$ meson in the final state and decays of the top through an off-shell $W$ with virtual mass $M_{W^*}$ near to some resonance $M$, like $\pi^+$, $\rho^+$, $K^+$, $D_s^+$, were considered. An estimate for the latter case is

$$\Gamma(t \to b\,M) \approx \frac{G_F^2\, m_t^3}{144\pi} f_M^2 |V_{qq'}|^2. \tag{68}$$

The typical values of the corresponding branching ratios are too small to be measured:

$$\mathrm{BR}(t \to b\pi) \sim 4 \cdot 10^{-8} \quad , \quad \mathrm{BR}(t \to bD_s) \sim 2 \cdot 10^{-7}. \tag{69}$$

In Table 24 we summarize the expected decay rates for the main top decay channels in the SM.

### 8.2 Beyond the Standard Model decays

The fact that a measurement of the top width is not available and that the branching ratio $\mathrm{BR}(t \to bW)$ is a model dependent quantity makes the present experimental constraints on the top decays beyond the SM quite weak. Hence, the possibility of $t$ decays into new massive states with branching fraction of order $\mathrm{BR}(t \to bW)$ is not excluded. Apart from the production of new final states with large branching fractions, we will see that new physics could also give rise to a considerable increase in the rates of many decay channels that in the SM framework are below the threshold of observability at the LHC.

Table 24: Branching ratios for the main SM top decay channels.

| channel | $BR_{\rm SM}$ | channel | $BR_{\rm SM}$ |
|---|---|---|---|
| $bW$ | $1$ | $sW$ | $1.6 \cdot 10^{-3}$ |
| $dW$ | $\sim 10^{-4}$ | $bWg$ | $0.3$ ($E_g > 10$ GeV) |
| $bW\gamma$ | $3.5 \cdot 10^{-3}$ ($E_\gamma > 10$ GeV) | $bWZ$ | $2 \cdot 10^{-6}$ |
| $cW^+W^-$ | $\sim 10^{-13}$ | $bW^+H$ | $< 10^{-7}$ |
| $qg$ | $5 \cdot 10^{-11}$ | $q\gamma$ | $5 \cdot 10^{-13}$ |
| $qZ$ | $1.3 \cdot 10^{-13}$ | $cH$ | $< 10^{-13}$ |

### *8.21 $4^{th}$ fermion family*

Extending the SM with a $4^{th}$ fermion family can alter considerably a few $t$ decay channels. First of all, when adding a $4^{th}$ family to the CKM matrix the present constraints on the $|V_{tq}|$ elements are considerably relaxed. In particular, $|V_{ts}|$ and $|V_{td}|$ can grow up to about 0.5 and 0.1, respectively [192]. Correspondingly, assuming $|V_{tb}| \sim 1$ for the sake of normalisation, one can have up to :

$$\mathrm{BR}_4(t\to sW) \sim 0.25 \;\; \text{and} \;\; \mathrm{BR}_4(t\to dW) \sim 0.01, \tag{70}$$

to be confronted with the SM expectations in (57).

The presence of a $4^{th}$ fermion family could also show up in the $t$ direct decay into a heavy $b'$ quark with a relatively small mass ($m_{b'} \sim 100$ GeV) [239]. This channel would contribute to the $t\to cWW$ decay, with a rate:

$$\mathrm{BR}(t\to W^+b'(\to W^-c)) \sim 10^{-3}\ (10^{-7}) \quad \text{at} \quad m_{b'} = 100\ (300)\ \ \mathrm{GeV}, \tag{71}$$

to be confronted with the SM prediction in (64).

### *8.22 Two Higgs Doublet models (2HDM's)*

The possibility that the EW symmetry breaking involves more than one Higgs doublet is well motivated theoretically. In particular, three classes of two Higgs doublet models have been examined in connection with rare top decays, called model I, II and III. The first two are characterised by an *ad hoc* discrete symmetry which forbids tree-level FCNC [240], that are strongly constrained in the lightest quark sector. In model I and model II, the up-type quarks and down-type quarks couple to the same scalar doublet and to two different doublets, respectively (the Higgs sector of the MSSM is an example of model II). In model III [241, 242], the above discrete symmetry is dropped and tree-level FCNC are allowed. In particular, a tree-level coupling $tcH$ is predicted with a coupling constant $\lesssim \sqrt{m_t m_c}/v$ (where $v$ is the Higgs vacuum expectation value).

Since enlarging the Higgs sector automatically implies the presence of charged Higgs bosons in the spectrum, one major prediction of these new frameworks is the decay $t\to bH^+$, possibly with rates competitive with $\mathrm{BR}(t\to bW)$ for $m_{H^+} \lesssim 170$ GeV. In the MSSM, one expects $\mathrm{BR}(t\to bH^+) \sim 1$, both at small and large values of $\tan\beta$. The interaction Lagrangian describing the $H^+t\,\bar{b}$-vertex in the MSSM is [243]:

$$\mathcal{L}_{Htb} = \frac{g}{\sqrt{2}M_W}\, H^+\, \left[\bar{t}\,(m_t \cot\beta\, P_L + m_b \tan\beta\, P_R)\, b + \bar{\nu}\,(m_\ell \tan\beta\, P_R)\, \ell\right] \,+\, \mathrm{h.c.}\,, \tag{72}$$

where $P_{L,R} = 1/2(1 \mp \gamma_5)$ are the chiral projector operators.

At tree level the corresponding decay widths of $t\to bH^+$, $H^+\to\tau\nu$, and $H^+\to t\bar{b}$ (or, analogously, of $H^+\to c\bar{s}$) are equal to [243]

$$\Gamma(t\to bH^+) \;\; = \;\; \frac{g^2}{64\pi M_W^2 m_t}|V_{tb}|^2\lambda^{1/2}\left(1, \frac{m_b^2}{m_t^2}, \frac{m_H^2}{m_t^2}\right) \times$$

$$\left[(m_t^2+m_b^2-m_H^2)(m_t^2\cot^2\beta+m_b^2\tan^2\beta)+4m_t^2m_b^2\right], \tag{73}$$

$$\Gamma(H^+\to\tau^+\nu) = \frac{g^2 m_H}{32\pi M_W^2} m_\tau^2 \tan^2\beta, \tag{74}$$

$$\Gamma(H^+\to t\bar{b}) = \frac{3g^2}{32\pi M_W^2 m_H}|V_{tb}|^2\lambda^{1/2}\left(1,\frac{m_b^2}{m_H^2},\frac{m_t^2}{m_H^2}\right)\times \left[(m_H^2-m_t^2-m_b^2)(m_t^2\cot^2\beta+m_b^2\tan^2\beta)-4m_t^2m_b^2\right], \tag{75}$$

where $\lambda(a,b,c)=a^2+b^2+c^2-2(ab+ac+bc)$, and $m_H\equiv m_{H^+}$.

Consequently, if $m_H < m_t - m_b$, one expects $H^+\to\tau^+\nu$ (favoured for large $\tan\beta$) and/or $H^+\to c\bar{s}$ (favoured for small $\tan\beta$) to be the dominant decays. Hence, for $\tan\beta > 1$ and $H^+\to\tau^+\nu$ dominant, one can look for the channel $t\to bH^+$ by studying a possible excess in the $\tau$ lepton signature from the $t$ pair production [244]. On the other hand, if $\tan\beta < 2$ and $m_H > 130$ GeV, the large mass (or coupling) of the $t$-quark causes $\mathrm{BR}(H^+\to t^*\bar{b}\to W^+b\bar{b})$ to exceed $\mathrm{BR}(H^+\to c\bar{s})$ (Fig. 44, see [245] for details).

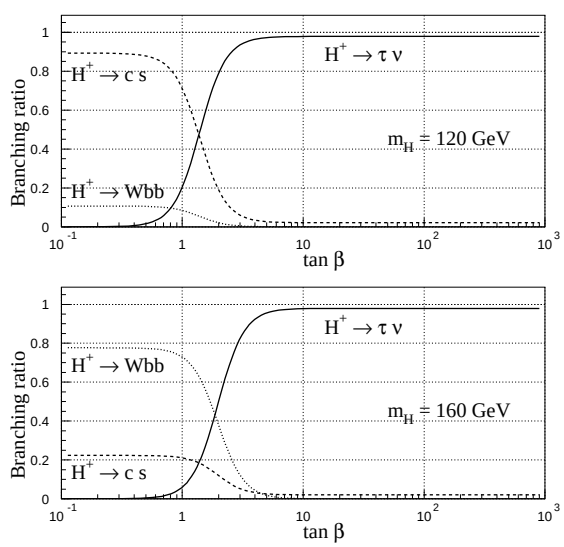


Fig. 44: Branching fractions for three $H^+$ decay modes for two values of $m_{H^+}$ vs. $\tan\beta$.

As a consequence, new interesting signatures at LHC such as leptons plus multi-jet channels with four $b$-tags, coming from the gluon-gluon fusion process $gg\to t\bar{b}H^-$, followed by the $H^-\to\bar{t}b$ decay, have been studied [246]. These processes could provide a viable signature over a limited but interesting range of the parameter space.

One should recall however that both $\mathrm{BR}(t\to bH^+)$ and $\mathrm{BR}(H^+\to W^+b\bar{b})$ are very sensitive to higher-order corrections, which are highly model dependent [247].

In model III, the tree-level FCNC decay $t\to ch$ can occur with branching ratios up to $10^{-2}$ [242]. In [248], the rate for the channel $t\to ch\to cWW(cZZ)$ has been studied. Accordingly, $\mathrm{BR}(t\to cWW)$ can be enhanced by several orders of magnitude with respect to its SM value. In particular, for an on-shell decay with $2M_W \lesssim m_h \lesssim m_t$, one can have up to $\mathrm{BR}(t\to cWW)\sim 10^{-4}$ from this source. The same process was considered in a wider range of models, where the decay $t\to cWW$ can occur not only through a scalar exchange but also through a fermion or vector exchange [239]. In this framework, the fermion exchange too could lead to detectable rates for $t\to cWW$, as in (71).

In 2HDM's, the prediction for the FCNC decays $t\to cg$, $t\to c\gamma$ and $t\to cZ$ can also be altered. While in models I and II the corresponding branching fractions cannot approach the detectability threshold [249], in model III predicts values up to $\mathrm{BR}(t\to cg) \simeq 10^{-5}$, $\mathrm{BR}(t\to c\gamma) \simeq 10^{-7}$ and $\mathrm{BR}(t\to cZ) \simeq 10^{-6}$ [217].

By further extending the 2HDM's Higgs sector and including Higgs triplets, one can give rise to a vertex $HWZ$ at tree level in a consistent way [250]. Accordingly, the $t\to bWZ$ decay can be mediated by a charged Higgs (coupled with $m_t$) that can enhance the corresponding branching fraction up to $\mathrm{BR}(t\to bWZ) \sim 10^{-2}$. Large enhancements can also be expected in similar models for the channels $t\to sWZ$ and $t\to dWZ$.

### *8.23 Minimal Supersymmetric Standard Model (MSSM)*

Supersymmetry could affect the $t$ decays in different ways. (Here, we assume the MSSM framework [26], with (or without, when specified) $R$ parity conservation.)

First of all, two-body decays into squarks and gauginos, such as $t\to\tilde{t}_1\tilde{g}$, $t\to\tilde{b}_1\tilde{\chi}_1^+$, $t\to\tilde{t}_1\tilde{\chi}_1^0$, could have branching ratios of order $\mathrm{BR}(t\to bW)$, if allowed by the phase space (see, i.e. [251] for references). QCD corrections to the channel $t\to\tilde{t}_1\tilde{g}$ have been computed in [252] and were found to increase its width up to values even larger than $\Gamma(t\to bW)$. Three-body $t$ decays in supersymmetric particles were surveyed in [251].

The presence of light top and bottom squarks, charginos and neutralinos in the MSSM spectrum could also give rise to a CP asymmetry of the order $10^{-3}$ in the partial widths for the decays $t\to bW^+$ and $\bar{t}\to\bar{b}W^-$ [140, 253].

Explicit $R$-parity violating interactions [254] could provide new flavour-changing $t$ decays, both at tree-level (as in the channels $t\to\tilde{\tau}b$ and $t\to\tau b\tilde{\chi}_1^0$ [255]) and at one loop (as in $t\to c\tilde{\nu}$ [256]), with observable rates. For instance, $\mathrm{BR}(t\to c\tilde{\nu}) \sim 10^{-4} - 10^{-3}$ in particularly favourable cases.

Another sector where supersymmetric particles could produce crucial changes concerns the one-loop FCNC decays $t\to cg$, $t\to c\gamma$, $t\to cZ$ and $t\to cH$ , which in the SM are unobservably small. In the MSSM with universal soft breaking the situation is not much affected, while, by relaxing the universality with a large flavour mixing between the $2^{nd}$ and $3^{rd}$ family only, one can reach values such as [257, 258]:

$$\mathrm{BR}_{\mathrm{MSSM}}(t\to cg) \sim 10^{-6} \quad , \quad \mathrm{BR}_{\mathrm{MSSM}}(t\to c\gamma) \sim 10^{-8} \quad , \quad \mathrm{BR}_{\mathrm{MSSM}}(t\to cZ) \sim 10^{-8}, \tag{76}$$

which, however, are still not observable. The introduction of baryon number violating couplings in broken $R$-parity models could on the other hand give large enhancements [218], and make some of these channels observable:

$$\mathrm{BR}_{\not{R}}(t\to cg) \sim 10^{-3} \quad , \quad \mathrm{BR}_{\not{R}}(t\to c\gamma) \sim 10^{-5} \quad , \quad \mathrm{BR}_{\not{R}}(t\to cZ) \sim 10^{-4}. \tag{77}$$

A particularly promising channel is the FCNC decay $t\to ch$ in the framework of MSSM, where $h = h^0, H^0, A^0$ is any of the supersymmetric neutral Higgs bosons [259]. By including the leading MSSM contributions to these decays (including gluino-mediated FCNC couplings), one could approach the detectability threshold, especially in the case of the light CP-even Higgs boson, for which one can get up to:

$$\mathrm{BR}_{\mathrm{MSSM}}(t\to ch^0) \sim 10^{-4}. \tag{78}$$

### *8.24 Anomalous couplings*

In the framework of the top anomalous couplings described in Section 7., one can predict large enhancements in different FCNC top decay channels. While the $t\to cg$, $t\to c\gamma$, and $t\to cZ$ processes are analysed in section 7., here we concentrate on the possible FCNC contributions to the top decays into two gauge

bosons, $t \to qVV$, where $V$ is either a $W$ or a $Z$ and $q = c, u$:

$$t \to qW^+Z \quad , \quad t \to qW^+W^- \quad , \quad t \to qZZ. \tag{79}$$

In the SM, the first two decays occur at tree level, while $t \to qZZ$ proceeds only through loop contributions. We will see that within the present experimental limits on the top anomalous couplings, the rates for these processes can be large with respect to the SM prediction, but are still below the detectability threshold at the LHC.

The FCNC contribution to the first channel in (79), for the anomalous coupling $\kappa_z \approx 0.3$, has a rate of the the same order of magnitude as the SM $\mathrm{BR}(t \to bWZ)$ [260]:

$$\mathrm{BR}_{\mathrm{FCNC}}(t \to cWZ) \sim 10^{-6} \approx \mathrm{BR}_{\mathrm{SM}}(t \to bWZ). \tag{80}$$

Top anomalous FCNC interactions with both a photon and a $Z$-boson contribute to the second process in eq.(79). Contrary to the SM case this amplitude has no GIM suppression. As a result, the corresponding branching ratio can have almost the same value as that of the $t \to qWZ$ decay [260]:

$$\mathrm{BR}_{\mathrm{FCNC}}(t \to cW^+W^-) \sim 10^{-7} \gg \mathrm{BR}_{\mathrm{SM}}(t \to cWW). \tag{81}$$

For the $t \to qZZ$ decay mode, a coupling $\kappa_z \sim 0.3$ gives a branching ratio much greater than the corresponding SM one ( $\lesssim 10^{-13}$ [260]):

$$\mathrm{BR}_{\mathrm{FCNC}}(t \to qZZ) \sim 10^{-8} \gg \mathrm{BR}_{\mathrm{SM}}(t \to qZZ), \tag{82}$$

but still too small to be detected at LHC.

In summary, the observation of any of these decays at LHC would indicate new physics not connected with the top FCNC interactions (see, for example, [248]).

### 8.3 ATLAS studies of (rare) top quark decays and couplings

In ATLAS various analyses have been performed on top decays, using the PYTHIA Monte-Carlo interfaced to a fast detector simulation (ATLFAST). In the following, the most relevant results are reported.

#### *8.31* $\mathrm{BR}(t \to bX)$ *and measurement of* $|V_{tb}|$

The SM prediction $\mathrm{BR}(t \to W^+b) \approx 1$ can be checked by comparing the number of observed (1 or 2) $b$-tags in a $t\bar{t}$ sample. The first $b$-tag is used to identify the event as a $t\bar{t}$ event, and the second $b$-tag (if seen) is used to determine the fraction of top decays producing a $b$ quark. Within the three-generation SM, and assuming unitarity of the CKM matrix, the ratio of double $b$-tag to single $b$-tag events is given by:

$$\mathrm{R}_{2b/1b} = \mathrm{BR}(t \to Wb)/\mathrm{BR}(t \to Wq) = |V_{tb}|^2/(|V_{tb}|^2 + |V_{ts}|^2 + |V_{td}|^2) = |V_{tb}|^2 \tag{83}$$

The CDF collaboration has used the tagging method in leptonic $t\bar{t}$ events to obtain the result $\mathrm{R}_{2b/1b} = 0.99 \pm 0.29$ [261], which translates to a limit of $|V_{tb}| > 0.76$ at the 95% CL assuming three-generation unitarity. If this constraint is relaxed, a lower bound of $|V_{tb}| > 0.048$ at the 95% CL is obtained, implying only that $|V_{tb}|$ is much larger than either $|V_{ts}|$ or $|V_{td}|$.

The LHC will yield a much more precise measurement of $\mathrm{R}_{2b/1b}$. For example, $t\bar{t}$ events in the single lepton plus jets mode can be selected by requiring an isolated electron or muon with $p_T > 20$ GeV, $E_T^{miss} > 20$ GeV, and at least four jets with $p_T > 20$ GeV. Requiring that at least one of the jets be tagged as a $b$-jet produces a clean sample of $t\bar{t}$ events, with $S/B$ = 18.6, with the remaining background coming mostly from $W$+jet events [30]. Assuming a $b$-tagging efficiency of 60%, a sample of 820 000 single $b$-tagged events would be selected for an integrated luminosity of 10 fb$^{-1}$. Of these,

276 000 would be expected to have a second $b$-tag, assuming the SM top quark branching ratios. This ATLAS study indicates that the statistical precision achievable would correspond to a relative error of $\delta\mathrm{R}_{2b/1b}/\mathrm{R}_{2b/1b}$ (stat.) = 0.2% for an integrated luminosity of 10 fb$^{-1}$. The final uncertainty will be dominated by systematic errors due to the uncertainty in the $b$-tagging efficiency and fake $b$-tag rates, as well as correlations affecting the efficiency for $b$-tagging two different jets in the same event. Further study is needed to estimate the size of these systematic uncertainties.

### *8.32* $\mathrm{BR}(t\to WX)$

The measurement of the ratio of di-lepton to single lepton events in a $t\bar{t}$ sample can be used to determine $\mathrm{BR}(t\to WX)$. In this case, the first lepton tags the $t\bar{t}$ event, and the presence of a second lepton is used to determine the fraction of top quark decays producing an isolated lepton, which can be then be related to the presence of a $W$ (or other leptonically decaying states) in the decay. The SM predicts that $\mathrm{R}_{2l/1l}$ = $\mathrm{BR}(W\to\ell\nu)\approx$ 2/9 where $\ell=(e,\mu)$. Deviations from this prediction could be caused by new physics, for example, the existence of a charged Higgs boson. The dominant $H^+$ decays in such instances are usually considered to be $H^+\to\tau\nu$ or $H^+\to c\bar{s}$. In either case, the number of isolated electrons and muons produced in top decay would be reduced, and $\mathrm{R}_{2l/1l}$ would be less than the SM prediction.

A study performed by ATLAS [30] shows that with an integrated luminosity of 10 fb$^{-1}$, a clean sample of about 443 000 $t\bar{t}$ events in the single lepton plus jets mode could be selected by requiring an isolated electron or muon with $p_T>$ 20 GeV, $E_T^{miss}>$ 20 GeV, and at least two $b$-tagged jets with $p_T>$ 20 GeV. To determine $\mathrm{R}_{2l/1l}$, one then measures how many of these events have a second isolated electron or muon, again with $p_T>$ 20 GeV, and of the opposite sign to the first lepton. Assuming the SM, one would expect a selected sample of about 46 000 di-lepton events with these cuts. Given these numbers, the statistical precision achievable would correspond to a relative error of $\delta\mathrm{R}_{2l/1l}/\mathrm{R}_{2l/1l}$ (stat.) = 0.5% for an integrated luminosity of 10 fb$^{-1}$. Further study is required to estimate the systematic uncertainty on $\mathrm{R}_{2l/1l}$ due to the lepton identification and fake rates.

### *8.33 Radiative Decays:* $t\to WbZ, t\to WbH$

The 'radiative' top decay $t\to WbZ$ has been suggested [233] as a sensitive probe of the top quark mass, since the measured value of $m_t$ is close to the threshold for this decay. For the top mass of (173 $\pm$ 5.2) GeV [192], the SM prediction, based on the $Z\to ee$ signature and a cut $m_{ee}>0.8M_Z$ (see Section 8.1), is $\mathrm{BR}_{cut}(t\to WbZ)$ = $(5.4^{+4.7}_{-2.0})\times10^{-7}$ [233]. Thus, within the current uncertainty $\delta m_t\approx$ 5 GeV, the predicted branching ratio varies by approximately a factor of three. A measurement of $\mathrm{BR}(t\to WbZ)$ could therefore provide a strong constraint on the value of $m_t$. Similar arguments have been made for the decay $t\to WbH$, assuming a relatively light SM Higgs boson.

ATLAS has studied the experimental sensitivity to the decay $t\to WbZ$ [30, 262], with the $Z$ being reconstructed via the leptonic decay $Z\to ll$ ($\ell=e,\mu$), and the $W$ through the hadronic decay $W\to jj$. The efficiency for exclusively reconstructing $t\to WbZ$ is very low, due to the soft $p_T$ spectrum of the $b$-jet in the $t\to WbZ$ decay. Instead, a semi-inclusive technique was used, where a $WZ$ pair close to threshold was searched for as evidence of the $t\to WbZ$ decay. Since the $t\to WbZ$ decay is so close to threshold, the resolution on $m_{WZ}$ is not significantly degraded with respect to the exclusive measurement. The selection of $Z\to ll$ candidates required an opposite-sign, same-flavor lepton pair, each lepton having $p_T>$ 30 GeV and $|\eta|<$ 2.5. The clean $Z\to ll$ signal allows a wide di-lepton mass window to be taken (60 GeV $<m_{\ell\ell}<$ 100 GeV) in order to have very high efficiency. Candidates for $W\to jj$ decay were formed by requiring at least two jets, each having $p_T>$ 30 GeV and $|\eta|<$ 2.5, and satisfying 70 GeV $<mjj<$ 90 GeV. The $lljj$ invariant mass resolution was $\sigma[m_{WZ}]$ = 7.2 $\pm$ 0.4 GeV, and the signal efficiency was 4.3%.

The dominant backgrounds come from processes with a $Z$ boson in the final state, primarily $Z$+jet production, and to a much lesser extent from $W$Z and $t\bar{t}$ production. In order to reduce the

$Z$+jet background, an additional cut requiring a third lepton with $p_T > 30$ GeV was made. For the signal process $t\bar{t} \to (WbZ)(Wb)$, this cut selects events in which the $W$ from the other top decays leptonically. After this selection, and with a cut on $m_{WZ}$ of $\pm 10$ GeV around the top mass, the total expected background was reduced to $\approx 1.5$ events (mostly from $WZ$ production) per 10 fb$^{-1}$. Requiring at least five events for signal observation leads to a branching ratio sensitivity of order $10^{-3}$. Since the background has been reduced essentially to zero, the sensitivity should improve approximately linearly with integrated luminosity. However, even with a factor of ten improvement for an integrated luminosity of 100 fb$^{-1}$, the sensitivity would still lie far above the SM expectation of order $10^{-7} - 10^{-6}$.

Given this result, observation of the decay $t \to WbH$ does not look possible. The current LEP limit on $m_H$ implies that the Higgs is sufficiently heavy that, in the most optimistic scenario that the Higgs mass is just above the current limit, $\mathrm{BR}(t \to WbH) \lesssim \mathrm{BR}(t \to WbZ)$. As $m_H$ increases further, $\mathrm{BR}(t \to WbH)$ drops quickly. Assuming $m_H \approx m_Z$, one would have to search for $t \to WbH$ using the dominant decay $H \to b\bar{b}$. The final state suffers much more from background than in the case of $t \to WbZ$, where the clean $Z \to \ell^+\ell^-$ signature is a key element in suppressing background. Although $\mathrm{BR}(H \to b\bar{b})$ in this $m_H$ range is much larger than BR($Z \to \ell^+\ell^-$ ), the large increase in background will more than compensate for the increased signal acceptance, and so one expects the sensitivity to $\mathrm{BR}(t \to WbH)$ to be worse than for $\mathrm{BR}(t \to WbZ)$. The decay $t \to WbH$ has therefore not been studied in further detail.

### *8.34* $t \to H^+b$

Limits on the mass of the charged Higgs have been obtained from a number of experiments. An indirect limit obtained from world averages of the $\tau$ branching ratios excludes at 90% CL any charged Higgs with $m_{H^+} < 1.5 \tan\beta$ GeV [263], where $\tan\beta$ is the ratio of the vacuum expectation values of the two Higgs doublets. CLEO indirectly excludes $m_{H^+} < 244$ GeV for $\tan\beta > 50$ at 95% CL, assuming a two-Higgs-doublet extension to the SM [212], while the LEP experiments directly exclude $m_{H^+} < 59.5$ GeV/$c^2$ at 95% CL [264]. Searches at the Tevatron have extended the region of excluded $[m_{H^\pm}, \tan\beta]$ parameter space, particularly at small and large $\tan\beta$, and set a limit on the branching ratio $\mathrm{BR}(t \to H^+b) <$ 0.45 at 95% CL [265]. Run 2 at the Tevatron will be sensitive to branching fractions $\mathrm{BR}(t \to H^+b) >$ 11% [266].

ATLAS has performed an analysis of the experimental sensitivity to the $t \to H^+b$ decay, followed by $H^+ \to \tau\nu$, in the context of the MSSM [30, 267]. Since the relevant $t \to H^+b$ branching ratio is proportional to $(m_t^2 \cot^2\beta + m_b^2 \tan^2\beta)$ (see (73)), for a given value of $m_{H^\pm}$ the branching ratio for such decays is large at small and at large $\tan\beta$, but has a pronounced minimum at $\tan\beta \sim \sqrt{m_t/m_b} \sim$ 7.5. The exact position of this minimum and its depth is sensitive to QCD corrections to the running $b$-quark mass.

In the ATLAS analysis, an isolated high-$p_T$ lepton with $|\eta| < 2.5$ is required to trigger the experiment, which in signal events originates from the semi-leptonic decay of the second top quark. One identified hadronic tau is then required, and at least three jets with $p_T > 20$ GeV and $|\eta| < 2.5$, of which two are required to be tagged as $b$-jets. This reduces the potentially large backgrounds from $W$+jet and $b\bar{b}$ production to a level well below the $t\bar{t}$ signal itself. These cuts enhance the $\tau$-lepton signal from $H^\pm$ decays with respect to that from $W$ decay, and select mostly single-prong $\tau$-decays. After the selection cuts and the $\tau$ identification criteria are applied, $t \to H^+b$ decays appear as final states with an excess of events with one isolated $\tau$-lepton compared to those with an additional isolated electron or muon.

A signal from charged Higgs-boson production in $t\bar{t}$ decays would be observed for all values of $m_{H^\pm}$ below $m_t - 20$ GeV over most of the $\tan\beta$ range. For moderate values of $\tan\beta$, for which the expected signal rates are lowest, the accessible values of $m_{H^\pm}$ are lower than this value by 20 GeV. The limit on the sensitivity to $\mathrm{BR}(t \to H^+b)$ is dominated by systematic uncertainties, arising mainly from imperfect knowledge of the $\tau$-lepton efficiency and of the number of fake $\tau$-leptons present in the final sample. These uncertainties are estimated to limit the achievable sensitivity to $\mathrm{BR}(t \to H^+b)$ = 3%.

For charged Higgs masses below 150 GeV and for low values of $\tan\beta$, the $H^{\pm}\rightarrow cs$ and $H^{\pm}\rightarrow cb$ decay modes are not negligible. In the same mass range, the three-body off-shell decays $H^{\pm}\rightarrow hW^{*}$, $H^{\pm}\rightarrow AW^{*}$ and $H^{\pm}\rightarrow bt^{*}\rightarrow bbW$ also have sizeable branching ratios. When the phase-space increases, for 150 GeV $< m_{H^{\pm}} <$ 180 GeV, both the $bbW$ and the $hW^{*}$ mode could be enhanced with respect to the $\tau\nu$ mode. Decays into the lightest chargino $\tilde{\chi}_1^{\pm}$ and neutralino $\tilde{\chi}_1^0$ or decays into sleptons would dominate whenever kinematically allowed. For large values of $\tan\beta$ the importance of these SUSY decay modes would be reduced. However, for values as large as $\tan\beta$ = 50, the decay $H^{\pm}\rightarrow\tilde{\tau}\tilde{\nu}$ would be enhanced, provided it is kinematically allowed and would lead to $\tau$'s in the final state. Their transverse momentum spectrum is, however, expected to be softer than that of $\tau$'s from the direct $H^{\pm}\rightarrow\tau\nu$ decays.

The $H^{\pm}\rightarrow cs$ decay mode has been considered as a complementary one to the $H^{\pm}\rightarrow\tau\nu$ channel by ATLAS for low values of $\tan\beta$. In the ATLAS analysis, one isolated high $p_T$ lepton with $|\eta| <$ 2.5 is required to trigger the experiment, which in signal events originates from the semi-leptonic decay of the second top quark. Two $b$-tagged jets with $p_T >$ 15 GeV and $|\eta| <$ 2.5 are also required, with no additional $b$-jet. Finally, at least two non-$b$ central jets with $|\eta| <$ 2.0 are required for the $H^{\pm}\rightarrow cs$ reconstruction, and no additional jets above 15 GeV in this central region. Evidence for $H^{\pm}$ is searched for in the two-jet mass distribution. The mass peak from an $H^{\pm}$ decay can be reconstructed with a resolution of $\sigma = (5-8)$GeV if the mass of the $H^{\pm}$ is in the range between 110 and 130 GeV. In this mass range, the peak sits on the tail of the reconstructed $W\rightarrow jj$ distribution from $t\bar{t}$ background events which decay via a $Wb$ instead of a $H^{\pm}b$. In the mass range 110 $< H^{\pm} <$ 130 GeV, the $H^{\pm}$ peak can be separated from the dominant $W\rightarrow jj$ background, with $S/B \approx$ 4-5% and $S/\sqrt{B} \sim$ 5. This channel is complementary to the $H^{\pm}\rightarrow\tau\nu$ channel for low $\tan\beta$ values. Whereas the $H^{\pm}\rightarrow\tau\nu$ channel allows only the observation of an excess of events, it is possible to reconstruct a mass peak in the $H^{\pm}\rightarrow cs$ decay mode.

The $H^{\pm}\rightarrow hW^{*}$, $H^{\pm}\rightarrow AW^{*}$ and $H^{\pm}\rightarrow bt^{*}\rightarrow bbW$ have not been studied so far by ATLAS. With the expected $b$-tagging efficiency, these multi-jet decay modes are very interesting for a more detailed investigation.

### *8.35 $t\rightarrow Zq$ decay*

The sensitivity to the FCNC decay $t\rightarrow Zq$ (with $q = u, c$) has been analyzed [268] by searching for a signal in the channel $t\bar{t}\rightarrow(Wb)(Zq)$, with the boson being reconstructed via the leptonic decay $Z\rightarrow ll$. The selection cuts required a pair of isolated, opposite sign, same flavor leptons (electrons or muons), each with $p_T >$ 20 GeV and $|\eta| <$ 2.5 and with $|m_{ll} - m_Z| <$ 6 GeV. The dominant backgrounds come from $Z + jet$ and $WZ$ production. Not only cuts were applied on the $Zq$ final state, but also on the $Wb$ decay of the other top quark in the event, to further reduce the background. Two different possible decay chains have been considered: the first ("leptonic mode") where the $W$ decays leptonically $W\rightarrow\ell\nu$, and the second ("hadronic mode") with $W\rightarrow jj$. The hadronic $W$ decay signature has a much larger branching fraction, but suffers from larger backgrounds. The search in the leptonic mode required, in addition to the leptons from the Z boson decay, a further lepton with $p_T >$ 20 GeV and $|\eta| <$ 2.5, $E_T^{miss}$ $>$ 30 GeV, and at least two jets with $p_T >$ 50 GeV and $|\eta| <$ 2.5. Exactly one of the high $p_T$ jets was required to be tagged as a $b$-jet. The invariant mass spectrum of each $Zq$ combination was then formed from the $Z\rightarrow ll$ candidates taken with each of the non $b$-tagged jets. The $Zq$ invariant mass resolution was 10.1 GeV. Combinations were accepted if $m_{Zq}$ agreed with the known top mass within $\pm$ 24 GeV. Assuming an integrated luminosity of 100 fb$^{-1}$, 6.1 signal events survive the cuts with 7 background events. A value of $\mathrm{BR}(t\rightarrow Zq)$ as low as $2\cdot10^{-4}$ could be discovered at the 5$\sigma$ level.

The search in the hadronic mode required, in addition to the $Z\rightarrow ll$ candidate, at least four jets with $p_T >$ 50 GeV and $|\eta| <$ 2.5. One of the jets was required to be tagged as a $b$-jet. To further reduce the background, the decay $t\rightarrow jjb$ was first reconstructed. A pair of jets, among those not tagged as a $b$-jet, was considered a W candidate if $|m_{jj} - M_W| <$ 16 GeV. $W$ candidates were then combined with the $b$-jet, and considered as a top candidate if $|m_{jjb} - m_t| <$ 8 GeV. For those events with an accepted

$t \to jjb$ candidate, the invariant mass of the $Z$ candidate with the remaining unassigned high $p_T$ jets was calculated to look for a signal from $t \to Zq$ decays. Combinations were accepted in case $|m_{Zq} - m_t|$ $<$ 24 GeV. Assuming an integrated luminosity of 100 fb$^{-1}$, one would get 0.4 signal events, with 2 background events.

### *8.36 $t \to \gamma q$ decay*

The FCNC decay $t \to \gamma q$ (with $q = u, c$) can be searched for as a peak in the $M_{\gamma j}$ spectrum in the region of $m_t$. The requirement of a high $p_T$ isolated photon candidate in $t\bar{t} \to (Wb)(\gamma q)$ events is not sufficient to reduce the QCD multi-jet background to a manageable level. Therefore, the $t \to Wb$ decay of the other top (anti-) quark in the event was reconstructed using the leptonic $W \to \ell\nu$ decay mode, and looking for the $t\bar{t} \to (Wb)(\gamma q) \to (\ell\nu b)(\gamma q)$ final state. For the event selection, the ATLAS collaboration [30, 262] required the presence of an isolated photon with $p_T >$ 40 GeV and $|\eta| <$ 2.5, an isolated electron or muon with $p_T >$ 20 GeV and $|\eta| <$ 2.5, and $\mathrm{E}_T^{miss} >$ 20 GeV. Exactly 2 jets with $p_T$ $>$ 20 GeV were required, in order to reduce the $t\bar{t}$ background. At least one of the jets was required to be tagged as a $b$-jet with $p_T >$ 30 GeV and $|\eta| <$ 2.5. The $t \to \ell\nu b$ candidate was first reconstructed. The combination was accepted as a top quark candidate if $m_{\ell\nu b}$ agreed with $m_t$ within $\pm$20 GeV. For these events the $t \to \gamma q$ decay was sought by combining the isolated photon with an additional hard jet with $p_T >$ 40 GeV and $|\eta| <$ 2.5. The invariant mass of the $\gamma j$ system was required to agree with the known value of $m_t$ within $\pm$20 GeV. The $m_{\gamma j}$ resolution with the cuts described above was 7.7 GeV, and the signal efficiency (not counting branching ratios) was 3.3%, including a $b$-tagging efficiency of 60%. The background (155 events for an integrated luminosity of 100 fb$^{-1}$) is dominated by events with a real $W \to \ell\nu$ decay and either a real or a fake photon. These processes include $t\bar{t}$, single top production, $W + jets$ and $Wbb$ production. The corresponding $5\sigma$ discovery limit is

$$\mathrm{BR}(t \to \gamma q) = 1.0 \times 10^{-4}. \tag{84}$$

### *8.37 $t \to gq$ decay*

The search for a FCNC $tgq$ coupling (with $q = u, c$) through the decay $t \to gq$ was analyzed in [229] for the Tevatron. However, as can be seen from Table 23 in Section 7., the sensitivity for such a coupling turns our to be much larger in the $t$ production processes than in the decay $t \to gq$, whose signal will be overwhelmed by the QCD background. We refer the reader to Section 7. for a detailed discussion of this point.

## 8.4 CMS studies of FCNC top quark decays and t$\to$ H$^+$b

The CMS sensitivity to $t \to \gamma(Z)(u, c)$ decays was studied recently (see [230] for details). The PYTHIA 5.7 [52] generator was used for the signal and background simulations and the detector response was simulated at the fast MC level (CMSJET [177]). For the $t \to \gamma(u, c)$ signal the exact $2 \to 5$ matrix elements $gg(q\bar{q}) \to t\bar{t} \to \gamma u(c) + W^* b(\to \ell\nu b)$ were calculated and included in PYTHIA. The $t \to \gamma(Z)(u, c)$ decays would be seen as peaks in the $M_{\gamma(Z),jet}$ spectrum in the region of $m_t$. To separate the signal from the background one has to exploit the presence of the additional top decaying to the $\ell\nu b$ in the same event. The signature with the hadronic decay of the additional top was found to be hopeless.

### *8.41 $t \to \gamma(u, c)$*

In order to separate the $(\gamma q)(\ell\nu b)$ final state from the backgrounds several selection criteria were found to be effective. First, the presence of one isolated photon with $E_t \geq 75$ GeV and $|\eta| \geq 2.5$, one isolated lepton $(\mu, e)$ with $E_t \geq 15$ GeV and $|\eta| \geq 2.5$, and at least two jets with $E_t \geq 30$ GeV and $|\eta| \geq 2.4$ is required. One top quark has to be reconstructed from the photon and jet ($M_{\gamma,jet} \subset m_t \pm 15$ GeV), the corresponding jet is not allowed to be $b$-tagged. On the contrary, the jet with maximal $E_t$,

which is not involved in the $(\gamma, \text{jet})$ system has to be $b$-tagged, should have $E_t \geq 50$ GeV and contribute to another reconstructed top quark ($M_{\ell\nu j} \subset m_t \pm 25$GeV). There must be no additional jets with $E_t \geq 50$ GeV. The $b$-tagging efficiency was assumed to be $60\%$ for the purity $1\%(10\%)$ with respect to the gluon and light quark jets ($c$-quark jets). After this selection, approximately 270 background events dominated by the $t\bar{t}$ and $W$ + jets, including $Wb\bar{b}$, survive for the integrated luminosity of 100 fb$^{-1}$, while the signal efficiency is $9.1\%$. The $S/B$ ratio is about 1 for $\mathrm{BR}(t \to \gamma(u,c)) = 10^{-4}$ and the 5 $\sigma$ discovery limit is as low as $3.4 \times 10^{-5}$ for 100 fb$^{-1}$.

### *8.42* $t \to Zq$

The $t \to Zq$ signal was searched for in the $t\bar{t} \to (\ell\bar{\ell}q)\ell\nu b$ final state. Three isolated leptons with $E_t \geq 15$ GeV and $|\eta| \leq 2.5$, and exactly two jets with $E_t \geq 30$ GeV and $|\eta| \leq 2.5$ are required. The pair of the opposite-sign same-flavour leptons has to be constrained to the $Z$ mass ($M_{\ell\bar{\ell}} \subset M_Z \pm 6$ GeV) and one jet, combined with the reconstructed Z, has to form the top system ($M_{\ell\bar{\ell}j} \subset m_t \pm 15$ GeV). This jet is not allowed to be the $b$-jet, but the last "free" jet in the event has to be $b$-tagged. For the integrated luminosity of 100 fb$^{-1}$ just $\sim 9$ background events coming from the $WZ$, $t\bar{t}Z$ and $Z + jets$ processes survive. The signal efficiency is about $6.8\%$ which corresponds, however, only to $\sim 12$ events for $\mathrm{BR}(t \to Z(u,c)) = 10^{-4}$. The indication is that one can reduce the background rate to the nearly zero level tightening the selection criteria. In particular, requiring in addition $E_t^{miss} \geq 30$ GeV and a harder jet involved in the top $(\ell\bar{\ell}j)$ system ($E_t \geq 50$ GeV) one can reduce the background to the level of $\sim 0.6$ events still keeping $\sim 3.7\%$ of the signal (6.6 events for $\mathrm{BR}(t \to Z(u,c)) = 10^{-4}$ and 100 fb$^{-1}$). One can conclude that the $t \to Z(u,c)$ signal should be very clean but, due to the low signal event rate, only $\sim 3 \times 100$fb$^{-1}$ of integrated luminosity would allow one to probe $\mathrm{BR}(t \to Z(u,c))$ as low as $10^{-4}$, provided the present background understanding is correct and the detector performance will not be deteriorated during the long run. The $5\sigma$ reach for 100 fb$^{-1}$ is $\sim 1.9 \times 10^{-4}$.

### *8.43* $t \to H^+b$

CMS has investigated the production of the light charged Higgs, $m_{H^\pm} < m_t$, in $t\bar{t}$ events using the decay chain $t\bar{t} \to H^\pm bWb \to (\tau^\pm\nu_\tau b) + (\ell\nu b)$ [269]. The $H^\pm \to \tau\nu$ branching ratio is large $\sim$98% in this mass range for $\tan\beta >$2 and only slightly dependent on $\tan\beta$. The $t \to H^\pm b$ branching ratio is large both at high and at low $\tan\beta$ values and has a minimum of $\sim$0.8% around $\tan\beta \sim$6. Since the Higgs mass cannot be reconstructed in this process the signal can be only inferred from the excess of $\tau$ production over what is expected from the SM $t \to Wb$, $W^\pm \to \tau^\pm\nu$ decay.

An isolated lepton with $p_t > 20$ GeV is required to identify the top decay and to trigger the event. The $\tau$'s are searched starting from calorimeter jets with $E_t >$40 GeV within $|\eta| <$2.4. For the $\tau$ identification the tracker information is used, requiring one hard isolated charged hadron with $p_t >$30 GeV within the cone of $\Delta R <$0.1 inside the calorimeter jet. The algorithm thus selects the one prong $\tau$ decays.

The main backgrounds are due to the $t\bar{t}$ events with $t\bar{t} \to WbWb \to (\tau^\pm\nu_\tau b) + (\ell\nu b)$ and $W$ + jet events with $W \to \tau\nu$. The $t\bar{t}$ background is irreducible, but can be suppressed by exploiting the $\tau$ polarisation effects [270]. Due to the $\tau$ polarisation the charged pion from $\tau \to \pi^\pm\nu$ decay has a harder $p_t$ spectrum when coming from $H^\pm \to \tau\nu$ than from $W^\pm \to \tau\nu$. The decay matrix elements with polarisation [271] were implemented in PYTHIA [52]. Due to the polarisation, the efficiency of the above $\tau$ selection is significantly better for $H^\pm \to \tau\nu$ ($\sim$19%) than for $W^\pm \to \tau\nu$ ($\sim$6%).

The events were required to have at least one $b$-jet with $E_t > 30$ GeV tagged with an impact parameter method [272]. This $b$-tagging suppresses efficiently, by a factor of $\sim$70, the background from $W$+jet events. The efficiency for $t\bar{t}$ events is $\sim$35%. The expected $5\sigma$ discovery range for 10 fb$^{-1}$ in the MSSM $(m_A, \tan\beta)$ parameter space was found to be: $m_A < 110$ GeV for all $\tan\beta$ values and somewhat extended ($m_A \lesssim$ 140) for $\tan\beta \lesssim$ 2.

### 8.5 Conclusions on rare top decays

In the framework of the SM, the top rare decays (that is any channel different from $t \to qW$) are definitely below the threshold for an experimental analysis at LHC. On the other hand, LHC experiments will be able to probe quite a few predictions of possible extensions of the SM.

An extended Higgs sector will be looked for through the tree-level decay $t \to bH^+$. ATLAS estimates its sensitivity to this channel in the MSSM, through an excess in the tau lepton signal, to be around $\mathrm{BR}(t \to H^+ b)$ = 3% (that is almost 4 times better than what expected from Run 2 at the Tevatron). This would allow to probe all values of $m_{H^\pm}$ below $m_t - 20$ GeV over most of the $\tan\beta$ range. For low $\tan\beta$, the complementary decay mode $H^\pm \to cs$ has been considered. In the mass range $110 < H^\pm <$ 130 GeV, the $H^\pm$ peak can be reconstructed and separated from the dominant $W \to jj$ background.

For CMS, using the $\tau$ excess signature, the expected $5\sigma$ discovery range for 10 fb$^{-1}$ in the MSSM ($m_A, \tan\beta$) parameter space is $m_A < 110$ GeV, for all $\tan\beta$ values, and somewhat extended ($m_A \lesssim$ 140), for $\tan\beta \lesssim$ 2.

Other interesting signatures like $H^\pm \to hW^*$, $H^\pm \to AW^*$ and $H^\pm \to bt^* \to bbW$ are very promising in particular parameter ranges, but have not yet been thoroughly investigated.

ATLAS has studied its sensitivity to the radiative decay $t \to WbZ$. This has been found to be at most of the order $10^{-4}$, that is insufficient for the study of a SM signal ($\sim 10^{-6}$), but possibly useful for exploring the predictions of some extended Higgs-sector model, for which $\mathrm{BR}(t \to WqZ) \lesssim 10^{-2}$. On the other hand, the radiative Higgs decay $t \to WbH$ seems out of the reach of LHC in any realistic model.

The LHC reach for the FCNC decays $t \to qZ$, $t \to q\gamma$ and $t \to qg$ has also been thoroughly investigated. Apart from the $t \to qg$, which is completely overwhelmed by the hadronic background, both ATLAS and CMS have a sensitivity of about $2 \times 10^{-4}$ to the $t \to qZ$ channel, while the CMS reach for the $t \to q\gamma$ channel is about $3.4 \times 10^{-5}$, that is slightly better than the ATLAS sensitivity ($1.0 \times 10^{-4}$), assuming an integrated luminosity of 100 fb$^{-1}$. These thresholds could be largely sufficient to detect some manifestation of possible FCNC anomalous couplings in the top sector.

ATLAS has also investigated its sensitivity to a measurement of $|V_{tb}|$ through a determination of the rate $\mathrm{BR}(t \to bX)$, by comparing the number of observed (1 or 2) $b$-tags in a $t\bar{t}$ sample. Within the three-generation SM, the ratio of double $b$-tag to single $b$-tag events is $\mathrm{R}_{2b/1b} = |V_{tb}|^2$. LHC will allow a much more precise determination of $\mathrm{R}_{2b/1b}$ with respect to the Tevatron (where, presently, one gets $|V_{tb}| > 0.76$ at the 95% CL). On a purely statistical basis, the expected relative error on $\mathrm{R}_{2b/1b}$ is $\delta\mathrm{R}_{2b/1b}/\mathrm{R}_{2b/1b}$ (stat.) = 0.2% for an integrated luminosity of 10 fb$^{-1}$, that would imply a relative error on $|V_{tb}|$ of about $1^0\!/_{00}$ . On the other hand, the final uncertainty will be dominated by systematic errors related to the $b$-tagging. Further study is needed to estimate the size of these systematic uncertainties.

## 9. ASSOCIATED TOP PRODUCTION[24]

The associated production of a Higgs boson (both SM-like and MSSM) with a top-antitop pair, is one of the most promising reactions to study both top quark and Higgs boson physics at the LHC.

The $pp \to t\bar{t}H$ channel can be used in the difficult search for an intermediate mass Higgs ($m_H \simeq 100 - 130$ GeV), as first proposed in [273]. In this mass region, the associated top production cross section is quite high but still smaller than the leading $gg \to H$ and $qq \to Hqq$ cross sections by two orders and one order of magnitude, respectively. However, since the final state $t\bar{t}H$ signature is extremely distinctive, even such a small signal production rate can become relevant, especially if identifying the Higgs through its dominant $H \to b\bar{b}$ decay becomes realistic, as will be discussed in the following.

Associated $t\bar{t}H$ production will furthermore provide the first direct determination of the top quark Yukawa coupling, allowing to discriminate, for instance, a SM-like Higgs from a more general MSSM Higgs. Processes like $gg \to H$ or $H \to \gamma\gamma$ are also sensitive to the top Yukawa coupling, but only

[24]Section coordinators: A. Belyaev, L. Reina, M. Sapinski (ATLAS), V. Drollinger (CMS).

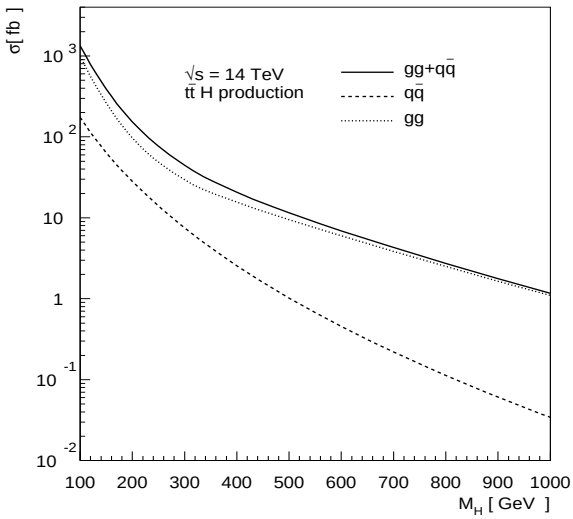


Fig. 45: Cross section for $t\bar{t}H$ production at the LHC as a function of the Higgs mass, for $\mu = m_H$.

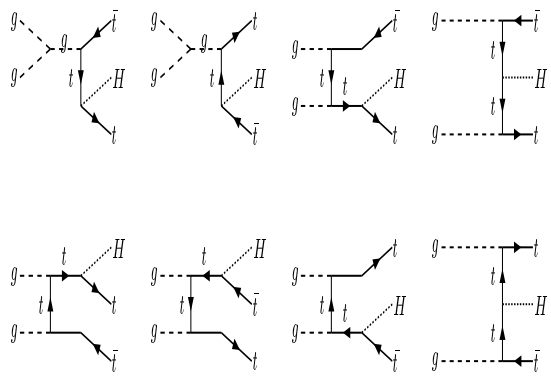

Fig. 46: Diagrams for $gg \to t\bar{t}H$, the leading parton level process for $pp \to t\bar{t}H$.

through large top loop corrections. Therefore loop contributions from other sources of new physics can pollute the interpretation of the signal as a measurement of the top Yukawa coupling.

In the following we will concentrate on the case of a SM-like Higgs boson, whose top Yukawa coupling ($y_t = 2^{3/4} G_F^{1/2} m_t$) is enhanced with respect to the corresponding MSSM (scalar Higgs) coupling for $\tan\beta > 2$, the region allowed by LEP data. Predictions for the MSSM case can be easily obtained by rescaling both the $t\bar{t}H$ coupling and any other coupling that appears in the decay of the Higgs boson.

The cross section for $pp \to t\bar{t}H$ at LO in QCD has been known for a long time [274] and has been confirmed independently by many authors. We have recalculated it and found agreement with the literature. Of the two parton level processes ($q\bar{q} \to t\bar{t}H$ and $gg \to t\bar{t}H$), $gg \to t\bar{t}H$ dominates at the LHC due to the enhanced gluon structure function. The complete gauge invariant set of Feynman diagrams for $gg \to t\bar{t}H$ is presented in Fig. 46. The corresponding analytical results are too involved to be presented here. The numerical results for $\sqrt{s} = 14$ TeV and a few values of the QCD scale $\mu$ are given in Table 25, and illustrated in Fig. 45 as functions of $m_H$, for $\mu = m_H$. For consistency, we have used the leading order CTEQ4L PDFs [115] as well as the leading order strong coupling constant (for reference, $\alpha_s^{LO}(\mu = M_Z) = 0.1317$ for $\Lambda_{QCD}^{(5)} = 0.181$). The cross section, as expected from a LO calculation, shows a strong scale dependence, as can be see in Table 25 , where results for $\mu = m_H$ , $m_t$, $m_H + 2m_t$ and $\sqrt{\hat{s}}$ are presented. In comparison with $\mu = 2m_t + m_H$, for $\mu = m_H$ we have 80-50% higher cross sections, when 100 GeV $< m_H <$ 200 GeV. Since the choice of the QCD scale at LO is pretty arbitrary, and since we expect NLO QCD corrections to enhance the LO cross section, we decide to use $\mu = m_H$ in Fig. 45 and in the following presentation. These calculations have been performed independently using the CompHEP software package [275] and MADGRAPH [276]+HELAS [277].

The NLO QCD corrections are expected to enhance the cross section, but their complete evaluation is still missing at the moment. Associated top production is in fact the only Higgs production mode for which the exact NLO QCD corrections have not been calculated yet. The task is very demanding, since it requires the evaluation of several one loop five-point functions for the virtual corrections and the integration over a four-particle final state (three of which massive) for the real corrections.

For large $m_H$, the cross section for $t\bar{t}H$ has been calculated including a complete resummation of potentially large logarithms, of order $\ln(m_H/m_t)$, to all orders in the strong coupling [278]. These effects can almost double the cross section for $m_H = 1$ TeV.

Table 25: Leading order cross sections for $t\bar{t}H$ production at the LHC. The individual parton level channels ($q\bar{q} \to t\bar{t}H$ and $gg \to t\bar{t}H$) as well as their sum are given for a few values of the renormalization scale $\mu$.

| $m_H$[GeV] | $q\bar{q}$ [fb] $\mu = m_H$ | $gg$ [fb] $\mu = m_H$ | $q\bar{q}$+$gg$ [fb] $\mu = m_H$ | $q\bar{q}$+$gg$ [fb] $\mu = m_t$ | $q\bar{q}$+$gg$ [fb] $\mu = 2m_t + m_H$ | $q\bar{q}$+$gg$ [fb] $\mu = \sqrt{\hat{s}}$ |
|---|---|---|---|---|---|---|
| 100 | 348. | 990. | 1340. | 1070. | 765. | 685. |
| 110 | 279. | 740. | 1020. | 840. | 596. | 534. |
| 120 | 227. | 558. | 785. | 674. | 473. | 422. |
| 130 | 186. | 428. | 613. | 542. | 379. | 338. |
| 140 | 153. | 334. | 487. | 445. | 308. | 273. |
| 150 | 128. | 263. | 391. | 367. | 251. | 224. |
| 160 | 107. | 210. | 317. | 306. | 207. | 184. |
| 170 | 90.5 | 169. | 260. | 257. | 173. | 152. |
| 180 | 76.8 | 139. | 216. | 218. | 145. | 128. |
| 190 | 65.7 | 115. | 181. | 187. | 124. | 108. |
| 200 | 56.4 | 97.1 | 153. | 162. | 106. | 92.4 |
| 300 | 15.0 | 29.5 | 44.5 | 55.7 | 33.2 | 28.4 |
| 400 | 5.11 | 15.6 | 20.7 | 29.6 | 16.2 | 13.8 |
| 500 | 2.04 | 9.51 | 11.5 | 18.4 | 9.32 | 7.98 |
| 600 | 0.909 | 6.00 | 6.91 | 12.1 | 5.73 | 4.93 |
| 700 | 0.439 | 3.86 | 4.29 | 8.20 | 3.63 | 3.14 |
| 800 | 0.226 | 2.50 | 2.72 | 5.62 | 2.34 | 2.04 |
| 900 | 0.122 | 1.65 | 1.76 | 3.90 | 1.54 | 1.35 |
| 1000 | 0.0684 | 1.10 | 1.16 | 2.73 | 1.02 | 0.900 |

For an intermediate mass Higgs, the $K$ factor ($\sigma_{NLO}/\sigma_{LO}$) has been estimated in the Effective Higgs Approximation (EHA) [279]. The EHA neglects terms of $O(m_H/\sqrt{s})$ and higher and works extremely well for $e^+e^- \to t\bar{t}H$ already at $\sqrt{s}=1$ TeV. However, it is a much poorer approximation in the $pp \to t\bar{t}H$ case, since it does not include the $t$-channel emission of a Higgs boson for $gg \to t\bar{t}H$. Indicatively, at $\sqrt{s} = 14$ TeV, for a SM-like Higgs boson with $m_H \simeq 100-130$ GeV, the EHA gives $K \simeq 1.2 - 1.5$, with some uncertainty due to scale and PDF dependence. Only the complete knowledge of the NLO level of QCD corrections will allow to reduce the strong scale and PDF dependence of the LO and EHA cross sections. For the following analysis we choose to use the pure LO cross section with no K-factor, both due to the uncertainty of the result and for consistency with the corresponding background cross sections. However, one should point out that, due to the choice of a quite low QCD scale ($\mu = m_H$), a sort of *effective* K-factor has been automatically included in our analysis.

In the following subsection we present the analysis and results from the ATLAS collaboration as well as a discussion of the main backgrounds. The analysis mainly focuses on the search and study of an intermediate mass Higgs boson. To introduce the study, it is useful to discuss and qualitatively understand the size of the possible irreducible backgrounds in the $100 < m_H < 140$ GeV mass region.

Given the relatively small number of events that will be available, one should try to consider all possible decay channels of the Higgs boson in the intermediate mass region: $H \to b\bar{b}$, $\tau\bar{\tau}$, $\gamma\gamma$, $WW$ and $ZZ$. The corresponding irreducible backgrounds are: 1) $t\bar{t}b\bar{b}$, 2) $t\bar{t}\tau\bar{\tau}$, 3) $t\bar{t}\gamma\gamma$, 4) $t\bar{t}WW$, and 5) $t\bar{t}ZZ$. The number of events expected from signal and background signatures for 1)-5) are presented in Fig. 47. This figure shows the number of signal and background events in each bin of the corresponding invariant mass: $M_{bb}$, $M_{\tau\tau}$, $M_{\gamma\gamma}$, $M_{WW}$ or $M_{ZZ}$. They are obtained multiplying the $t\bar{t}H$ cross section by the respective Higgs boson branching ratios. In order to take into account finite mass resolution effects, we have chosen 10 GeV bins for the $M_{\gamma\gamma}$ distribution and 50 GeV for the others. The presented

Table 26: Leading-order cross sections for various $t\bar{t}XX$ backgrounds.

| | $t\bar{t}b\bar{b}$ | $t\bar{t}\tau\bar{\tau}$ | $t\bar{t}\gamma\gamma$ | $t\bar{t}WW$ | $t\bar{t}ZZ$ |
|---|---|---|---|---|---|
| cuts | $\lvert\eta_b\rvert < 3$<br>$E_T^b > 15$ GeV<br>$m_{bb} > 90$ GeV | $\lvert\eta_\tau\rvert < 3$<br>$E_T^\tau > 15$ GeV | $\lvert\eta_\gamma\rvert < 2.5$<br>$E_T^\gamma > 15$ GeV<br>$M_{\gamma\gamma} > 90$ GeV | | |
| $\sigma$ [fb] $q\bar{q}$ | 41.2 | 2.9 | 2.73 | 0.50 | 1.11 |
| $gg$ | 846. | 15.7 | 1.82 | 1.52 | 0.567 |
| $q\bar{q}$+$gg$ | 887. | 18.6 | 4.55 | 2.53 | 1.68 |

numbers correspond to 30 fb$^{-1}$ of integrated luminosity. The corresponding total cross sections are given in Table 26.

Cross sections for backgrounds 1)-3) were calculated with the kinematic cuts shown in Table 26, while for processes 4) and 5) no cuts were applied. We have used CTEQ4L PDF and $\mu^2 = M_{XX}$, where $XX$ is $b\bar{b}$, $\tau^+\tau^-$, $\gamma\gamma$, $W^+W^-$ or $ZZ$ depending on the channel. One can see that the $t\bar{t}b\bar{b}$ signature has the highest signal (and background) event rate. It has been the object of the study of the ATLAS collaboration and will be discussed in the next section. The $t\bar{t}\gamma\gamma$ channel has also been the subject of [280] where signal as well as reducible and irreducible backgrounds have been studied in details at the parton level. However, one can see that other signatures could also be interesting and helpful in searching for the Higgs boson and measuring the $t\bar{t}H$ Yukawa coupling, and should be taken into account in future studies.

### 9.1 $\mathrm{t\bar{t}H}$ : Analyses and Results

The ATLAS collaboration has studied several channels in which the discovery of a SM-like Higgs boson would be possible and obtained a quite complete Higgs discovery potential [30]. One of the most important channels for discovery of a low mass Higgs boson ($100-130$ GeV) is the $t\bar{t}H$, $H \to b\bar{b}$ channel, in which it is possible to obtain quite large signal significance [281] and also to measure the top-Higgs Yukawa coupling.

The final state of this channel consists of two $W$ bosons and four $b-$jets: two from the decay of the top quarks, and two from the decay of the Higgs boson. In order to trigger signal events, one $W$ boson is required to decay leptonically. The second $W$ boson is reconstructed from the decay to a $q'\bar{q}$ pair. This channel could be also investigated with both $W$ bosons decaying leptonically. However, for this signature the total branching ratio is much smaller and, in addition, it is more difficult to reconstruct two neutrino momenta from the measured missing energy.

In the analysis both top quarks are fully reconstructed, and this reduces most of the $W$+jets background. The reconstruction is done using strategies similar to those discussed in Section 3.5 for the kinematic studies of $t\bar{t}$ production. The main backgrounds for this process are:

- the irreducible continuum $t\bar{t}b\bar{b}$ background;
- the irreducible resonant $t\bar{t}Z$ background, which is not very important for this channel as it has a very small cross section;
- the reducible backgrounds which contain jets misidentified as $b$-jets, such as $t\bar{t}jj$, $Wjjjjjj$, $WWb\bar{b}jj$, etc.

After the reconstruction of the two top quarks, it has been found that the most dangerous background is $t\bar{t}b\bar{b}$ (56% of all $t\bar{t}$+jets background). In Table 27 we give $\sigma\times$BR, where BR represents the product of the branching ratios for $t \to Wb, W_1 \to \ell\nu, W_2 \to q_1\bar{q}_2$, and $H \to b\bar{b}$. We also give the number of events expected after the reconstruction procedure for 3 years of low luminosity operation ($b$-tagging efficiency $\epsilon_b = 60\%$; probability to mistag $c$-jet as $b$-jet $\epsilon_c = 10\%$; probability to

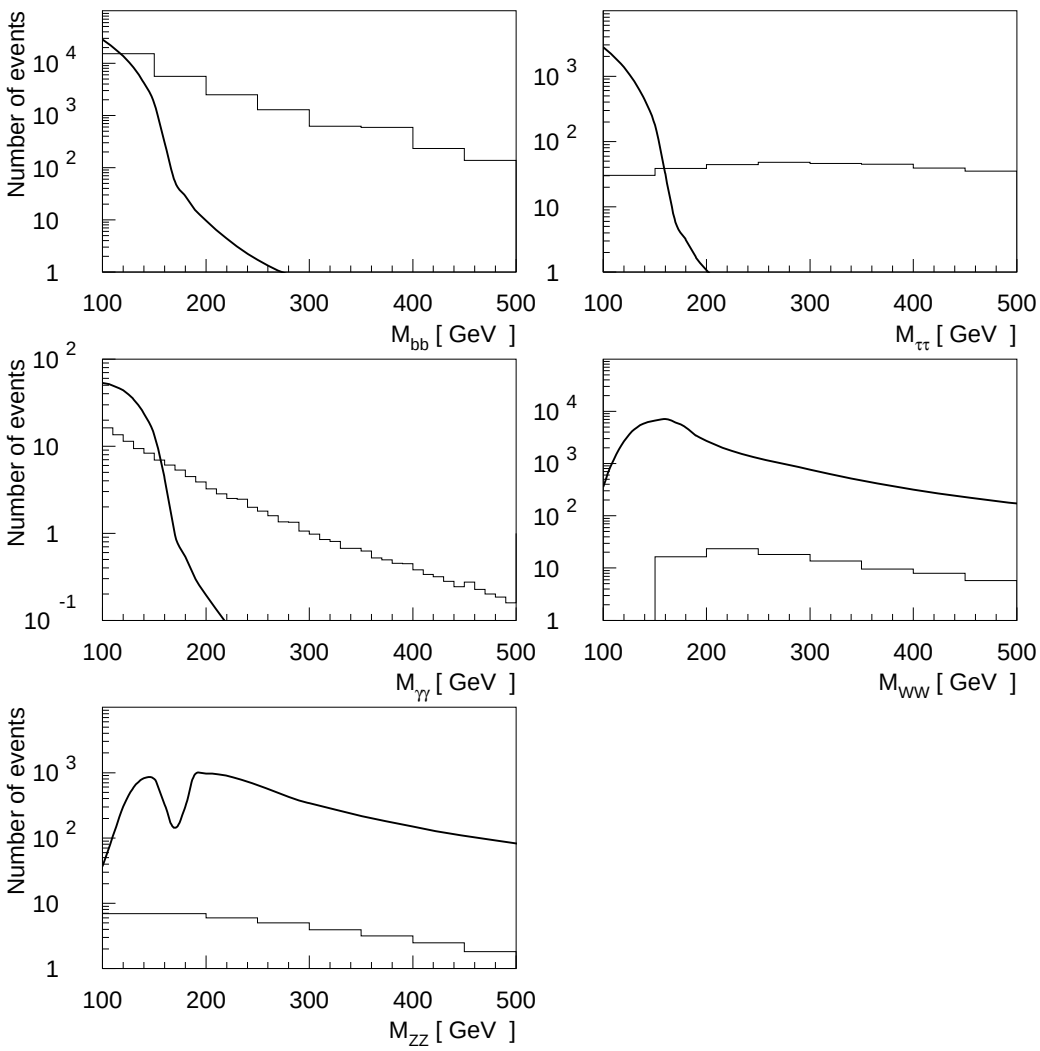


Fig. 47: Number of events for $t\bar{t}H$ signal (solid line) and background $t\bar{t}b\bar{b}$, $t\bar{t}\gamma\gamma$, $t\bar{t}WW$, $t\bar{t}ZZ$ signatures (histogram), as a function of the corresponding invariant masses $M_{XX}$, assuming 30 fb$^{-1}$ of integrated luminosity at $\sqrt{s}=14$ TeV. The bin size is 10 GeV for the $M_{\gamma\gamma}$ distribution and 50 GeV for the others.

mistag any other jet as $b$-jet $\epsilon_j = 1\%$; $p_T^{jet} > 15$ GeV; lepton identification efficiency $\epsilon_\ell = 90\%$; $p_T^{e,\mu} > 20$ GeV), and after one year of high luminosity operation (for high luminosity the $b$-tagging efficiency is degraded to $\epsilon_b = 50\%$ ($\epsilon_c$, $\epsilon_j$ and $\epsilon_\ell$ remain unchanged), the threshold on jet reconstruction is raised to $p_T > 30$ GeV and the electron $p_T$ threshold is raised to $p_T^e > 30$ GeV). Combined results are also shown.

Figure 48 shows the signal and background shapes for $m_H = 120$ GeV and 100 fb$^{-1}$ of integrated luminosity obtained with combined detector performance (30 fb$^{-1}$ with low luminosity and 70 fb$^{-1}$ with high luminosity). On the other hand, Fig.49 illustrates the signal shape for $m_H = 100$ GeV, as obtained by using the full (GEANT) simulation of the detector. In this figure, the shaded area represents the true signal where both $b$-jets come from the Higgs boson, and the solid line stands for the signal obtained through the method that we described above. The *combinatorial background*, which comes from taking at least one $b$-jet from a top instead the one from the Higgs, is quite large and the signal purity is at the level of 60% for low luminosity.

For the fast simulation the $m_{b\bar{b}}$ peak mass resolution is $\sigma_{m_{b\bar{b}}} = 19.0$ GeV, while for the full simulation, including the influence of electronic noise and the threshold on cell energy, a resolution $\sigma_{m_{b\bar{b}}} = 20.0$ GeV has been obtained.

Table 27: Cross sections multiplied by branching ratios and numbers of events after all cuts, including the $\pm 30\ m_{b\bar{b}}$ mass window cut, for 30 fb$^{-1}$ (low luminosity detector performance), 100 fb$^{-1}$ (high luminosity detector performance) and combined 100 fb$^{-1}$ (30 fb$^{-1}$ with low luminosity and 70 fb$^{-1}$ with high luminosity detector performance) of integrated luminosity.

| process | $\sigma \times$ BR (pb) | nr. of reconstructed events | | |
|---|---|---|---|---|
| | | low lumi | high lumi | combined |
| $t\bar{t}H,\ m_H = 120$ GeV | 0.16 | 40 | 62 | 83 |
| $t\bar{t} + jets$ | 87 | 120 | 242 | 289 |
| $Wjjjjjj$ | 65200 | 5 | 10 | 12 |
| $t\bar{t}Z$ | 0.02 | 2 | 5 | 6 |
| total background | - | 127 | 257 | 307 |
| $S/B$ | - | 0.32 | 0.24 | 0.27 |
| $S/\sqrt{(B)}$ | - | 3.6 | 3.9 | 4.8 |
| $S_{H\to b\bar{b}}/S_{total}$ | - | 59% | 50% | - |
| $\delta y_t/y_t$ (stat.) | - | 16.2% | 14.4% | 11.9% |

Similar analyses have been performed for the $t\bar{t}H,\ H \to \gamma\gamma$ channel. Since the signal rate for this channel is very small, it will not be useful during the low luminosity period. However, thanks to the high purity of the signal, it will be possible to obtain between 4 or 5 signal events above 1 event from $t\bar{t}\gamma\gamma$ background per one year of high luminosity operation [282]. To increase the signal rate, $WH$ and $ZH$ with $H \to \gamma\gamma$ channels have been included into the analysis and 14 signal events above 5 background events ($W\gamma\gamma$, $Z\gamma\gamma$, $t\bar{t}\gamma\gamma$ and $b\bar{b}\gamma\gamma$) are expected for one year of high luminosity operation [30].

The statistical uncertainty in the determination of the top-Higgs Yukawa coupling $y_t$ is given in the last row of Table 27. These results assume that the theoretical uncertainty is small, as we expect to be the case by the time the LHC turns on. Many statistical uncertainties of the direct measurement of $y_t$, such as those associated with uncertainties in the integrated luminosity and in the $t\bar{t}$ reconstruction efficiency, could be controlled by comparing the $t\bar{t}H$ rate with the $t\bar{t}$ rate.

To conclude, the $t\bar{t}H,\ H \to b\bar{b}$ and $H \to \gamma\gamma$ channels are very useful for Higgs boson discovery as well as for the measurement the of top-Higgs Yukawa coupling.

### *9.11 A closer look at the $t\bar{t}b\bar{b}$ background: CompHEP versus PYTHIA*

It is necessary to stress that the correct understanding of the $t\bar{t}b\bar{b}$ background is one of the main points of this study. One can simulate this background using PYTHIA, by generating events of top pair production and emitting $b\bar{b}$ pairs from the gluon splitting after the initial and final state radiation. In order to understand how good or bad this approximation is, one needs to calculate and simulate the complete $t\bar{t}b\bar{b}$ process. We have done this using the CompHEP package [275].

In order to compare CompHEP and PYTHIA on the same footing, one should take into account the effects of the initial and final state radiation in CompHEP. This has been done through a CompHEP-PYTHIA interface [283]. We use parton level events generated by CompHEP and link them to PYTHIA in order to include initial and final state radiation effects as well as hadronization effects.

Table 28 presents parton level CompHEP and PYTHIA cross sections including branching ratios of the $W$-boson decay, for the same choice of structure function (CTEQ4L [115]) and QCD scale ($\mu^2 = m_t^2 + p_T^2$(average)). We can see a good agreement for the total cross sections between the exact calculation and the gluon splitting approximation.

In Fig. 50 we present the distribution of $b$-jet separation in $t\bar{t}b\bar{b}$ events. One can see a quite good agreement between CompHEP and PYTHIA. Figures 51 and 52 compare the transverse momentum distributions of the most energetic $b$-jet and of the least energetic $b$-jet in $t\bar{t}b\bar{b}$ production, as reproduced

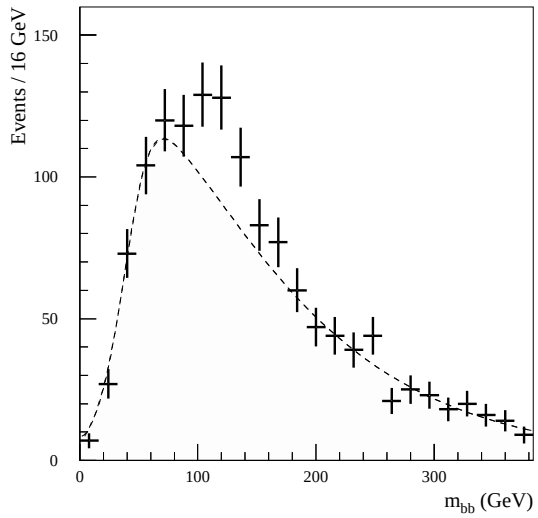


Fig. 48: Invariant mass distribution of tagged $b$-jet pairs in fully reconstructed $t\bar{t}H$ signal events and background events, obtained using the fast simulation of the ATLAS detector, for $m_H = 120$ GeV and integrated luminosity of 100 fb$^{-1}$ (30 fb$^{-1}$ at low plus 70 fb$^{-1}$ at high luminosity). The points with error bars represent the result of a single experiment and the dashed line represents the background distribution.

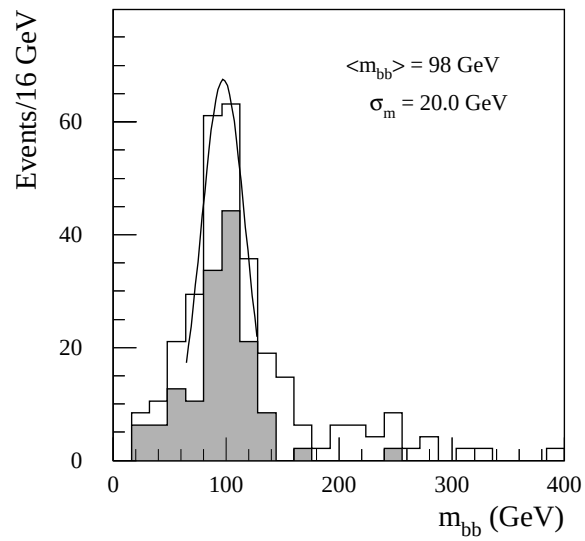


Fig. 49: Invariant mass distribution of tagged $b$-jet pairs in fully reconstructed $t\bar{t}H$ signal events, obtained using a full (GEANT) simulation of the ATLAS detector, for $m_H = 100$ GeV and low luminosity performance. The shaded area denotes those events for which the jet assignment in the Higgs boson reconstruction is correct.

Table 28: Results for the $t\bar{t}b\bar{b}$ background, assuming an integrated luminosity $\mathcal{L}_{\rm int} = 30$ fb$^{-1}$: CompHEP (ISR and FSR included) versus PYTHIA (default).

| Selection | CompHEP | PYTHIA | CompHEP / PYTHIA |
|---|---|---|---|
| 4 $b$-quarks with<br>$p_T > 15$ GeV$/c$ ; $\|\eta\| < 2.5$ | 92000 events<br>$\sigma = 3.1$ pb | 87600 events<br>$\sigma = 2.9$ pb | 1.05 |
| $\Delta$R($b$,$b$) $> 0.5$<br>$b$-quarks not from top decay | 54000 events<br>59% of prev. Step | 48900 events<br>56% of prev. Step | 1.10 |

using PYTHIA and CompHEP respectively. These distributions also confirm that PYTHIA describes well the $t\bar{t}b\bar{b}$ background.

### 9.2 Summary and conclusions for $\mathrm{t\bar{t}H}$ production

The associated production of a Higgs boson with a top-antitop pair is important for the discovery of an intermediate mass Higgs boson ($m_H \simeq 100-130$ GeV) and provides a direct determination of the top-Higgs Yukawa coupling. From studies of the couplings and of the CP-parity of the Higgs boson [284] it will be possible to discriminate, for instance, a SM-like Higgs boson from a generic MSSM one.

The ATLAS analysis has focused on the $t\bar{t}H$ , $H \to b\bar{b}$ channel for the low luminosity run of the LHC (30 fb$^{-1}$ of integrated luminosity). The results presented in Section 9.1 are very encouraging and indicate that a signal significance of 3.6 as well as a precision of 16% in the determination of the Yukawa coupling can be reached (for $m_H = 120$ GeV). Better results can be obtained from the high luminosity run of the LHC (100 fb$^{-1}$ of integrated luminosity), when also the high purity $t\bar{t}H, H \to \gamma\gamma$ channel is available.

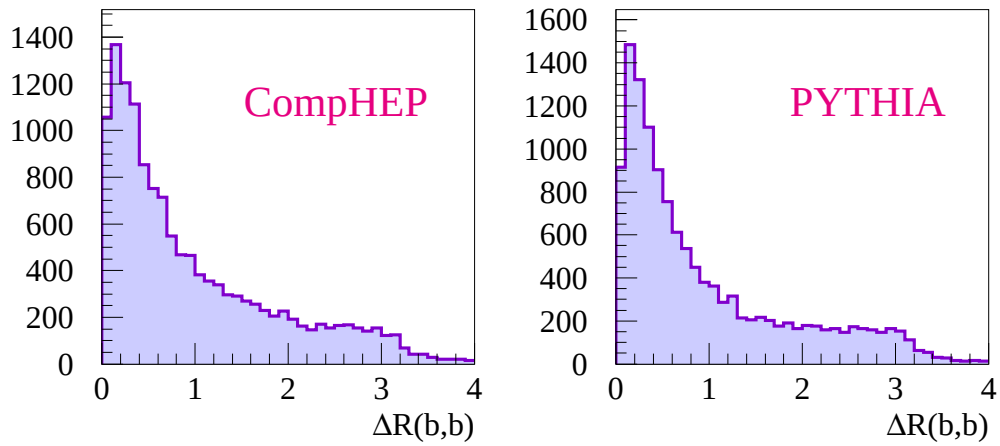


Fig. 50: Results for $t\bar{t}b\bar{b}$ background, assuming an integrated luminosity $L_{\rm int} = 4.4$ fb$^{-1}$: CompHEP (ISR and FSR included) versus PYTHIA (default).

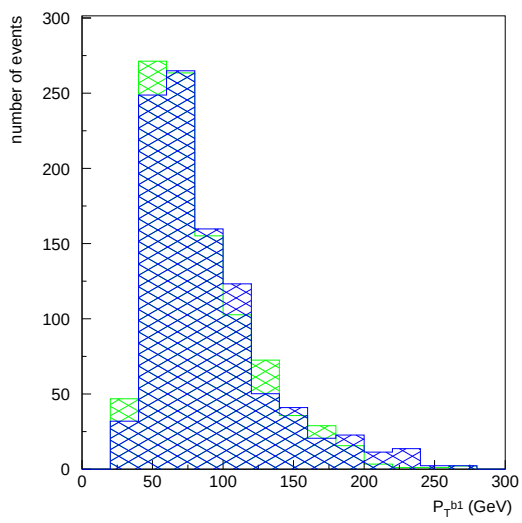


Fig. 51: Transverse momentum distribution of the most energetic $b$-jet from $t\bar{t}b\bar{b}$ processes at the LHC: CompHEP (dark-grey histogram) versus PYTHIA (light-grey)

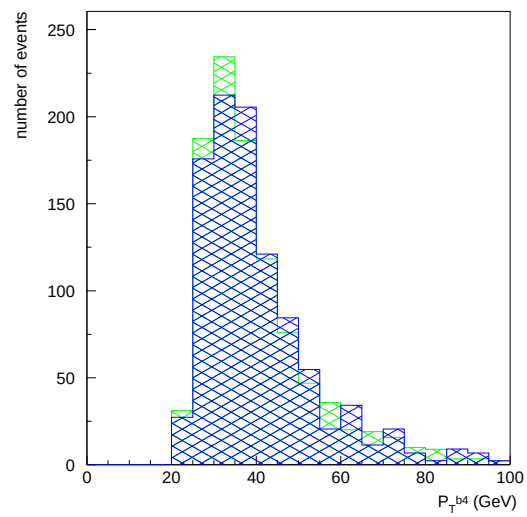


Fig. 52: Transverse momentum distribution of the least energetic $b$-jet from $t\bar{t}b\bar{b}$ processes at the LHC: CompHEP (dark-grey histogram) versus PYTHIA (light-grey)

## A APPENDIX: b-TAGGING AND JET E-SCALE CALIBRATION IN TOP EVENTS[25]

For the reconstruction of the top events and in particular for the precision measurement of the top mass two important aspects in the detector performance have to be considered:

- the $b$-quark jet tagging capabilities and efficiency in top events, and
- the jet energy scale calibration for the light quark jets but in particular for the $b$-jets.

In both experiments ATLAS and CMS several studies have been made on these, highlights of which are presented here. From the preliminary results available so far, there is confidence that the numbers used or implied in the analyses presented in this report are realistic. Needless to say that these are preliminary results and several detailed studies need to be performed with the final detector simulations and the first LHC data.

[25]Section coordinator: I. Efthymiopoulos

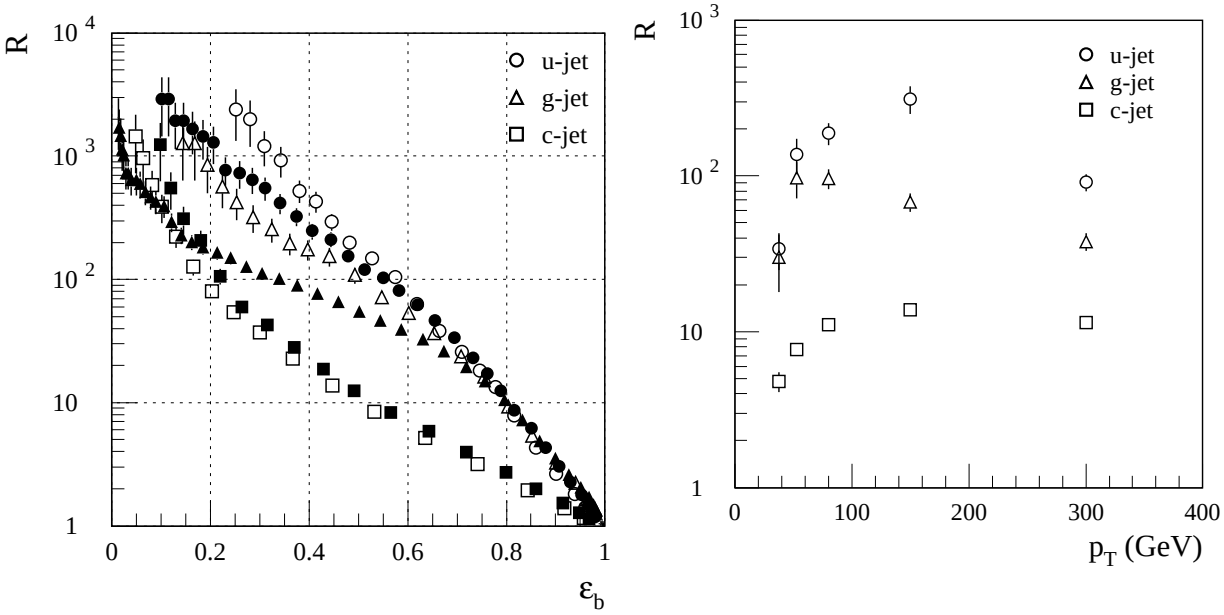


Fig. 53: Left: jet rejection factors for the vertex $b$-tagging method, with high luminosity pile-up. Open symbols: $m_H = 100$ GeV, full symbols: $m_H = 400$ GeV. Right: background rejections as a function of the $p_T$ for $\epsilon_b = 50\%$ with high luminosity pile-up included. From [30], Chapter 10.

### A1 b-jet tagging in the top events

ATLAS has done extensive studies for the $b$-tagging performance using jets from the decay of 100 and 400 GeV Higgs bosons ([30], Chapter 10). In Fig. 53 the rejection factors for the light quark jets versus the $b$ tagging efficiency and the jet $p_T$ are shown.

Typically in the ATLAS analyses discussed here, and in particular for the fast simulation studies, an overall $b$-jet tagging efficiency of 60% (50%) for low (high) luminosity of LHC is used. The mis-tagging inefficiencies for the $c$-jets (or other light quark jets) were 10% (1%) for the $p_T$ range interesting for the top physics. Although most of the studies were done with events from the Higgs decays, the results were verified with the top events themselves and no significant differences were found.

### A2 Absolute jet energy scale calibration

Determining the absolute jet energy scale at LHC will be a rather complex issue because it is subject to both physics (initial-final state radiation, fragmentation, underlying event, jet algorithm etc.) and detector (calorimeter response over a wide range of energies and over the full acceptance of the detector, non-linearities at high energies, $e/h$ ratio etc.) effects. All these have to be understood at the level of a fraction of a percent in terms of systematic uncertainties as required for the precision measurements of the top mass.

ATLAS has done an extensive study of the possible *in situ* jet scale calibration methods using specific data samples available at LHC ([30], Chapter 12). In general, good candidate event classes at LHC will be:

- reconstruction of $W \to jj$ decays within the top events themselves [12] to obtain the light quark jet calibration and,
- events containing a $Z$ boson decaying into leptons balanced with one high-$p_T$ jet to cross-check the light quark jet calibration but in addition to calibrate the $b$-jets and extend the energy reach to the TeV range.

In Fig. 54 the results obtained are shown. As can be seen (left plot) for the case of $W \to jj$ events,

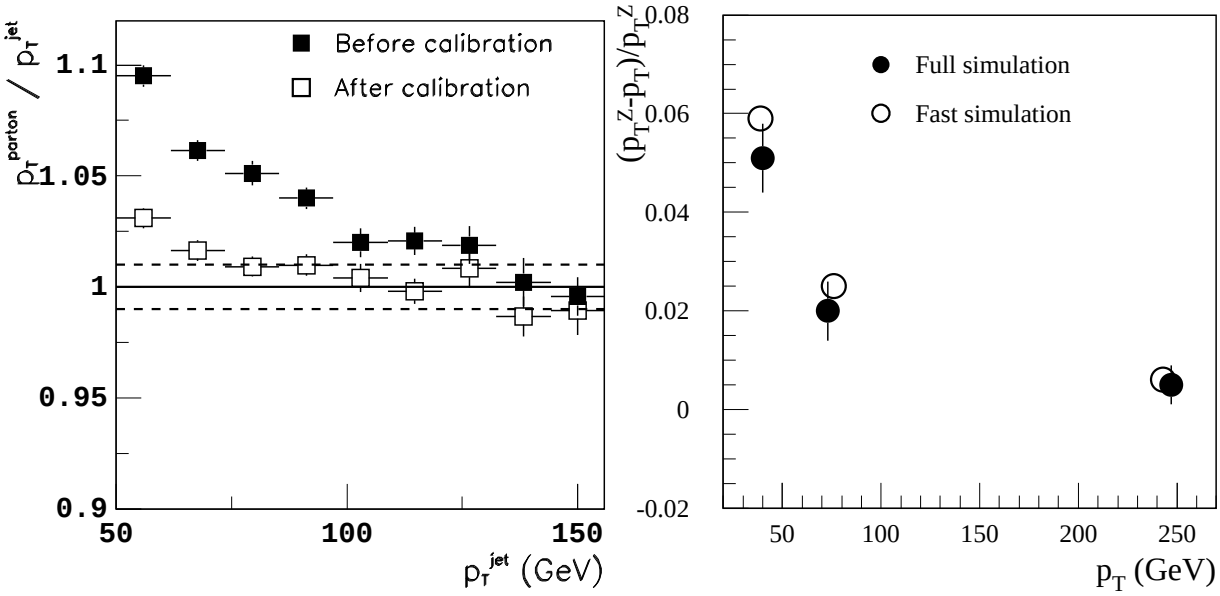


Fig. 54: Left: Ratio of the original parton $p_T$ to the $p_T$ of the reconstructed jet as a function of the $p_T$ of the jet for the $W \to jj$ decays reconstructed in include $t\bar{t}$ events. The jets were reconstruced using a fixed cone jet algorithm with cone size DR$= 0.4$, (optimized for high luminosity operation of LHC). Right: Average fractional imbalance between the $p_T$ of the $Z$ boson and the $p_T$ of the leading jet as a function of the $p_T$ of the jet for the sample of $Z$ + jets events. A cone of DR$= 0.7$ is used to collect the jet energy.

once the jet 4-vectors are rescaled using the $M_W$ constraint the required 1% uncertainty is reached for jets with $p_T >$ 70 GeV up to several hundred GeV. The lower and upper end of this range will depend on how well residual systematic effects can be controlled in the data and the Monte Carlo simulation [285].

The use of the $Z$ + jets sample in LHC is a bit less straightforward than at the Tevatron [286] due to the ISR radiation which produces an additional high-$p_T$ jet which degrades the quality of the $p_T$-balance between the $Z$ boson and the leading jet. In Fig. 54 (right) the variation of the average fractional imbalance between the $p_T$ of the leading jet and the $Z$ boson as a function of the $p_T$ of the jet. Rescaling the jet $p_T$ to satisfy $p_T$ balance with the $Z$ boson and applying tight selection criteria (jet veto and difference in azimuth $\delta\phi$ between the reconstructed $Z$ and the leading jet) the desired goal of $\pm 1\%$ systematic uncertainty on the absolute jet energy scale can be achieved for jets with $p_T > 50$ GeV and up to the TeV range [287].

However, as shown in Fig. 54 (right), it is possible, taking advantage of the large rate and requiring tight event selection criteria, to obtain the required precision for jets with $p_T >$ 40 GeV and up to the TeV range.

Clearly more studies are needed, and will be done in the years to come, to understand the limitations of the proposed methods and to devise possible improvements.

## B APPENDIX: DIRECT MEASUREMENT OF TOP QUANTUM NUMBERS[26]

### B1 Top spin and experimental tests

Evidence to date is circumstantial that the top events analysed in Tevatron experiments are attributable to a spin-1/2 parent. The evidence comes primarily from consistency of the distribution in momentum of the decay products with the pattern expected for the weak decay $t \to b + W$, with $W \to \ell + \nu$ or $W \to \text{jets}$, where the top $t$ is assumed to have spin-1/2.

[26]Section coordinators: E.L. Berger, U. Baur.

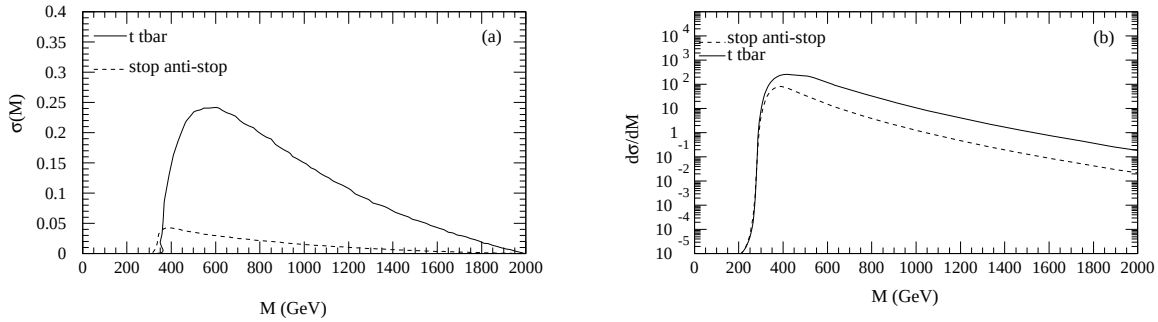


Fig. 55: (a) Partonic cross sections $\hat{\sigma}(M)$ as functions of partonic sub-energy $M$ for the $gg$ channel. (b) Hadronic cross sections $d\sigma/dM$ in proton-proton collisions at 14 TeV as functions of pair mass. The top quark mass $m_t = 175$ GeV, and the top squark (stop) mass $m_{\tilde{t}} = 165$ GeV.

It is valuable to ask whether more definitive evidence for spin-1/2 might be obtained in future experiments at the Tevatron and LHC. We take one look at this question by studying the differential cross section $d\sigma/dM_{t\bar{t}}$ in the region near production threshold [288]. Here $M_{t\bar{t}}$ is the invariant mass of the $t\bar{t}$ pair. We contrast the behaviour of $t\bar{t}$ production with that expected for production of a pair of spin-0 objects. We are motivated by the fact that in electron-positron annihilation, $e^+ + e^- \to q + \bar{q}$, there is a dramatic difference in energy dependence of the cross section in the near-threshold region for quark spin assignments of 0 and 1/2.

For definiteness, we compare top quark $t$ and top squark $\tilde{t}$ production since a consistent phenomenology exists for top squark pair production, obviating the need to invent a model of scalar quark production. Moreover, top squark decay may well mimic top quark decay. Indeed, if the chargino $\tilde{\chi}^+$ is lighter than the light top squark, as is true in many models of supersymmetry breaking, the dominant decay of the top squark is $\tilde{t} \to b + \tilde{\chi}^+$. If there are no sfermions lighter than the chargino, the chargino decays to a $W$ and the lightest neutralino $\tilde{\chi}^o$. In another interesting possible decay mode, the chargino decays into a lepton and slepton, $\tilde{\chi}^+ \to \ell^+\tilde{\nu}$. The upshot is that decays of the top squark may be very similar to those of the top quark, but have larger values of missing energy and softer momenta of the visible decay products. A recent study for Run II of the Tevatron [289] concluded that even with 4 fb$^{-1}$ of data at the Tevatron, and including the LEP limits on chargino masses, these decay modes remain open (though constrained) for top squarks with mass close to the top quark mass.

At the energy of the CERN LHC, production of $t\bar{t}$ pairs and of $\tilde{t}\bar{\tilde{t}}$ pairs is dominated by $gg$ subprocess, and the threshold behaviours in the two cases do not differ as much as they do for the $q\bar{q}$ incident channel. In Fig. 55(a), we show the partonic cross sections $\hat{\sigma}(\sqrt{\hat{s}})$ as functions of the partonic sub-energy $\sqrt{\hat{s}}$ for the $gg$ channel. In Fig. 55(b), we display the hadronic cross sections for $pp \to t\bar{t}X$ and $pp \to \tilde{t}\bar{\tilde{t}}X$ at proton-proton center-of-mass energy 14 TeV as a function of pair mass. We include the relatively small contributions from the $q\bar{q}$ initial state. After convolution with parton densities, the shape of the $\tilde{t}\bar{\tilde{t}}$ pair mass distribution is remarkably similar to that of the $t\bar{t}$ case.

Based on shapes and the normalisation of cross sections, it is difficult to exclude the possibility that some fraction (on the order of 10%) of top squarks with mass close to 165 GeV is present in the current Tevatron $t\bar{t}$ sample. The invariant mass distribution of the produced objects, $M_{t\bar{t}}$, is quite different at the partonic level for the $q\bar{q}$ initial state (dominant at the Tevatron), but much less so for the $gg$ initial state (dominant at the LHC). However, after one folds with the parton distribution functions, the difference in the $q\bar{q}$ channel at the Tevatron is reduced to such an extent that the $M_{t\bar{t}}$ distribution is not an effective means to isolate top squarks from top quarks.

Ironically, the good agreement of the absolute rate for $t\bar{t}$ production with theoretical expectations [45, 47] would seem to be the best evidence now for the spin-1/2 assignment in the current Tevatron sample.

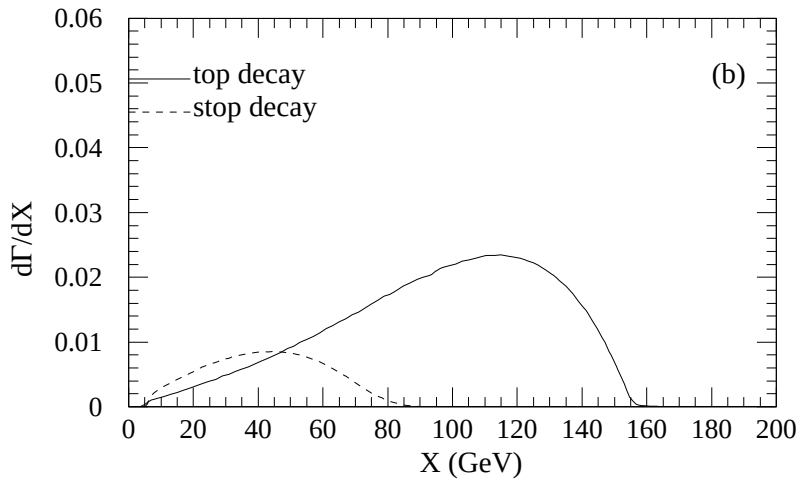


Fig. 56: Distribution in the invariant mass of a bottom quark and charged lepton ($X$) for a top quark or top squark decay, with relative size normalized to the cross sections at the LHC. The top squark decay and sparticle masses are discussed in the text.

A promising technique to isolate a top squark with mass close to $m_t$ would be a detailed study of the momentum distribution of the top quark decay products (presumably in the top quark rest frame). One could look for evidence of a chargino resonance in the missing transverse energy and charged lepton momentum, or for unusual energy or angular distributions of the decay products owing to the different decay chains. One could also look for deviations from the expected correlation between angular distributions of decay products and the top spin [167].

As a concrete example of an analysis of this type, in Fig. 56 we present the distribution in the invariant mass $X$ of the bottom quark and charged lepton, with $X^2 = (p_b + p_{\ell^+})^2$, where the bottom quark and lepton are decay products of either a top quark with $m_t = 175$ GeV or a top squark $\tilde{t} \to \tilde{\chi}^+ b \to W^+ \tilde{\chi}^0 b \to \ell^+ \nu_\ell \tilde{\chi}^0 b$, with $m_{\tilde{t}} = 165$ GeV, $m_{\tilde{\chi}^+} = 130$ GeV, $m_{\tilde{\chi}^0} = 40$ GeV, and $m_b = 5$ GeV. The $X$ distribution is a measure of the degree of polarisation of the $W$ boson in top quark decay [290], and the figure shows that the different dynamics responsible for top squark decay result in a very different distribution, peaked at much lower $X$. The areas under the curves are normalised to the inclusive $t\bar{t}$ and $\tilde{t}\bar{\tilde{t}}$ rates at the LHC.

In this simple demonstration potentially important effects are ignored such as cuts to extract the $t\bar{t}$ signal from its backgrounds, detector resolution and efficiency, and ambiguities in identifying the correct $b$ with the corresponding charged lepton from a single decay. Detailed simulations would be required to determine explicitly how effective this variable would be in extracting a top squark sample from top quark events. Nevertheless, such techniques, combined with the large $t\bar{t}$ samples at the Tevatron Run II and LHC, should prove fruitful in ruling out the possibility of a top squark with mass close to the top quark mass, or alternatively, in discovering a top squark hidden in the top sample.

### B2 Direct Measurement of the Top Quark Electric Charge

In order to confirm that the electric charge of the top quark is indeed $Q_{top} = 2/3$, one can either measure the charge of the $b$-jet and $W$ boson, or attempt to directly measure the top quark electro-magnetic coupling through photon radiation in

$$pp \to t\bar{t}\gamma, \qquad pp \to t\bar{t},\ t \to Wb\gamma. \tag{85}$$

Since the process $pp \to t\bar{t}\gamma$ is dominated by $gg$ fusion at the LHC, one expects that the $t\bar{t}\gamma$ cross section is approximately proportional to $Q_{top}^2$. For radiative top decays the situation is more complicated because

the photon can also be radiated off the $b$-quark or the $W$ line.

The charge of the $b$-jet can most easily be measured by selecting events where the $b$-quarks are identified through their semi-leptonic decays, $b \to \ell\nu c$ with $\ell = e,\ \mu$. The small semi-leptonic branching ratio of the $b$-quark (Br$(b \to \ell\nu c) \approx 10\%$) and wrong sign leptons originating from $B - \bar{B}$ mixing are the main problems associated with this method. For a quantitative estimate realistic simulations are needed. Nevertheless, we believe that the enormous number of top quark events produced at the LHC should make it possible to use semi-leptonic $b$-tagging to determine the electric charge of the top quark.

In our analysis, we focus on top charge measurement through the photon radiation processes listed in (85), concentrating on the lepton+jets mode,

$$pp \to \gamma\ell\nu jjb\bar{b}. \tag{86}$$

We assume that both $b$-quarks are tagged with a combined efficiency of 40%. Top quark and $W$ decays are treated in the narrow width approximation. Decay correlations are ignored. To simulate detector response, the following transverse momentum, rapidity and separation cuts are imposed:

$$p_T(b) > 15 \text{ GeV}, \qquad |y(b)| < 2, \tag{87}$$
$$p_T(\ell) > 20 \text{ GeV}, \qquad |\eta(\ell)| < 2.5, \tag{88}$$
$$p_T(j) > 20 \text{ GeV}, \qquad |\eta(j)| < 2.5, \tag{89}$$
$$p_T(\gamma) > 30 \text{ GeV}, \qquad |\eta(\gamma)| < 2.5, \tag{90}$$
$$\not{p}_T > 20 \text{ GeV}, \qquad \text{all } \Delta\text{R}'\text{s} > 0.4. \tag{91}$$

In addition, to suppress contributions from radiative $W$ decays, we require that

$$m(jj\gamma) > 90 \text{ GeV} \quad \text{and} \quad m_T(\ell\gamma; \not{p}_T) > 90 \text{ GeV}, \tag{92}$$

where $m_T$ is the cluster transverse mass of the $\ell\gamma$ system.

The events passing the cuts listed in (88) – (92) can then be split into three different subsamples:

1. By selecting events which satisfy

$$m(bjj\gamma) > 190 \text{ GeV} \quad \text{and} \quad m_T(b\ell\gamma; \not{p}_T) > 190 \text{ GeV}, \tag{93}$$

   radiative top quark decays can be suppressed and an almost pure sample of $t\bar{t}\gamma$ events is obtained ("$t\bar{t}\gamma$ cuts").
2. For

$$m_T(b_{1,2}\ell\gamma; \not{p}_T) < 190 \text{ GeV} \quad \text{and} \quad m(b_{2,1}jj\gamma) > 190 \text{ GeV}, \tag{94}$$

   the process $pp \to t\bar{t}$, $t \to Wb\gamma$, $W \to \ell\nu$ dominates ("$t \to Wb\gamma$, $W \to \ell\nu$ cuts").
3. Requiring

$$m_T(b_{1,2}\ell\gamma; \not{p}_T) > 190 \text{ GeV} \quad \text{and} \quad 150 \text{ GeV} < m(b_{2,1}jj\gamma) < 190 \text{ GeV}, \tag{95}$$

   one obtains an event sample where the main contribution originates from the process $pp \to t\bar{t}$, $t \to Wb\gamma$, $W \to jj$ ("$t \to Wb\gamma$, $W \to jj$ cuts").

For $m_t = 175$ GeV, $Q_{top} = 2/3$, and $\int \mathcal{L}dt = 100 \text{ fb}^{-1}$, one expects about 2400, 11000 and 9400 events in the regions of phase space corresponding to the three sets of cuts. We have not studied any potential background processes. The main background should originate from $W\gamma+$ jets production and should be manageable in a way similar to the $W+$ jets background for regular $t\bar{t}$ production.

The differential cross section for the photon transverse momentum at the LHC is shown in Fig. 57. Results are shown for $m_t = 175$ GeV and three "top" quark charges: $Q_{top} = 2/3$, $Q_{top} = -4/3$, and

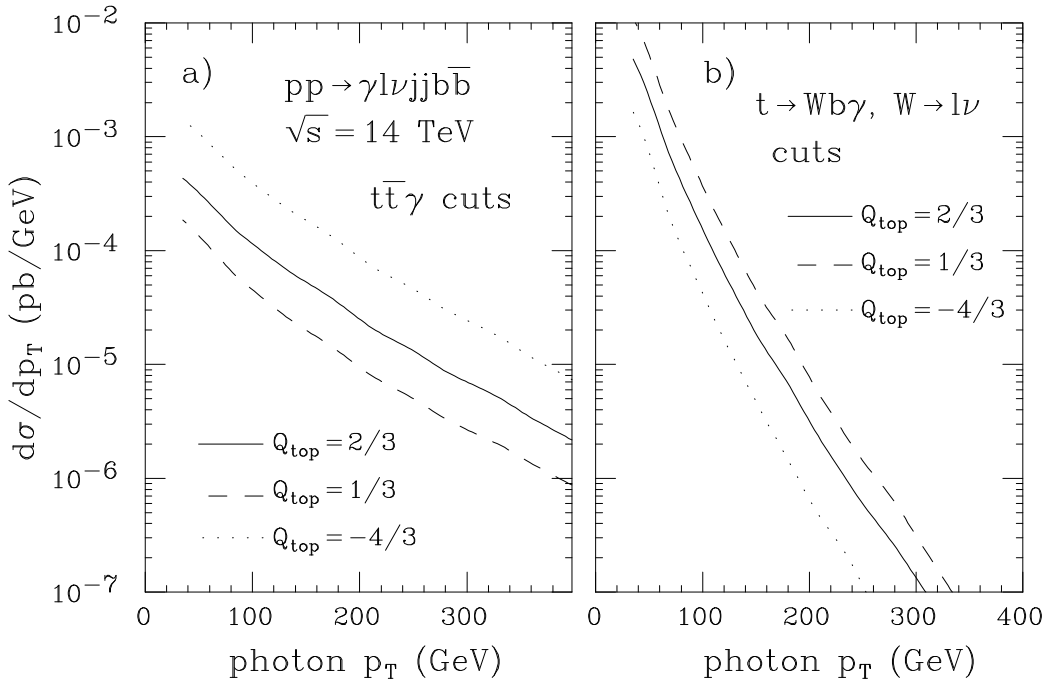


Fig. 57: The differential cross section for the photon transverse momentum in the reaction $pp{\to}\gamma\ell\nu jjb\bar{b}$ at the LHC for three different "top" quark charges.

$Q_{top} = 1/3$. For $Q_{top} = -4/3$, the "top" quark decays into a $W^-$ and a $b$-quark instead of $t{\to}W^+b$. If $Q_{top} = 1/3$, the "$b$"-quark originating from the "top" decay is a (exotic) charge $-2/3$ quark. In the $t\bar{t}\gamma$ region (Eq. (93) and Fig. 57a), the $pp{\to}\gamma\ell\nu jjb\bar{b}$ cross section for a charge $-4/3$ ($1/3$) "top" quark is uniformly a factor $\approx 3.3$ larger ($\approx 2.3$ smaller) than that for $Q_{top} = 2/3$, reflecting the dominance of the $gg{\to}t\bar{t}\gamma$ process for which the cross section scales with $Q^2_{top}$. On the other hand, for the $pp{\to}t\bar{t}$, $t{\to}Wb\gamma$, $W{\to}\ell\nu$ selection cuts (Eq. (94) and Fig. 57b), the cross section for $Q_{top} = -4/3$ is a factor 3 to 5 smaller than that for a charge $2/3$ top quark, due to destructive interference effects in the $t{\to}Wb\gamma$ matrix element. If $Q_{top} = 1/3$, the interference is positive, and the cross section is about a factor 2 to 2.5 larger than for $Q_{top} = 2/3$. The results for the $t{\to}Wb\gamma$, $W{\to}jj$ selection cuts ((95)) are similar to those shown in Fig. 57b, and are therefore not shown here. Note that the photon $p_T$ distribution for radiative top decays is much softer than that for $t\bar{t}\gamma$ production.

From our (simplified) calculation we conclude that the large number of double-tagged $\gamma\ell\nu jjb\bar{b}$ events, together with the significant changes in the $t\bar{t}\gamma$ and the $t\bar{t}$, $t{\to}Wb\gamma$ cross sections should make it possible to accurately determine $Q_{top}$ at the LHC.

## C APPENDIX: 4$^{th}$ GENERATION QUARKS[27]

For completeness, we present here results for the total cross section of possible heavy quarks above the top quark mass. The scale and PDF dependences are shown in Fig. 58. The uncertainty due to the choice of scale is comparable to that of the $t\bar{t}$ cross section, although the effects of the higher order corrections are more and more important at large masses (see Fig. 59). The uncertainty induced by PDF changes becomes very large at large masses, in particular if one considers sets such as CTEQ5HJ which have harder gluons. Notice however that the relative effect due to the resummation corrections depends only very weakly upon the choice of PDF's (cf. Section 3.2).

[27]Section coordinator: M.L. Mangano

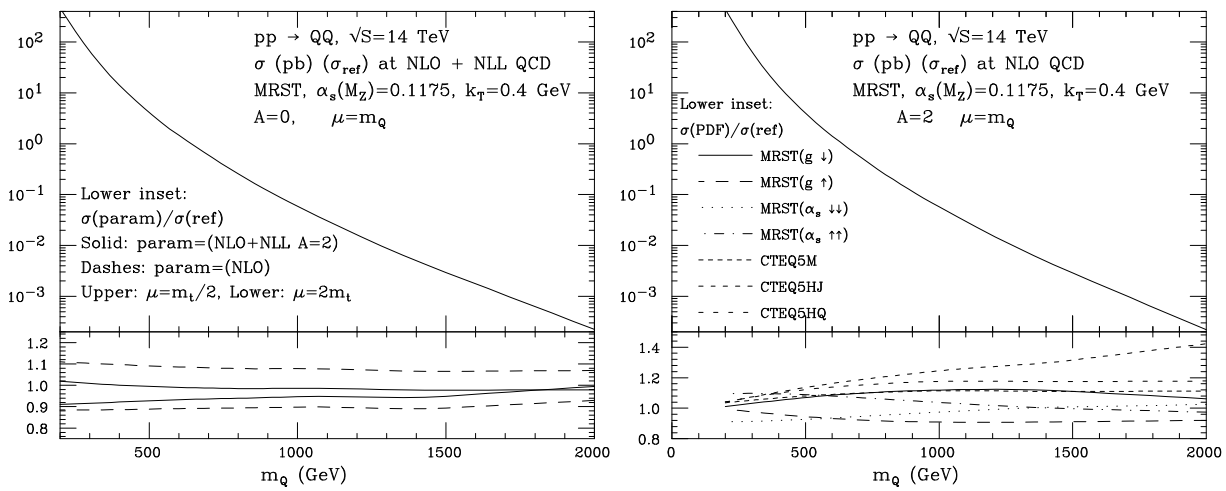


Fig. 58: Heavy quark total production rates. Left figure: scale dependence at fixed NLO (dashed lines in the lower inset), and at NLO+NLL (solid lines). Right figure: PDF dependence. See the Section 3.2 for details.

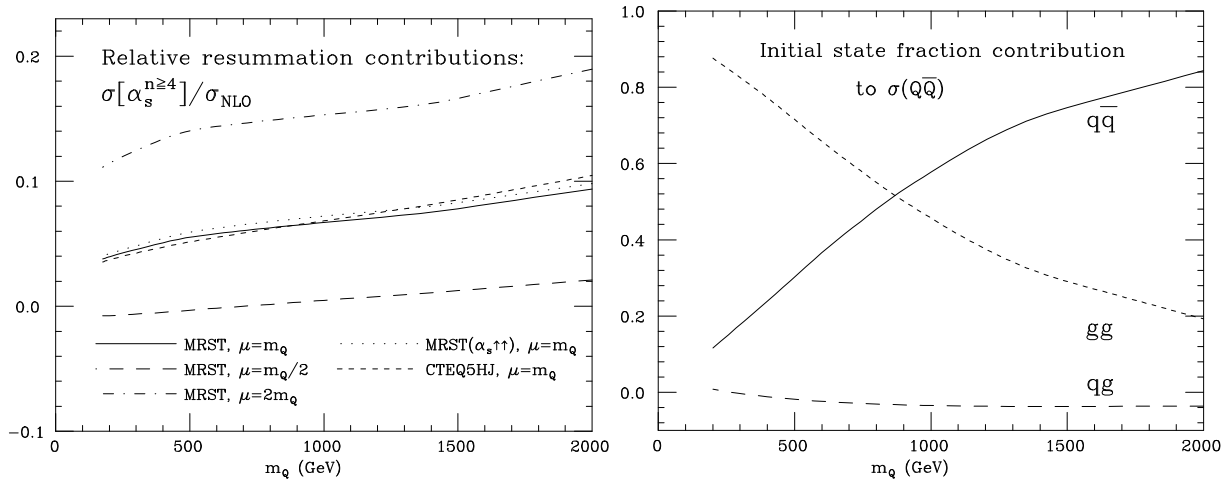


Fig. 59: Heavy quark total production rates. Left figure: fractional contribution induced by resummation contributions of order $\mathcal{O}(\alpha_S^{\geq 4})$. Right figure: initial state composition.

# D APPENDIX: MONTE CARLO TOOLS[28]

## D1 Parton shower Monte Carlos

General purpose Monte Carlo event generators like HERWIG, PYTHIA and ISAJET are essential tools for measuring the top quark cross section, mass and other production and decay properties. They are complementary to the QCD tools described in Section 3.1 since, although they are less reliable for inclusive quantities like the total cross section, they provide a fully exclusive description of individual events at the hadron level. These can be analysed in exactly the same way as experimental data and can be put through full or fast detector simulations to estimate experimental systematics. In certain kinematic regions, particularly the quasi-elastic limit in which accompanying radiation is suppressed, they give more reliable QCD predictions than the available calculations. They include approximate treatments of higher order perturbative effects, hadronisation, secondary decays and underlying events.

The three programs we discuss have the same basic structure, although the precise details vary enormously. Events are generated by starting with the hardest (highest momentum scale) interaction, described by exact QCD (or EW) matrix elements. This is usually only done to leading order so describes

[28]Section coordinators: M.L. Mangano, M. Seymour.

a $2\rightarrow2$ scattering process. The production of multi-parton final states is described as the emission of additional partons from the incoming and outgoing partons of the hard process. This is simulated by a parton shower algorithm in which the partons evolve downwards in some energy-like scale according to perturbatively-calculable probabilistic distributions. When the evolution scale becomes small the running coupling grows, phase space fills with (mostly soft) partons and perturbation theory breaks down. At this point a model of the non-perturbative physics is needed: the perturbative emission is cutoff by a fixed infrared cutoff and the system of partons is confined into hadrons. Having treated all outgoing partons we are left with the remnants of the incoming protons, stripped of the partons that participated in the hard process. These remnants can interact with each other, to produce additional soft hadrons in the event, known as the underlying event.

Parton shower algorithms are developed by studying the amplitude to emit an additional parton into a given process. This is enhanced in two kinematic regions: collinear, where two massless partons are much closer to each other than any others or where a massless parton is close to the incoming proton direction; and soft, where a gluon is much softer than any other parton. In both cases the enhanced terms are universal, allowing a factorisation of emission by a system of partons from the process that produced them. In the collinear case, this factorisation works at the level of cross sections, so it is not surprising that a probabilistic approach can be set up. In the soft case however, the factorisation theorem is valid at amplitude level and it turns out that in any given configuration, many different amplitudes contribute equally. It therefore seems impossible to avoid quantum mechanical interference and so to set up the evolution in a probabilistic way. The remarkable result though is that, due to coherence between all the coloured partons in an event, the interference is entirely destructive outside angular-ordered regions of phase space. This means that the soft emission can be incorporated into a collinear algorithm, simply by choosing the emission angle as its evolution variable, as is done in HERWIG. The most important effects of coherence can be approximately incorporated by using some other evolution variable, like virtuality, and vetoing non-angular-ordered emission, as is done in PYTHIA. If the colour-coherence is not treated at all, one obtains the wrong energy-dependence of jet properties. Such models, like ISAJET, are completely ruled out by $e^+e^-$ annihilation data. Colour coherence effects are also important in determining the initial conditions for the parton evolution, resulting in physically-measurable inter-jet effects [292], which are also in disagreement with ISAJET.

Since the top quark decays faster than the typical hadronisation time, its width cuts off the parton shower before the infrared cutoff. Its decay then acts as an additional hard process and the resulting bottom quark (and two more partons if the W decays hadronically) continue to evolve. Additional coherence effects mean that radiation from the top quark is suppressed in the forward direction (the dead cone effect), as is radiation in the W direction in the top decay. These effects are again included in HERWIG, partially included in PYTHIA and not included in ISAJET. Since the top quark is coloured, the $b$ quark in its decay is colour-connected to the rest of the event, meaning that its properties are not necessarily the same as in a 'standard' $b$ production event. As mentioned in Section 4.6 and as discussed in more detail in [64], such non-universal effects are small.

Although parton showers are reliable for the bulk of emission, which is soft and/or collinear, it is sometimes the rare hard emissions that are most important in determining experimental systematics and biases. Such non-soft non-collinear emission should be well described by NLO perturbation theory, since it is far from all divergences. However, it is not straightforward to combine the advantages of the parton shower and NLO calculation, so it has only been done for a few specific cases. Most notable for hadron-hadron collisions are the Drell-Yan process, for which matrix element corrections are included in both HERWIG and PYTHIA, and top decay, which is included in HERWIG and discussed earlier in Section 4.62 in this report. The corrections to Drell-Yan events are particularly important at high transverse momenta, where the uncorrected algorithms predict far too few events. It is likely that implementing corrections to $t\bar{t}$ pair production would cure the analogous deficit at high $p_T^{t\bar{t}}$ seen in Fig. 7.

Hadronisation models describe the confinement of partons into hadrons. Although this process

is not well understood from first principles, it is severely constrained by the excellent data from LEP, SLD and HERA. The string model, used by PYTHIA, and the cluster model, used by HERWIG, both take account of the colour structure of the perturbative phase of evolution, with colour-connected pairs producing non-perturbative singlet structures that decay to hadrons. The biggest difference between these models is in how local these colour-singlet structures are. In the string model they stretch from a quark (or anti-di-quark) via a series of colour-connected gluons to an antiquark (or di-quark). In the cluster model each gluon decays non-perturbatively to a quark-antiquark pair and each resulting quark-antiquark singlet (coming one from each of two colour-connected gluons) decays to hadrons. The independent fragmentation model, used by ISAJET, on the other hand, treats each parton as an independent source of hadrons and is strongly ruled out by $e^+e^-$ data, for example on inter-jet effects in three-jet events, the so-called string effect. Of the other two models, PYTHIA gives the better description of $e^+e^-$ data, but HERWIG also gives an adequate description, despite having a lot fewer adjustable parameters.

Models of the underlying event are not strongly constrained by either theoretical understanding or experimental data. Two extreme models are available and the truth is likely to lie between them. In the soft model, used in HERWIG, the collision of the two proton remnants is assumed to be like a minimum bias hadron-hadron collision at the same energy. A simple parametrisation of minimum bias data (from UA5 [293]) is used with little additional physics input. In the mini-jet model, used in PYTHIA and available as an additional package for HERWIG, on the other hand, the remnant-remnant collisions act as a new source of perturbative scattering, which ultimately produce the hadrons of the underlying event. To avoid regions of unstable perturbative predictions and problems with unitarity, a cutoff must be used, $p_{t,min} \sim 1$ GeV. Presumably for a complete description, some soft model should describe the physics below $p_{t,min}$ such that the results do not depend critically on its value. Unfortunately no such model exists at present. Although the two models give rather similar predictions for average properties of the underlying event, they give very different probabilities for the rare fluctuations that can be most important in determining jet uncertainties. This is an area that needs to be improved before LHC running begins.

## D2 Parton-level Monte Carlos

With few exceptions (e.g. 3 or 4-jet final states in $e^+e^-$ collisions) multi-jet final states are not accurately described by the shower MC's described above. This is because emission of several hard and widely separated partons is poorly approximated by the shower evolution algorithms, and exact (although perhaps limited to the tree level) matrix elements need to be used to properly evaluate quantum correlations. Parton-level Monte Carlos are event generators for multi-parton final states, which incorporate the exact tree-level matrix elements. They can be used for parton-level simulations of multi-jet processes, under the assumption that each hard parton will be identified with a final-state physical jet with momentum equal to the momentum of the parent parton. Selection and analysis cuts can be applied directly to the partons. In some cases, the partonic final states can be used as a starting point for the shower evolution performed using a shower MC such as HERWIG, PYTHIA, or ISAJET. For a discussion of the problems involved in ensuring the colour-coherence of the shower evolution when dealing with multi-parton final states, see [294].

In the following, we collect some information on the most frequently used parton-level MCs used in connection with top quark studies.

### *D21 VECBOS*[29]

VECBOS [150] is a Monte Carlo for inclusive production of a $W$-boson plus up to 4 jets or a $Z$-boson plus up to 3 jets. VECBOS is therefore a standard tool used in the simulation of backgrounds to $t\bar{t}$ production. The matrix elements are calculated exactly at the tree level, and include the spin correlations of the vector boson decay fermions with the rest of the event. Various parton density functions are

[29] VECBOS authors: F.A. Berends, H. Kuijf, B. Tausk and W.T. Giele. Contacts: giele@fnal.gov

available and distributions can be obtained by using the kinematics of the final state, available on an event-by-event basis together with the corresponding event weight. The code and its documentation can be obtained from:

`http://www-theory.fnal.gov/people/giele/vecbos.html`

Documentation on the use of VECBOS within ATLAS can be found in [295].

### *D22 CompHEP*[30]

CompHEP is a package for the calculation of elementary particle decay and collision properties in the lowest order of perturbation theory (the tree approximation). The main purpose of CompHEP is to generate automatically transition probabilities from a given Lagrangian, followed by the automatic evaluation of the phase-space integrals and of arbitrary distributions. The present version has 4 built-in physical models. Two of them are the versions of the Standard Model (SU(3)xSU(2)xU(1)) in the unitary and t'Hooft-Feynman gauges. The user can change the models or even create new ones.

The symbolic part of CompHEP allows the user to perform the following operations:

1. to select a process by specifying incoming and outgoing particles for the decays of $1 \to 2, \ldots, 1 \to 5$ types and the collisions of $2 \to 2, \ldots, 2 \to 4$ types,
2. to generate Feynman diagrams, calculating the analytical expressions for the squared matrix elements,
3. to save the algebraic symbolic results and to generate the optimized Fortran and C codes for the squared matrix elements for further numerical calculations.

The numerical part of CompHEP allows to convolute the squared matrix element with structure functions and beam spectra, to introduce various kinematic cuts, to introduce a phase space mapping in order to smooth sharp peaks of a squared matrix element, to perform a Monte Carlo phase space integration by VEGAS, to generate events and to display distributions for various kinematic variables. Recently, an interface with PYTHIA has been created [283]. This allows to perform realistic simulations of the process including hadronisation effects as well as the effects of the initial and final state radiation.

The CompHEP codes and manual are available from the following Web sites:

`http://theory.npi.msu.su/~comphep`
`http://www.ifh.de/~pukhov`

### *D23 ALPHA*[31]

ALPHA is an algorithm introduced in [296] for the evaluation of arbitrary multi-parton EW matrix elements. This algorithm determines the matrix elements from a (numerical) Legendre transform of the effective action, using a recursive procedure which does not make explicit use of Feynman diagrams. The algorithm has a complexity growing like a power in the number of particles, compared to the factorial-like growth that one expects from naive diagram counting. This is a necessary feature of any attempt to evaluate matrix elements for processes with large numbers of external particles, since the number of Feynman diagrams grows very quickly beyond any reasonable value.

An implementation of ALPHA for hadronic collisions was introduced in [294], where the algorithm was extended to the case of QCD amplitudes (see also [297]). The main aim of the hadronic version of ALPHA is to allow the QCD parton-shower evolution of the multi-parton final state, in a way consistent with the colour-coherence properties of the soft gluon emission dynamics. This is achieved by evaluating the QCD amplitudes in an appropriate colour basis [294], such that the assignement of a specific colour flow configuration on an event-by-event basis. The pattern of colour flow defines the colour currents

[30] CompHEP authors: A. Pukhov, E. Boos, M. Dubinin, V. Edneral, V. Ilyin, D. Kovalenko, A. Kryukov, V. Savrin, S. Shichanin, A. Semenov. Contacts: pukhov@theory.npi.msu.su, ilyin@theory.npi.msu.su

[31] ALPHA authors: F. Caravaglios, M. Moretti. The version for hadronic collisions received additional contributions from M.L. Mangano and R. Pittau. Contact: moretti@fe.infn.it

required to implement the angular ordering prescription which embodies, at the leading order in the $1/N_c$ expansion, the quantum coherence properties of soft-gluon radiation, as discussed in Appendix D1. A version of the code is being completed [298], which incorporates the evaluation of $Wb\bar{b}+n$ jets ($n \leq 4$), with all $b$-mass effects included. This program will allow a complete evaluation of the $W+$ multijet backgrounds to single top and $t\bar{t}$ production. The code contains 3 modules: the first for the generation of parton-level events, with the assignement of partonic flavours, helicities and colour flows. The second for the unweigthing of the events, and the third for the parton-shower evolution of the initial and final states, done using the HERWIG MC. The code will soon be available from the URL:

`http://home.cern.ch/~mlm/alpha`

**References**


[1] F. Abe *et al.* [CDF], Phys. Rev. Lett. **73**, 225 (1994) hep-ex/9405005; Phys. Rev. **D50**, 2966 (1994).

[2] F. Abe *et al.* [CDF], Phys. Rev. Lett. **74**, 2626 (1995) hep-ex/9503002.
S. Abachi *et al.* [D0], Phys. Rev. Lett. **74**, 2632 (1995) hep-ex/9503003.

[3] F. Abe *et al.* [CDF], Phys. Rev. **D51**, 4623 (1995) hep-ex/9412009; Phys. Rev. Lett. **75**, 3997 (1995) hep-ex/9506006; Phys. Rev. **D52**, 2605 (1995).

[4] F. Abe *et al.* [CDF], Phys. Rev. **D59**, 092001 (1999).

[5] S. Abachi *et al.* [D0], Phys. Rev. Lett. **79**, 1197 (1997) hep-ex/9703008; B. Abbott *et al.* [D0], Phys. Rev. Lett. **80**, 2063 (1998) hep-ex/9706014; Phys. Rev. **D58**, 052001 (1998) hep-ex/9801025; Phys. Rev. **D60**, 052001 (1999) hep-ex/9808029.

[6] F. Abe *et al.* [CDF], Phys. Rev. Lett. **80**, 2767 (1998) hep-ex/9801014; Phys. Rev. Lett. **80**, 2779 (1998) hep-ex/9802017; Phys. Rev. Lett. **82**, 271 (1999) hep-ex/9810029.

[7] S. Abachi *et al.* [D0], Phys. Rev. Lett. **79**, 1203 (1997) hep-ex/9704015.

[8] F. Abe *et al.* [CDF], Phys. Rev. Lett. **80**, 2773 (1998) hep-ex/9710008.

[9] F. Abe *et al.* [CDF], Phys. Rev. Lett. **79**, 1992 (1997).

[10] B. Abbott *et al.* [D0], Phys. Rev. **D60**, 012001 (1999) hep-ex/9808034; Phys. Rev. Lett. **83**, 1908 (1999) hep-ex/9901023.

[11] F. Abe *et al.* [CDF], Phys. Rev. Lett. **79**, 3585 (1997) hep-ex/9704007.

[12] F. Abe *et al.* [CDF], Phys. Rev. Lett. **80**, 5720 (1998) hep-ex/9711004.

[13] F. Abe *et al.* [CDF], Phys. Rev. Lett. **80**, 2525 (1998).

[14] T. Affolder *et al.* [CDF], Phys. Rev. Lett. **84**, 216 (2000) hep-ex/9909042.

[15] B. Abbott *et al.* [D0], hep-ex/0002058.

[16] `http://weblib.cern.ch/weblib2/Home/Internal_Notes/ATLAS_Notes/index.php`

[17] `http://cmsdoc.cern.ch/cms.html`

[18] `http://home.cern.ch/~mlm/lhc99/topwg.html`

[19] The LEP Electroweak Working Group and the SLD Heavy Flavour Group, CERN-EP/99-15; D. G. Charlton, hep-ex/9912019; M. L. Swartz, hep-ex/9912026.

[20] R. Hempfling and B. A. Kniehl, Phys. Rev. **D51**, 1386 (1995).

[21] K. Melnikov and T. van Ritbergen, hep-ph/9912391; K. G. Chetyrkin and M. Steinhauser, Phys. Rev. Lett. **83**, 4001 (1999).

[22] A. Czarnecki and K. Melnikov, Nucl. Phys. **B544**, 520 (1999).

[23] K. G. Chetyrkin, R. Harlander, T. Seidensticker and M. Steinhauser, Phys. Rev. **D60**, 114015 (1999).

[24] A. Denner and T. Sack, Nucl. Phys. **B358**, 46 (1991); G. Eilam, R. R. Mendel, R. Migneron and A. Soni, Phys. Rev. Lett. **66**, 3105 (1991).

[25] I. I. Bigi, Y. L. Dokshitzer, V. Khoze, J. Kühn and P. Zerwas, Phys. Lett. **B181**, 157 (1986).

[26] For reviews see, e.g., J. Bagger and J. Wess, *Supersymmetry And Supergravity* (2nd Edition),

Princeton University Press, 1992; H. P. Nilles, Phys. Rept. **110**, 1 (1984); H. E. Haber and G. L. Kane, Phys. Rept. **117**, 75 (1985).
[27] M. Veltman, Nucl. Phys. **B123**, 89 (1977).
[28] A. Sirlin, Phys. Rev. **D22**, 971 (1980); W. J. Marciano and A. Sirlin, Phys. Rev. **D22**, 2695 (1980).
[29] H. E. Haber and R. Hempfling, Phys. Rev. Lett. **66**, 1815 (1991); Prog. Theor. Phys. **85**, 1 (1991); J. Ellis, G. Ridolfi and F. Zwirner, Phys. Lett. **B257**, 83 (1991).
[30] ATLAS Collab., "ATLAS Detector and Physics Performance Technical Design Report", CERN LHCC 99-14/15 (1999).
[31] J. H. Kühn and M. Steinhauser, Phys. Lett. **B437**, 425 (1998) hep-ph/9802241; M. Davier and A. Höcker, Phys. Lett. **B435**, 427 (1998) hep-ph/9805470.
[32] D. Bardin, M. Grünewald and G. Passarino, hep-ph/9902452; G. Degrassi, P. Gambino and A. Sirlin, Phys. Lett. **B394**, 188 (1997) hep-ph/9611363.
[33] G. Degrassi, P. Gambino, M. Passera and A. Sirlin, Phys. Lett. **B418**, 209 (1998) hep-ph/9708311.
[34] S. Heinemeyer, T. Mannel and G. Weiglein, hep-ph/9909538.
[35] S. Heinemeyer, W. Hollik and G. Weiglein, Eur. Phys. J. **C9**, 343 (1999) hep-ph/9812472.
[36] J. H. Kühn and G. Rodrigo, Phys. Rev. **D59**, 054017 (1999) hep-ph/9807420.
[37] P. Nason, "Heavy quark production", in *Heavy Flavours*, eds A.J. Buras and M. Lindner, Advanced Series on Directions in High Energy Physics, vol. 10 (World Scientific, Singapore, 1992); S. Frixione, M.L. Mangano, P. Nason and G. Ridolfi, in *Heavy Flavours II*, eds A.J. Buras and M. Lindner, Advanced Series on Directions in High Energy Physics, vol. 15 (World Scientific, Singapore, 1998), hep-ph/9702287.
[38] P. Nason, S. Dawson and R.K. Ellis, Nucl. Phys. **B303**, 607 (1988); W. Beenakker, H. Kuijf, W.L. van Neerven and J. Smith, Phys. Rev. **D40**, 54 (1989).
[39] P. Nason, S. Dawson and R.K. Ellis, Nucl. Phys. **B327**, 49 (1989); W. Beenakker, W.L. van Neerven, R. Meng, G.A. Schuler and J. Smith, Nucl. Phys. **B351**, 507 (1991).
[40] M.L. Mangano, P. Nason and G. Ridolfi, Nucl. Phys. **B373**, 295 (1992).
[41] Code available from `http://home.cern.ch/~nason`
[42] S. Frixione, M.L. Mangano, P. Nason and G. Ridolfi, Phys. Lett. **B351**, 555 (1995) hep-ph/9503213.
[43] G. Sterman, Nucl. Phys. **B281**, 310 (1987); S. Catani and L. Trentadue, Nucl. Phys. **B327**, 323 (1989).
[44] S. Catani, M.L. Mangano, P. Nason and L. Trentadue, Phys. Lett. **B378**, 329 (1996) hep-ph/9602208; Nucl. Phys. **B478**, 273 (1996) hep-ph/9604351.
[45] E.L. Berger and H. Contopanagos, Phys. Rev. **D57**, 253 (1998) hep-ph/9706206.
[46] N. Kidonakis and G. Sterman, Nucl. Phys. **B505**, 321 (1997) hep-ph/9705234.
[47] R. Bonciani, S. Catani, M.L. Mangano and P. Nason, Nucl. Phys. **B529**, 424 (1998) hep-ph/9801375.
[48] E. Laenen, G. Oderda and G. Sterman, Phys. Lett. **B438**, 173 (1998) hep-ph/9806467.
[49] L. H. Orr, T. Stelzer and W. J. Stirling, Phys. Rev. **D56**, 446 (1997) hep-ph/9609246; L. H. Orr and W. J. Stirling, Phys. Rev. **D51**, 1077 (1995) hep-ph/9409238.
[50] B. Masuda, L. H. Orr and W. J. Stirling, Phys. Rev. **D54**, 4453 (1996) hep-ph/9605369.
[51] G. Marchesini and B. R. Webber, Nucl. Phys. **B310**, 461 (1988); G. Marchesini, B. R. Webber, G. Abbiendi, I. G. Knowles, M. H. Seymour and L. Stanco, HERWIG 5.1, Comput. Phys. Commun. **67**, 465 (1992); G. Corcella *et al.*, HERWIG 6.1, hep-ph/9912396. Unless otherwise stated, the default public version 5.9 of HERWIG was used. Version features and various parameter tunings can be found at: `http://hepwww.rl.ac.uk/theory/seymour/herwig/`
[52] T. Sjöstrand and M. Bengtsson, Comput. Phys. Comm. **43**, 367 (1987); T. Sjostrand, PYTHIA 5.7, Comput. Phys. Commun. **82**, 74 (1994).
[53] F. E. Paige and S. D. Protopopescu, BNL-29777; H. Baer, F. E. Paige, S. D. Protopopescu and X. Tata, ISAJET 7.48, hep-ph/0001086; ISAJET 7.40, hep-ph/9810440; ISAJET 7.37, hep-

ph/9804321.
[54] G. Corcella and M. H. Seymour, Phys. Lett. **B442**, 417 (1998) hep-ph/9809451.
[55] H.L. Lai *et al.* [CTEQ], hep-ph/9903282.
[56] A.D. Martin, R.G. Roberts, W.J. Stirling and R.S. Thorne, Eur. Phys. J. **C4**, 463 (1998) hep-ph/9803445.
[57] A. D. Martin, R. G. Roberts, W. J. Stirling and R. S. Thorne, hep-ph/9907231.
[58] M.A. Aivazis, J.C. Collins, F.I. Olness and W. Tung, Phys. Rev. **D50**, 3102 (1994) hep-ph/9312319.
[59] M. Cacciari, hep-ph/9910412.
[60] A. Petrelli, M. Cacciari, M. Greco, F. Maltoni and M. L. Mangano, Nucl. Phys. **B514**, 245 (1998) hep-ph/9707223; F. Maltoni, M. L. Mangano and A. Petrelli, Nucl. Phys. **B519**, 361 (1998) hep-ph/9708349.
[61] M. Cacciari and S. Catani, private communication and work in progress.
[62] S. Frixione, Nucl. Phys. **B507**, 295 (1997) hep-ph/9706545.
[63] G. Corcella and M. H. Seymour, hep-ph/9911536; hep-ph/9908388.
[64] G. Corcella, M.L. Mangano and M.H. Seymour, to appear.
[65] S. Catani, Y. L. Dokshitzer, M. H. Seymour and B. R. Webber, Nucl. Phys. **B406**, 187 (1993); M. H. Seymour, Nucl. Phys. **B421**, 545 (1994).
[66] The final report of the Physics at Run II Workshop: Supersymmetry/Higgs and Top-quark physics at Run II (*t*hinkshop), `http://fnth37.fnal.gov/run2.html`
[67] W. Beenakker, A. Denner, W. Hollik, R. Mertig, T. Sack and D. Wackeroth, Nucl. Phys. **B411**, 343 (1994).
[68] C. Kao, G. A. Ladinsky and C. P. Yuan, Int. J. Mod. Phys. **A12**, 1341 (1997).
[69] A. Stange and S. Willenbrock, Phys. Rev. **D48**, 2054 (1993) hep-ph/9302291.
[70] H. Zhou, C. Li and Y. Kuang, Phys. Rev. **D55**, 4412 (1997) hep-ph/9603435.
[71] W. Hollik, W. M. Mösle and D. Wackeroth, Nucl. Phys. **B516**, 29 (1998) hep-ph/9706218.
[72] C.Kao and D.Wackeroth, in preparation.
[73] K.J.F. Gaemers and G. Hoogeveen, Phys. Lett. **B146**, 347 (1984).
[74] D. Dicus, A. Stange and S. Willenbrock, Phys. Lett. **B333**, 126 (1994) hep-ph/9404359.
[75] W. Bernreuther, M. Flesch and P. Haberl, Phys. Rev. **D58**, 114031 (1998) hep-ph/9709284.
[76] J. Yang and C. Li, Phys. Rev. **D52**, 1541 (1995); J. M. Yang and C. S. Li, Phys. Rev. **D54**, 4380 (1996) hep-ph/9603442.
[77] C. Li, R. J. Oakes, J. M. Yang and C. P. Yuan, Phys. Lett. **B398**, 298 (1997) hep-ph/9701350.
[78] J. Kim, J. L. Lopez, D. V. Nanopoulos and R. Rangarajan, Phys. Rev. **D54**, 4364 (1996) hep-ph/9605419.
[79] H. Zhou and C. Li, Commun. Theor. Phys. **30**, 465 (1998) hep-ph/9805372.
[80] C. Li, H. Zhou, Y. Zhu and J. Yang, Phys. Lett. **B379**, 135 (1996) hep-ph/9606271; C. Li, B. Hu, J. Yang and C. Hu, Phys. Rev. **D52**, 5014 (1995); S. Alam, K. Hagiwara and S. Matsumoto, Phys. Rev. **D55**, 1307 (1997) hep-ph/9607466.
[81] Z. Sullivan, Phys. Rev. **D56**, 451 (1997) hep-ph/9611302.
[82] C. S. Li, C. P. Yuan and H. Zhou, Phys. Lett. **B424**, 76 (1998) hep-ph/9709275.
[83] D. Wackeroth, hep-ph/9807558.
[84] H. Zhou and C. Li, Phys. Rev. **D55**, 4421 (1997); Z. Yu, H. Pietschmann, W. Ma, L. Han and J. Yi, Eur. Phys. J. **C9**, 463 (1999) hep-ph/9804331.
[85] W. Hollik, W.M. Mösle and D.Wackeroth, in preparation.
[86] W. Bernreuther, A. Brandenburg and M. Flesch, hep-ph/9812387.
[87] C. Kao, Phys. Lett. **B348**, 155 (1995) hep-ph/9411337.
[88] C. Kao and D. Wackeroth, hep-ph/9902202.
[89] M. L. Mangano, Nucl. Phys. **B405**, 536 (1993).
[90] A. Lagatta, L. La Rotonda and M. Cobal, "Top mass evaluation in the $t\bar{t}$ dilepton channel", ATLAS

Internal Note ATL-COM-PHYS-99-044 (1999).
[91] Lj. Simic, G. Skoro and D. Popovic, "Signal and background study for $t\bar{t}$ all hadronic decay at the LHC", ATLAS Internal Note ATL-COM-PHYS-99-057 (1999).
[92] K. Lane and E. Eichten, Phys. Lett. **B352**, 382 (1995); E. Eichten and K. Lane, Phys. Lett. **B327**, 129 (1994).
[93] C. T. Hill and S. J. Parke, Phys. Rev. **D49**, 4454 (1994); R. Casalbuoni et al., Z. Phys. **C69**, 519 (1996).
[94] C.T. Hill, Phys. Lett. **B266**, 419 (1991); C.T. Hill, Phys. Lett. **B345**, 483 (1995).
[95] E. Simmons, Phys. Rev. **D55**, 1678 (1997).
[96] N. Cartiglia and J. Parsons, "Study of ATLAS sensitivity to a heavy resonance decaying to $t\bar{t}$", ATLAS Internal Note ATL-COM-PHYS-99-038 (1999).
[97] S. Gonzalez de la Hoz, "MSSM Higgs decay to top quarks", ATLAS Communication ATL-COM-PHYS-99-016 (1999).
[98] R. Frey *et al.*, FERMILAB-CONF-97/085.
[99] See the Proceedings of the ECFA Large Hadron Collider Workshop, Eds. G. Jarlskog and D. Rein, CERN 09-10, ECFA 90-133, in particular: G. Unal and L. Fayard, vol. II, p.360.
[100] E. Accomando *et al.* [ECFA/DESY LC Physics Working Group Collaboration], Phys. Rept. **299**, 1 (1998).
[101] M. Beneke, A. Signer and V. A. Smirnov, Phys. Lett. **B454**, 137 (1999) hep-ph/9903260; A. H. Hoang and T. Teubner, Phys. Rev. **D60**, 114027 (1999) hep-ph/9904468; T. Nagano, A. Ota and Y. Sumino, Phys. Rev. **D60**, 114014 (1999) hep-ph/9903498; A. H. Hoang *et al.*, hep-ph/0001286.
[102] M. Beneke and V. M. Braun, Nucl. Phys. **B426**, 301 (1994) hep-ph/9402364; I. I. Bigi, M. A. Shifman, N. G. Uraltsev and A. I. Vainshtein, Phys. Rev. **D50**, 2234 (1994) hep-ph/9402360.
[103] M. C. Smith and S. S. Willenbrock, Phys. Rev. Lett. **79**, 3825 (1997) hep-ph/9612329.
[104] M. Beneke, Phys. Lett. **B434**, 115 (1998) hep-ph/9804241.
[105] E. Richter-Was, D. Froidevaux and L. Poggioli, "ATLFAST 2.0 a fast simulation package for ATLAS", ATL-PHYS-98-131 (1998).
[106] P. Grenier et al., "Measurement of the top quark mass in the inclusive single lepton plus jets channel", ATL-COM-PHYS-99-024 (1999).
[107] A. Artamonov et.al., ATLAS Internal Note ATL-SOFT-95-104 (1995).
[108] I. Efthymiopoulos, ATLAS Internal Note ATL-COM-PHYS-99-050 (1999).
[109] C. Peterson et al., Phys. Rev. **D27**, 105 (1983).
[110] ALEPH, Phys. Rep. **294**, 1 (1998).
[111] CMS Letter of Intent, CERN/LHCC 92-3 (1992) 90; I. Iashvili *et al.*, CMS TN/92-34 (1992).
[112] A. Kharchilava, hep-ph/9912320.
[113] A. Kharchilava and P. Pralavorio, CMS TN/96-116 (1996).
[114] G. Wrochna *et al.*, CMS TN/96-060 (1996) and references therein.
[115] H. L. Lai *et al.*, Phys. Rev. **D51**, 4763 (1995) hep-ph/9410404.
[116] H. L. Lai *et al.*, Phys. Rev. **D55**, 1280 (1997) hep-ph/9606399.
[117] S. R. Slabospitsky, in preparation; implemented into PYTHIA with L. Sonnenschein.
[118] LEP Heavy Flavour Working Group, LEPHF/98-01.
[119] K. Abe *et al.* [SLD Coll.], hep-ex/9908032.
[120] S.S. Willenbrock and D.A. Dicus, Phys. Rev. **D34**, 155 (1986); C.P. Yuan, Phys. Rev. **D41**, 42 (1990); R.K. Ellis and S. Parke, Phys. Rev. **D46**, 3785 (1992).
[121] S. Cortese and R. Petronzio, Phys. Lett. **B253**, 494 (1991).
[122] T. Stelzer and S. Willenbrock, Phys. Lett. **B357**, 125 (1995) hep-ph/9505433.
[123] A.P. Heinson, A.S. Belyaev and E.E. Boos, Phys. Rev. **D56**, 3114 (1997) hep-ph/9612424.
[124] T. M. Tait, Phys. Rev. **D61**, 034001 (2000) hep-ph/9909352.
[125] T. Stelzer, Z. Sullivan and S. Willenbrock, Phys. Rev. **D56**, 5919 (1997) hep-ph/9705398.

[126] M.C. Smith and S. Willenbrock, Phys. Rev. **D54**, 6696 (1996) hep-ph/9604223.
[127] D. Amidei *et al.* [TeV-2000 Study Group], FERMILAB-PUB-96-082.
[128] G.A. Ladinsky and C.P. Yuan, Phys. Rev. **D43**, 789 (1991); A. Stange, W. Marciano and S. Willenbrock, Phys. Rev. **D50**, 4491 (1994) hep-ph/9404247; S. Moretti, Phys. Rev. **D56**, 7427 (1997) hep-ph/9705388.
[129] D.O. Carlson and C.P. Yuan, Phys. Lett. **B306**, 386 (1993).
[130] G. Mahlon and S. Parke, Phys. Rev. **D55**, 7249 (1997) hep-ph/9611367.
[131] G. Mahlon and S. Parke, hep-ph/9912458.
[132] D.O. Carlson, E. Malkawi and C.P. Yuan, Phys. Lett. **B337**, 145 (1994) hep-ph/9405277; A. Datta and X. Zhang, Phys. Rev. **D55**, 2530 (1997) hep-ph/9611247.
[133] T. Tait and C. P. Yuan, hep-ph/9710372.
[134] K. Hikasa, K. Whisnant, J. M. Yang and B. Young, Phys. Rev. **D58**, 114003 (1998) hep-ph/9806401.
[135] E. Boos, L. Dudko and T. Ohl, Eur. Phys. J. **C11**, 473 (1999) hep-ph/9903215.
[136] D. Atwood, S. Bar-Shalom, G. Eilam and A. Soni, Phys. Rev. **D54**, 5412 (1996) hep-ph/9605345.
[137] E.H. Simmons, Phys. Rev. **D55**, 5494 (1997) hep-ph/9612402.
[138] C.S. Li, R.J. Oakes and J.M. Yang, Phys. Rev. **D55**, 1672 (1997) hep-ph/9608460.
[139] C.S. Li, R.J. Oakes and J.M. Yang, Phys. Rev. **D55**, 5780 (1997) hep-ph/9611455; C. Li, R.J. Oakes, J. Yang and H. Zhou, Phys. Rev. **D57**, 2009 (1998) hep-ph/9706412.
[140] S. Bar-Shalom, D. Atwood and A. Soni, Phys. Rev. **D57**, 1495 (1998) hep-ph/9708357.
[141] E. Malkawi and T. Tait, Phys. Rev. **D54**, 5758 (1996) hep-ph/9511337; A. Datta, J.M. Yang, B. Young and X. Zhang, Phys. Rev. **D56**, 3107 (1997) hep-ph/9704257; R.J. Oakes, K. Whisnant, J.M. Yang, B. Young and X. Zhang, Phys. Rev. **D57**, 534 (1998) hep-ph/9707477.
[142] T. Han, M. Hosch, K. Whisnant, B. Young and X. Zhang, Phys. Rev. **D58**, 073008 (1998) hep-ph/9806486.
[143] G. Bordes and B. van Eijk, Nucl. Phys. **B435**, 23 (1995).
[144] T. Stelzer, Z. Sullivan and S. Willenbrock, Phys. Rev. **D58**, 094021 (1998) hep-ph/9807340.
[145] A.S. Belyaev, E.E. Boos and L.V. Dudko, Phys. Rev. **D59**, 075001 (1999) hep-ph/9806332.
[146] R.M. Barnett, H.E. Haber and D.E. Soper, Nucl. Phys. **B306**, 697 (1988); F.I. Olness and W. Tung, Nucl. Phys. **B308**, 813 (1988).
[147] B. Harris, E. Laenen, Z. Sullivan, and S. Weinzierl, in progress.
[148] J. Huston, S. Kuhlmann, H.L. Lai, F. Olness, J.F. Owens, D.E. Soper and Phys. Rev. **D58**, 114034 (1998) hep-ph/9801444.
[149] D. Green *et al.*, "A Study of Single Top at CMS," CMS Note 1999/048, unpublished.
[150] F. A. Berends, H. Kuijf, B. Tausk and W. T. Giele, Nucl. Phys. **B357**, 32 (1991).
[151] J. Bennloch, in Proc. of the 1992 Meeting of the APS, Division of Particles and Fields, Fermilab, 10-14 Nov, 1992, eds. C. Albright et al, World Scientific (1993), p.1091; J. Benlloch, A. Caner, M.L. Mangano, T. Rodrigo, CDF Note : CDF/DOC/MONTECARLO/PUBLIC/1823 (1992).
[152] B. González Piñeiro, D. O'Neil, R. Brock and M. Lefebvre, "Measuring $V_{tb}$ and Polarization via Boson Gluon Fusion at the LHC", ATLAS Note: ATL-COM-PHYS-99-027, unpublished.
[153] D. O. Carlson, UMI-96-05840; S. Mrenna, T. Tait, and C.-P. Yuan, private communication.
[154] D. O'Neil, "Performance of the ATLAS Hadronic Endcap Calorimeter and the Physics of Electroweak Top Quark Production at ATLAS", University of Victoria Ph. D. Thesis, December 1999.
[155] A. Ahmedov, A.P. Cheplakov, V.V. Kukhtin, R. Mehdiyev, Z. Metreveli, and D. Salihagic, "Single Top quark production via W-gluon fusion at LHC, simulation with PYTHIA 5.7 Event Generator," ATLAS Note: ATL-COM-PHYS-99-026, unpublished.
[156] M. Dittmar, F. Pauss and D. Zurcher, Phys. Rev. **D56**, 7284 (1997) hep-ex/9705004.
[157] W.T. Giele, S. Keller and E. Laenen, Phys. Lett. **B372**, 141 (1996) hep-ph/9511449.
[158] M. Jezabek and J. H. Kühn, Nucl. Phys. **B320**, 20 (1989); M. Jezabek, "Top quark physics," Nucl. Phys. Proc. Suppl. **37B**, 197 (1994) hep-ph/9406411.

[159] B. Abbott *et al.* [D0], hep-ex/9906025.
[160] R.K. Ellis and S. Veseli, Phys. Rev. **D60**, 011501 (1999) hep-ph/9810489.
[161] R. Kleiss and W. J. Stirling, Z. Phys. **C40**, 419 (1988).
[162] V. Barger, J. Ohnemus and R. J. Phillips, Int. J. Mod. Phys. **A4**, 617 (1989).
[163] Y. Hara, Prog. Theor. Phys. **86**, 779 (1991); T. Arens and L. M. Sehgal, Phys. Lett. **B302**, 501 (1993).
[164] A. Brandenburg, Phys. Lett. **B388**, 626 (1996) hep-ph/9603333.
[165] T. Stelzer and S. Willenbrock, Phys. Lett. **B374**, 169 (1996) hep-ph/9512292.
[166] G. Mahlon and S. Parke, Phys. Rev. **D53**, 4886 (1996) hep-ph/9512264.
[167] G. Mahlon and S. Parke, Phys. Lett. **B411**, 173 (1997) hep-ph/9706304.
[168] D. Chang, S. Lee and A. Sumarokov, Phys. Rev. Lett. **77**, 1218 (1996) hep-ph/9512417.
[169] W. Bernreuther and A. Brandenburg, Phys. Rev. **D49**, 4481 (1994) hep-ph/9312210.
[170] W. Bernreuther, A. Brandenburg and P. Uwer, Phys. Lett. **B368**, 153 (1996) hep-ph/9510300; W. G. Dharmaratna and G. R. Goldstein, Phys. Rev. **D53**, 1073 (1996).
[171] A. Czarnecki, M. Jezabek and J. H. Kühn, Nucl. Phys. **B351**, 70 (1991).
[172] W. Bernreuther, O. Nachtmann, P. Overmann and T. Schröder, Nucl. Phys. **B388**, 53 (1992).
[173] J. P. Ma and A. Brandenburg, Z. Phys. **C56**, 97 (1992).
[174] M. Jezabek and J. H. Kühn, Phys. Lett. **B329**, 317 (1994) hep-ph/9403366.
[175] C. R. Schmidt, Phys. Rev. **D54**, 3250 (1996) hep-ph/9504434; M. Fischer, S. Groote, J. G. Körner, M. C. Mauser and B. Lampe, Phys. Lett. **B451**, 406 (1999) hep-ph/9811482.
[176] V. Šimàk, P.Homola, J. Valenta, R. Leitner, ATL-COM-PHYS-99-073 (1999).
[177] S. Abdullin, A. Khanov, N. Stepanov, *CMSJET*, CMS TN/94-180 (1999).
[178] P. Haberl, O. Nachtmann and A. Wilch, Phys. Rev. **D53**, 4875 (1996) hep-ph/9505409.
[179] K. Cheung, Phys. Rev. **D55**, 4430 (1997) hep-ph/9610368.
[180] D. Atwood, A. Aeppli and A. Soni, Phys. Rev. Lett. **69**, 2754 (1992).
[181] D. Atwood, A. Kagan and T. G. Rizzo, Phys. Rev. **D52**, 6264 (1995) hep-ph/9407408.
[182] G. L. Kane, G. A. Ladinsky and C. P. Yuan, Phys. Rev. **D45**, 124 (1992); A. Brandenburg and J. P. Ma, Phys. Lett. **B298**, 211 (1993).
[183] C. P. Yuan, Mod. Phys. Lett. **A10**, 627 (1995) hep-ph/9412214.
[184] F. Larios and C. P. Yuan, Phys. Rev. **D55**, 7218 (1997) hep-ph/9606397; B. Grzadkowski, B. Lampe and K. J. Abraham, Phys. Lett. **B415**, 193 (1997) hep-ph/9706489.
[185] H. Zhou, Phys. Rev. **D58**, 114002 (1998) hep-ph/9805358.
[186] V. Simak, J. Smolik, A. Lagatta, ATL-COM-PHYS-99-049 (1999).
[187] C. R. Schmidt, Phys. Lett. **B293**, 111 (1992).
[188] S. Weinberg, Phys. Rev. **D42**, 860 (1990); W. Bernreuther, T. Schröder and T. N. Pham, Phys. Lett. **B279**, 389 (1992).
[189] A. Pilaftsis, Phys. Lett. **B435**, 88 (1998) hep-ph/9805373.
[190] C. R. Schmidt and M. E. Peskin, Phys. Rev. Lett. **69**, 410 (1992).
[191] W. Bernreuther and A. Brandenburg, Phys. Lett. **B314**, 104 (1993).
[192] C. Caso *et al.*, Eur. Phys. J. **C3**, 1 (1998), and 1999 off-year partial update for the 2000 edition available on the PDG WWW page: `http://pdg.lbl.gov/`
[193] W. Buchmüller and D. Wyler, Nucl. Phys. **B268**, 621 (1986); K. Hagiwara, S. Ishihara, R. Szalapski and D. Zeppenfeld, Phys. Rev. **D48**, 2182 (1993).
[194] G. J. Gounaris, F. M. Renard and C. Verzegnassi, Phys. Rev. **D52**, 451 (1995) hep-ph/9501362; G. J. Gounaris, F. M. Renard and N. D. Vlachos, Nucl. Phys. **B459**, 51 (1996) hep-ph/9509316.
[195] K. Whisnant, J. Yang, B. Young and X. Zhang, Phys. Rev. **D56**, 467 (1997) hep-ph/9702305; J. M. Yang and B. Young, Phys. Rev. **D56**, 5907 (1997) hep-ph/9703463.
[196] R. D. Peccei and X. Zhang, Nucl. Phys. **B337**, 269 (1990); R. D. Peccei, S. Peris and X. Zhang, Nucl. Phys. **B349**, 305 (1991).
[197] E. Malkawi and C. P. Yuan, Phys. Rev. **D50**, 4462 (1994) hep-ph/9405322.

[198] F. del Aguila, J.A. Aguilar-Saavedra and R. Miquel, Phys. Rev. Lett. **82**, 1628 (1999).
[199] W. Hollik, J. I. Illana, S. Rigolin, C. Schappacher and D. Stockinger, Nucl. Phys. **B551**, 3 (1999) hep-ph/9812298.
[200] G. J. Feldman and R. D. Cousins, Phys. Rev. **D57**, 3873 (1998) [physics/9711021]; J.A. Aguilar-Saavedra, hep-ex/9911024.
[201] J. F. Donoghue, Phys. Rev. **D18**, 1632 (1978); E. P. Shabalin, Yad. Fiz. **31**, 1665 (1980) [Sov. J. Nucl. Phys. **31**, 864 (1980)].
[202] A. Soni and R. M. Xu, Phys. Rev. Lett. **69**, 33 (1992); C. R. Schmidt and M. E. Peskin, Phys. Rev. Lett. **69**, 410 (1992).
[203] B. Lampe, Phys. Lett. **B415**, 63 (1997) hep-ph/9709493.
[204] J. Lee, S. Y. Choi and C. S. Kim, hep-ph/9801236; S. Y. Choi, C. S. Kim and J. Lee, Phys. Lett. **B415**, 67 (1997) hep-ph/9706379.
[205] K. Cheung, Phys. Rev. **D53**, 3604 (1996) hep-ph/9511260; P. Haberl, O. Nachtmann and A. Wilch, Phys. Rev. **D53**, 4875 (1996) hep-ph/9505409; T. G. Rizzo, Phys. Rev. **D53**, 6218 (1996) hep-ph/9506351.
[206] T. G. Rizzo, in *1996 DPF/DPB Summer Study on New Directions for High Energy Physics*, Snowmass, CO, July 1996, eds. D.G. Cassel, L.Trindle Gennari and R.H. Siemann, hep-ph/9609311.
[207] D. Atwood, A. Aeppli and A. Soni, Phys. Rev. Lett. **69**, 2754 (1992).
[208] E. Boos, A. Pukhov, M. Sachwitz and H. J. Schreiber, Z. Phys. **C75**, 237 (1997) hep-ph/9610424; E. Boos, A. Pukhov, M. Sachwitz and H. J. Schreiber, Phys. Lett. **B404**, 119 (1997) hep-ph/9704259.
[209] S. Parke, Proc. of the 1994 Meeting of the APS, (DPF 94), Albuquerque, NM, 2-6 Aug 1994, DPF Conf.1994:0726-730 (QCD161:A6:1994), hep-ph/9409312.
[210] F. Larios, E. Malkawi and C.-P. Yuan, Lectures given by C.-P. Yuan at the CCAST Workshop on 'Physics at TeV Energy Scale ' July 15-26, 1996, Beijing, China, hep-ph/9704288.
T. M. Tait, hep-ph/9907462.
[211] G. L. Kane, G. A. Ladinsky and C. P. Yuan, Phys. Rev. **D45**, 124 (1992).
[212] M. S. Alam *et al.* [CLEO], Phys. Rev. Lett. **74**, 2885 (1995).
[213] F. Larios, M. A. Perez and C. P. Yuan, Phys. Lett. **B457**, 334 (1999) hep-ph/9903394.
[214] E. E. Boos, M. N. Dubinin, V. A. Ilin, A. E. Pukhov and V. I. Savrin, hep-ph/9503280; P. Baikov et.al, in: Proc. of X Workshop on High Energy Physics and Quantum Field Theory, ed. by B. Levtchenko, V. Savrin, Moscow, 1996, p.101.
[215] J. Cao, J. Wang, J. M. Yang, B. Young and X. Zhang, Phys. Rev. **D58**, 094004 (1998) hep-ph/9804343.
[216] B. Grzadkowski, J. F. Gunion and P. Krawczyk, Phys. Lett. **B268**, 106 (1991).
[217] D. Atwood, L. Reina and A. Soni, Phys. Rev. **D55**, 3156 (1997), hep-ph/9609279; L. Reina, Fermilab Thinkshop on Top Physics at Run II (Oct 19-21 1998).
[218] J.M. Yang, B.-L. Young and X. Zhang, Phys. Rev. **D58**, 055001 (1998). hep-ph/9705341,
[219] T. Han, R. D. Peccei and X. Zhang, Nucl. Phys. **B454**, 527 (1995) hep-ph/9506461.
[220] Y. P. Gouz and S. R. Slabospitsky, Phys. Lett. **B457**, 177 (1999) hep-ph/9811330.
[221] ALEPH Coll., ALEPH-Conf 99-023.
[222] P. Abreu *et al.* [DELPHI], Phys. Lett. **B446**, 62 (1999) hep-ex/9903072.
[223] DELPHI Coll., DELPHI Note 99-85, DELPHI Note 99-146.
[224] V. F. Obraztsov, S. R. Slabospitsky and O. P. Yushchenko, Phys. Lett. **B426**, 393 (1998) hep-ph/9712394; T. Han and J. L. Hewett, Phys. Rev. **D60**, 074015 (1999) hep-ph/9811237.
[225] M. Hosch, K. Whisnant and B. L. Young, Phys. Rev. **D56**, 5725 (1997) hep-ph/9703450.
[226] F. del Aguila, J. A. Aguilar-Saavedra and L. Ametller, Phys. Lett. **B462**, 310 (1999) hep-ph/9906462.
[227] F. del Aguila and J. A. Aguilar-Saavedra, hep-ph/9909222.
[228] A. D. Martin, W. J. Stirling and R. G. Roberts, Phys. Rev. **D50**, 6734 (1994) hep-ph/9406315.

[229] T. Han, K. Whisnant, B. L. Young and X. Zhang, Phys. Lett. **B385**, 311 (1996) hep-ph/9606231.
[230] N. Stepanov and S. Slabospitsky, in preparation.
[231] T. G. Rizzo, hep-ph/9910255.
[232] R. Decker, M. Nowakowski and A. Pilaftsis, Z. Phys. **C57**, 339 (1993) hep-ph/9301283.
[233] G. Mahlon and S. Parke, Phys. Lett. **B347**, 394 (1995) hep-ph/9412250.
[234] E. Jenkins, Phys. Rev. **D56**, 458 (1997) hep-ph/9612211.
[235] L. Conti et al., in preparation.
[236] G. Mahlon, hep-ph/9810485.
[237] B. Mele, S. Petrarca, A. Soddu, Phys. Lett. **B435**, 401 (1998), hep-ph/9805498; G. Eilam, J.L. Hewett and A. Soni, Erratum-Phys. Rev. **D59**, 039901 (1999).
[238] L. T. Handoko and C. Qiao, hep-ph/9907375; L. T. Handoko, Nuovo Cim. **A111**, 1275 (1998) hep-ph/9803262.
[239] D. Atwood and M. Sher, Phys. Lett. **B411**, 306 (1997) hep-ph/9707229.
[240] S. Glashow and S. Weinberg, Phys. Rev. **D15**, 1958 (1977).
[241] L.J. Hall and S. Weinberg, Phys. Rev. **D48**, R979 (1993), hep-ph/9303241; M. Luke and M.J. Savage, Phys. Lett. **B307**, 387 (1993), hep-ph/9303249.
[242] W.S. Hou, Phys. Lett. **B296**, 179 (1992).
[243] V. Barger and R. J. Phillips, "Collider Physics," Addison-Wesley (1987) (Frontiers in Physics, vol.71).
[244] CDF Collaboration, hep-ex/9912013.
[245] E. Ma, D. P. Roy and J. Wudka, Phys. Rev. Lett. **80**, 1162 (1998) hep-ph/9710447.
[246] D.J. Miller, S. Moretti, D.P. Roy, W.J. Stirling, hep-ph/9906230.
[247] J.A. Coarasa, J. Guasch and J. Sola, hep-ph/9903212; J.A. Coarasa, J. Guasch, W. Hollik and J. Sola, Phys. Lett. **B442**, 326 (1998), hep-ph/9808278; Xiao-Jun Bi, Yuan-Ben Dai, Xiao-Yuan Qi, Phys. Rev. **D61**, 015002 (2000), hep-ph/9907326.
[248] S. Bar-Shalom, G. Eilam, A. Soni and J. Wudka, Phys. Rev. **D57**, 2957 (1998) hep-ph/9708358; Phys. Rev. Lett. **79**, 1217 (1997) hep-ph/9703221.
[249] G. Eilam, J. L. Hewett and A. Soni, Phys. Rev. **D44**, 1473 (1991).
[250] J.L. Diaz Cruz and D.A. López Falcón, hep-ph/9911407.
[251] J. Guasch and J. Sola, Z. Phys. **C74**, 337 (1997) hep-ph/9603441.
[252] S.H. Zhu and L.Y. Shan, hep-ph/9811430.
[253] M. Aoki, N. Oshimo, Mod. Phys. Lett. **A13**, 3225 (1998) hep-ph/9808217.
[254] For reviews on $R$-parity violation, see *e.g.*: D.P. Roy, Pranama **41**, S333 (1993) hep-ph/9303324; G. Bhattacharyya, Nucl. Phys. Proc. Suppl. **52A**, 83 (1997).
[255] T. Han and M.B. Magro, hep-ph/9911442.
[256] S. Bar-Shalom, G. Eilam and A. Soni, Phys. Rev. **D60**, 035007 (1999) hep-ph/9812518.
[257] G. M. de Divitiis, R. Petronzio and L. Silvestrini, Nucl. Phys. **B504**, 45 (1997) hep-ph/9704244; J.L. Lopez, D.V. Nanopoulos and R. Rangarajan, Phys. Rev. **D56**, 3100 (1997), hep-ph/9702350.
[258] C. S. Li, R. J. Oakes and J. M. Yang, Phys. Rev. **D49**, 293 (1994); J. Yang and C. Li, Phys. Rev. **D49**, 3412 (1994); G. Couture, C. Hamzaoui and H. König, Phys. Rev. **D52**, 1713 (1995) hep-ph/9410230; G. Couture, M. Frank and H. König, Phys. Rev. **D56**, 4213 (1997) hep-ph/9704305.
[259] J. Guasch and J. Solà, hep-ph/9906268.
[260] S.R. Slabospitsky, in preparation.
[261] G. F. Tartarelli, The CDF Collaboration, FERMILAB-CONF-97/401-E. Published Proceedings International Europhysics Conference on High Energy Physics, Jerusalem, Israel, August 19-26, 1997.
[262] J. Dodd, S. McGrath and J. Parsons, ATLAS Communication ATL-COMP-PHYS-99-039 (1999).
[263] A. Stahl and H. Voss, Z. Phys. **C74**, 73 (1997).
[264] R. Barate *et al.* [ALEPH], hep-ex/9902031; M. Acciarri *et al.* [L3], Phys. Lett. **B466**, 71 (1999) hep-ex/9909044; G. Abbiendi *et al.* [OPAL], Eur. Phys. J. C **7**, 407 (1999).

[265] F. Abe *et al.* [CDF], Phys. Rev. Lett. **79**, 357 (1997) hep-ex/9704003; B. Abbott *et al.* [D0], Phys. Rev. Lett. **82**, 4975 (1999) hep-ex/9902028.
[266] "Future Electroweak Physics at the Fermilab Tevatron: Report of the TeV2000 Study Group", eds. D. Amidei and R. Brock, Fermilab-Pub-96/082 (1996).
[267] D. Cavalli *et al.*, ATLAS Internal Note-PHYS-94-053 (1994).
[268] L.D. Chikovani and T.D. Djobava, ATLAS Internal Note ATL-COM-PHYS-99-034 (1999).
[269] R. Kinnunen, J. Tuominiemi and D. Denegri, Search for the charged Higgs boson from top decays in CMS, CMS TN/94-233, 1994.
[270] D.P. Roy, Phys. Lett. **B277**, 183 (1992); Phys.Lett. **B283**, 403 (1992).
[271] P. Aurenche and R. Kinnunen, Z. Phys. **C28**, 261 (1985).
[272] R. Kinnunen and D. Denegri, B-tagging with Impact Parameter in the CMS Tracker, CMS TN/96-045, 1996.
[273] W. J. Marciano and F. E. Paige, Phys. Rev. Lett. **66**, 2433 (1991).
[274] Z. Kunszt, Nucl. Phys. **B247**, 339 (1984); Z. Kunszt, S. Moretti and W. J. Stirling, Z. Phys. **C74**, 479 (1997) hep-ph/9611397.
[275] A. Pukhov *et al.*, hep-ph/9908288; see also `http://theory.npi.msu.su/~comphep`
[276] T. Stelzer and W. F. Long, Comput. Phys. Commun. **81**, 357 (1994) hep-ph/9401258.
[277] H. Murayama, I. Watanabe and K. Hagiwara, KEK-91-11.
[278] D. A. Dicus and S. Willenbrock, Phys. Rev. **D39**, 751 (1989).
[279] S. Dawson and L. Reina, Phys. Rev. **D57**, 5851 (1998) hep-ph/9712400.
[280] M. N. Dubinin, V. A. Ilyin and V. I. Savrin, CMS-NOTE-97-101, Sep 1997. 21pp., Proc. of 12th International Workshop High-Energy Physics and Quantum Field Theory (QFTHEP 97), Samara, Russia, 4-10 Sep 1997, hep-ph/9712335.
[281] E. Richter-Was, M. Sapinski Acta Phys. Pol. **B30**, 1001 (1999)
[282] G. Eynard, 'Etude de la production associee du boson de Higgs $WH$, $t\bar{t}H$, $ZH$ with $H \to \gamma\gamma$ avec le detecteur ATLAS, aupres du LHC', ATLAS Ph.D. Thesis 1997, LAPP Annecy.
[283] V. Ilyin et al, CompHEP-PYTHIA interface, to appear.
[284] J. F. Gunion and J. Pliszka, Phys. Lett. **B444**, 136 (1998) hep-ph/9809306.
[285] P. Savard "The $W$ to jet-jet and top quark mass reconstruction with the ATLAS detector", ATL-CAL-97-092 (1997).
[286] B. Abbott *et al.* [D0 Collaboration], Nucl. Instrum. Meth. **A424**, 352 (1999) hep-ex/9805009.
[287] R. Mehdiyev and I. Vichou, ATLAS Internal Note, ATL-COM-PHYS-99-054 (1999).
[288] E.L. Berger and T. Tait, hep-ph/0002305.
[289] R. Demina, J. Lykken, K. Matchev, and A. Nomerotski, hep-ph/9910275.
[290] D. O. Carlson, Ph.D. Thesis, Michigan State University, MSUHEP 050727.
[291] U. Baur, M. Buice and L.H. Orr, in preparation.
[292] F. Abe *et al.* [CDF], Phys. Rev. **D50**, 5562 (1994); B. Abbott *et al.* [D0], Phys. Lett. **B464**, 145 (1999) hep-ex/9908017.
[293] G. J. Alner *et al.* [UA5], Phys. Rept. **154**, 247 (1987).
[294] F. Caravaglios, M. L. Mangano, M. Moretti and R. Pittau, Nucl. Phys. **B539**, 215 (1999) hep-ph/9807570.
[295] M. Cobal, D. Costanzo and S. Lami, Atlas note ATL-PHYS-96-084.
[296] F. Caravaglios and M. Moretti, Phys. Lett. **B358**, 332 (1995) hep-ph/9507237.
[297] P. Draggiotis, R. H. Kleiss and C. G. Papadopoulos, Phys. Lett. **B439**, 157 (1998) hep-ph/9807207.
[298] M.L. Mangano, M. Moretti and R. Pittau, work in progress.